Construction of versatile biomolecule nano-platforms via Dip-pen Nanolithography and their application in bio-sensing and cell differentiation

Sabine Oberhansl

UNIVERSITAT DE BARCELONA

Tesis doctoral

Construction of versatile biomolecule nano-platforms via Dip-pen Nanolithography and their application in bio-sensing and cell differentiation

Memoria presentada por

Sabine Oberhansl

Para optar al grado de **Doctor en Nanociencias**

Universitat de Barcelona

Departament d'Electrònica

Programa de doctorado de Nanociencias

2008-2012

Tesis doctoral dirigida por

Dr. Elena Martínez Fraiz

Tutor de la tesis

Prof. Josep Samitier Martí

Barcelona, 2012

Für meine Eltern

Bärbel und Heinz

Acknowledgements / Danksagung / Agradecimientos

So this is it… Ya está…. Endlich.... Time is a strange phenomenon: Sometimes 5 minutes seem like forever. And then, sometimes, 5 years seem like just a very short time…During those years, I met a lot of people, some of them collaborations and some of them colleagues/friends. The following pages are dedicated to those people, without whose help I wouldn´t have had such a good time.

I would like to start by thanking the two people who made it possible for me to be here: First of all, the person who interviewed me and accepted me as a PhD student and guided me along the ups and downs of the thesis – the director of my thesis: Dr. Elena Martinez. Thank you for believing in me, motivating me, pushing me when necessary and for always being present and listening to me. And most importantly, thanks for being a calming influence and rescuing me in situations of crisis (5 min before my conference presentation the beamer shuts down – Menorca 2008; Chapter 2 of the present thesis disappears suddenly – one day before handing in). Also, I would like to thank the tutor of my thesis, Professor Samitier, who allowed me to work in the Nanobiolab and facilitated the access to instrumentation and research material. Thanks for providing an excellent environment for the daily work.

A very important part of my time in Barcelona I spent with the people from the Nanobiolab, especially with my group, the "Elenos". Thank you very much to all of you (present and former members) for creating such a nice atmosphere in the lab! First to mention, the best and most fashionable Post Doc in the world, Anna Lagunas, who understood and helped me defend the "Chemist's point of view". Thanks for your help in- and outside of the lab and for teaching me useful Spanish proverbs ("o…todos o…al rio"). Also to Jordi (el guapo), thank you very much for sharing the lab space and time with me and for your indispensable help with software problems/plug-ins/processing (all the "theoretical stuff"); and for teaching me important Spanish words (falacia). Vero, a cordial "thank you" for being a "balancing" element, always having a word of good advice for me, for cheering me up and for making me laugh. To Maria and Albert, the relatively new members of the group, thank you for the nice time together, for the laughter and for helping me with my work. Not to forget, the former Elenos, firstly Maruxa! I really appreciate your help when I arrived here and had no clue how to find my way around in Barcelona! Thanks also for taking care of me (I really didn't mind that you fell asleep watching a movie). And also to Santi, thank you for the time we shared together in the lab and for discussions and advice.

From the rest of the Nanobiolab people I would like to thank everybody for helping me out with problems and discussing experiments and results with me. Also

for the hours we spent together outside the lab, thanks for having such a great time! My sincere thanks go to Marilia and Coco, who are more than just good colleagues to me, thanks for your advice and for being my friends! Also a special thanks to JuanJo (organizer of many rainy events), Juan Pablo (sending funny links and brightening up the lab routine), Reyes (for the second hand market experience and the jokes), Patti (for having an open ear and giving good advice), Marta (for always being friendly and smiling and also for helpful discussions), David "Papa Pitufo" Izquierdo (por siempre animarnos y estar preocupado por nosotros), Sergio (por ser el major compi de oficina que puede haber), Oscar (por hacerme reir - queté queté?). Furthermore, I would like to thank Patricia, Ernest, Rosella, Monica, Bogachan, Wilmer, Xavi F, JuanMa, Toni, AnaMaria, Jose Luis, and Javi for making the everyday life in the lab more pleasant. I don't want to forget to mention the former lab members: David Caballero (momento estrella al pelar la naranja), Muriel (the spectacular BBQ at your place), Marc, Xavi S. (thanks for helping me at the beginning and with the DPN!!), Eli, Eva, Lorena, Sam, Bea, Chris Mills, Nadia, Errachid and Christian Sporer, a "big thanks" for sharing the lab time and free time and many happy memories with me! And also the former "foreigners group" who adopted me just after starting in Barcelona: Marta Mattotti, Thomas, Gert-Jan, Mike, Jesus, Mathias and Ruth, thank you very much! From the Helix lab I would like to thank Tiziano, Aitor, Isil and Kay.

My sincere thanks also go to the IBEC support service: to Miriam, Laura and Isa, always willing to help, thank you very much for managing and organizing the lab and making my life and work easier (and for the good memories outside the lab, too)! And also the people in the administration (Mayte, Ricard, Fran B., Judith, Ester, Teresa, JuanFran, Fran C., Pilar J., Esther, Carolina, Arantxa, Ana, Vienna, and Marta R.) thank you for helping me with the paper work! A "special thanks" goes to Pilar C. for encouraging me to participate in the annual Carrera de la Mujer.

Furthermore I would like to mention and express my gratitude to: the former and present staff of the *Plataforma de Nanotecnologia*, thank you very much for providing a good service and always being there and helping out (Marta Poch, Silvia, Raul, Marina, Maria Jesus, Yolanda and Alvaro); the staff from the *Servei Cientific de la UB*; Lidia and Anna from the *ADM Core Facility* (thank you so much for your help with the microscopes) and also to Silvia Rovira from the *Facultad de Fisica (UB)* (for being the most efficient secretary I know).

During the course of my thesis, I was able to collaborate with several different people whom I would like to sincerely thank. From *NanoInk Inc.*: Tom L, Karen, Andy, Al, Jose R, Jason H, Anthony, Raymond, Sergey, Frank, Bob Marchmont, Rob Stokes and the rest of the NanoInk team; a special thanks goes to Jose C, Anne, Donato, Sarah for caring for me and making my stay such a great one! From the *Universidad Autonoma de Barcelona (UAB)*: Daniel Maspoch (for scientific advice, helpful discussions and providing the lab space), Elena, Alberto and Carlos (essential help with the NLP). From the *Institute for Research in Biomedicine (IRB)*: Professor

Albericio, Marta Paradis and Eli Prats (for the never-ending supply of biotin-thiol). Also from the *IRB*: Ramon Eritja (for indispensable scientific advice and helpful discussions) and his group. From the *NT Buchs*: Professor Bernard, Klaus, David and Valentin (for starting the collaboration on the piezoelectric device and for the delicious Swiss chocolate). From the *Karlsruhe Institut für Technologie (KIT)*: Professor Fuchs, Sylwia, Michael, Falko and Thomas (for helping me solve problems and placing at my free disposal equipment and their advice). Finally, I would like to express my gratitude to the *EuminaFAB Project* for accepting two project proposals and facilitating my stay at the KIT.

Outside of the university and lab routine, there are been several important people (some would call them friends) whom I would like to thank especially: Ana Rodriguez (por su felicidad y buen humor), Sara (por ser amiga y compi de piso), Alice, Hanne and Aitor, Alda, Samantha (para la receta inmejorable de Guacamole), Richard (las clases de LindyHop) and Lars (die vielen Tees und den seelischen und sonstigen Beistand). Gracias Javi y Rocio por vuestra amistad y por preocuparos por mi. A los miembros de la Coral de Gospel "The New Zombis" quiero agradecer los buenos momentos que pasamos juntos, en los ensayos y conciertos (en especial, Wally y Clooney). Muchas gracias también a mis nuevos compañeros de trabajo, en especial Daniela, Bouchra, Angel, Mireia, Thomas y Marcello and Louise (never forget this year's St. Patrick's). Marta (Pelay), petarda, gracias por socorrerme, escucharme y llevarme a comer sushi cuando hacía falta! Muchisimas gracias a Rosuca por siempre escucharme, dar buenos consejos y por tu felicidad y cariño. Eskerrik asco Lidia por compartir conmigo el master y el piso y muchos buenos e inolvidables momentos! Gracias también a Eugenio por compartir piso conmigo y por ser critico en las discussiones. Merci beaucoup Nadege pour être la meilleure colocatrice et très bonne amie!

Bei meinen Freunden aus Deutschland möchte ich mich auch noch ganz herzlich bedanken. Herzlichen Dank an Ralph Moser, Marc Mottl, Nadine Walter und Billy. Nadine Perschmann, vielen herzlichen Dank für die unzähligen Stunden Telefonseelsorge über Skype und für Deine langjährige Freundschaft. Ebenfalls mille grazie an Solli, meine wohl älteste Freundin! Ich hoffe daß wie nie den Kontakt verlieren werden! I would also like to thank my former neighbor, Frau Matsutani who convinced me that it is very important to emigrate at least once in your life. Vielen herzlichen Dank dass Sie eine so vorzügliche Nachbarin waren und immer noch sind.

Finally, I would like to thank the most important people in my life. How does the saying go… behind every great girl there is a great family (well, similar somehow). Ohne meine Familie wäre ich sicherlich nicht bis hierher gelangt. Vielen Dank an Micha und Olga, und auch an Thomas, für Euer Interesse und Eure Unterstützung. Meinem Cousin Steffen „Brüderle" möchte ich auch ganz herzlich danken für die Unterstützung und den Rückhalt (and of course also for the amazing

cover design). Herzlichen Dank auch an meine beiden Omas, die immer für mich da waren und alles für mich gemacht haben. Diese Arbeit ist meinen Eltern, Bärbel und Heinz gewidmet. Ich danke Euch von Herzen für Eure Unterstützung, Euren unerschütterlichen Glauben in mich und Eure Liebe. Nur dank der Sicherheit, die Ihr mir gebt, kann ich meine Träume verwirklichen.

Gracias a todos – Euch allen vielen Dank – Thank you to everybody!

- GENERAL INDEX -

Abbreviations

µCP	Microcontact printing
Å	Ångström (10^{-10} m)
AFM	Atomic force microscope/microscopy
APTES	3-aminopropyltrimethoxysilane
BMP-2	Bone morphogenetic protein 2
BSA	Bovine serum albumin
C2C12	Myoblastic cell line
cat	Catalyst (in this case Cu(I)I, TBTA, DIPEA)
DIPEA	*N,N*-diisopropylethylamine
D-MEM	Dulbecco's modified eagle's medium
DMF	Dimethylformamide
DMSO	Dimethyl sulfoxide
DNA	Desoxyribonucleic acid
DPN	Dip-pen Nanolithography
dt	Dwell time for Dip-pen Nanolithography (dots)
DTT	Dithiothreitol
ECM	Extracellular matrix
EDTA	Ethylenediaminetetraacetic acid
ELISA	Enzyme-linked immunosorbent assay
FBS	Foetal bovine serum
FAM	Fluorescein (fluorophore)
GPTMS	3-glycidyloxypropyl)trimethoxysilane
HIV	Human immunodeficiency virus
LFM	Lateral force microscopy / image

MHA	16-mercaptohexadecanoic acid
NHS	N-hydroxysuccinimide
NSOM	Near field scanning optical microscope/microscopy
ODT	Octadecanethiol
PBS	Phosphate buffer saline
PDMS	Poly(dimethylsiloxane)
RH	Relative humidity (in %)
RT	Room temperature (generally 21°C)
SAM	Self-assembled monolayer
SAV	Streptavidin
SAV-TR	Streptavidin with Texas Red ® fluorophore
SEM	Scanning electron microscope/microscopy
SMPB	4-(p-maleimidophenyl)butyrate
SPL	Scanning probe lithography
STM	Scanning tunnelling microscope/microscopy
T	Temperature
TBTA	Tris[(1-benzyl-1*H*-1,2,3-triazol-4-yl)methyl]amine
THF	Tetrahydrofuran
ToF-SIMS	Time-of-Flight Secondary Ion Mass Spectrometry
TRIS base	2-amino-2-hydroxymethyl-propane-1,3-diol
v	Writing velocity for Dip-pen Nanolithography (lines)
VdW	Van-der-Waals forces
XPS	X-ray photoelectron spectroscopy

General Introduction

“Equipped with his five senses, man explores the universe around him and calls the adventure Science.”

Edwin Powell Hubble

"Men love to wonder, and that is the seed of science.”

Ralph Waldo Emerson

Mankind has always been curious. After discovering almost everything at the visible range, the next challenges were things invisible to the naked eye. The resolving power of the human eye is around 100 µm, which corresponds to the size of a human hair.[1] This led to the invention of the light microscope in the 16th century and by that, it was possible to visualize features down to 200 nm. But scientists had to wait until 1931, when the first electron microscope was being built, before they could study even smaller features. Today, it is possible to investigate tiniest object, having a size of 0.5 Å (with the high-resolution transmission electron microscope, HRTEM) or, and this is laboratory routine, objects of 1-20 nm (with the scanning electron microscope, SEM). Figure 1 shows the length scale diagram from meter to Ångström (Å) and illustrates the size of a human being compared to an atom. Along the length scale, several examples from everyday live are given with their corresponding sizes.

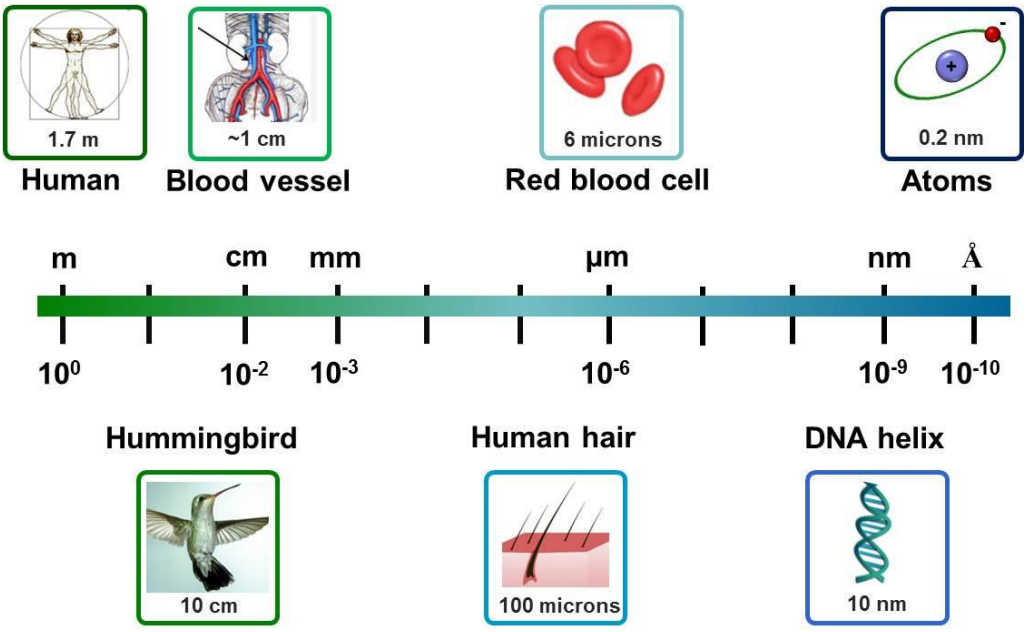

Figure 1: Length scale diagram showing nanometer in context.

Importance of nanometer sized features

Thanks to these new visualization techniques it could be discovered that nature itself uses nanofeatures. Below, two examples show how access to the micro- and nanoscale could shed light on curious facts, the lotus leave and the gecko's toes.

A Confucian scholar once said “I love lotus because while growing from mud, it is unstained”.[2] Not until almost one thousand years later science could reveal the secret of the lotus: looking at a lotus leaf with a SEM, we discover that it is equipped with a uniform distribution of hills and valleys and a combination of micro and nano features which extremely confine the surface contact area of water drops on the leaf, making the drops adopt an almost spherical shape. This phenomenon is called superhydrophobicity and permits the self-cleansing property of the lotus leaf – water and dirt will roll off the surface.[3]

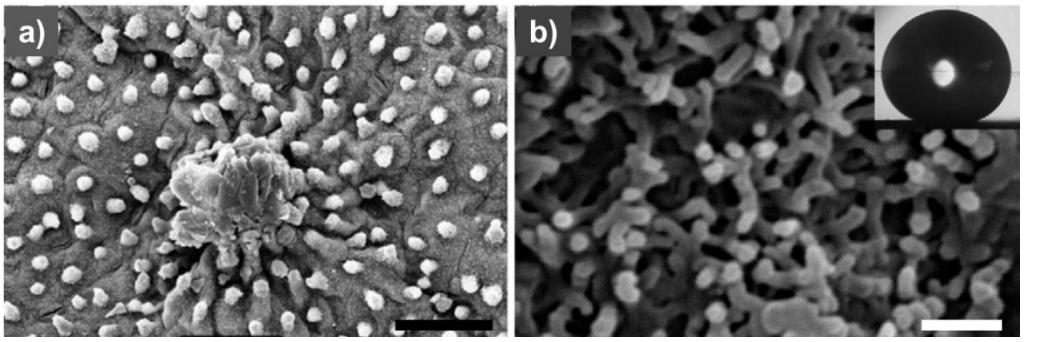

Figure 2: SEM images of lotus leaves with different magnifications. The inset of b) represents a water contact angle measurement on a lotus leaf with a value of 161 ± 2º. Images are taken from reference 3. The scale bars equal 50 µm in a) and 1 µm in b).

Who hasn't wondered how a gecko is able to walk up a slippery glass wall or stick to the ceiling? The answer also lies in the nano regime and actually, researchers are trying to take advantage of and mimic this amazing ability. The toes of a gecko have more to them than meets the eye (without microscope). As shown in Figure 3, at higher resolution it was discovered that every square millimeter of a gecko's footpad contains about 14.000 hair-like setae, each having a diameter of about 5 µm (compare: the human hair is 18 – 180 µm in diameter). Each seta in turn is tipped with 100 – 1000 of so called spatulae, each being 0.2 µm long.[4] These spatulae facilitate attractive forces called Van der Waals (VdW) forces to arise between the spatulae and the surface, which in turn enable the gecko to walk up the wall or stick to the ceiling. For detaching their toes, gecko change the angle of adhesion by bending their toes in the opposite direction from human fingers (and thus overcoming these VdW forces) and finally peeling the toes off of the surface. Only substrates with very low VdW forces,

like Teflon, are difficult for geckos to adhere to. The fact that geckos can attach and remove their feet reversibly without using any kind of chemical (glue, liquid, etc.) and furthermore, this attachment is very strong and can hold weights of over 100 kg made scientists mimic the setae and spatulae features and develop a kind of "reversible glue".[4]

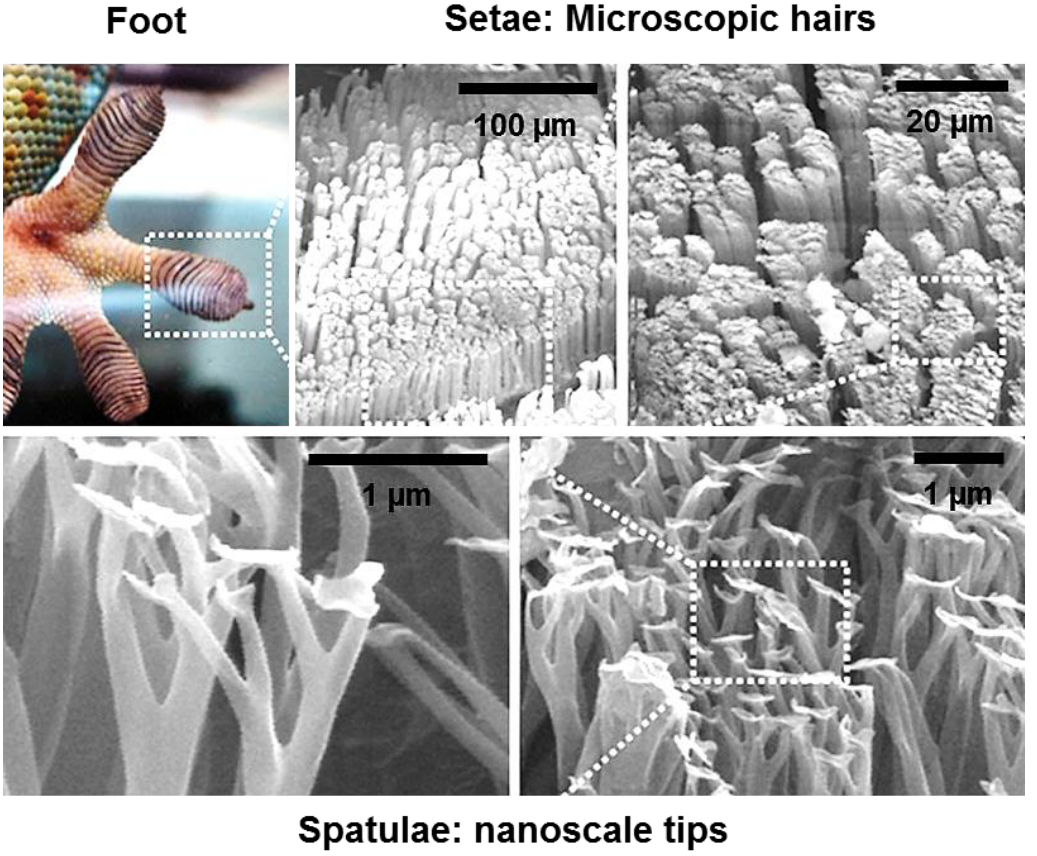

Figure 3: SEM images of the micro and nanofeatures of the gecko foot. Millions of fine microscopic foot hairs (setae) split into hundreds of nanoscale ends (setae). Images were adapted from reference 4.

Surface modification at the micro- and nanoscale

The modification of a surface in general (not only at the micro- and nanoscale) can be distinguished into two different techniques: **structuring** or **patterning** (or a combination of both). Surface structuring involves changes in the topographical features of the surface; examples include the above shown Lotus leave and gecko feet. Surface patterning, on the other hand, consists in a chemical modification of the surface while the topography usually stays the same. Examples are the coating of

kitchenware or clothes with Teflon to render them water-repellent, a similar effect to the one seen for the lotus leaf, obtained with nanostructures. Teflon, by the way, is also used in medicine for transplants, especially as a bypass for arteries. A very recent example for surface coating is the modification of a glass bottle to avoid the ketchup or mayonnaise sticking to the inside of the bottle but rather have them flow out easily.[5] Both techniques are altering the physical and/or chemical properties of the surface.

Origin of Nanotechnology

A very good definition of Nanotechnology was given in 2005: "Nanotechnology is an umbrella term used to define the products and processes at the nano/micro scale that have resulted from the convergence of the physical, chemical, and life sciences".[6]

Two famous individuals who are closely linked with and laid the foundations for the field of nanotechnology are Richard P. Feynman and Gordon E. Moore. In 1959, Feynman gave his famous speech at the Caltech Institute called "plenty of room at the bottom" where he introduced the idea of nano to a broad audience and encouraged scientists to do research in this area by posting rewards.[7] Gordon Moore is one of the founders of Intel and probably best known for the "Moore's law" which he published in an article in 1965, stating that the number of transistors of a computer would increase exponentially and be doubling approximately every two years.[8] Both men can be regarded as visionaries at their time because they revealed that the future trend would be miniaturization towards the nanorange in order to meet the needs of society. And this extreme miniaturization called for new and effective fabrication methods.

Micro- and nanofabrication methods can be divided into two different approaches: top-down and bottom-up

A **top-down** approach will usually start from a bigger piece of material and try to make it smaller by physical or chemical treatment. The most common top-down techniques include: lithographic methods like e-beam lithography, focused ion beam lithography (FIB) and photolithography; molding and embossing methods like Nanoimprint lithography (NIL) and printing methods like the well-known microcontact printing (μCP; this technique is explained in more detail in appendix F)

or ink-jet printing. Those and more techniques are discussed in more detail in a review from the group of Professor Whitesides.[9]

The **bottom-up** approach takes advantage of molecular interactions due to which molecules arrange themselves on a surface in a determined and controllable way. This auto-organization is called self-assembly and can be observed in systems with one or more components. The adsorption of an alkanethiol on gold is one of the most studied self-assembly systems (self-assembled monolayer, SAM).[9] The multi-component systems usually include a mixture of components, ranging from a mixture of alkanethiols with different functional groups over block copolymers to nanoparticles. The beauty of the self-assembly systems lies in the relative facility with which these systems can be custom tailored to yield the desired features.

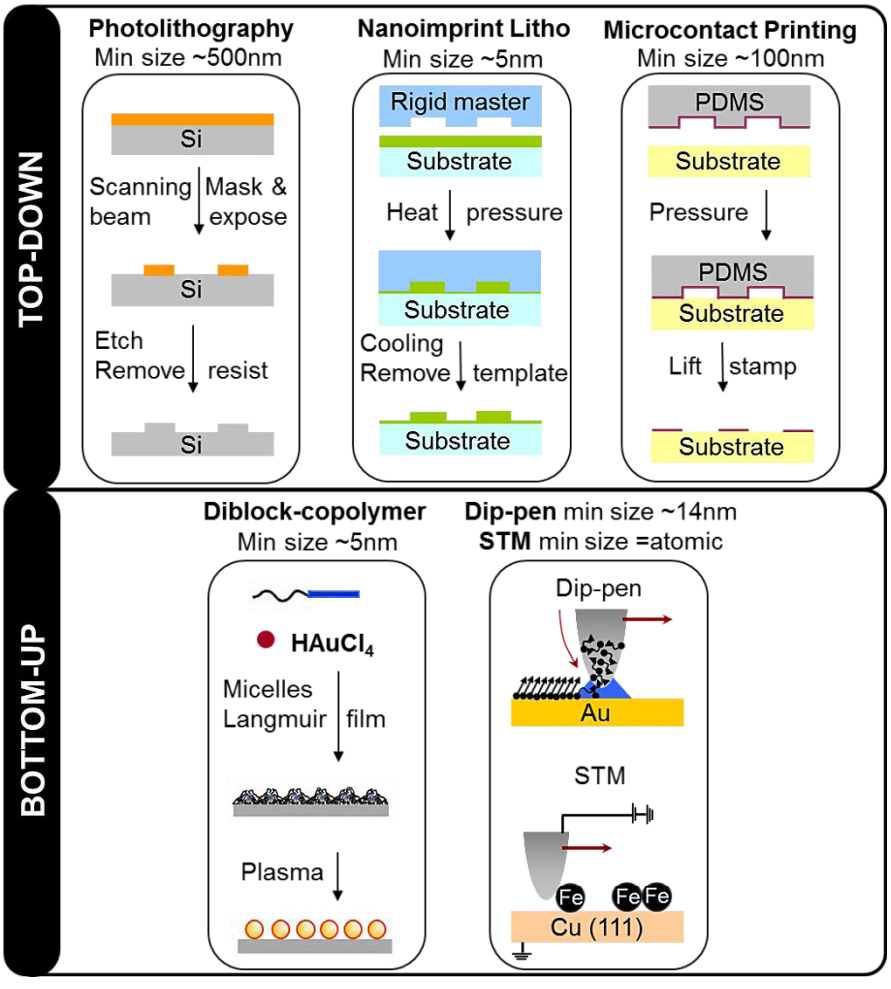

Figure 4: Overview over some top-down and bottom-up methods presented in the text.

Finally, a **combination** of both top-down and bottom-up fabrication methods is applied for template self-assembly, edge lithography and scanning probe lithography (SPL). Latter method contains quite different tools but the common feature is a micro- or nano sized probe which is scanned over a surface. SPL techniques include scanning tunnelling microscopy (STM), atomic force microscopy (AFM) and near-field scanning optical microscopy (NSOM) and even though they are all microscopy techniques (microscopy: from greek mikros = small and skopein = to watch), they can be used both for patterning and for evaluation of said patterning step. Their applications are numerous and range from deposition of single atoms to parallel writing of large molecules. The most versatile technique hereby is AFM since the surface doesn't have to be conductive (like with STM) and the patterning can be done with many different molecules (see appendix A for a more detailed overview of AFM and Chapter 1 for more information about Dip-pen Nanolithography).

Molecular biorecognition

Bottom-up nanofabrication strategies usually take advantage of a mechanism called "molecular biorecognition" when engineering the nanostructures, which is based on strong biological interactions. A well-known and well-studied example is the binding of **streptavidin to biotin**, which exclusively and quite fast bind each other and is one of the strongest non-covalent interactions known in nature.[10] In the presence of a protein-repelling (= passivation) layer, very good recognition results can be achieved by patterning of biotin with the subsequent incubation in a streptavidin solution.[11] Once established on the surface, the biotin-steptavidin pair gives rise to a universal platform for attaching any type of molecule which can be biotinylated. A further and not less interesting biorecognition mechanism is the one of **DNA or oligonucleotides**. It is well known that the hybridization of two complementary oligonucleotides is very selective, fast and stable under adequate conditions. Especially the high selectivity makes oligonucleotides the ideal tool for the construction of multiple analyte platforms, since more than one oligonucleotide sequence can be immobilized on the surface and the hybridization can be carried out in a mixture of all complementary strands, always provided the sufficient difference in the oligonucleotide sequences. On top of that, many molecules, which have a

complementary sequence attached to them, can be anchored on a surface via oligonucleotide hybridization in a more or less stable and non-destructive manner.

The present thesis entitled **"Construction of versatile biomolecule nano-platforms via Dip-pen Nanolithography and their application in bio-sensing and cell differentiation"** aims at contributing to the field of Nanobiotechnology, best defined as miniaturized biotechnology where nanofabrication technology is used for biological purposes. To this end, this research work employs the relatively novel nanofabrication technique called Dip-pen Nanolithography (DPN) for direct patterning of biologically relevant molecules at the micro- and nanoscale, both for biosensor applications and cell differentiation studies. Several covalent immobilization methods for gold and glass surfaces were evaluated for the respective applications in order to ensure highest stability and reproducibility for the lithography process, as well as biological compatibility, especially important for cell experiments. The fabricated substrates were extensively tested for their stability of the covalent immobilization. This thesis is divided into three experimental chapters:

In **Chapter 1,** we aimed at contributing to the development of the Dip-pen Nanolithography technique by solving one of the basic problems when working in constant height mode. The leveling of a 1D multi-pen array with respect to the surface is crucial for two reasons: firstly for a homogeneous patterning outcome. Secondly, especially when working with soft substrates, all tips must exert the same amount of pressure on the surface in order to avoid damaging the substrate. On the other hand, when working with constant force mode and more than one cantilever at the same time (multi-pens), only one of them will give feedback of the force exerted on the substrate. Nevertheless, it would be advantageous to have a force feedback from each cantilever. To address these problems, a piezoelectric device was designed and implemented into the Dip-pen Nanolithography instrument. The results showed that the leveling process can be optimized and the force can be measured at all times (for molecular inks) and thus, the damaging of soft substrates can be avoided. This work was carried out in collaboration with the group of Prof. André Bernard at the Interstaatliche Hochschule für Technik Buchs, Institut für Mikro- und Nanotechnologie (NTB, Switzerland).

In **Chapter 2,** Dip-pen Nanolithography was used to miniaturize an already in-house developed biosensor platform. Therefore, oligonucleotide sequences were immobilized on both gold and glass substrates. For the immobilization on glass, several chemical surface modifications were tested for their suitability concerning covalent attachment and surface characteristics during the lithography process. Surface click chemistry proved to be the best approach because of, both, the surface properties and the stability of the created covalent bond. Minimization of the spot diameter was achieved from ± 200 μm to ± 6 μm and the sensitivity of the obtained sensor array was assessed with fluorescence microscopy. This work was performed in collaboration with the group of Dr. Daniel Maspoch, Centro de Investigación en Nanociencias y Nanotecnología, Esfera Universidad Autonoma de Barcelona (UAB, Spain), and NanoInk Inc. (USA).

In **Chapter 3,** Dip-pen Nanolithography was used for the construction of a versatile substrate for cell experiments and subsequent application in cell differentiation. Therefore, a biotinylated molecule was patterned over a big area on both gold and glass substrates. Subsequently, the obtained substrates were functionalized with streptavidin and biotinylated BMP-2. The successful immobilization of BMP-2 with the simultaneous preservation of its biological activity was assessed by cell culture experiments with C2C12 fibroblast cells. The obtained results are promising, even though having a lower overall cell differentiation percentage, and encourage further studies with this type of surfaces. This work was performed in collaboration with the group of Prof. Fuchs at the Karlsruhe Nano Micro Facility, Karlsruhe Institute of Technology (KIT, Germany), and NanoInk Inc. (USA).

Each chapter is provided with a special introductory section into the respective areas, addressing the current state of the art and the working hypothesis. Following the results and discussion section, the main findings and contribution of each chapter are summarized in the conclusions section. Following the last experimental chapter, there is a section with the **general conclusions** of the achievements of the performed studies.

The thesis ends with an **appendix section,** explaining in more detail the fabrication or characterization methodologies which were employed for the

experiments but were only shortly mentioned in the materials and methods section of the corresponding chapter: Appendix A deals with Atomic Force Microscopy (AFM), appendix B with Scanning Electron Microscopy (SEM), appendix C with X-Ray Photoelectron Spectroscopy (XPS), appendix D with Time-of-Flight Secondary Ion Mass Spectrometry (ToF-SIMS), appendix E with the Nano Plotter™, appendix F with Microcontact Printing (μCP) and appendix G with Western Blot Analysis.

References

[1] Taken from http://www.nobelprize.org/educational/physics/microscopes/discoveries/index.html; accessed in June 2012.

[2] Taken from http://en.wikipedia.org/wiki/Nelumbo_nucifera#cite_note-5; accessed in June 2012.

[3] Z. Guo and W. Liu. *Biomimic from the superhydrophobic plant leaves in nature: Binary structure and unitary structure.* Plant Science 2007. **172**: p. 1103-1112.

[4] H.E. Jeoung and K.Y. Suh. *Nanohairs and nanotubes: Efficient structural elements for gecko-inspired artificial dry adhesives*. Nanotoday 2009. **4 (4)**: p. 335-346.

[5] Taken from http://mit100k.org/bpc/bpc-semi-finalists/liquiglide/; accessed in June 2012.

[6] R. Bawa, S.R. Bawa, S.B. Maebius, T. Flynn and C. Wei. *Protecting new ideas and inventions in nanomedicine with patents*. Nanomedicine: Nanotechnology, biology and Medicine 2005. 1 (2): p. 150-158.

[7] R.P. Feynman. *There's plenty of room at the bottom*. Engineering and Science (California Institute of Technology) 1960. **23 (5)**: p. 22-36.

[8] G.E. Moore. *Cramming more components onto integrated circuits*. Electronics 1965. **38 (8)**. Taken from the website "http://download.intel.com/museum/Moores_Law/Articles-Press_Releases/Gordon_Moore_1965_Article.pdf"; accessed in June 2012.

[9] B.D. Gates, Q. Xu, M. Stewart, D. Tyan, C.G. Willson and G.M. Whitesides. *New Approaches to Nanofabrication: Molding, Printing, and Other Techniques*. Chemical Reviews 2005. **105 (4)**: p. 1171-1196.

[10] E. A. Bayer, M. Wilchek and E. Skutelsky. *Affinity cytochemistry: The localization of lectin and antibody receptors on erythocytes via the avidin-biotin complex.* FEBS Letters 1976. **68**: p. 240-244.

[11] E. Prats-Alfonso, F. Garcia-Martin, N. Bayo, L.F. Cruz, M. Pla-Roca, J. Samitier, A. Errachid and F. Albericio. *Facile solid-phase synthesis of biotinylated alkyl thiols*. Tetrahedron 2006. **62**: p. 6876-6881.

Chapter 1.

Development of cantilevers with integrated piezoresistive sensors for Dip-pen Nanolithography

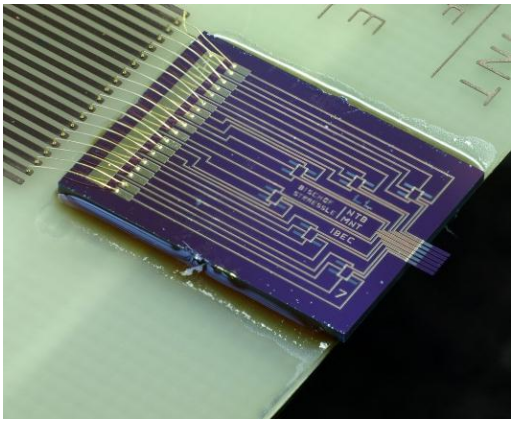

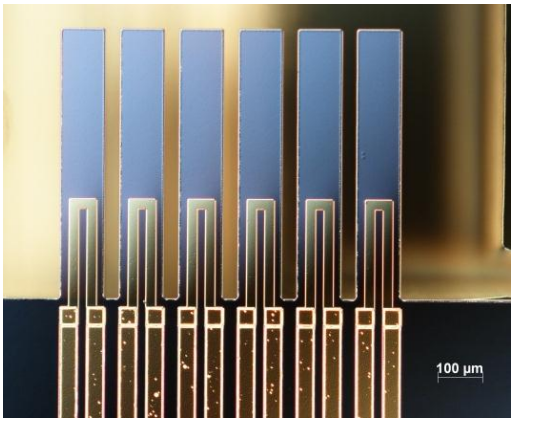

1.1. INTRODUCTION

In the year 1986, Binning and Rohrer were given the Nobel Price in Physics for the invention of the so called scanning tunnelling microscope (STM). This was the beginning of the increasing popularity of the scanning probe microscopes, amongst them the atomic force microscope (AFM). In comparison with other microscopy techniques, AFM has some mayor advantages: atomic resolution, measurements in air (no vacuum is necessary!) and in liquid (especially attractive for biological problems since this is the natural environment of proteins, cells, DNA, etc.) and the possibility of direct manipulation and measurement of inter- and intramolecular forces down to the pico Newton (pN) range.

The set-up of an AFM is shown in Figure 5 (for more information about the AFM technique, see appendix A). It consists of a silicon cantilever (200 x 45 μm^2) which is provided with a sharp silicon tip (curvature radius of 5 – 10 nm), a laser diode and a photodetector. The cantilever tip is scanned over the sample surface while the laser beam is focused onto the back of tip. There it is reflected towards the photodetector. During the scanning process, changes in the sample topography cause the movement of the cantilever and therefore a change in the laser reflection. This is registered by the photodetector and transformed into the resulting topography data.

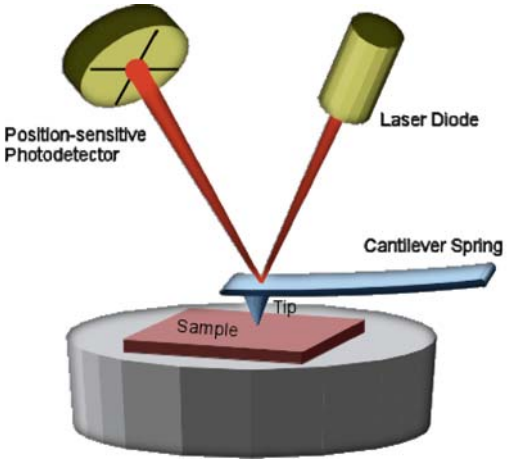

Figure 5: Basic set-up of an atomic force microscope (AFM). Taken from reference 1.

A major problem when operating the AFM in air is the formation of a water meniscus between the tip and the surface (Figure 6), which can alter and even falsify the results. In 1994, Binggeli and Mate published an article about the influence of the ambient humidity on the size of the water meniscus[2], reporting that on hydrophilic surfaces the values of adhesive force and friction are altered due to a large meniscus; on hydrophobic surfaces, only the value of the adhesive force is affected. In 2005, an extensive study of this problem was published by Weeks *et al*.[3]

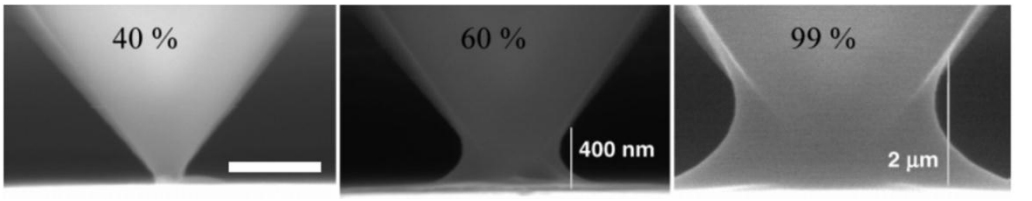

Figure 6: Water meniscus which is automatically formed at different humidities between tip and surface (taken from reference 3). The scale bar equals 1 µm.

In 1995, shortly after the paper of Binggeli and Mate, Jaschke and Butt were the first to report that after scanning a surface with 1-octadecanthiol (ODT), they accidentally deposited these molecules from AFM tips to another surface, suggesting that the tip had been contaminated during the scanning process.[4] What they didn't know at this time was that the water meniscus was the reason for the deposition of ink from a tip to the substrate. Several years later, the group of Chad Mirkin from the Northwestern University in Chicago came up with the idea of taking advantage of the almost inevitable water meniscus in order to intentionally deposit molecules from a "chemically modified" cantilever tip onto a surface.[5] This way, ODT was the first substance to be deposited on purpose with an AFM tip onto a gold substrate.

This was the start of the so called Dip-pen Nanolithography (DPN) which is based on conventional AFM technique. Soon after its invention in 1999, DPN turned out to be a very versatile method for the chemical patterning of surfaces with nano size resolution (smallest linear features 15 nm)[6]. Within only a few years, the number of publications using DPN increased from 4 in 1999 to over hundred just 5 years later (Figure 7, data taken from Isi Web of Knowledge, searching for Dip-pen).

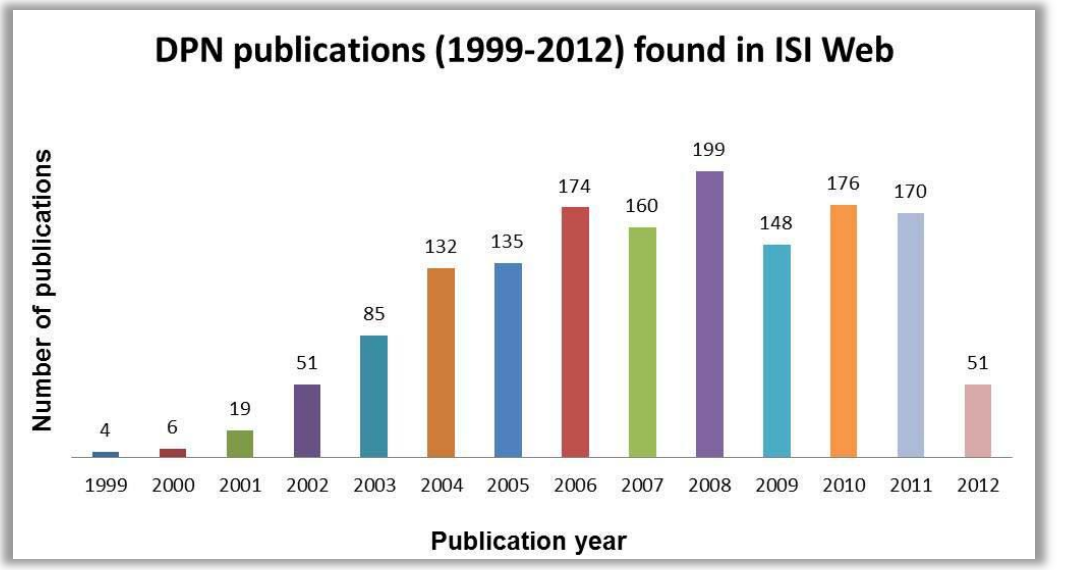

Figure 7: Dip-pen Nanolithography publications 1999-2012 found in ISI Web of Knowledge.

DPN surely would not have been as successful a technique as it is if only one single tip was used for patterning. Nevertheless, so called single pens do exist and are used when a new ink has to be characterized for its deposition properties (like finding optimal temperature, humidity or ink composition). In contrast to the conventional AFM tips, DPN has several different types of so called multi-pen arrays (i.e. chips with multiple cantilevers), allowing for parallelization and thus for faster and larger-scale patterning. While only one tip of the array is monitored as conventional AFM tip (laser controlled feedback), all the other tips of the array will repeat exactly the same in a passive manner.[7]

Addressing the different inks that might be used along with the different types of substrates, there are cantilevers with different shapes and stiffness, as shown in Figure 8a and b). The ultimate approach to parallelization was given by the introduction of the 2D nano print array which contains 55000 identical cantilevers (see Figure 8c for a small section of the 2D array), making it possible to nano-pattern several mm^2 in a short time (throughputs range from 10 mm^2/h to 30000 mm^2/h)[8]. Its only drawback so far lies in the ink, which has to be applied to the 2D array by vapor coating, thus limiting the variety of inks down to only a few. No liquid solvents can be used because a solvent-meniscus would be formed automatically between the

cantilever back and the lower part of the 2D chip (directly above the cantilever end, where they are fixed to) which would lead to all the cantilevers being stuck to the "ceiling" and being worthless for patterning.

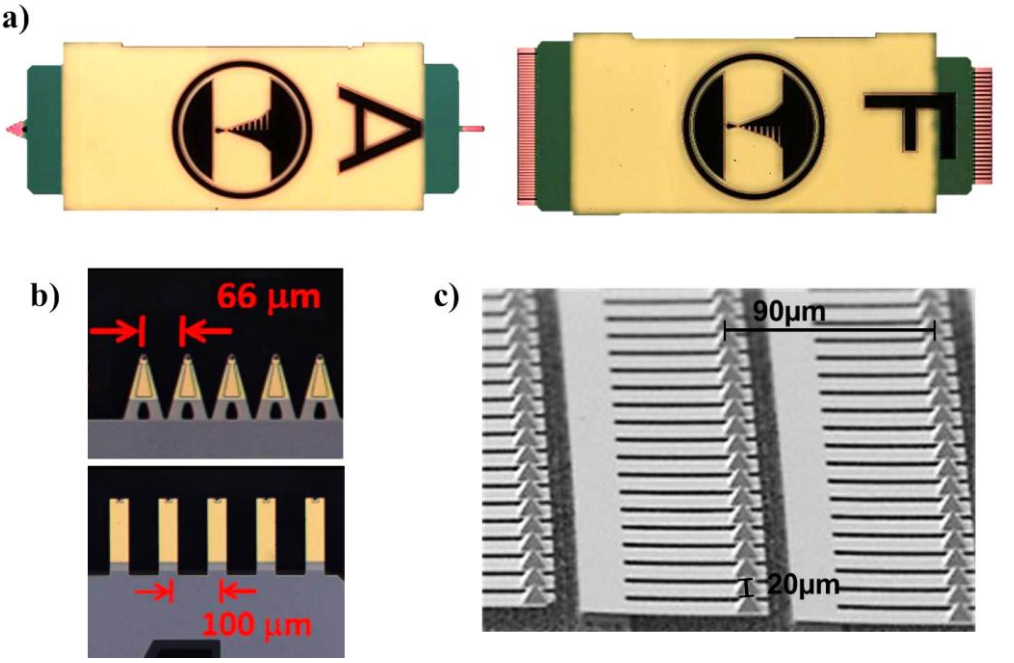

Figure 8: a) A-type single pen and F-type multi-pen (right side 26 and left side 52 cantilever). b) Cantilever shapes: A-frame (above) and diving board (below). c) Detail of the 2D array.

As already mentioned before, the first inks used for DPN consisted basically of alkanethiols in ethanol, which were patterned on gold. Examples are 1-octadecanethiol (ODT)[5,9,10] or 12-mercaptohexadecanol (MHA)[11,12,13], which can be used as a resist for etching[14,15,16] or for anchoring other molecules on the surface.[17] Soon afterwards, the field of applications opened up to inks which can be used on other substrates like glass[18] or silicon[19], which contain nanoparticles[20] or which can be used for fabrication of nanowires.[21,22] Ultimately and quite recently, it was discovered that DPN can also be used to deposit droplets of a liquid. This cleared the way for inks which consist of polymers[23,24,25,26] (a very nice example is the deposition of a PEG polymer with subsequent crosslinking[27]) or which contain biologically sensitive molecules like proteins,[28,29,30] peptides,[31] viruses[32] or DNA,[28] where guaranteeing the integrity and

biological activity is of vital importance. A more detailed description of the different types of inks is given below in section 1.1.1.

The great variety of inks gives rise to a broad field of applications for DPN, as can be seen in Figure 9 (data provided by NanoInk Inc.).

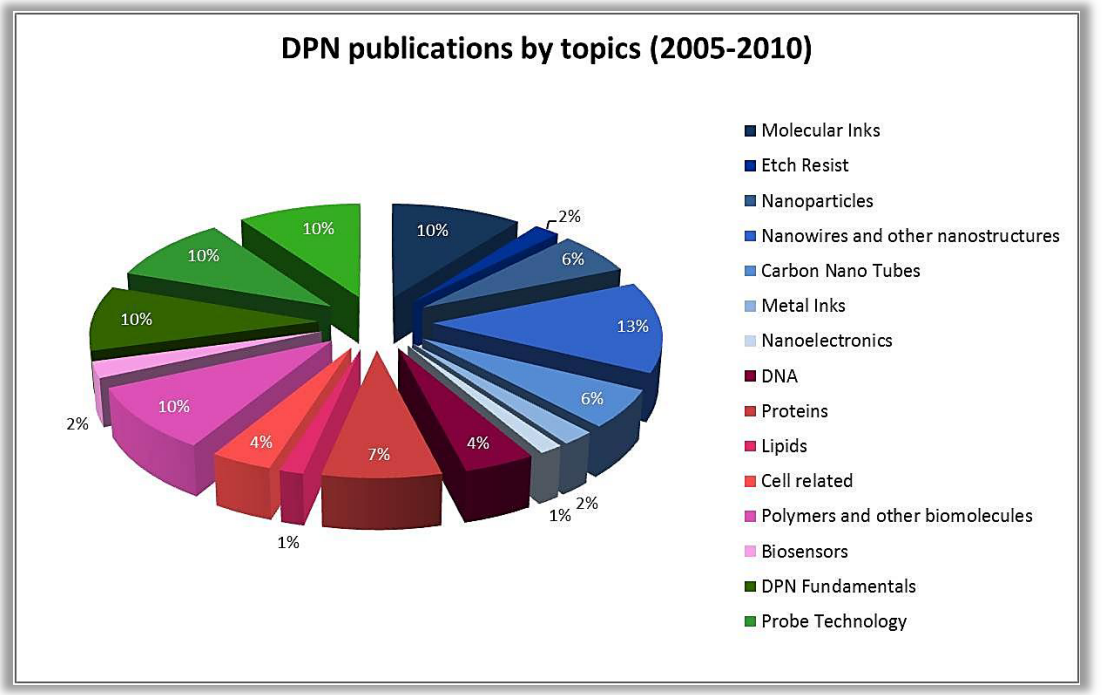

Figure 9: DPN publications sorted by topic (2005-2010). Blue slices represent Nanoengineering, red Biomaterials and green DPN technology, respectively.

The fields of application can be categorized into three main sectors: Nanoengineering (blue slices) which include the fields of nanoelectronics, nanowires, etch resists and templating, and where inks contain for example nanoparticles or carbon nanotubes. A second sector is the one of biomaterials (red slices), where DNA, proteins, viruses or polymers are deposited and the applications include biosensor or cell related research. The third sector (green slices) is related with the DPN process itself like ink delivery or improvement of tips, or even investigation of the deposition mechanism itself. Furthermore, by creating an electric field at the end of the tip and having a current flowing through the tip-sample junction, reduction/oxidation reactions can be induced on a functionalized substrate and these molecules can be

chemically modified.[33,34] To the day, there are more than 1300 publications in very different fields. Obviously, DPN is applicable to a large range of materials but requires careful selection of ink and substrate to ensure a stable formation of the nanopattern on the surface.

An interesting review about the applications of DPN was published in 2007 by Salaita *et al.*[35] Even though there has been a lot of development in the field of applications this review gives some very nice examples.

1.1.1. Inks for DPN – molecular and liquid inks

The quite different types of ink can be distinguished into two classes: the so called molecular inks and the so called liquid inks. Depending on the class of ink, the deposition process is different: the molecular inks are deposited in constant force mode and the liquid inks in constant height mode.

Molecular Inks

Molecular inks are typically composed of small organic molecules which can be coated on the tip either by vapor coating (like ODT[36]) or by dissolving the molecule in an organic solvent like ethanol, acetonitrile[37] or similar. These molecules have to be stable towards drying or denaturing. The cantilever is immersed into the solution containing the molecule (typical solution of MHA in ethanol might be 1-5 mM) and dried prior to deposition. Thereby, the desired molecules are coating the tip of the cantilever and will be delivered from the tip to the surface through a water meniscus (see Figure 10). The deposition rate is determined by the diffusion rate of the ink, which can differ a lot depending on the molecule and for example the interaction ink-surface. The diffusion rate, on the other hand, is highly dependent on the size of the water meniscus, i.e. the ambient humidity, and to a lesser extent also on the temperature. The feature size of dots can be controlled by the dwell-time, meaning the time which the tip remains at the same point on the surface. For writing lines, the tip has to touch the surface and then move in a determined direction with a constant

velocity. The parameter which controls the line width is the writing velocity during lithography.

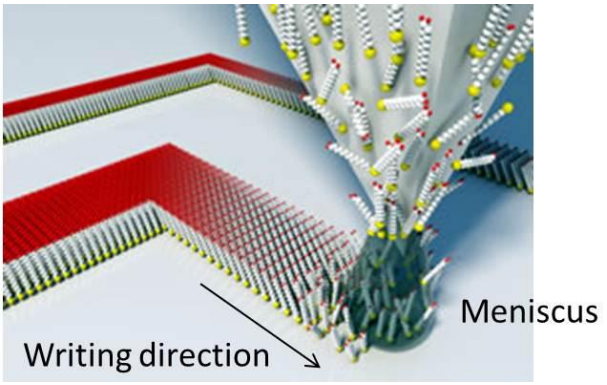

Figure 10: Deposition of a molecular ink through the water meniscus.

The operating AFM mode for molecular inks is the constant force mode (sub-category of contact mode), meaning that one of the tips in the array is constantly controlled by "laser feedback", as well as the force exerted on the substrate, which is kept constant during lithography. (N.B: laser feedback in this case means that the laser is used to control the electronic feedback and z-axis correction by the piezo). This prevents the making of holes on soft substrates like gold. On the other hand, since the tips are in "feedback mode", the patterning can be verified directly after ink deposition. This is thanks to the DPN being a conventional AFM. Without the need of changing the tips or removing the substrate, the patterned area is scanned in contact mode and the pattern can be evaluated by a fast scanning software; the scanning velocity is usually much higher than the writing velocity in order to minimize deposition during scanning: writing ~1Hz, scanning ~5Hz. A very well characterized and easily controllable ink is MHA. Figure 11 shows the calibration of MHA by varying the dwell-time/velocity and also the humidity. As can be seen for the dots (upper part), the calibration curves are more or less linear, also for varying humidity. For a patterning experiment, it is therefore beneficial to work at an elevated humidity and use dwell times as short as possible to decrease the total patterning time. At the lowest dwell time used, it is important to keep in mind that there is a minimum dwell time which cannot be minimized, due to the instrument itself and its response time. This should best be determined for each instrument. On the other hand, as can be seen

for the lines (bottom part) there is a huge difference in the performance of the ink when the humidity is changed. In this case, lower humidities yield not very reliable calibration curves.

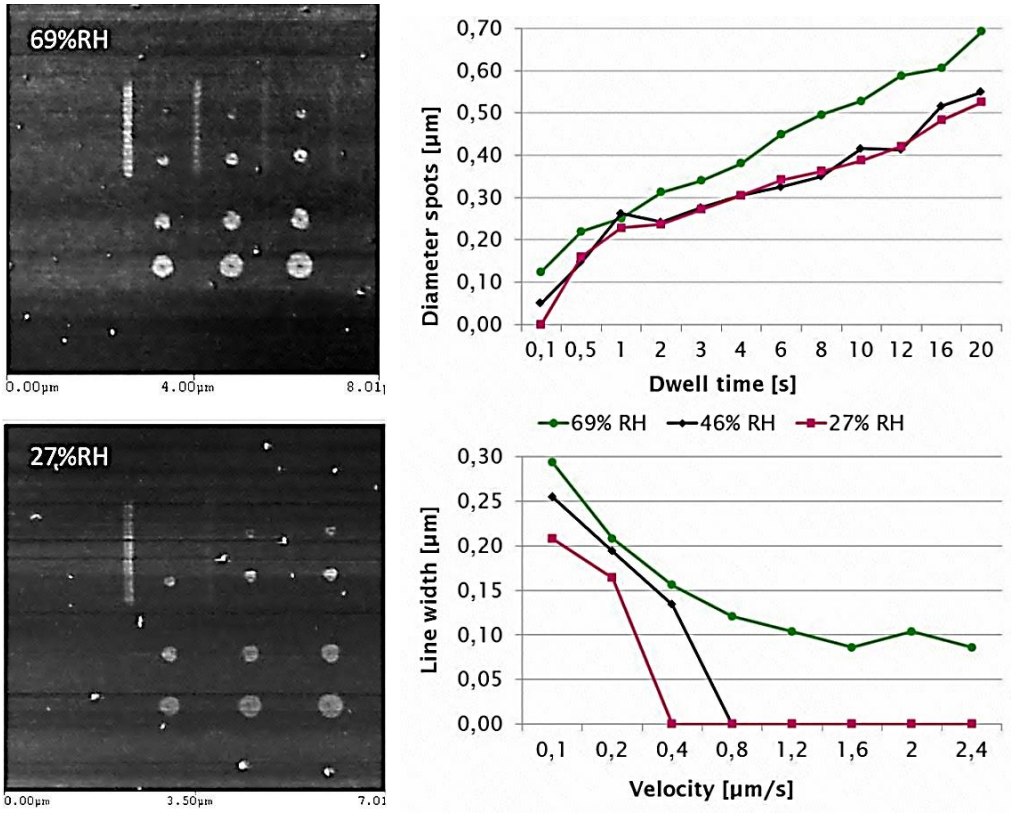

Figure 11: Calibration of a 1mM MHA solution in ethanol. Different dwell times (above) and velocities (below) are determined for 3 different ambient relative humidities (RH).

This calibration process has to be carried out for each ink in order to find the optimal patterning conditions, since these can differ dramatically. Typical examples of molecular inks include alkanethiols on gold or silanes on silicon oxide[38]. The created patterns on the surface can achieve a resolution of 15 - 50 nm and a lateral resolution better than 10 nm.[39]

Especially non-gold surfaces need a prior chemical modification in order to covalently immobilize the molecules to the surface. When working with silicon oxide surfaces, the easiest modification is treatment with piranha acid (1 part H_2O_2 and 3 parts H_2SO_4), leaving hydroxyl-groups (-OH) on the surface which can be reacted

with silanes. Furthermore, the mentioned silanes can have a functional group which in turn can be used to attach another molecule: a silane with a carboxyle group can react with an incoming amine; a silane with an alkyne group can react with an incoming azide – the last example is the so called click chemistry. Recently, surface click chemistry has received increasing interest and the group of Jane Frommer was the first to prove that click chemistry can also be performed with DPN.[40] Click chemistry is explained in more detail in the introduction of Chapter 2, but shortly, it is the name of a chemical reaction which is used to covalently couple two molecules. The term "click" refers to the fast and selective reaction of these two molecules. When used for surfaces, molecules can be stably anchored on these surfaces.

Click chemistry inks are at the interface of both ink types (molecular and liquid inks) and, depending on the molecule to be deposited, can belong to one class or the other. In Chapter 2, DPN click chemistry is used for the miniaturization of a biosensor and results were obtained when a liquid ink was used (no results were obtained on the other hand with a molecular ink). In Chapter 3, DPN click chemistry is used in order to construct a surface for cell differentiation experiments and the ink belongs to the molecular ink type.

Liquid Inks

Liquid inks include any material that is liquid at deposition conditions or any molecule that cannot be dried on the tips. Examples are fluid materials like hydrogels, sol gels or lipids, or simply biomolecules which have to be maintained in a buffered solution in order to prevent their denaturing (proteins, peptides, DNA or viruses).[28,29,30,31,32] The deposition properties of liquid inks differ greatly from the ones of molecular inks and are determined by the interactions of the interfaces of ink - tip, ink - substrate and finally the viscosity of the ink itself. These interactions limit the minimum feature size of the liquid ink to around 500 nm, depending on the contact angle of the liquid. A very sophisticated recent work by O'Connell *et al.* determined the volume of droplets deposited with DPN and they found that the volumes are in the regime of attoliters (aL, 10^{-18} L; compare with volumes of picoliters – 10^{-12} L obtained with ink-jet deposition techniques).[41] In general, higher viscosities offer greater control over feature size and are desirable, as well as a slow evaporation process of the

solvent. This can be achieved by adding for example glycerol to an aqueous buffer solution or by using a so called carrier material (for example lipids).[27,28,42] The dependence of the feature size on the water meniscus and ultimately on the ambient humidity is negligible, what makes it easier to control the lithography process. Furthermore, it is possible to perform multiplexed depositions (depositing different molecules at the same time) by using inkwells (commercially available microfluidic chips), where each cantilever can be incubated separately in a small well or the end of the channel (see Figure 12).[27]

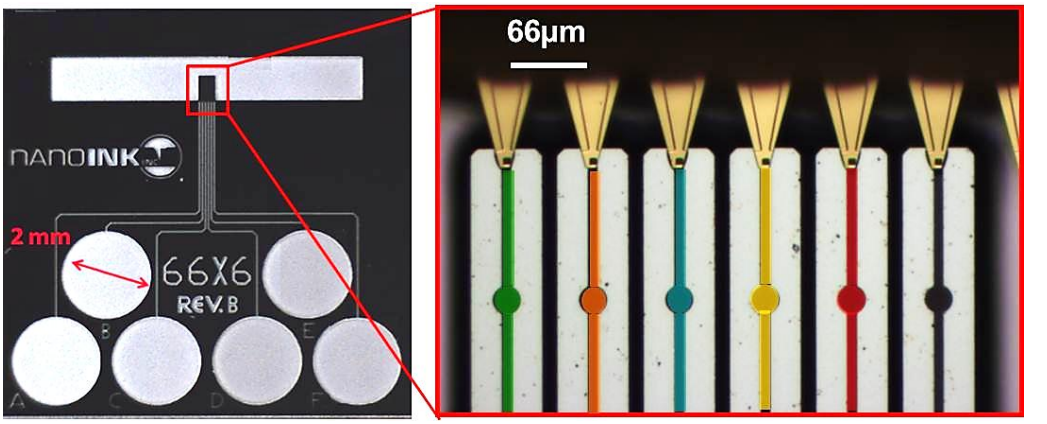

Figure 12: Inkwells (2 mm diameter) and separate channels leading to the inking area (red square). Inset: Tips inking in the channels, which could each contain a different ink indicated by the different colors.

After the incubation of the cantilevers in the ink, they are retracted abruptly to destroy the formed meniscus between liquid and tip and repeatedly brought into contact with the surface to reduce the size of the ink drop which covers the tip (so called bleeding dots) until the resulting dot is suitable for the writing of a small but homogeneous pattern. Since the deposited drops are usually quite big at the beginning of the writing process (micrometer range), they can be detected by the equipment's built in optical microscope. The operating mode for liquid inks is the constant height mode, which is, similar to constant force mode, a sub-category of AFM contact mode. It is not possible to use feedback controlled lithography because the ink usually spreads onto the back of the cantilever where the laser is reflected towards the photodiode, which leads to an uncontrollable deflection of the laser through the ink drops: no stable signal can be obtained from the photodiode. Therefore, the tips have

to be brought into contact with the surface manually. When a tip touches the surface, the cantilever back bends and "changes its color" due to the change in the deflection of light from the cantilever back (this can be detected with the built-in microscope, see Figure 13).

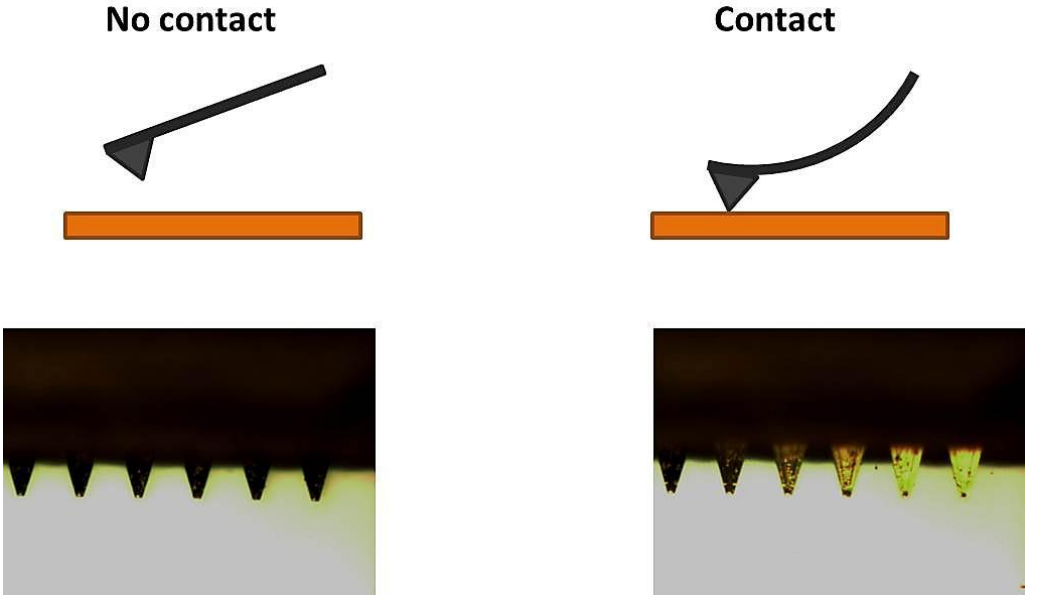

Figure 13: Cantilevers over a surface: not touching (left side) and touching (right side). When the cantilevers touch the surface their back bends. This results in a change in the deflection of light from the cantilever back which can be perceived as color change.

This manual approach will only cause problems when working with soft substrates like polymers or gold and cantilevers with a relatively high spring constant (0.6 N/m, compared to "soft" tips with 0.03 – 0.05 N/m). In this case, due to the cantilever being stiffer than the substrate, when it changes its color indicating that it is touching, the exerted force is already too much and the tips can damage the substrate (making holes in the case of gold or tearing the polymer). On the other hand, when using a liquid ink and a cantilever with a spring constant that is too small, the meniscus, which builds up between tip and surface, might influence the patterning in a negative way because the cantilever bends too easily. Also, the shape of the cantilevers influences the ink deposition characteristic and using a different shape might result in decreased ink flow.

Since liquid inks work without laser feedback, it is not necessary to use a conventional AFM for patterning, even more since the scanner range is usually limited to around 90 x 90 μm^2 (this is how far the piezo elements can extend, without using the motors). This area is quite small when the pattern is designed for biological applications especially when cell experiments are considered. In order to be able to pattern bigger areas, the tips need to be displaced manually to a new 90 x 90 μm^2 area, where the patterning can be continued. This displacement involves using the motors, what inevitably goes along with an offset displacement of some micrometers (intrinsic to the motor movement; when the AFM is used only for scanning the surface, a much lower precision of alignment of the tip and the pattern is needed). Therefore, the patterning with liquid inks over a large distance can be performed in an easier way by using a DPN which is not based on a conventional AFM but uses the same tips.

1.1.2. Instruments for DPN

As already mentioned before, there are two different types of ink which need a different way of operating the instrument: With a molecular ink, the instrument can be used with laser control (in feedback), whereas on the other hand, a liquid ink needs manual control over the cantilevers since the ink interferes with the laser and no signal can be obtained. The first commercially available DPN instrument is the so called **NScriptor** (NanoInk Inc., US), consisting of a conventional AFM with a specially designed software in order to simplify the design of the pattern. Since it was known that molecular inks change their deposition properties depending on the humidity, an ambient control chamber was included, in order to control and adjust humidity and temperature during the patterning procedure (see Figure 14).

Patterning is done by bringing the tips in a determined height over the substrate, which stays constant during the whole lithography process. For creating the pattern, the piezos, which bring the tip towards the surface, extend to maximum (12 μm) and retract afterwards; in the case of a dot, the tip does not move and in the case of a line, the tip touches, moves and retract. This extension-retraction is always the same and given by the maximum extension of the piezos. Therefore, for not damaging a soft

substrate, when the patterning height is determined, the tips have to touch only very lightly when the piezo is fully extended. With this instrument, the substrate does not move, only the tips move over the surface, whereas the piezos have a range of 90 x 90 μm^2 and beyond this range, the motors have to be used to move the tips.

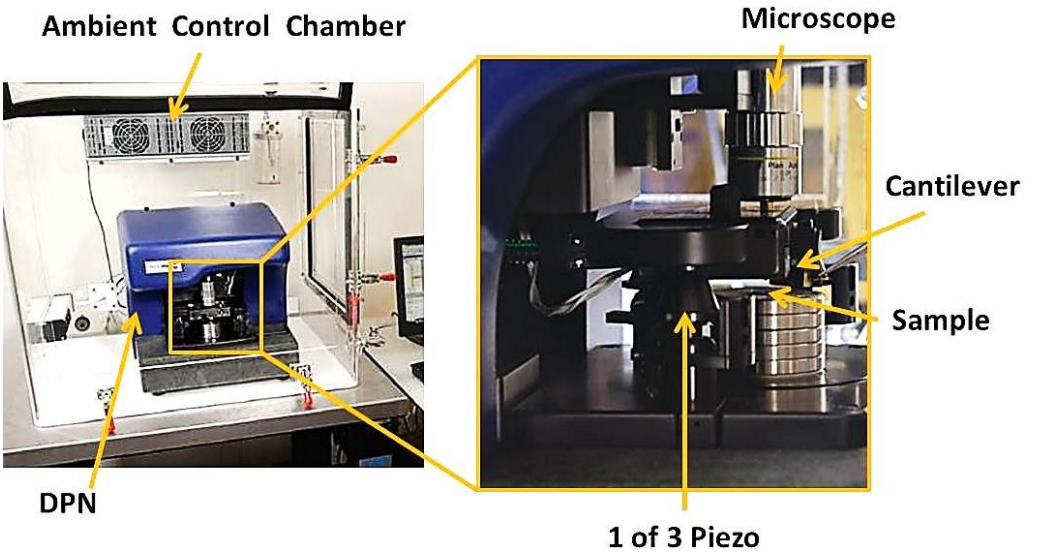

Figure 14: Set-up of the NScriptor DPN instrument (NanoInk Inc., US). Inset: close-up with sample puck.

The AFM based DPN meets its limits when a larger area of pattern is needed or when the patterning process is to be automatized. Therefore, quite recently, a different DPN instrument has been introduced by the same company, which does not rely on the AFM technique. This so called **NLP2000**, see Figure 15, doesn't use the laser to control the cantilevers and is mainly intended for the use of liquid inks and biological applications. It has an increased travel range (several cm) and due to that also includes a plane leveling feature: over the length of a bigger substrate there can be variations of several micrometers in height due to uneven placement of the substrate. Furthermore, it allows for automation of the patterning meaning that large patterns can be previously programmed, and even re-inking of the tips can be included and does not have to be done manually. In contrast to the NScriptor, the cantilever stay in place during patterning and the substrate moves, controlled by three encoded piezo-driven stages and two encoded goniometer stages.[43] The great advantage here lies in the possibility to adjust the retraction of the substrate during lithography, whereas for the

NScriptor the maximum distance is 12 µm. This is a very crucial point when working with liquid inks: Due to the liquid consistence of the ink, a meniscus will form spontaneously when the ink comes into contact with the surface. This meniscus has to be broken in order to avoid smearing of the pattern when the tip changes locations. A retraction distance of 12 µm (NScriptor) might not always be sufficient, whereas 30 µm would be. The continuous adjustment of the retraction distance is therefore of great value for liquid inks. The probably only drawback is that the touching force of the tips has to be controlled by eye (since there is no laser in the instrument).

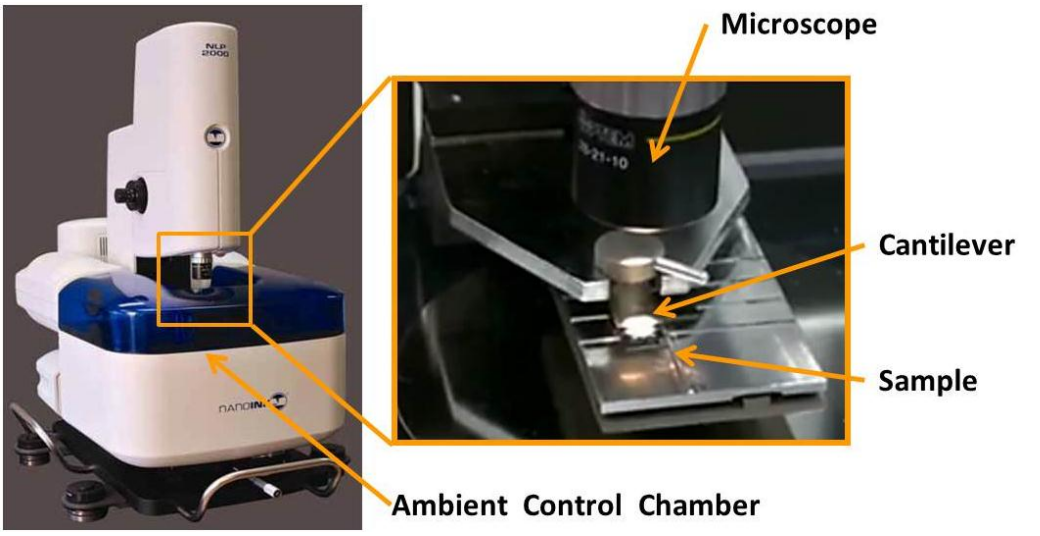

Figure 15: Set-up of the NLP2000 (NanoInk Inc., US). Inset: close-up with sample stage and tip holder.

1.1.3. Working with multi-pen arrays

Whenever using a multi-pen array, tip leveling is a crucial factor and has to be performed for both instruments (NScriptor and NLP2000) and for both lithography types (with and without "laser feedback"). Up to now, there is no automated leveling routine for the multi-pen arrays and this process has to be done more or less manually and by eye/microscope camera. In the case of laser feedback controlled lithography, the leveling has to be done before patterning and, even though the lithography process is controlled by laser, the tips have to be leveled by eye because the laser cannot be split up to read out two tips at the same time. The laser in fact is aligned on the back of

one cantilever of choice which then serves for all other cantilevers in the array as well. In the case of lithography completely without laser feedback, where the whole lithography is controlled by eye, the leveling has to be done before inking the tips in the liquid ink and the force exerted on the surface has to be controlled by eye during the whole lithography.

Tip leveling is so important in both cases because only perfectly leveled tips with respect to the surface will be able to perform homogeneously during lithography, because the touching force of all the tips is the same. Not perfectly leveled tips will cause inhomogeneous patterning, even when the leveling is only slightly off. When there is a huge offset in the leveling, one side of the array may be patterning, while the other side may be making holes in the substrate (see Figure 16).

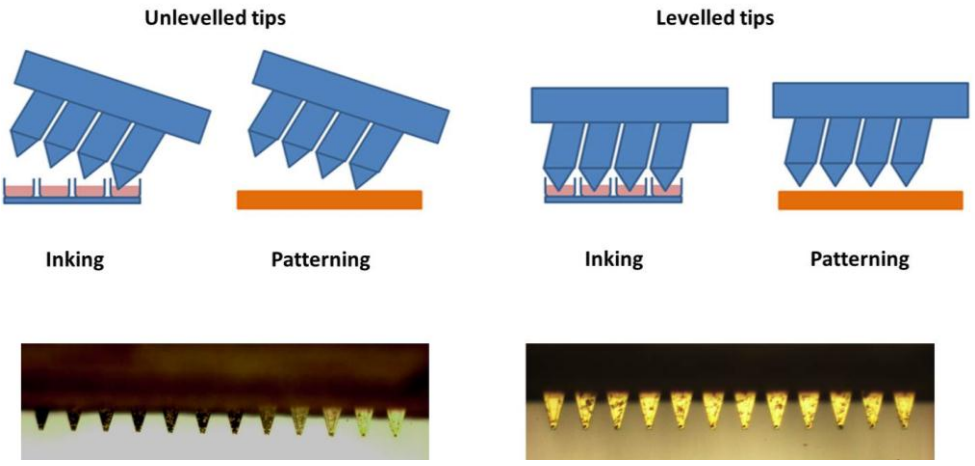

Figure 16: The leveling of the tips is crucial for lithography.

As already mentioned before, tip leveling is performed by relying only on the optics of the instrument (microscope and computer screen) and the own eye. Up to now, there is no automated solution or even an assisted leveling option. The work developed in this chapter aimed at addressing this general problem when working with multi tip arrays. In a first attempt, some manual improvements were implemented into the leveling routine. These included zoom-in leveling assisted by an excel-sheet for the calculation of the offset angle and also a manual 3 point plane leveling. But these improvements still relied on the optics and the eye. Therefore, an optics-independent solution was pursued. Thanks to a collaboration that carried out the clean room

fabrication part and followed the instructions in order to meet the needs for assisted leveling, we developed a piezoelectric device and applied it with the DPN instrument. Thanks to this new device, it is not only possible to have an almost perfect array leveling but, and this can be very handy, it is possible to read out and control the pressure exerted on the surface of each tip of the array.

1.2. EXPERIMENTAL SECTION

1.2.1. Multi-pen tip leveling on the NScriptor instrument

The leveling of the tips is done by eye and for the whole array of tips; the 1-D cantilever array (M-type, NanoInk Inc., USA) contains 12 Si_3N_4 tips which are all visible at the same time. For leveling, the tips are brought into close proximity with the surface, without touching it. Then, slowly, the tips are approached in steps of 2 µm until they change their color, what means that the cantilever backs bend and the deflection of the light changes, see Figure 17. The degree of color change indicates if the tips are touching with the same force. If the outermost tips seem to have the same color, the array can be considered leveled. If this is not the case, the leveling has to be corrected manually. Therefore, the inclination of the array is corrected in small steps, until the tips are all touching equally.

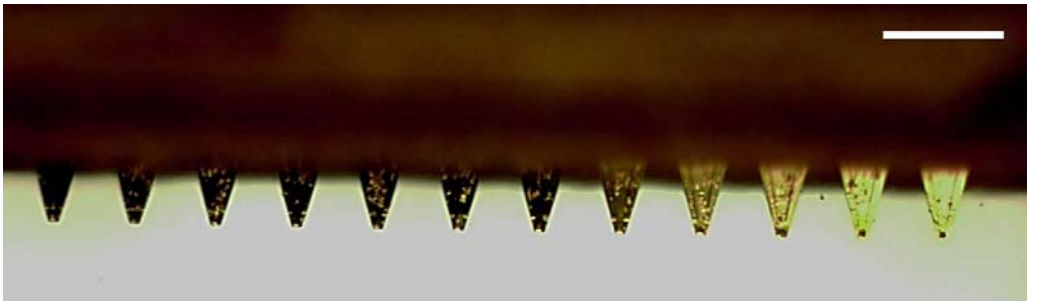

Figure 17: Gradual change in the deflection (seen as color change) due to the bending of the cantilever when they touch the surface and exert more force onto it (force increases from left to right). The scale bar equals 100 µm.

Patterning of a liquid ink with a 1-D cantilever array containing 12 Si_3N_4 tips (M-type) was performed on gold. For lithography, the tips have to be brought into "patterning height" by eye and this height is not changed during the whole lithography (constant height mode). This might cause a heterogeneous patterning outcome if the substrate is not 100% flat (tilted over x-axis, see section 1.2.3. and Figure 18) and the tips have a different distance from the substrate at the beginning of the pattern and the end.

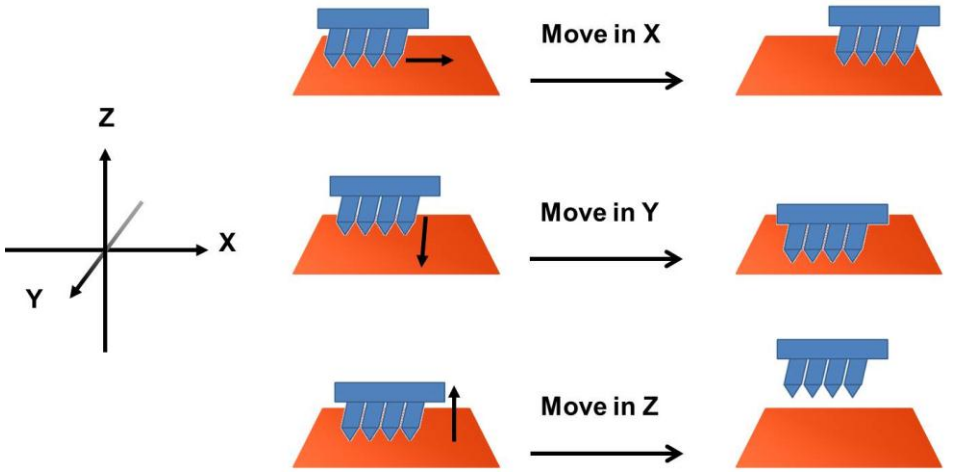

Figure 18: Motion axes in the DPN instruments and corresponding movements of the tips.

For the improved leveling process, changes can be made in two different "axes": leveling of the cantilever array with respect to the x-axis so that the extreme left and extreme right tips touch at the same time (section 1.2.2). The second option is the leveling of the cantilever array with respect to the y-axis so that the tips touch with the same force at the front of the substrate and the back of the substrate (in the y-axis, section 1.2.3). This is especially important for larger substrates since there can be a significant difference in height due to dust particles or the sticky tape. The y-axis leveling has to be performed after the x-axis leveling.

So to sum up, there are two possible causes of inhomogeneity during lithography: inhomogeneity in x coming from insufficient "tip-leveling" and inhomogeneity in y coming from insufficient "surface-leveling".

1.2.2. Manually improved array leveling (x-axis)

In order to improve the leveling accuracy, the procedure was performed with maximum zoom, where only 3 tips are visible at the same time instead of the whole array of 12 tips. Adapting a procedure from the instrument NLP2000, an excel sheet with the data for all relevant tips was created. The correction angle α was calculated with Equation 1 following the geometric set-up shown in Figure 19.

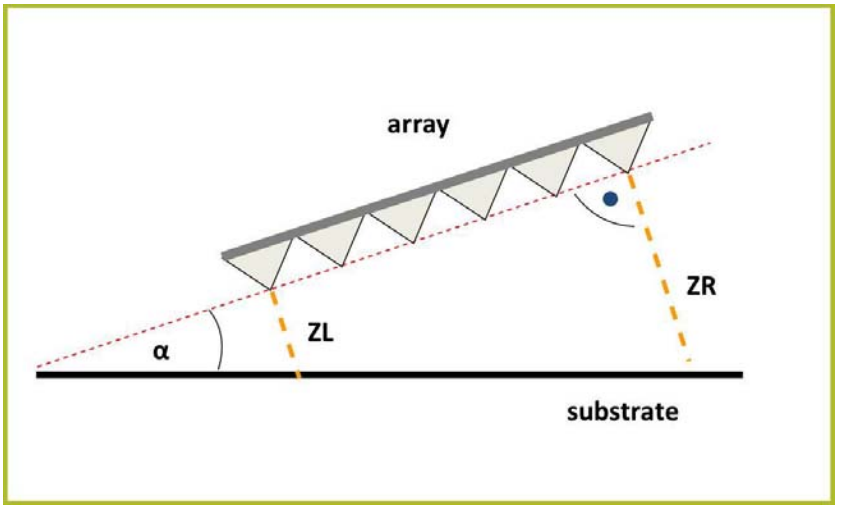

Figure 19: Determining the angle for tip leveling at maximum zoom.

Equation 1: $\alpha = \arctan((ZL-ZR)/\Delta(LR))$

Where ZL = the height in Z when the left tip touches the surface; ZR= the height in Z where the right tip touches the surface and Δ(LR) = the distance between the left and the right tip, calculated from the chip parameters. The heights in Z are given by the software and have to be entered into the excel database to yield the angle. Table 1 is taken from the excel sheet and is an example for the 1-D cantilever array containing 12 tips (M-type). The values for ZL and ZR are read out from the instrument and are entered into the chart to obtain the angle. Here, the values for ZL and ZR in italics are example values, as well as the obtained value for the angle.

Table 1: Example for calculating the angle for 1-D cantilever array with 12 tips (M-type).

No. tips	d(tip-tip) µm	Δ(LR) µm	Tip type	Distance ZL (µm)	Distance ZR (µm)	Angle α
12	66	726	M	*5978.38*	*5974.18*	*0.33°*

1.2.3. Plane leveling of the substrate (y-axis)

In order to further improve the patterning and avoid the inhomogeneity between front and back of the substrate (with respect to the y-axis), a plane leveling of the substrate was included. Therefore, 2 points in Y-direction were determined on the surface (the front and the back of the substrate) and the height difference is calculated in order to determine the correction factor. Then, for each motor movement in Y-direction, the correction in the Z height was applied.

The SEM images shown in the results section 1.3.2 were obtained by patterning of an oligonucleotide on gold. Therefore, the oligonucleotide „20down“ (see Chapter 2 for the oligonucleotide sequences) was diluted in PBS (Sigma Aldrich, Spain) and passed through a NAP^{TM}-10 column (GE Healthcare, USA) to yield a final concentration of 0.05 mM. Subsequently, 10 µl of glycerol (Sigma Aldrich, Spain) were added to 90 µl of oligo solution, mixed well and transferred into an inkwell (M-type; NanoInk Inc., USA). A 1D cantilever array with 12 tips (M-type) was incubated in the ink in the corresponding ink wells for 10 min at RT. The pattern consisted of an array of 14 x 14 dots with a distance of 2 µm and a dwell time of 0.8 s. After lithography, the sample was examined in a Nova NanoSEM 230-FEI (FEI Company, The Netherlands) with an inclination of 52.0° in order to better determine whether the features were holes or deposited material.

1.2.4. Multi-pen tip leveling by new piezoresistive tips

A description of the custom fabricated piezoresistive device along with a photo is given in section 1.3.2. In order to check the performance of the piezoresistive device in the NScriptor, the tips were functionalized with streptavidin-Texas Red (SAV-TR; Cultek, Spain), and mercaptohexadecanoic acid (MHA; Aldrich, Spain) in a second experiment. The pattern was created in both cases on a gold surface.

The gold substrates were rinsed with THF (Sigma Aldrich, Spain), acetone (Aldrich, Spain), ethanol (Panreac, Spain) and MilliQ water and subsequently incubated in piranha acid for 30 min. After rinsing the samples with copious amounts

of MilliQ water, they were dried under a nitrogen stream. For the pattern with SAV-TR, the gold was incubated overnight in a solution of 1 mM biotin-thiol (from the collaboration with Prof. Albericio, IRB Barcelona, Spain) in ethanol, subsequently rinsed with ethanol and dried under a nitrogen stream. The ink was SAV-TR (0.1 mg/mL in PBS) with 2% glycerol. The tips were incubated in the ink during 10 min at room temperature and a relative humidity (RH) of 52%. The tips were then brought into contact with the surface to deposit droplets of ink. After a dwell time of 1 s on the surface, the tip was lifted up manually y motors around 30 μm and moved in Y-direction 50 μm. Another drop of ink was deposited then and so on. The substrate was incubated overnight in a humid atmosphere. The patterned area was visualized with fluorescence microscopy using an Eclipse E1000 upright microscope (Nikon, Netherlands) equipped with a charge-coupled-device (CCD) camera and working with a green excitation G-2A long-pass emission filter. Pictures were processed with freeware image analysis software ImageJ (NIH, http://rsb.info.nih.gov/ij/).

For the pattern with MHA, the cantilever were cleaned with PBS, PBS with 0.1% of Triton-X (a detergent; Sigma Aldrich, Spain), MilliQ water and ethanol and dried gently under a nitrogen stream. Subsequently they were activated in an ozone cleaner (UV/Ozone Pro Cleaner^{TM} from BioForce Nanosciences, United States) for 10 min and directly afterwards incubated in a 1 mM solution of MHA in ethanol for 5 min. Then, they were dipped into ethanol and incubated again in the MHA solution. This procedure was repeated two more times. Finally, the cantilevers were dried gently under a nitrogen stream and mounted into the NScriptor. The patterning was performed a RH of 42% and a temperature of around 21.5ºC. Dwell times ranged from 6 – 50 s and 0.7 x 0.7 μm^2 squares were written at a scanning rate of 0.5 Hz.

After lithography, the samples were incubated overnight and subsequently subjected to wet etching in order to remove the gold where no MHA was deposited (the etching procedure was chosen for the visualization of the pattern because AFM tapping mode turned out to destroy the patterned area by dispersing the MHA on the surface by the tip movement). Therefore, a solution of 20 mM iron nitrate ($Fe_2(NO_3)_3$ x 9 H_2O; Panreac, Spain) and 30 mM thiourea (Panreac, Spain) in MilliQ was prepared freshly before the etching process. The substrate was immersed completely

into the solution and, under stirring at room temperature, was left there for 7 min until the gold without MHA was etched away and only the protected areas were still visible. The sample was then rinsed with MilliQ water, dried under a nitrogen stream and examined with contrast microscopy, using an Eclipse E1000 upright microscope (Nikon, Netherlands) equipped with a charge-coupled-device (CCD) camera and working with a phase contrast filter set. Pictures were processed with freeware image analysis software ImageJ (NIH, http://rsb.info.nih.gov/ij/).

For the second experiment, several inclinations were tested in order to find the correct one, where only the tips are touching. Figure 20 shows the schematic set-up of the DPN instrument with the 3 motors attached to the scanner base which are used to control the Z-height of the tip over the substrate (*Remark: 0 would be completely retracted and the higher the value, the more the motor is down to the substrate*). By changing this Z-height, it is possible to change the inclination of the scanner base. In this case, motors 2 and 3 were kept constant, only motor 1 was used to move the tips upwards as indicated by the red arrow. By doing so, instead of having scenario a (red inset), at the end of the experiment, scenario c, where only the tips are touching. The Z-height of the motor was changed in steps of 200 µm with subsequent lithography in order to test lithography. The values tested in lithography are given in Table 2.

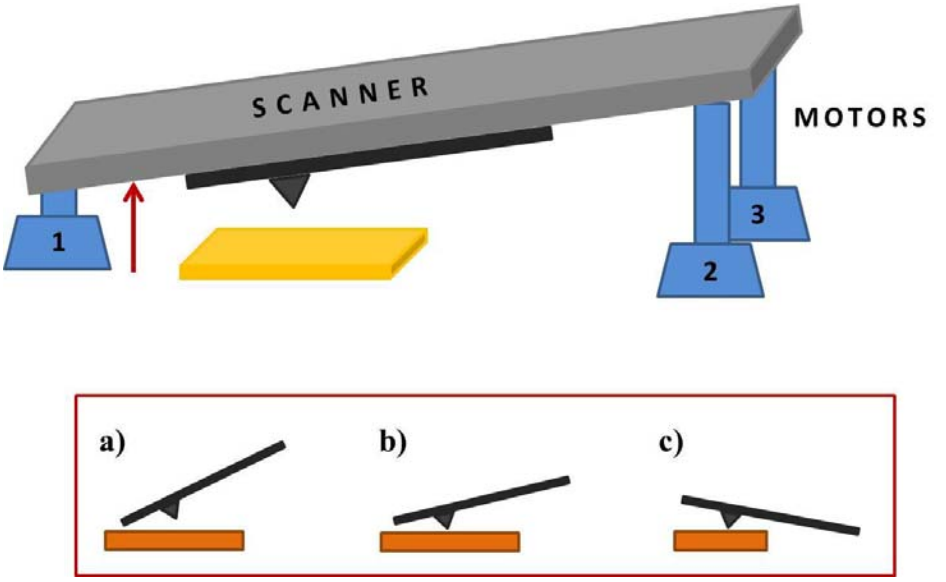

Figure 20: Schematic set-up of the DPN instrument with the cantilever in black, the substrate in golden, the scanner base in grey and the 3 motors for controlling the Z-height in blue.

Table 2: Different inclinations tested for lithography in order to overcome the inclination problem. Only motor 1 was used and the position of the tips was changed in steps of 200 µm.

Total change in Z-position	Z-position (µm) motor 1	Z-position (µm) motor 2	Z-position (µm) motor 3
Start	6542,65	5201.28	7564.16
200 µm up	6342.96	5201.28	7564.16
400 µm up	6143,27	5201.28	7564.16
600 µm up	5943,90	5201.28	7564.16
800 µm up	5744,22	5201.28	7564.16
1000 µm up	5544,53	5201.28	7564.16

1.3. RESULTS AND DISCUSSION

1.3.1. Manually improved multi-pen array leveling

The leveling of the tips has to be done by eye, meaning in a qualitative manner. Up to now, there is no device for automated or even assisted leveling and the whole process relies on the video equipment of the instrument and the user's eye. Nevertheless, in order to improve the leveling of the tips, a procedure was adapted from the NLP2000 instrument, which is part of the routine leveling implemented in the software. By determining the distance of the two outermost tips to the surface, the leveling angle was determined.

The higher accuracy was achieved by using maximum zoom, which allows the earlier detection of the cantilever deflection when touching the surface. An improvement of 0.08° for the leveling was obtained (measured for M-type tips), meaning the tips are "more leveled" in respect to before. A difference in 0.1° over the whole array corresponds to a height difference 1.4 μm for the two outside tips and can already lead to the making of holes on one side of the cantilever array.

Leveling is, as already mentioned, very important for the homogeneity of the pattern created by the different tips. Despite the improvement with the zoom-in, this method has its limits, for example in the microscopy optics. On the other hand, when a soft substrate such as gold or polymer is used, the high spring constant of the tips for liquid inks are the main cause of damaging the substrate. The tips will make holes in the substrate before the cantilever back is bending and the deflection can be detected. Therefore, the combination of stiff cantilevers and optical detection method of the touching will always give rise to problems when working with soft substrates. In order to overcome this issue, a different detection method is needed (see section 1.3.3.).

1.3.2. Plane leveling of the substrate

In practice, a substrate is never 100% flat on the sample holder, normally due to dust particles underneath the substrate or simply due to the adhesive pad with which the sample is mounted on the sample holder to avoid movement during lithography. While working with laser feedback, this unevenness will cause no problem because the Z-height will be automatically corrected. This is the so called constant force mode, meaning, that during lithography, the force exerted on the substrate never changes. In the case of constant height mode, where the cantilevers are brought to a desired height over the substrate, this height never changes, especially when working without laser feedback. This means that when the surface is uneven, no automatic regulation of the Z-height will be done. If the substrate comes closer to the tips (only a few µm is already sufficient), this might cause indentation instead of pure ink deposition.

Therefore, a manual plane leveling was included into the leveling procedure. Before lithography, the substrate is measured for the Z-height in the front and in the back and a correction factor for the desired shift in y-direction can be calculated, thus avoiding indentation into soft substrates or changing the force during patterning which can alter the deposition properties.

For example: the distance between the two measured spots is 3000 µm (in the front and in the back) and the difference in Z is 17.55 µm, then there has to be a Z-correction of 0.24 µm for every movement of 50 µm in y-direction. This may seem insignificantly small but when the pattern stretches over 500 µm in y-direction, this is already 2.4 µm, which means that either the tips might be touching too much and be creating holes or might have lost contact and stopped patterning at all.

Figure 21 shows an extreme example of what can happen, when the plane leveling is not performed before lithography. The white arrows indicate patterning direction. The white square in a) is an outline of the whole array which consists of 14 x 14 dots with a spacing of 2 µm, all written by the same tip. As can be seen both in a) as in the enlarged section in b), the substrate was tilted because the tips exerted more force at the beginning of the lithography than at the end. This is evident because of the large holes at the beginning and almost no holes at the end.

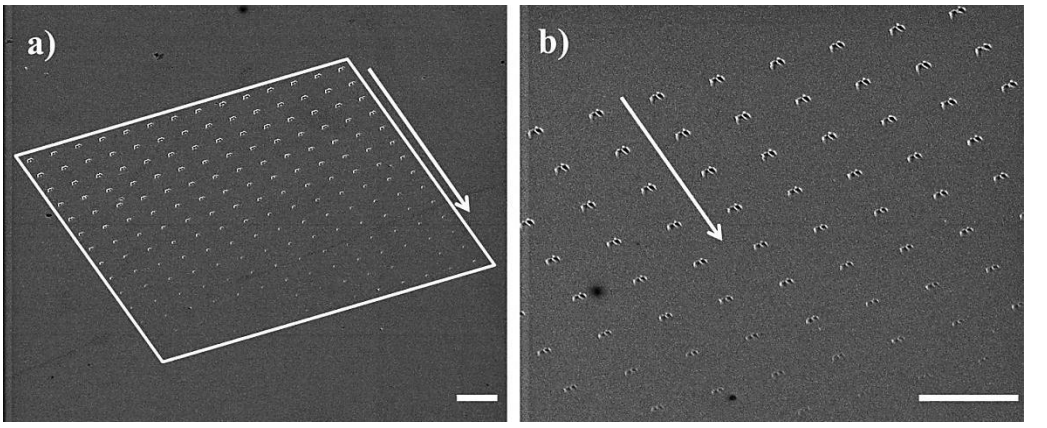

Figure 21: SEM image of a pattern on gold. The arrows indicate the patterning direction. The white square in a) indicates the outline of the whole pattern (14 x 14 dots). b) shows an enlarged section and reveals the big difference in the touching force of the tip at the beginning and at the end of the pattern. Scale bars equal 3 µm.

After implementing the plane leveling correction, inhomogeneous arrays in y-direction could be avoided. That means that either all the arrays in y-direction had holes, or no holes at all were made (for this ideal case see Chapter 2.2.3). Even though possible inhomogeneities could be eliminated by improved leveling procedure, there is still the problem that the tips might be touching the substrate with too much force and create holes during lithography (on soft substrates). This is because the whole leveling process (both in x- and y-direction) relies on optics (microscope and user's eye) and only qualitative information is obtained.

1.3.3. Multi-pen tip leveling by new piezoresistive tips

In order to improve the leveling procedure and also have more control over the touching force before and during lithography, a piezoresistive device was custom-fabricated for implementation into the DPN instrument (the NScriptor). The tips in this device have a resistor included in the back of the cantilever (see Figure 22) which changes under mechanical tension. This means that when the tips come into contact with the substrate, they bend and their resistance changes, what can be measured. After adjusting the prototype and improving the measuring sensitivity, the device was

fully functional. Figure 23 shows the whole device with the wire-connections for signal transmission to the readout software.

The sensitivity of the device was tested by bringing the tips close to the surface in order to establish contact. When the tips were brought into contact with the device and the included software, the touching point could be determined sooner than when using the eye: the difference was significant with 18 µm less! This means that it is less likely to make indentation during patterning. Furthermore, the tip leveling can be performed much easier due to automatically calculated correction angle given by the software. A further advantage is that it is not necessary anymore to rely on the quite unreliable combination of video image and eye judgment for the leveling procedure because both are only qualitative approaches.

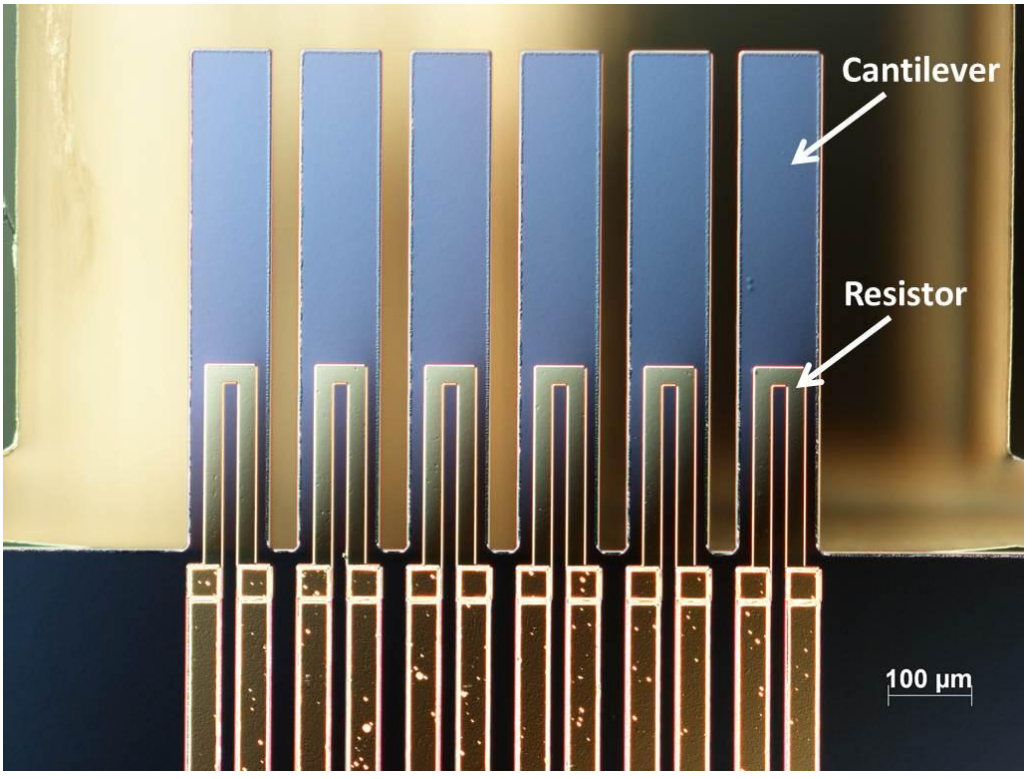

Figure 22: Cantilever backs with integrated resistor as a sensor. Image is a courtesy of NTB Buchs, Switzerland.

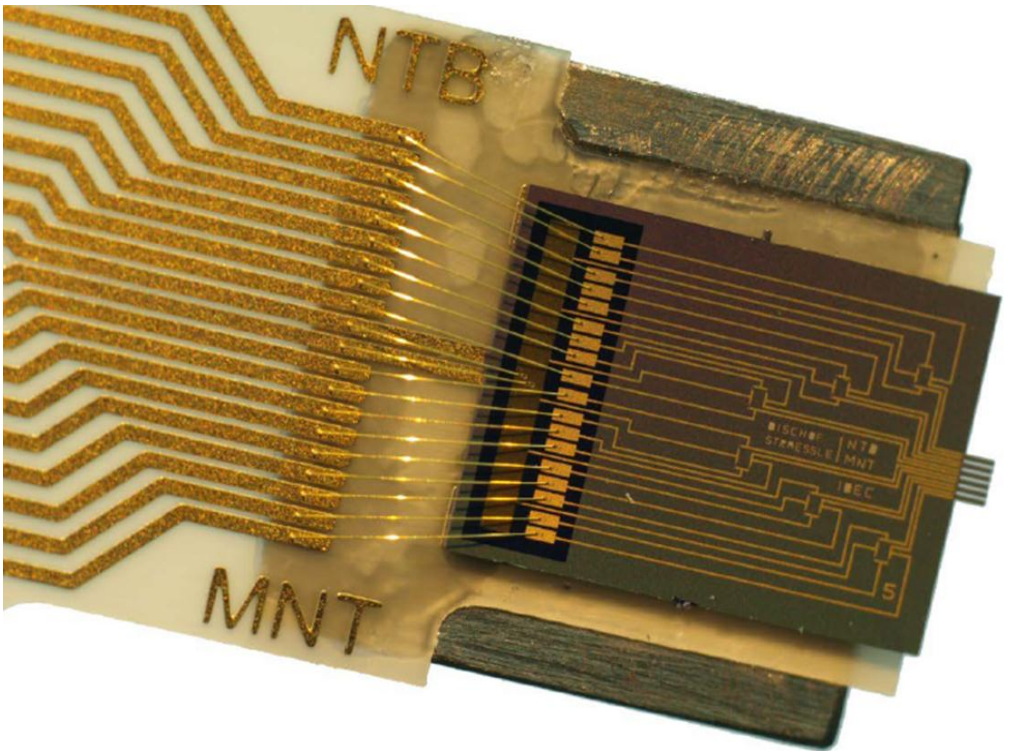

Figure 23: Piezoresistive device fabricated in collaboration with the NTB Buchs (Switzerland). On the right side, the 6 cantilevers are visible which have the integrated deflection sensors in their back. The wires enable the connection to the readout software. Image is a courtesy of NTB Buchs, Switzerland.

Figure 24 shows a screen shot of the software MNT LeverSens for controlling the piezoresistive device. The letter A in a) highlights the different levers which can be turned on (green light) or off (grey light), meaning their feedback is taken into account when determining the correction angle for the leveling procedure (red square). The blue beams correspond to the contact force and, when the tip touches the surface and the lever bends, decrease their height depending on the contact force. In b), the red square indicates the decrease in the blue beams. The blue square gives the values for the contact force exerted from the tips on the substrate (here in the order of 10^{-6} N, which equals μN).

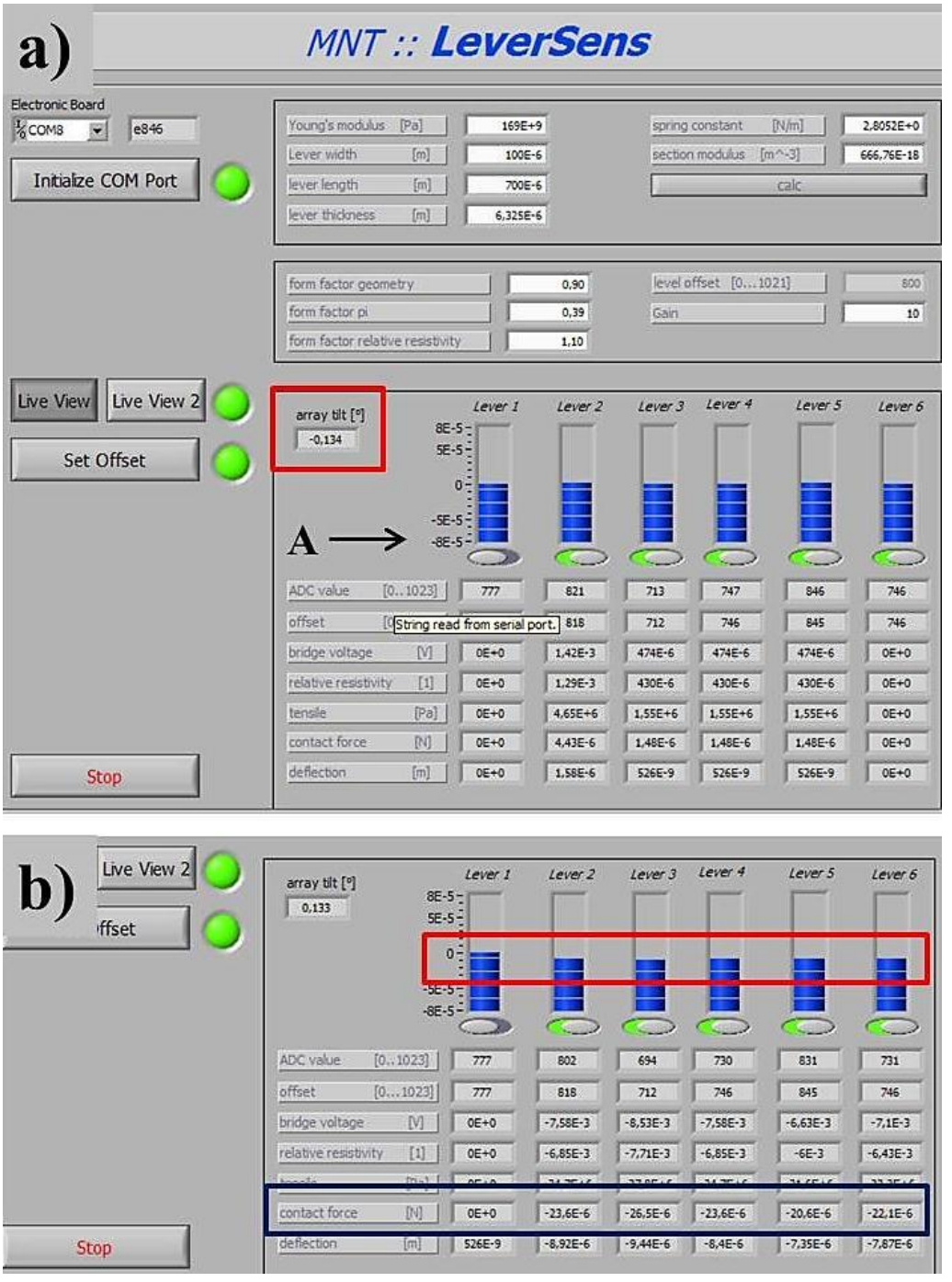

Figure 24: Screenshot MNT LeverSens software for controlling the piezoresistive device (in collaboration with NTB Buchs, Switzerland).

For patterning, the tips were incubated with Streptavidin Texas Red (SAV-TR, a liquid ink) and a series of pattern was written on a gold substrate functionalized with biotin-thiol. Deposition of the ink (SAV-TR) was possible even though the deposition properties of the tips have to be improved for liquid inks. Figure 25 shows the fluorescence microscopy image of the SAV-TR pattern of 4 tips, where one tip did not deposit at all (3rd tip from the left). The tips did not deposit equally, most likely due to the fabrication process. The second tip from the left had a very big drop of ink which was smeared along the pattern (movements between the dots of 20 µm), indicated by the big red stripe. Only two tips are performing normal, even though also they show a small amount of smearing of excess ink.

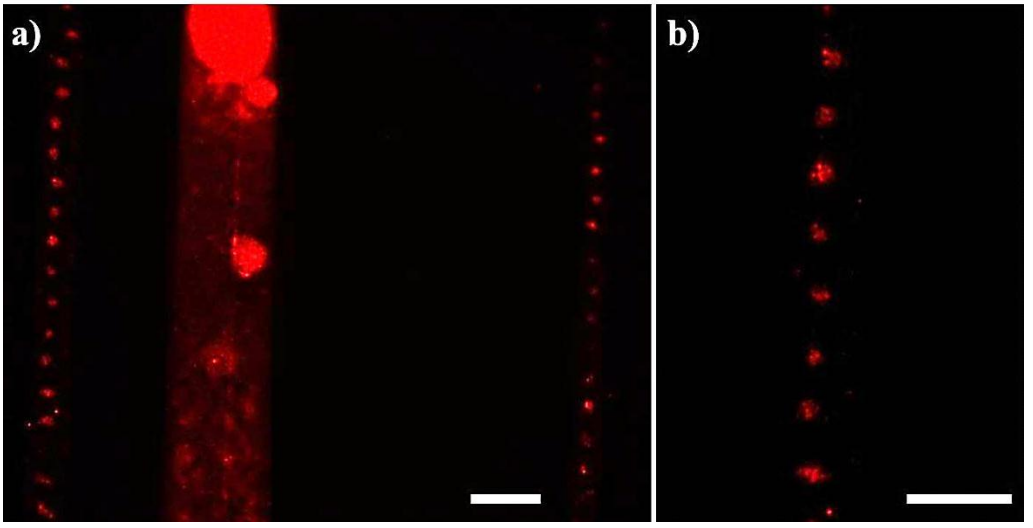

Figure 25: Fluorescence microscopy image of STV-TR patterned on a biotin-thiol functionalized gold surface. a) is an overview over the pattern of 3 tips, where the black area in the middle represents a 4th tip which did not deposit properly. b) is an enlarged area of the normal pattern. The patterning direction was from bottom to top. The scale bars equal 50 µm.

In a second experiment, mercaptohexadecanoic acid (MHA, a molecular ink) was patterned directly on gold. Subsequently, the not patterned gold was etched away, leaving only the gold which was "protected" by MHA. The pattern of all the tips is shown in Figure 26 a) and the numbers indicate the respective tips. The blue square is the enlarged section b) where the red arrows indicate the real pattern created by the tips. The extra MHA, which has been deposited and can be seen as interrupted lines originates from the cantilever edge. This is due to a too big inclination during

patterning, where not only the tip is touching but also the cantilever front edge. This has to be addressed in the fabrication process of the tips and the cantilever properties have to be corrected respectively.

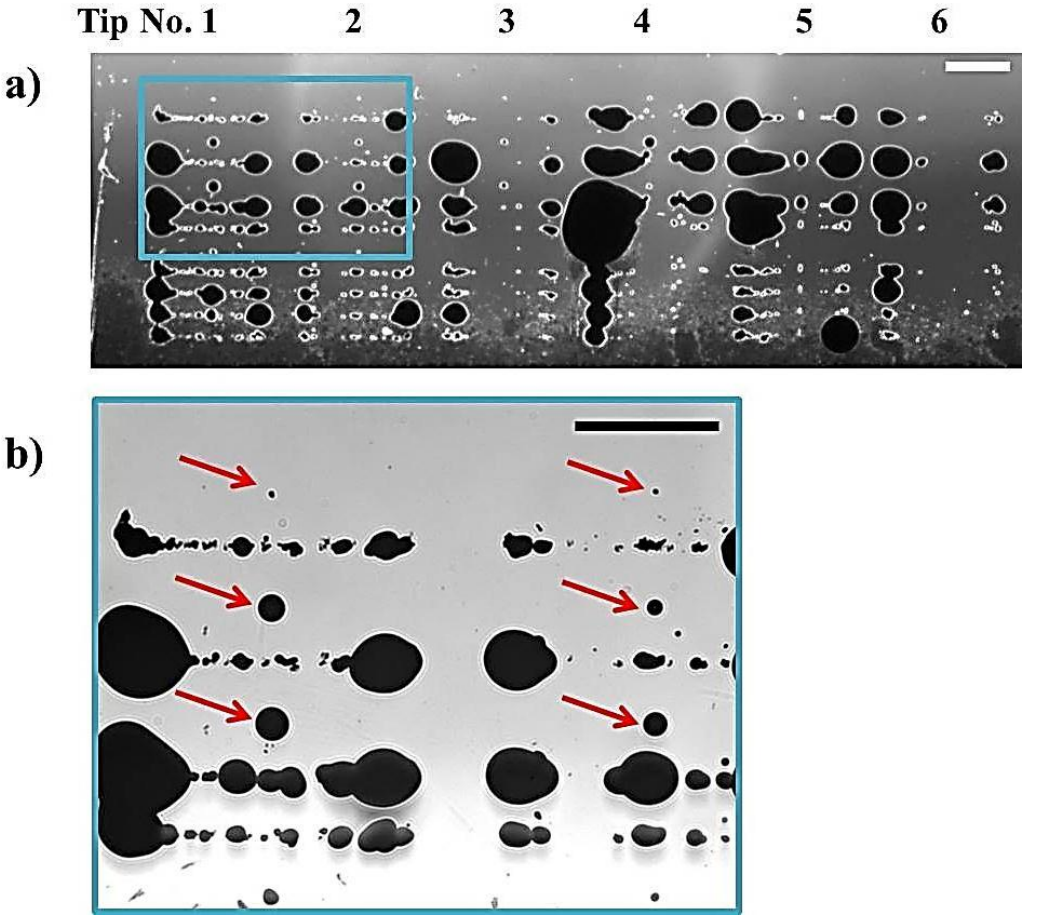

Figure 26: Phase contrast image of MHA patterned on gold and the not coated gold etched away. a) shows the pattern created by the 6 different tips. b) is an enlarged section and arrows indicate the actual pattern created by the tip. Scale bars in the upper right corner equal 50 µm.

In a third experiment, also with MHA on gold, the problem of the inclination was solved by manually correcting the inclination of the whole device using several different inclinations (see Table 2 for all inclinations tested). Image a) of Figure 27 illustrates the commercially available cantilever which had been used for experiments before (from NanoInk Inc., USA) and images b-d) illustrate how for the custom fabricated cantilever, the tip is further inside, causing the edge of the cantilever to

touch first (b) or at the same time (c). Image d) shows how, with sufficient inclination of the whole device, only the tips are touching and depositing ink.

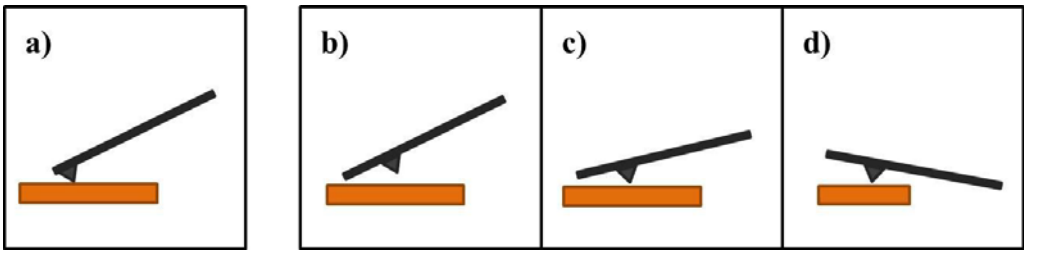

Figure 27: Illustration of how tilting the whole device solves the problem of the marks from the edge of the cantilever. Image a) stands for the commercially available cantilevers and images b-d) for the custom fabricated device. Whereas in image b) only the edge of the cantilever is touching, image d) has the inclination corrected sufficiently so that only the tip is touching.

As can be seen in Figure 28, this approach was successful and only the tips were depositing MHA. The correction factor for the inclination for these arrays was 600 µm upward (see experimental section for explanation). This is the minimum correction that has to be applied in order to avoid erroneous lithography as shown in Figure 26. Images b and c) of Figure 28 show the respective enlarged areas of image a), where the whole pattern can be appreciated. The white arrows indicate the different pattern structures and the numbers above image a) indicate the different cantilever (in total 6 on a chip). From image b) it is quite clear that there was no MHA deposited by the cantilever edge. Nevertheless, this issue has to be addressed in the future during the tip fabrication process because too much inclination of the DPN instrument will give rise to limitations during patterning. As an example, which was encountered here, patterning was only possible at the very edge of the substrate so that the lower cantilever side didn't touch the substrate (as indicated in Figure 27 c).

The tips are working for both liquid and molecular ink but the cantilever properties have to be adjusted for optimal patterning results. In any case, the tips are able to be implemented into the instrument and show good results for the leveling routine.

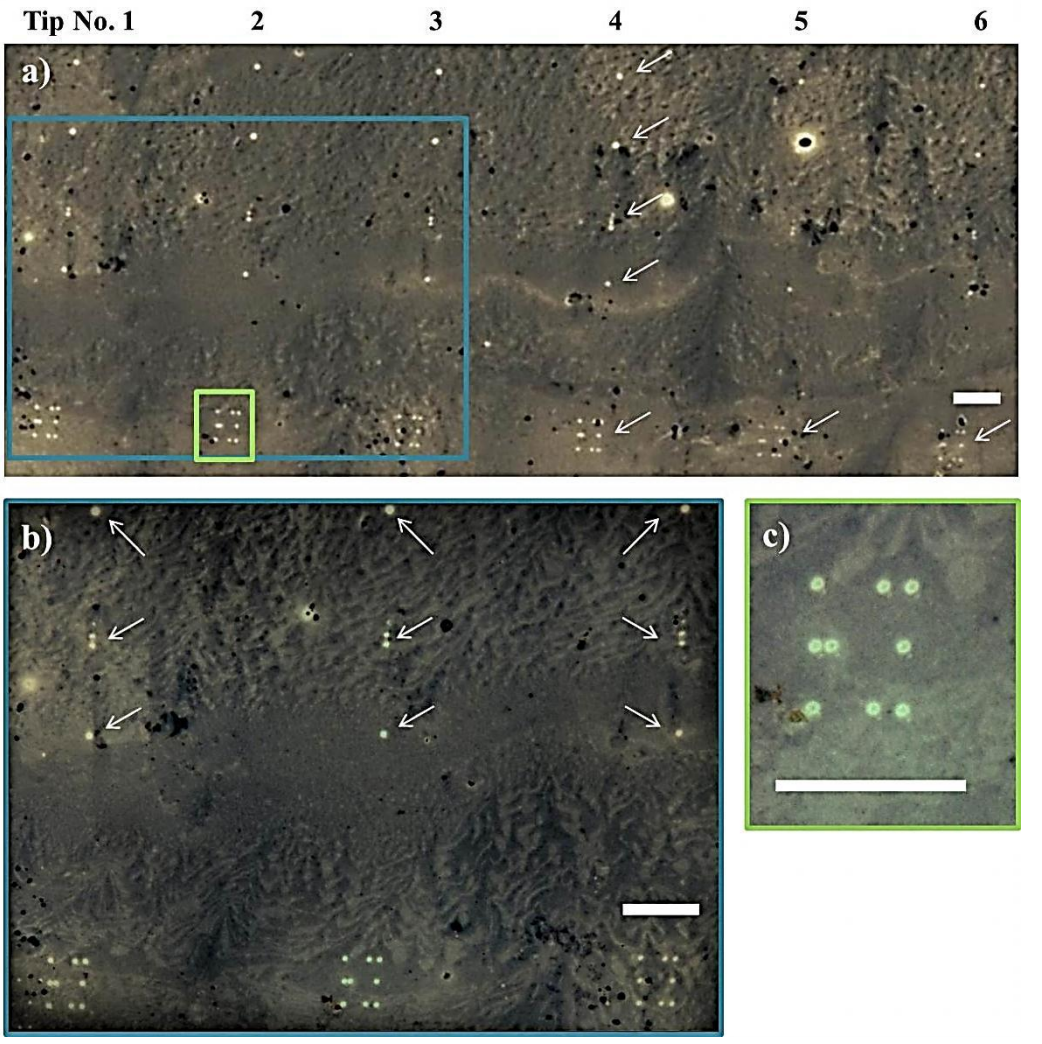

Figure 28: Brightfield microscopy image of MHA patterned on gold and the not coated gold etched away. In comparison to the previous image (figure 18), only the tips were depositing MHA. This can be seen because only the actual pattern is visible and no excess ink was deposited. The white arrows indicate the pattern areas of the 6 tips in image a). Images b and c are enlarged sections of a). All scale bars equal 30 µm.

1.4. CONCLUSIONS

When performing Dip-pen Nanolithography with more than one cantilever, the leveling of all tips with respect to the surface is still a critical issue. In this chapter several approaches were undertaken in order to improve manual leveling: As a first step, the zoom function of the microscope was used which resulted in an improved leveling of the whole array. As a second step, the introduction of a plane leveling was implemented in order to correct errors coming from the substrate plane. Even though these new routines could improve the leveling and diminish the chance of damaging the substrates, there was still no feedback of the pressure which the tips exert on the substrate.

Therefore, and also in order to make the tip leveling routine independent of any optical assistance, cantilevers with a piezoelectric sensor have been developed for implementation into the NScriptor instrument. After adjustment of tips and software, the device could be integrated successfully and was used to pattern two different inks (MHA and streptavidin). In order to enhance the deposition of liquid inks (streptavidin in this case), the tip properties need to be further adjusted. Also, MHA could be deposited on gold as with commercially available tips. Independently of the ink deposition, a higher sensitivity was determined for the point when the tips touch the surface.

This piezoresistive device is very promising for a big improvement of the leveling routine and also for quantitative measurements of the contact force of the tips on the substrate, which up to date is only indirectly possible.

1.5. REFERENCES

[1] Taken from www3.physik.uni-greifswald.de/method/afm/eafm.htm; accessed in June 2012.

[2] M. Binggeli and C.M. Mate. *Influence of capillary condensation of water on nanotribology studied by force microscopy.* Applied Physics Letters 1994. **65 (4)**: p. 415-417.

[3] B.L. Weeks, M.W. Vaughn and J.J. DeYoreo. *Direct Imaging of Meniscus Formation in Atomic Force Microscopy Using Environmental Scanning Electron Microscopy*. Langmuir 2005. **21 (18)**: p. 8096-8098.

[4] M. Jaschke and H.-J. Butt. *Deposition of Organic Material by the Tip of a Scanning Force Microscope.* Langmuir 1995. **11**: p. 1061-1064.

[5] R.D. Piner, J. Zhu, F. Xu, S. Hong and C.A. Mirkin. *"Dip-pen" Nanolithography.* Science 1999. **283 (5402)**: p. 661-663.

[6] D.S. Ginger, H. Zhang and C.A. Mirkin. *The Evolution of Dip-pen Nanolithography*. Angewandte Chemie, International Edition 2004. **43**: p. 30-45.

[7] S. Hong and C.A. Mirkin. *A Nanoplotter with Both Parallel and Serial Writing Capabilities.* Science 2000. **288 (5472)**: p. 1808-1811.

[8] Taken from the datasheet "*2D nano PrintArray™*", available at http://www.NanoInk.net; accessed in June 2012.

[9] P.E. Sheehan and L.J. Whitman. *Thiol Diffusion and the Role of Humidity in Dip Pen Nanolithography*. Physical Review Letters 2002. **88 (15)**: p. 1561041-1561044.

[10] S. Rozhok, R. Piner and C.A. Mirkin. *Dip-pen Nanolithography: What Controls Ink Transport?* The Journal of Physical Chemistry B 2003. **107**: p. 751-757.

[11] J. Hyun, S.J. Ahn, W.K. Lee, A. Chilkoti and S. Zauscher. *Molecular Recognition-Mediated Fabrication of Protein Nanostructures by Dip-pen Lithography.* Nano Letters 2002. **2 (11)**: p. 1203-1207.

[12] H. Zhang, S.-W. Chung and C.A. Mirkin. *Fabrication of Sub-50-nm Solid-State Nanostructures of the Basis of Dip-pen Nanolithography.* Nano Letters 2003. **3 (1)**: p. 43-45.

[13] H. Zhang, K.-B. Lee, Z. Li and C.A. Mirkin. *Biofunctionalized nanoarrays of inorganic structures prepared by Dip-pen nanolithography.* Nanotechnology 2003. **14**: p. 1113-1117.

[14] A. Kumar, H.A. Biebuyck, N.L Abbott and G.M. Whitesides. *The use of self-assembled monolayers and a selective etch to generate patterned gold features*. Journal of the American Chemical Society 1992. **114**: p. 9188-9189.

[15] M. Geissler, H. Wolf, R. Stutz, E. Delamarche, U.-W. Grummt, B. Michel and A. Bietsch. *Fabrication of Metal Nanowires Using Microcontact Printing.* Langmuir 2003. **19**: p. 6301-6311.

[16] G. Lu, Y. Chen, B. Li, X. Zhou, C. Xue, J. Ma, F.Y.C. Boey and H. Zhang. *Dip-pen Nanolithography-Generated Patterns Used as Gold Etch Resists: A Comparison Study of 16-Mercaptohexadecanoic Acid and 1-Octadecanethiol.* The Journal of Physical Chemistry C 2009. **113 (10)**: p. 4184-4187.

[17] D.G. Thompson, E.O. McKenna, A. Pitt and D. Graham. *Microscale mesoarrays created by Dip-pen nanolithography for screening of protein-proteins interactions.* Biosensors and Bioelectronics 2011. **26 (12)**: p. 4667-4673.

[18] S.E. Kooi, L.A. Baker, P.E. Sheehan and L.J Whitman. *Dip-pen nanolithography of chemical templates on silicon oxide.* Advanced Materials 2004. **16**: p. 1013-1016.

[19] B. Fabre, S. Ababou-Girard and F. Solal. *Covalent integration of pyrrolyl units with modified monocrystalline silicon surfaces for macroscale and sub-200nm-scale localized electropolymerization.* Journal of Material Chemistry 2005. **127 (13)**: p. 4564-4565.

[20] D. Prime, S. Paul, C. Pearson, M. Green and M.C. Petty. *Nanoscale patterning of gold nanoparticles using an atomic force microscope.* Materials Science and Engineering C 2005. **25**: p. 33-38.

[21] B.W. Maynor, J.Y. Li, C.G. Lu and J. Liu. *Site-specific fabrication of nanoscale heterostructures: Local chemical modification of GaN nanowires using electrochemical Dip-pen nanolithography.* Journal of the American Chemical Society 2004. **126 (20)**: p. 6409-6413.

[22] H. Taha, A. Lewis and C. Sukenik. *Controlled deposition of gold nanowires on semiconducting and nonconducting surfaces.* Nano Letters 2007. **7 (7)**: p. 1883-1887.

[23] M. Su, M. Aslam, L. Fu, N. Wu and V.P. Dravid. *Dip-pen nanopatterning of photosensitive conducting polymer using a monomer ink.* Applied Physics Letters 2004. **84 (21)**: p. 4200-4202.

[24] F.S. Teixeira, R.D. Mansano, M.C. Salvadori, M. Cattani and I.G. Brown. *Atomic force microscope nanolithography of polymethylmethacrylate polymer.* Review of Scientific Instruments 2007. **78**: p. 0537021-0537023.

[25] H. Nakashima, M.J. Higgins, C. O´Connell, K. Torimitsu and GG. Wallace. *Liquid Deposition Patterning of Conducting Polymer Ink onto Hard and Soft Flexible Substrates via Dip-pen Nanolithography.* Langmuir 2011. **28 (1)**: p. 804-811.

[26] J.-W. Jang, A. Smetana and P. Stiles. *Multi-Ink Pattern Generation by Dip-pen Nanolithograph*y. Scanning 2010. **32**: p. 24-29.

[27] P.L. Stiles. *Direct deposition of micro- and nanoscale hydrogels using Dip Pen Nanolithography (DPN)*. Nature Methods 2010. **7 (8)**: p. I-II.

[28] A.J. Senesi, D.I. Roykiewicz, D.N. Reinhoudt and C.A. Mirkin. *Agarose-Assisted Dip-pen Nanolithography of Oligonucleotides and Proteins.* ACS Nano 2009. **3 (8)**: p. 2394-2402.

[29] E. Bellido, R. de Miguel, D. Ruiz-Molina, A. Lostao and D. Maspoch. *Controlling the Number of Proteins with Dip-pen Nanolithography.* Advanced Materials 2010. **22**: p. 352-355.

[30] E.J. Irvine, A. Hernandez-Santana, K. Faulds and D. Graham. *Fabricating protein immunoassay arrays on nitrocellulose using Dip-pen lithography techniques.* Analyst 2011. **136**: p. 2925-2930.

[31] H. Jiang and S.I. Stupp. *Dip-pen Patterning and Surface Assembly of Peptide Amphiphiles.* Langmuir 2005. **21 (12)**: p. 5242-5246.

[32] Y.-H. Shin, S.-H. Yun, S.-H. Pyo, Y.-S. Lim, H.-J. Yoon, K.-H. Kim, S.-K. Moon, S.W. Lee, Y.G. Park, S.-I. Chang, K.-M. Kim and J.-H. Lim. *Polymer-Coated Tips for Patterning of Viruses by Dip-pen Nanolithography.* Angewandte Chemie, International Edition 2010. **49**: p. 9689-9692.

[33] S. Liu, R. Maoz and J. Sagiv. *Planned Nanostructures of Colloidal Gold via Self-Assembled on Hierarchically Assembled Organic Bilayer Template Patterns with In-situ Generated Terminal Amino Functionality.* Nano Letters 2004. **4 (5)**: p. 845-851.

[34] D. Chowdhury, R. Maoz and J. Sagiv. *Wetting Driven Self-Assembly as a New Approach to Template-Guided Fabrication of Metal Nanopatterns*. Nano Letters 2007. **7 (6)**: p. 1770-1778.

[35] K. Salaita, Y. Wang and C.A. Mirkin. *Applications of Dip-pen nanolithography.* Nature Nanotechnology 2007. **2**: p. 145-155.

[36] K. Salaita, Y. Wang, J. Fragala, R.A. Vega, C. Liu and C.A. Mirkin. *Massively Parallel Dip-pen Nanolithography with 55000-Pen Two-Dimensional Arrays.* Angewandte Chemie, International Edition 2006. **45**: p. 7220-7223.

[37] J.-W. Jang, R.G. Sanedrin, A.J. Senesi, Z. Zheng, X. Chen, S. Hwang, L. Huang and C.A. Mirkin. *Generation of Metal Photomasks by Dip-pen Nanolithography*. Small 2009. **5 (16)**: p. 1850-1853.

[38] H. Jung, R. Kulkarni and C.P. Collier. *Dip-pen nanolithography of reactive alkoxysilanes on glass.* Journal of the American Chemical Society 2003. **125 (40)**: p. 12096-12097.

[39] S. Hong, J. Zhu and C.A. Mirkin. *Multiple Ink Nanolithography: Toward a Multiple-Pen Nano-Plotter.* Science 1999. **86**: p. 523-525.

[40] D.A. Long, K. Unal, R.C. Pratt, M. Malkoch and J. Frommer. *Localized "Click" Chemistry Through Dip-pen Nanolithography.* Advanced Materials 2007, **19**: p. 4471-4473.

[41] C.D. O'Connell, M.J. Higgins, H. Nakashima, S.E. Moulton and G.G. Wallace. *Vapor Phase Polymerization of EDOT from Submicrometer Scale Oxidant Patterned by Dip-pen nanolithography.* Langmuir 2012. **28 (26)**: p. 9953-9960.

[42] S. Sekula, J. Fuchs, S. Weg-Remers, P. Nagel, S. Schuppler, J. Fragala, N. Theilacker, M. Franzreb, C. Wingren, P. Ellmark, C.A. Borrebaeck, C.A. Mirkin, H. Fuchs and S. Lenhert. *Multiplexed Lipid Dip-pen Nanolithography on Subcellular Scales for the Templating of Functional Proteins and Cell Culture*. Small 2008. **4**: p. 1785– 1793.

[43] Taken from the data sheet "*NLP 2000 System*" available at http://www.NanoInk.net; accessed in June 2012.

Chapter 2.

Immobilization of oligonucleotides via Dip-pen Nanolithography for the construction of a biosensor platform

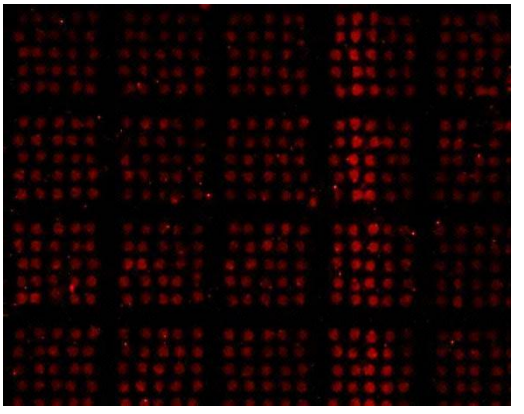

2.1. INTRODUCTION

Sensors play an important role in our everyday life, starting from a thermometer to measure temperature over a tactile sensor in the elevator button to the rain sensor in the windshield of the car. Generally spoken, a sensor is a device which measures a physical quantity and converts it into a signal which can be understood easily by the operator of the device. A special type of sensor is the so called biosensor, which is an analytical device consisting of a) a sensitive biological element which specifically binds the analyte (also called bioreceptor or recognition element), b) an interface architecture, c) a transducer or detector element, which transforms the signal of the interaction "analyte – biological element" into a quantifiable signal, and finally d) a computer software and e) an interface which allow the interpretation of the obtained signal (see Figure 29)[1]. Detection methods include optical, acoustic, electrical or magnetic response.

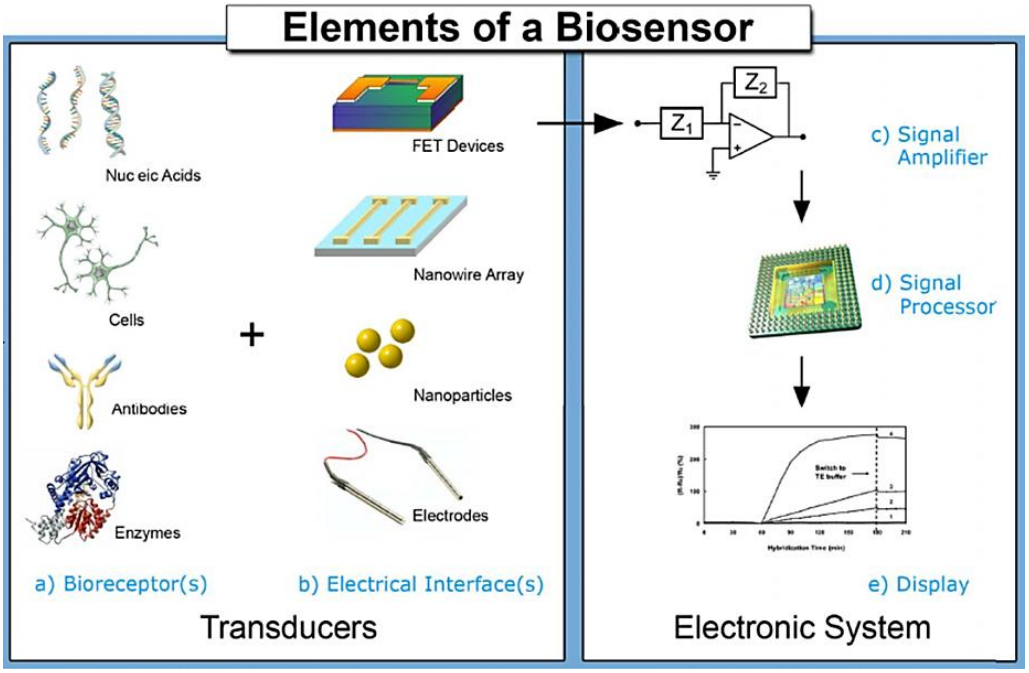

Figure 29: Elements and selected components of a typical biosensor. Image adapted from reference 1.

Biosensors are applied in many different areas. A canary in a cage used by miners in order to warn them of gas leaks could be considered the first routinely-used biosensor. A common example and the historical market driver is the commercially available blood glucose sensor for diabetes patients.[2] Other well-known applications of biosensors include detection of pesticides or pathogens in the environment[3] or in food[4], drug screening in food[5] or for medical purposes[6], and future applications aim at detection of diseases,[7] like cancer.[8,9] Also the military field has several applications for biosensors, for example the detection of chemicals or bombs with the so called Wasp-Hound.[10,11]

2.1.1. Classification of biosensors

A biosensor can be classified according to three different factors: a) the receptor, b) the immobilization technique for the receptor or c) the transducer, whereas option c) is the one normally used.[12] According to the operating principle of the transducer, which is responsible for converting the physical changes arising from the chemical or biological reaction in the sensor, biosensors can be divided into the following devices:

Calorimetric devices measure the heat given off or absorbed by a specific chemical reaction involving the analyte.

Potentiometric devices measure the accumulation of a charge potential at the working electrode compared to the reference electrode of the sensor, when zero or no significant current flows between the two electrodes.

Amperometric devices measure the current which results from the oxidation or reduction of an electroactive species in the sensor.

Piezoelectric devices measure the frequency change for a quartz oscillator plate which is caused by the adsorption of a mass (the analyte) to the oscillator plate.

Optical devices transform the changes of optical phenomena resulting from the interaction of the analyte with the receptor and can be further distinguished into measuring the a) absorbance, b) reflectance, c) luminescence, d) fluorescence,

e) refractive index, f) optothermal effect and g) light scattering. For a more detailed explanation of the subgroups, see reference 12.

2.1.2. Recognition elements for biosensors

As shown in Figure 29, the most common recognition elements of a biosensor include whole cells,[13] antibodies[14] or antibody fragments[15] and enzymes[16]. Furthermore, cell receptors[17], tissues[18] or microorganisms[19] have been used as well. And recently, a modified living organism (zebrafish) has been applied for biosensing.[20] The recognition elements used most widely are antibodies because of their high specificity of binding the antigen. Nevertheless, their surface immobilization can cause a severe loss of their biological activity (see section 2.1.4.). Another commonly used group of recognition elements are the nucleic acids which are popular for several advantages, amongst them because they are highly stable and easily reusable by thermal melting of the DNA duplex.[21]

A very important aspect for biosensors, which is closely linked to the recognition element, is the passivation of the surface against non-specific adsorption of the analyte or other mainly biological molecules present in the solution to be analyzed. This non-specific interaction can cause false results and significantly decrease the biosensor potential.

2.1.3. Nucleic acids as recognition elements

This family of recognition elements includes deoxyribonucleic acid (DNA), ribonucleic acid (RNA), single stranded oligonucleotides, specially designed aptamers[22] and nucleic acid analogues[23] like peptide nucleic acid (PNA) and locked nucleic acid (LNA).

Nucleic acids have several advantages over the other above mentioned biological recognition elements, and not only concerning the immobilization process.

They don't require a buffered solution, which means they will not lose their biological activity when dissolved in water or organic solvents. This allows for direct writing methods without the need of adjustments.[24] Furthermore, once immobilized on the surface, their storage is less complicated. They can also be easily adapted depending on the surface which is used for immobilization: custom synthesis of oligonucleotide sequences is already routinely performed and the desired oligonucleotides are accessible at reasonable prices and timeframes. Also, the incorporation of a chemical end group for anchoring purposes (thiol, amine, azide[25]…) is relatively easy and 100% controllable. Therefore, random anchoring can be almost completely avoided.

Applications of nucleic acids as recognition elements are numerous. They include the well-known DNA microarrays, which are used for the profiling of gene expression, detection and characterization of pathogens, genotyping, resequencing and the discovery of interactions between proteins and DNA.[26] A review about the use of DNA microarrays in toxicology and ecotoxicology is given in reference 27. Furthermore, nucleic acids are used for pure detection as biosensors. Aptamers, for example, are short oligonucleotide sequences that can bind not only to DNA or RNA but also to small molecules, proteins or even cells, tissues or organisms. Biosensors using aptamers are called aptasensors and their applications include detection of biomarkers like thrombin, clinical testing of cancer related markers, and also detection of microorganisms and viruses like E. coli or HIV-1.[28]

2.1.4. Immobilization strategies for recognition elements

In order to ensure a stable immobilization of the recognition element on the sensor surface, normally, covalent attachment is preferred over simple adsorption. When the sensing surface is gold or another metal, it can be coated with a self-assembled monolayer (SAM) containing a sulphide or disulphide anchor and a functional group in order to couple the recognition elements. Frequently used functionalities are carboxyl-, amine- or ester-groups, or the biotin-streptavidin coupling, whereas the first two groups require an additional activation step in order to facilitate further coupling reactions. Furthermore, very often used for the sensitive

enzymes are encapsulation techniques via hydrogel[29] or sol-gel[30] entrapment. Apart from homogeneous layers, patterning techniques are also employed, like microcontact printing[31] and direct spotting[32]. The local confinement of the sample area has several advantages: the biological assay can be miniaturized and less sample volume or fewer reagents are required. On the other hand, multiplexing on the same surface is possible and many assays can be run in parallel.

When immobilizing antibodies (AB) or antibody fragments, it is most important to avoid the loss of their functionality which can be caused by several factors, as indicated in Figure 30. On one hand, their random orientation on the surface can provoke that the active center is pointed in the wrong direction (image 2a, red AB). On the other hand, interactions with the surface may cause their unfolding (image 2b). And thirdly, if the antibodies are functionalized with a linker for surface attachment prior to the attachment, it can occur that the labeling with the linker itself can give rise to wrong orientation on the surface or can bind to or close to the active center (image 2c).

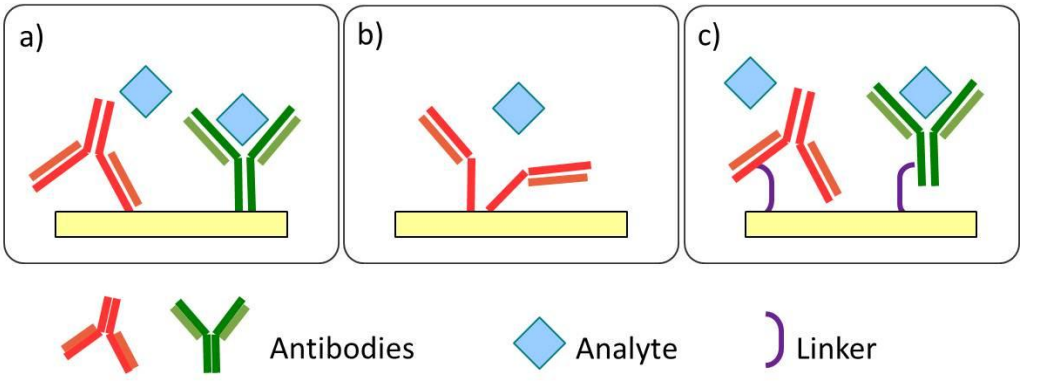

Figure 30: Immobilization of antibodies (AB) on a surface and problems arising thereby. The red AB represents a not recognizing AB where immobilization gave rise to problems; the green AB is the one who is still recognizing the analyte and immobilization was successful.

In comparison, the immobilization of nucleic acids can be a lot less troublesome, as explained in section 2.1.3. This is because their anchoring element can be included and – if necessary – custom tailored during synthesis without loss of their functionality. Their robustness against denaturing furthermore facilitates covalent attachment by chemical coupling reactions. Also, the potential facile regeneration of

the biosensor platform by thermal denaturing is beneficial. A general overview over different immobilization methods of nucleic acids for biosensors is given in a recent review by Labuda *et al*.,[33] where they mention the following immobilization methods: non-covalent binding (adsorption), affinity binding via avidin-biotin, chemisorption via SAMs and covalent binding. Latter strategy includes immobilization via the carbodiimide method and also via a synthetic polymer film, especially mentioning click chemistry as promising approach (see section below).

2.1.5. Advantages of the miniaturization of a biosensor

The most common detection method used for the construction of biosensors is the immunodetection, which is extensively applied in the fabrication of genomic and proteomic microarrays. Well-known examples are the enzyme-linked immunosorbent assay (ELISA) standard test[34] (determination of protein or antibody concentration) or the DNA microarrays (commercially available from many different distributors)[35]. The principle of these arrays is the immobilization of a so called probe on a previously functionalized sample surface and the subsequent conjugation with the target sequence. Figure 31 shows the example for a DNA array.

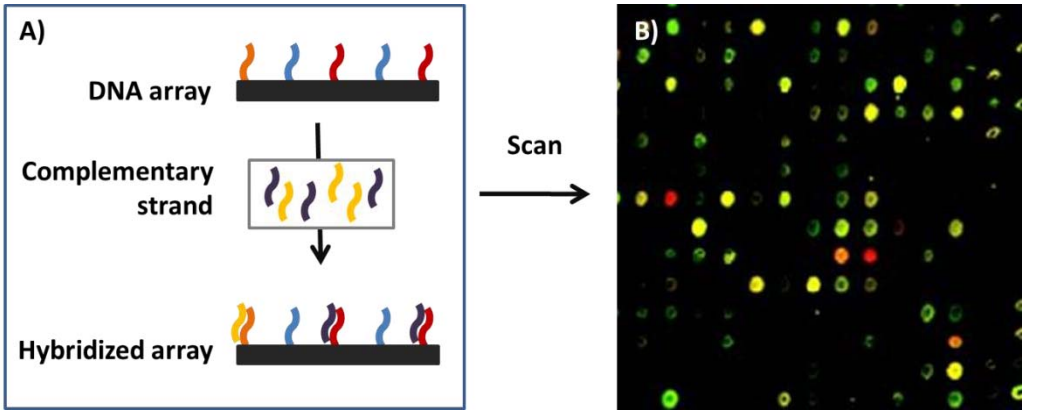

Figure 31: Example for a DNA microarray. A) set-up of a DNA microarray and incubation with the complementary strand (the target). After scanning the microarray, the read out could be as indicated in B). The image was taken from reference 36.

Detection is usually performed by fluorescence microscopy (introducing a fluorophore) or by colorimetry (adding an enzyme which reacts and thus leads to a change in color). As can be seen in Figure 31, the array can consist of many different spots and if every – in this case – complementary fluorophore had to have a different color, this would be impossible to realize. Therefore, the so called site-encoding strategy was developed. Site-encoding basically means that from the position of each spot of the array its composition can be deduced, because it's known what has been immobilized there.

Even though DNA microarray technique enables the detection millions of genomic sequences, this process is still expensive and laborious. Furthermore, up to now it's not possible to sequence entire simple DNA strands due to huge amount of material which would have to be analyzed.

Therefore, the development of arrays and ultimately also biosensors whose diameter of the site-encoding spots lies in the micro-nano regime has become of great interest. Furthermore, miniature biosensors have shown increased sensitivity, velocity and reliability, as well as lower production cost and possible higher feature surface density.[37] The fabrication of chips on which the surface density of immobilized probes is much higher leads to an increment of the capacities of immunodetection. This miniaturization can be accomplished thanks to novel nanofabrication techniques, which have been presented shortly in the General Introduction section. Particularly interesting hereby is Dip-pen Nanolithography (DPN) because it allows precise and also multiplexed positioning of molecules on a substrate in a predesigned array with complete control over spot density and spacing.

A very impressive example of a miniaturized biosensor was recently given by K.B. Lee *et al.*[38] who describe the fabrication of an antibody nanoarray created via DPN in order to detect HIV Type1 in blood plasma, where an antibody against the HIV-1 p24 antigen was immobilized on a gold surface (see Figure 32). Subsequently, clinical studies were carried out with uninfected and infected plasma samples and with different levels of virus RNA. They could successfully demonstrate that the fabricated nanoarray not only detected the antigen but even exceeded the detection limit of the conventional ELISA immunoassay by more than 1000-fold!

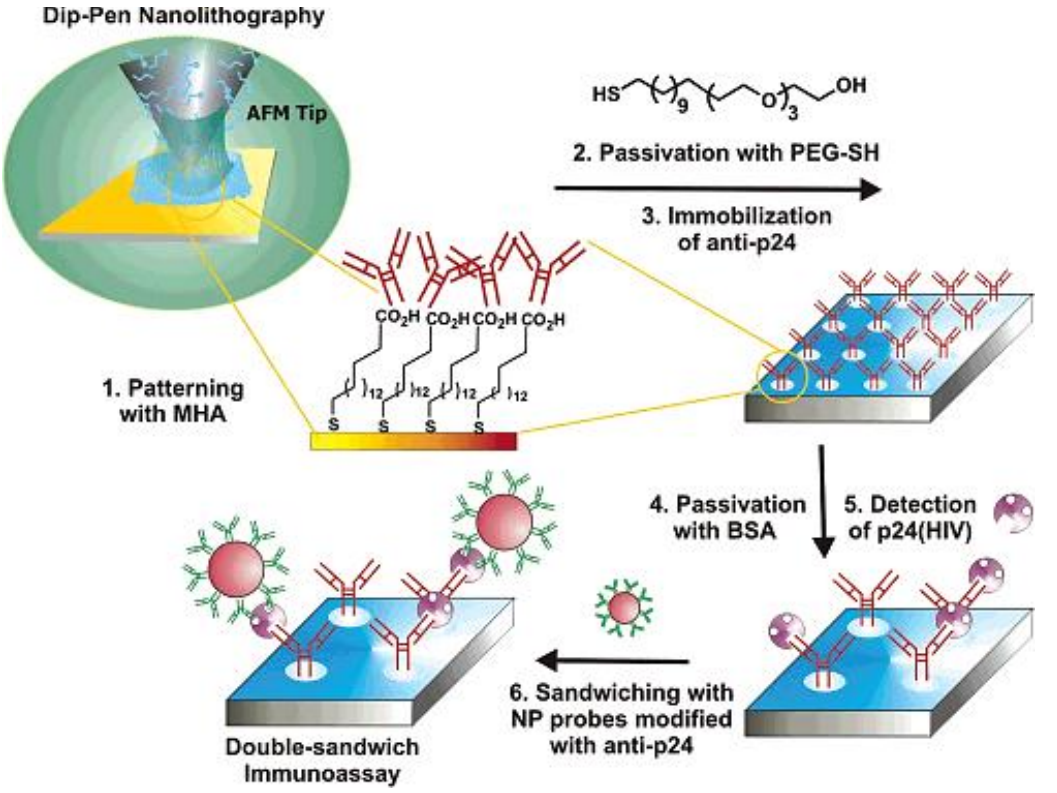

Figure 32: Schematic representation of the nano-biosensor fabricated via Dip-pen Nanolithography used to detect HIV-1 antigen with the anti-p24 antibody. Image taken from reference 38.

This excellent work already proves that these novel surface fabrication technologies yielding nanometer features promise to be very beneficial in the field of biomedicine, in particular in the area of nanomedicine. This new discipline is thought to have visible impact not only in early stage diagnosis of diseases via highly sensitive biosensor devices, but also in fields like tissue engineering, basic biology, regenerative medicine and treatment of many diseases ranging from cancer to diabetes.

Another beautiful example was given by Lee *et al.*,[39] who reported the development of a nanoarray protein chip for the quantitative analysis of human leptin in serum. The spot size is around 150 nm (achieved with DPN) and the sensitivity achieved is 1.95 x 10^7-fold higher than when using standard ELISA.

Furthermore, Irvine *et. al.*[40] report the fabrication of a prostate specific antigen (PSA) immunoassay with Dip-pen Nanolithography, with spot sizes of around 8 µm. The limit of detection (LOD: 0.095 ng/mL) is comparable to the standard commercial ELISA kits.

A miniaturized protein microarray for diagnosis of neonatal sepsis was presented by Buchegger *et al.*,[41] who could show that the protein chip fulfills the needs of a point-of-care device. In comparison to the already existing assay, the necessary sample volume could be decreased (from 20 µL to 4 µL), as well as the overall assay time (from 4 h to 2.5 h) while the sensitivity of the assay could be maintained.

2.1.6. Strategies for a miniaturized oligonucleotide-based biosensor

Direct immobilization of oligonucleotides at the micro-nano range has been successfully performed via DPN by several research groups. Demers *et al*. were the first researchers to publish the direct writing of thiol-modified oligos on gold and at the same time acrylamide-modified oligos on derivatized silica.[24] Based upon this work, other groups published deposition of thiol-[42], amine-[43] or silane-modified[44] oligos on the corresponding substrates. Even though none of these publications report a biosensor, they are good approaches for nanoscale immobilization of oligonucleotides. At present, the only already published biosensor, which is comparable to the one aimed at in this chapter, is the microarray sensor which has already been developed in-house.[45] Nevertheless, Table 3 presents several examples for different biosensors and their respective limits of detection. Detection methods are almost all based on fluorescence microscopy. AFM and SEM as read out methods are considered slower and less convenient.

Table 3: Examples of biosensors with different recognition elements, spot sizes and corresponding detection limits along with their references.

No.	Recognition element	Target	Spot size (diameter)	Detection method	Detection limit	*Ref.*
1	Nucleic acid (DNA)	DNA oligomer	Homogen.	Electro-chemical	152 pmol/mL	*46*
2	Nucleic acid (PNA)	DNA Hepatitis B	~ 250 µm	Fluo	10^2 copies /mL	*47*
3	Nucleic acid (oligo)	Metabolites and drugs	~ 200 µm	Fluo	< 1 µg/mL	*45*
4	Protein (ERK2)	Protein	~ 10 µm	Fluo	1 µM	*48*
5	Antibody ("attowells")	Protein	0.2 – 5 µm	Fluo	pg/mL	*49*
6	MHA + antibody	Antigen p24 HIV	~ 83 nm	SEM, AFM	0.025 pg/mL	*38*

2.1.7. Click chemistry for biosensors – a promising approach for miniaturization?

A strategy for immobilization of molecules on a surface which became popular only recently exploits click chemistry reactions, especially the Huisgen 1,3-dipolar cycloaddition of azides and alkynes. It originally presented a new strategy for the synthesis of triazoles[50,51] and was soon called the "cream of the crop" of the newly introduced concept of click chemistry.[52] In 2002, a significant breakthrough was reported independently by the groups of Meldal[53] and Sharpless[54], who showed that the use of a copper(I) catalyst significantly increases reaction efficiency and regioselectivity of the triazole formation. This so called copper(I)-catalyzed 1,3-diploar cycloaddition has been regarded as "the best click reaction to date" [55] and the "most efficient and widely used" one,[56] due to the mild reaction conditions and the high tolerance of functional groups. Recently, both the Huisgen's and the

copper(I)-catalyzed cycloaddition were discovered for surface modification, as click reaction of monolayers could be proven successfully on gold[57,58,59] and silica[60,61] surfaces. They were considered very useful for the synthesis and modification of polymers,[62,63,64,65] hydrogels[66] or bioactive surfaces[67], and for surface patterning techniques like microcontact printing[68,69,70,71], microarray fabrication[72] or Dip-pen Nanolithography [73,74,75].

In order to perform the click reaction, the presence of two functional groups is necessary: an alkyne group and an azide group. The reaction can be performed both with and without catalyst[60,69], whereby the catalyst not only influences reaction kinetics positively but also controls the regioselectivity.[55] Already existing strategies for click chemistry on surfaces generally focus on having the azide group on the reactive surface. Lin *et al.* compared surface click reactions with both the azide and alkyne group immobilized on the substrate and found higher reaction yields when having the azide group on the surface.[72] The azide group is usually introduced by immobilizing a silane with a bromide group and transforming the bromide into an azide. However, this process is time consuming, with 49 hours necessary for the reaction.[60,68] On the other hand there are different groups which have successfully performed, surface click chemistry with a surface bound alkyne, group,[61,68,69] which will be beneficial because of its higher stability.[73,76,77] An alkyne group can be introduced in an easy and well established way taking advantage of an already existing epoxy group, which reacts under ring-opening with an amine bearing an alkyne moiety.[78,79,80,81]

The **aim of this chapter** is the miniaturization of an already in-house developed oligonucleotide-based biosensor. Dip-pen Nanolithography was used to pattern two different substrates – gold and glass. Gold substrates were employed because they don't require any chemical modification and thiolated molecules are known to attach easily and in a sort of covalent manner to the gold surface. Thiolated oligonucleotides were used for the gold substrates. Glass substrates have the advantage that there is no quenching for fluorescence microscopy but their drawback is that they need a chemical modification enabling facile attachment of molecules. In our case, two

different surface modifications were tested: an aminosilane (APTES) was used to bind the heterobifunctional linker succinimidyl 4-(p-maleimidophenyl)butyrate (SMPB), which is commonly used in the linkage of two biomolecules like proteins or peptides. For this type of surface functionalization, thiolated oligonucleotides were used. The second functionalization route employed an epoxysilane (GPTMS) which was used to bind propargylamine, yielding a stable platform for surface click chemistry. Here, oligonucleotides with an azide moiety were used as "ink". Finally, the obtained sensor platform was evaluated concerning its sensitivity. Therefore, the fluorescent signal of the complementary strand was recorded for a series of experiments, using increasing concentrations of complementary strand for hybridization.

2.2. EXPERIMENTAL SECTION

The biosensor project emerged from a previously in house developed analogous biosensing platform in the μm range, created by means of a conventional DNA microarray plotter[45] and is a development towards miniaturization. Table 4 gives an overview over all oligonucleotide sequences used in this chapter.

Table 4: Oligonucleotide sequences used for the experiments.

Entry	Name	Sequence (5'-3')
1	RRSoja	**[Fluorescein]**-TTC ATG TTC GGC GGT CTC GCG-**SH** (cystein(Fm))
2	20down	**SH**-CGA GTC ATT GAG TCA TCG AG
3	15up	**Au**-GCT CAG TAA CTC AGT AGC TC (10 nm)
4	N1down	**SH**-CAG GAC AAT ATC GTT GCG TG
5	N1up	**Au**-GTC CTG TTA TAG CAA CGC AC (5 nm)
6	S2down	**SH**-CGG AGG TAC ATT CGA CTT GA
7	S2up	**Au**-TCA AGT CGA ATG TAC CTC CG (10 nm)
8	S2up	**[6Fluorescein]**-TCA AGT CGA ATG TAC CTC CG
9	N3down	**SH**-CGG ATA GAG CAC TAC GTT GT
10	N3up	**Au**-GCC TAT CTC GTG ATG CAA CA (20 nm)
11	N3up	**[Fluorescein]**-GCC TAT CTC GTG ATG CAA CA
12	CT	**N_3**-CTT CCT CCT CT
13	AG	**[Texas Red]-**AGA GGA GGA AG
14	GA	**[6Fluorescein]-**GAA GGA GGA GA

All oligonucleotides were provided lyophilized, except the complementary strands with gold nanoparticle which were provided in a buffered solution. The oligonucleotides RRSoja, 20down/15up, N1down/N1up, N2down/N2up/N2up, N3down/N3up/N3up and CT were provided by Dr. Ramon Eritja (IRB Barcelona, Spain). The ones with a thiol group were additionally protected with dithiothreitol (DTT) against the oxidation of the thiol group. To prepare the final "writing ink", the content of the provided vial was dissolved in 0.5 ml phosphate buffer saline (PBS; Sigma Aldrich, Spain) and passed through a NAP^{TM}-10 column[82] (GE Healthcare, USA) to cleave the DTT and obtain the deprotected thiol group.

2.2.1. Patterning on SMPB-glass via DPN using PBS/glycerol (liquid ink)

Functionalization of glass substrates

Glass slides (Corning, USA) were cut into 1 x 1 cm^2 pieces and cleaned in piranha acid (7:3 v/v solution of H_2SO_4 and H_2O_2; both from Panreac, Spain) for 30 min, rinsed with copious amounts of MilliQ water and dried very well with pressurized air. ***Caution: piranha acid is a strong oxidizer and a strong acid. It should be handled with extreme care, as it reacts violently with most organic materials***. The samples were then transferred into a desiccator along with a few drops of 3-aminopropyltrimethoxysilane (APTES; Aldrich, Spain), functionalized in vapor phase for 1 h at room temperature and then baked for 30 min at 80ºC. Figure 33 shows the reaction scheme for the silanization reaction with APTES.

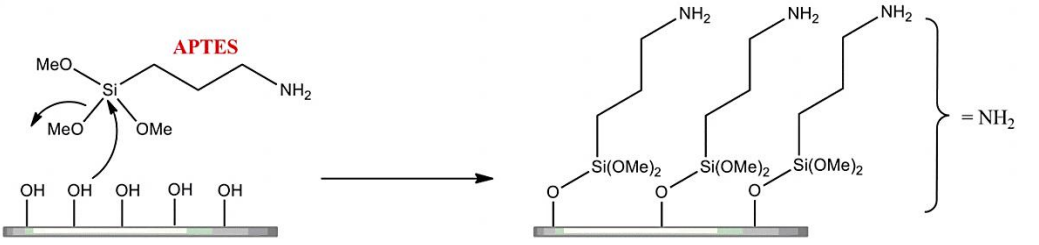

Figure 33: Reaction scheme of the silanization of previously piranha-cleaned glass with APTES.

In the following step, a linker was attached covalently by reacting the amino groups of the substrates with the N-hydroxysuccinimide ester group (NHS) present in the linker succinimidyl 4-(p-maleimidophenyl)butyrate (SMPB), whereby this reaction was carried out inside a glove bag under argon atmosphere and with anhydrous solvents since the NHS group is labile to hydrolysis. Figure 34 shows the reaction scheme for the coupling of the linker SMPB to the surface bound APTES.

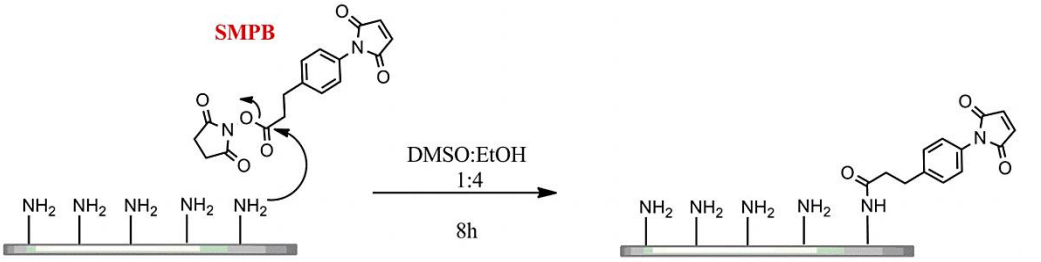

Figure 34: Reaction scheme of the heterobifunctional crosslinker SMPB with the amino group of the APTES functionalized glass.

Therefore, 9 mg SMPB (1 mM; Piercenet, USA) were dissolved in a mixture of DMSO (Fluka, Spain) and ethanol (1:4) and the pH was adjusted to pH=7. The substrates were incubated during 8h and rinsed with a mixture of DMSO and ethanol 1:4 and 1:9 and pure ethanol. The remaining free amino groups were blocked by incubating the substrates for 2 min in a freshly prepared solution of 1:1 Cap Mix A and Cap Mix B (Cap Mix A contains tetrahydrofuran (THF), 2,6-lutidine and acetic anhydride; Cap Mix B contains 6.5% 4-dimethylaminopyridine in THF; both from Eurogentech, USA). Subsequently, the samples were rinsed with THF (Sigma Aldrich, Spain), acetonitrile (Sigma Aldrich, Spain) and MilliQ water, dried with pressurized argon and stored under argon until use in order to avoid reaction of ambient thiol with the maleimide group. The maleimide group enables the covalent attachment of the thiolated oligonucleotide, as can be seen in the reaction scheme below. Figure 35 shows the covalent coupling of the thiolated oligonucleotide to the linker SMPB.

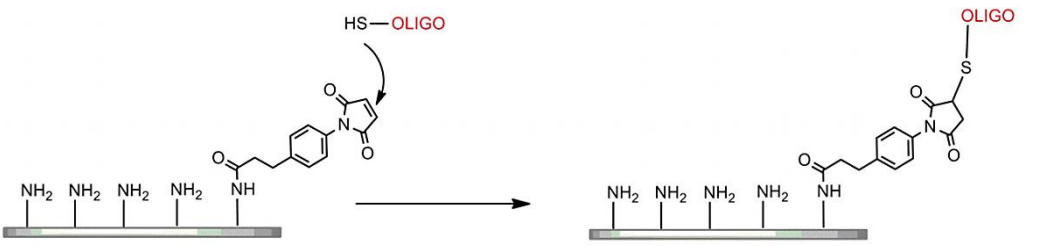

Figure 35: Reaction scheme of the addition of the thiolated oligo to the maleimide group of the SMPB, yielding a thioether.

Patterning of oligo "RRSoja" (thiol, FAM)

The oligonucleotide RRSoja was dissolved in PBS and passed through an illustra NAP^{TM}-10 column for purification. The final concentration was 0.2 mM in PBS. Subsequently, 90 µl of the oligonucleotide solution were mixed well with 10 µl of glycerol (Sigma Aldrich, Spain) and the mixture added to an M-type inkwell (NanoInk Inc., USA). A 1D cantilever array with 12 tips (M-type; NanoInk Inc., USA) was leveled with respect to the glass substrate (see Chapter 1 for more information), incubated in the ink well channel for 10 min and subsequently brought in contact with the substrate for patterning, having the relative humidity adjusted to 50% and the temperature to 21ºC. Before patterning the actual arrays, excessive ink had to be removed from the tips by bringing them repeatedly in contact with the surface. These resulting dots are called bleeding dots and the number differs for every new inking procedure of the tips. Patterning parameters for the arrays ranged from 5 x 5 dots to 20 x 20 dots, spacing between the dots from 2 µm to 3 µm and dwell times from 0.3 s to 0.8 s. Since the oligonucleotide has a fluorophore incorporated already, no further treatment was necessary after patterning. Fluorescence microscopy images were taken after patterning and also after rinsing the substrate with MilliQ water to remove unbound oligonucleotide. The microscope used for all fluorescence images was an Eclipse E1000 upright microscope (Nikon, The Netherlands) equipped with a charge-coupled-device (CCD) camera and working with a several excitation filters.

Patterning of oligo "N3down" (thiol)

The oligonucleotide "N3down" was dissolved in PBS and passed through an illustra NAP^{TM}-10 column for purification. The final concentration was 0.1 mM in PBS. Subsequently, 90 µl of the oligonucleotide solution were mixed well with 10 µl

of glycerol and the mixture added to an M-type inkwell. A 1D cantilever array with 12 tips (M-type) was leveled with respect to the glass substrate, incubated in the ink well channel for 10 min and subsequently brought in contact with the substrate for patterning, having the relative humidity adjusted to 50% and the temperature to 22ºC. Patterning parameters for the arrays were 10 x 10 dots, whereas the spacing between the dots ranged from 2 µm to 3 µm and dwell times from 0.5 s to 0.8 s. After patterning, the substrate was incubated under argon over-night to ensure the reaction of thiol group and maleimide group. Afterwards, the substrate was rinsed with MilliQ and incubated in a solution of 2% bovine serum albumin (BSA; Sigma Aldrich, Spain) in PBS for 1 h at room temperature in order to passivate the sample against unspecific protein adsorption. Subsequently, the sample was rinsed with PBS and hybridized with the complementary strand "N3up FAM" (19 µM in PBS) for 30 min at 35ºC. Finally, the sample was rinsed with PBS and a few drops of MilliQ water, dried with pressurized air and investigated with fluorescence microscopy.

2.2.2. Patterning on gold via DPN using PBS/glycerol (liquid ink)

Gold surfaces were obtained from the NTB Buchs (Switzerland) and provided as 1 x 1 cm^2 squares on blue foil. They consisted of float glass with a 2-5 nm titanium intermediate layer and an approximately 45 nm gold layer. Before using them, they were cleaned successively with THF, acetone (Aldrich, Spain), ethanol (Panreac, Spain) and piranha acid (7:3 v/v solution of H_2SO_4 and H_2O_2) for 30 min, rinsed with copious amounts of MilliQ water and dried with pressurized air.

Patterning of oligo "20down" (thiol)

The oligonucleotide "20down" was diluted in PBS and passed through a NAP™-10 column to yield a final concentration of 0.05 mM. Subsequently, 10 µl of glycerol were added to 90 µl of oligo solution, mixed well and transferred into an inkwell. A 1D cantilever array with 12 tips (M-type) was leveled with respect to the substrate, incubated in the ink well channel for 10 min and subsequently brought in repeated contact with the sample in order to remove the excess ink on the tips for patterning. The relative humidity was adjusted to 50% and the temperature to 22ºC.

Patterning parameters for the arrays ranged from 7 x 7 dots to 20 x 20 dots, spacing between the dots from 2 µm to 4 µm and dwell time from 0.5 s to 0.8 s. In order to passivate the substrates against unspecific adsorption, they were incubated in a 1 mM solution of 1-octadecanethiol (ODT; Sigma Aldrich, Spain) in ethanol for 1 h, subsequently rinsed with ethanol and MilliQ and dried with pressurized air. Following, the sample was hybridized with the respective complementary oligonucleotides by incubating the sample for 1 h at 30ºC in a 1 mM solution of oligo "15up" in PBS. Afterwards, it was rinsed with PBS and a few drops of MilliQ and dried with pressurized air and kept under argon atmosphere until inspection with a scanning electron microscope (SEM).

The SEM used for all images were either a High-resolution SEM Strata DB235 (FEI Company, The Netherlands) or a Nova NanoSEM 230-FEI (FEI Company, The Netherlands), which also allowed working at low vacuum with a water pressure of 0.5 mbar.

2.2.3. Patterning on gold via DPN using "Just Add DNA" (liquid ink)

Gold surfaces were obtained from NanoInk Inc. (USA) and used without further treatment. Oligonucleotide "S2down" was dissolved in solution A of the commercially available DNA printing kit "Just Add DNA" (NanoInk Inc., USA) and 1% of solution B was added, resulting in a final concentration of 0.3 mM. A 1D cantilever array with 12 tips (M-ED-type) with enhanced deposition properties was leveled with respect to the substrate, incubated in the ink well channel for 10 min and subsequently brought in contact with the substrate for patterning, having the relative humidity adjusted to 38% and the temperature to 24ºC. Patterning parameters for the arrays ranged from 4 x 4 dots to 6 x 6 dots, whereas the spacing between the dots ranged from 6 µm to 12 µm and dwell times from 0.2 s to 0.8 s. Arrays were repeatedly printed in y-direction between 7 and 16 times with a distance of 10 µm between the individual arrays. After patterning, samples were stored under argon atmosphere.

In order to evaluate the deposited matter, several surface characterization techniques were used on the untreated sample: The microscope used for all brightfield images was an Eclipse E1000 upright microscope (Nikon, The Netherlands) equipped with a charge-coupled-device (CCD) camera. The Scanning electron microscopes (SEM) used for all images were either a High-resolution SEM Strata DB235 (FEI Company, The Netherlands) or a Nova NanoSEM 230-FEI (FEI Company, The Netherlands), which also allowed working at low vacuum with a water pressure of 0.5 mbar. AFM images were obtained with a Dimension 3100 atomic force microscope (Veeco Instruments, USA) and the images were analysed with WSxM software (Nanotec^{TM}, Spain).

After examination of the untreated sample, it was rinsed with MilliQ in order to remove eventual salts on the surface resulting from the patterning solution, subsequently passivated with 0.2% solution of BSA in PBS for 1 h at room temperature and afterwards rinsed with PBS. In order to hybridize the immobilized oligonucleotide with its complementary strand "S2up", the complementary strand was dissolved in PBS to yield a stock solution with a concentration of 1 g/L, following diluted in hybridization buffer to a final concentration of 1 mg/L and incubated on the substrate for 30 min at room temperature. The hybridization buffer contained buffer 10 mM TRIS base (Sigma Aldrich, Spain), 1 mM EDTA (Sigma Aldrich, Spain) and 1 M NaCl (Sigma Aldrich, Spain) in MilliQ.

2.2.4. Patterning on gold via DPN using DMF/H_2O (molecular ink)

Gold surfaces were obtained from NTB Buchs (Switzerland) and cleaned as explained in section 2.2.2. The solvent for the DNA was prepared before dissolving the DNA and consisted of a mixture of DMF:H_2O = 9:1 (DMF, Sigma Aldrich, Spain), additionally containing 0.3 M $MgCl_2$ (Sigma Aldrich, Spain).

2.2.5. Patterning on glass with click chemistry

Modification of the glass with (3-Glycidyloxypropyl)trimethoxysilane

Glass Micro slides 75 x 25mm^2 (Corning Inc., USA) were used as delivered for Nanoplotter patterning and for Dip-pen experiments they were cut into 1 x 1cm^2 pieces prior to cleaning. Glass slides were cleaned in piranha acid (7:3 v/v solution of H_2SO_4 and H_2O_2) for 30 min, rinsed with copious amounts of MilliQ water and dried with pressurized air. The samples were then immersed in a 1% v/v solution of (3-Glycidyloxypropyl)trimethoxysilane (GPTMS, Aldrich, Spain) in toluene (Panreac, Spain) for 8 h at room temperature, afterwards rinsed with acetone and dried with pressurized air. Immediately afterwards, the epoxy ring-opening was performed by immersing the substrates in a 2% v/v solution of propargylamine (Aldrich, Spain) in acetonitrile (Sigma Aldrich, Spain) for 8 h at 45ºC. The samples were taken out of the solution, sonicated in ethanol for 5 min, rinsed thoroughly with ethanol and Milli-Q water and dried with pressurized air. If the samples were not used directly, they were stored at 4ºC under argon atmosphere. Figure 36 shows the reaction scheme for the functionalization of glass yielding an alkyne group.

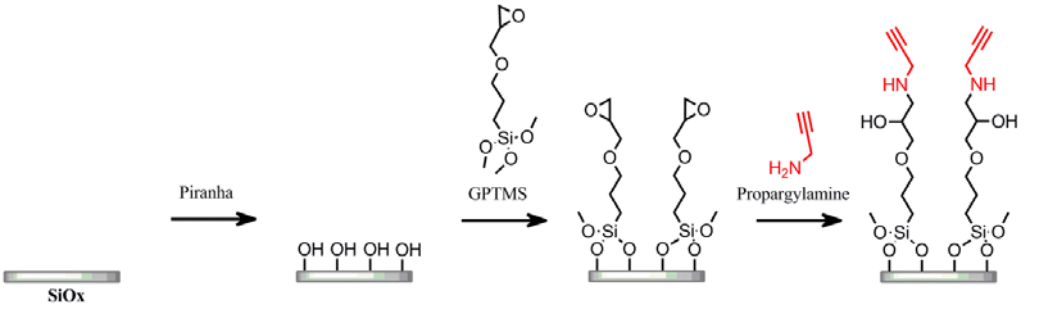

Figure 36: Reaction scheme of the functionalization of glass with GPTMS and propargylamine.

Surface characterization via X-ray photoelectron spectroscopy (XPS)

The two-step surface functionalization was monitored by XPS and measurements were performed using a PerkinElmer PHI 5500 Multitechnique System from Physical Electronics (Waltham, USA) with a monochromatic X-ray source (Aluminum KR line of 1486.6 eV energy and 350 W) placed perpendicular to the analyzer axis and calibrated using the 3d 5/2 line of Ag with a full width at

half-maximum (fwhm) of 0.8 eV. Core level scan spectra of carbon 1s, oxygen 1s, nitrogen 1s and silicon 2p were recorded, whereas the analysis area was ~0.5 mm^2). The resolution for the spectra was 187.5 eV of pass energy and 0.8 eV/step for general spectra, and 23.5 eV of pass energy and 0.1 eV/step for spectra of the different elements. All measurements were performed in an ultra-high vacuum (UHV) chamber with pressure levels between 7 x 10^{-9} and 3 x 10^{-8} mbar. When necessary, a low energy electron flood gun (0-3 eV) was used to discharge the samples. Peak fitting was performed using MultiPak V6.0A software from Physical Electronics Inc. (Chanhassen, USA).

Patterning of oligonucleotides at the microscale

The catalyst solution, containing Cu(I)I (Sigma Aldrich, Spain), Tris[(1-benzyl-1*H*-1,2,3-triazol-4-yl)methyl]amine (TBTA; Aldrich, Spain) and *N,N*-Diisopropylethylamine (DIPEA; Sigma Aldrich, Spain) was prepared separately in DMSO (Sigma Aldrich, Spain) and added to the oligonucleotide directly before patterning. The oligonucleotides "CT" and "GA" (Sigma Aldrich, Spain) were dissolved in MilliQ. The solvent for all mixtures and for plotting was DMSO:MilliQ = 1:1.

Table 5: Solutions used for patterning with the Nanoplotter.

Entry	Name	Concentration
1	E (CT + cat)	11 µM CT, 1.1 mM Cu(I)I, 1.1 mM TBTA, 1.3 mM DIPEA
2	B (CT)	11 µM CT
3	D (GA + cat)	11 µM GA, 1.1 mM Cu(I)I, 1.1 mM TBTA, 1.3 mM DIPEA
4	C (catalyst)	1.1 mM Cu(I)I, 1.1 mM TBTA and 1.3 mM DIPEA
5	A (solvent)	DMSO : MilliQ

Printing was carried out at 4ºC and 60% relative humidity with a robotic non-contact piezoelectric plotter (Nano-Plotter, GeSiM GmbH, Germany) using a so called Nanotip. The plotted volume was 0.4 nL and the correct formation of the droplet was

checked for each solution before patterning. Washing steps were done before and during patterning steps to minimize cross contamination.

After successful plotting, the surface was incubated overnight to ensure triazole formation and then rinsed with MilliQ and DMSO to remove unreacted oligonucleotides and catalyst. At this point, the sample was examined with Time-of-flight secondary ion mass spectrometry (ToF-SIMS) to compare the surface functionalization. Also, the autofluorescencce of the surface modification was ruled out by checking the substrate with fluorescence microscopy. Subsequently, the substrate was incubated for 1 h at room temperature in 1% BSA in PBS to block unspecific adsorption, rinsed with PBS and incubated for 1 h at 36ºC with 10 μM complementary oligonucleotide "AG" (Sigma Aldrich, Spain) in hybridization buffer (10 mM TRIS base, 1 mM EDTA and 1 M NaCl in MilliQ). Afterwards, the sample was rinsed with hybridization buffer and MilliQ and examined with fluorescence microscopy. The microscope used for all fluorescence images was an Eclipse E1000 upright microscope (Nikon, The Netherlands) equipped with a charge-coupled-device (CCD) camera and working with a several excitation filters.

Surface characterization via ToF-SIMS

Measurement of the phosphorus signature for DNA was performed using a ToF-SIMS IV instrument (ION-ToF, Germany) operated at a pressure of 5×10^{-9} mbar. Samples were bombarded with a pulsed bismuth liquid metal ion source (Bi 3þ), at 25 keV. The gun was operated with a 20 ns pulse width, 0.3 pA pulsed ion current for a dosage lower than 5×10^{11} ions/cm^2 , well below the threshold level of 1×10^{13} ions/cm^2 generally accepted for static SIMS conditions. Secondary ions were detected by a reflection time-of-flight analyzer, a multichannel plate (MCP) and time-to-digital converter (TDC). Measurements were performed with a typical acquisition time of 20 s, at a TDC time resolution of 200 ps. Charge neutralization was achieved with a low energy (20 eV) electron flood gun, thus no sample conductive coating was needed before the measurements. Secondary ions were extracted with 2 kV voltage and were post-accelerated to 10 keV kinetic energy just before hitting the detector. The maximum mass resolution, $R = m/\Delta m$, was around 8000, where m is the target ion mass and Δm is the resolved mass difference at peak half-width. Secondary ion

spectra in negative mode were acquired from randomly rastered surface areas of 500 μm x 500 μm along the slide.

Patterning of oligo "CT" with DPN as molecular ink

The catalyst solution, containing CuI, TBTA and DIPEA, had already been prepared separately and was added to the oligonucleotide directly before patterning. The final ink contained 61 μM oligo "CT", 6.1 mM Cu(I)I, 6.1 mM TBTA and 7.2 mM DIPEA in a solution of DMSO : MilliQ (1:1). A single cantilever (type CSC-17, MikroMasch, Germany) was activated in an ozone cleaner (UV/Ozone ProCleaner™ Plus, BioForce Nanosciences Inc, USA) and directly afterwards incubated in the freshly prepared solution for 20 min and dried in a nitrogen stream. Patterning was carried out in Dimension 3100 atomic force microscope (Veeco Instruments, USA) at a relative humidity of over 80%. As pattern, a square was chosen with an area of 1 μm² and the scanning rate for deposition was set to 0.5 Hz. In order to deposit sufficient material, every square was scanned twice. After patterning, the substrate was incubated overnight to ensure the formation of the triazole and then rinsed thoroughly with DMSO and MilliQ. Subsequently, the substrate was passivated with 1% BSA in PBS for 1 h at room temperature, rinsed with PBS and finally and incubated for 1 h at 36ºC with 10 μM complementary oligonucleotide "AG" in hybridization buffer (10 mM TRIS base, 1 mM EDTA and 1 M NaCl in MilliQ). Afterwards, the sample was rinsed with hybridization buffer and MilliQ and examined with fluorescence microscopy. The microscope used for all fluorescence images was an Eclipse E1000 upright microscope (Nikon, The Netherlands) equipped with a charge-coupled-device (CCD) camera and working with a several excitation filters. Subsequently, the sample was examined with fluorescence microscopy.

Patterning of oligo "CT" with DPN as liquid ink

The catalyst solution, containing CuI, TBTA and DIPEA, had already been prepared separately and was added to the oligonucleotide directly before patterning. The final ink contained 51 μM oligo "CT", 5.1 mM Cu(I)I, 5.1 mM TBTA and 6.0 mM DIPEA in a solution of DMSO : MilliQ (1:1) and 20 vol-% of glycerol. Since the dots deposited with DPN are smaller than the ones from the Nanoplotter, the concentration was increased five-fold in order to deposit sufficient material on the

surface. A single microcantilever print head with "ink cartridge" type SPT-S-C10S (BioForce Nanosciences Inc., USA) was activated for 10 min in an ozone cleaner (UV/Ozone ProCleaner^{TM} Plus, BioForce Nanosciences Inc, USA) and directly afterwards filled with approximately 2 µl of the freshly prepared ink solution. Patterning was carried out in an NLP2000 instrument (NanoInk Inc. USA) with a relative humidity of 30% and a temperature of 20°C. Patterning parameters for the arrays were 4 x 4 dots, 20 x 20 dots and 20 x 40 dots, whereas the spacing between the dots ranged from 10 µm to 20 µm and the dwell time was dt = 0.01 s. After patterning, the substrate was incubated overnight to ensure the formation of the triazole and then rinsed thoroughly with DMSO and MilliQ. Subsequently, the substrate was passivated with 1% BSA in PBS for 1 h at room temperature, rinsed with PBS and finally and incubated for 1 h at 36ºC with 10 µM complementary oligonucleotide "AG" in hybridization buffer (10 mM TRIS base, 1 mM EDTA and 1 M NaCl in MilliQ). Afterwards, the sample was rinsed with hybridization buffer and MilliQ and examined with fluorescence microscopy. The microscope used for all fluorescence images was an Eclipse E1000 upright microscope (Nikon, The Netherlands) equipped with a charge-coupled-device (CCD) camera and working with a several excitation filters. Subsequently, the sample was examined with fluorescence microscopy.

2.2.6. Assessment of the sensitivity of the sensor platform

The sensitivity of the created sensor platform was determined for 5 x 5 arrays by hybridizing it subsequently with different concentrations of complementary oligonucleotide (bearing a fluorophore). Between the hybridization steps, denaturing was performed by immersing the substrate for 2 min in 10 mM NaOH and subsequent rinsing with copious amounts of MilliQ-water. The surface was then passivated for 20 min in 1 % BSA and hybridized again for 1 h. After hybridization, the platform was washed carefully with MilliQ-water to remove the excess hybridization solution. The concentrations used for this experiment ranged from 100 pM to 10 µM: 100 pM, 1 nM, 10 nM, 100 nM, 1 µM and 10 µM.

The arrays were analyzed using ImageJ software with a special plug-in for Microarray Analysis. Using this software, the intensity for each spot in the array was calculated (25 spots per array) after background correction. The average of the 25 values and the standard deviation were calculated using MS Excel. Figure 37 shows the schematic representation of an array, indicating the spot numbers for analysis of all 5 spots. The spot diameter was set to the value "diameter for spots" = 25 in order to cover the whole area of the spots.

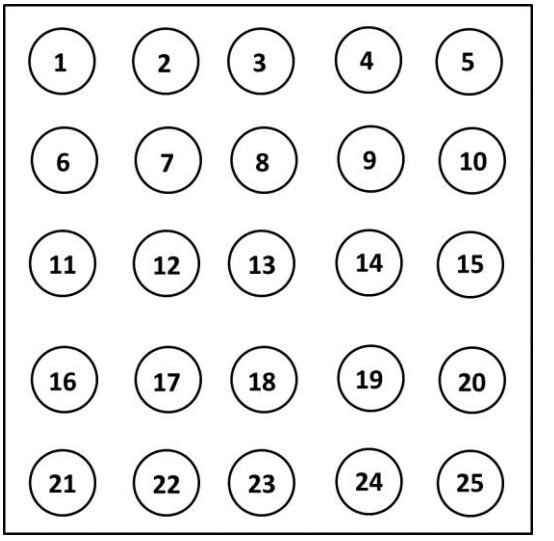

Figure 37: Schematic representation of the spot numbering in the analyzed 5 x 5 spot oligonucleotide arrays.

2.3. RESULTS AND DISCUSSION

2.3.1. Patterning on SMPB-glass via DPN using PBS/glycerol (liquid ink)

Patterning of "RRSoja" (thiol, FAM)

The first experiments of patterning an oligonucleotide on SMPB-modified glass were performed with a model oligo called RRSoja, which apart from the thiol group has a fluorophore already incorporated (fluorescein = FAM) in order to avoid the hybridization step. This way, possible errors coming from the hybridization step are eliminated and the sources are the deposition or attachment of the oligo itself.

The deposition of RRSoja oligonucleotide on glass via Dip-pen Nanolithography was verified with fluorescence microscopy directly after patterning. Figure 38 shows the so called "bleeding dots" which are created when the excess of ink on the tips has to be removed in order to ensure proper patterning. Above the bleeding dots are small squares which are the patterned arrays. In this case, there was still too much ink on the tips which caused a merging of the single dots and resulted in a completely filled square. The writing direction was from bottom to top.

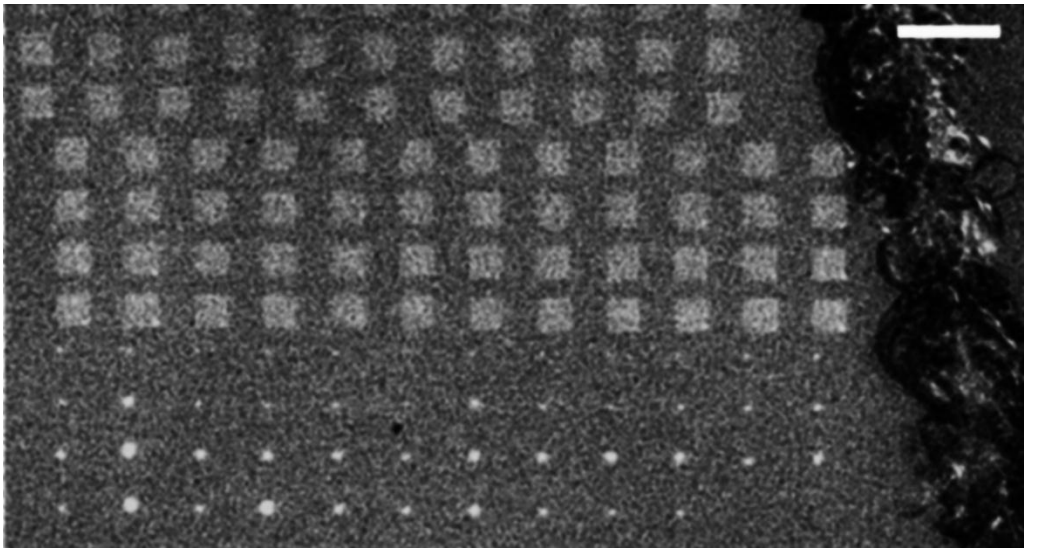

Figure 38: Fluorescence microscopy image of an oligonucleotide pattern created by Dip-pen Nanolithography. The scale bar equals 66 µm.

After sufficient removal of ink, the tips start patterning neatly single dots. Unfortunately, and this is a characteristic of each cantilever, not all tips start patterning at the same moment. Figure 39 is a merge of several images taken with fluorescence microscopy. The numbers 1 to 12 indicate the different tips (12 cantilevers on the M-type chip) and the arrows give the writing direction, whereas the small arrow indicates the patterning direction inside each array (left to right and top to bottom) and the large arrow indicates the order in which the different arrays were written. It is obvious that the tips have different patterning behavior which results in inhomogeneous deposition of the ink because the squares in each row are not equal (some have already well resolved and separated ink dots whereas others are still merging from an excess of ink).

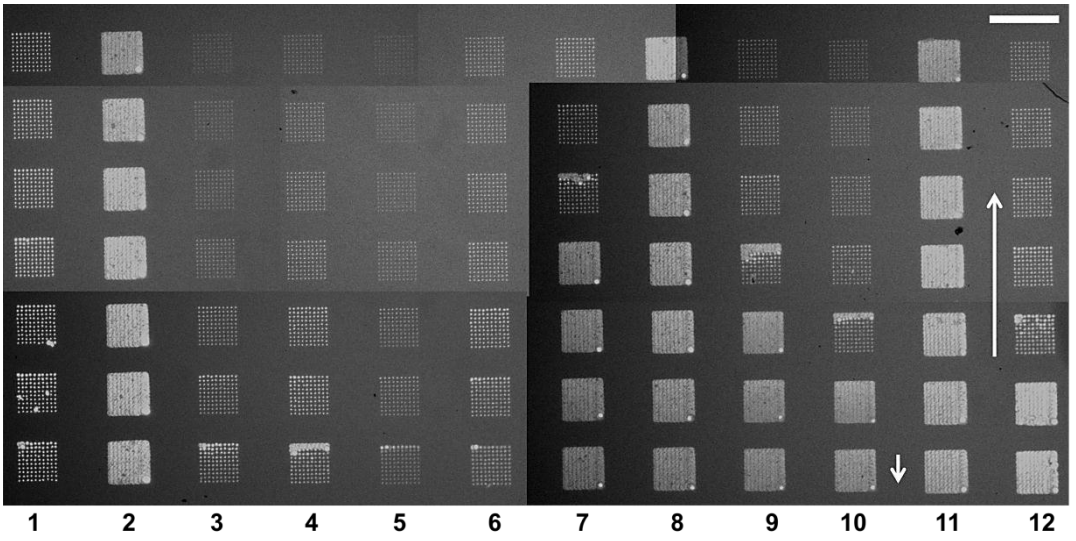

Figure 39: Merge of several fluorescence microscopy images of subsequently patterned arrays. The number indicate the 12 different tips which are on the M-type chip and the arrows indicate the in-array patterning direction (small) and the general writing direction (large). The scale bar equals 50 µm.

Figure 40 is a magnification of Figure 39 where a perfectly homogeneous array set can be appreciated. All images were taken directly after patterning and without previous rinsing of the surface.

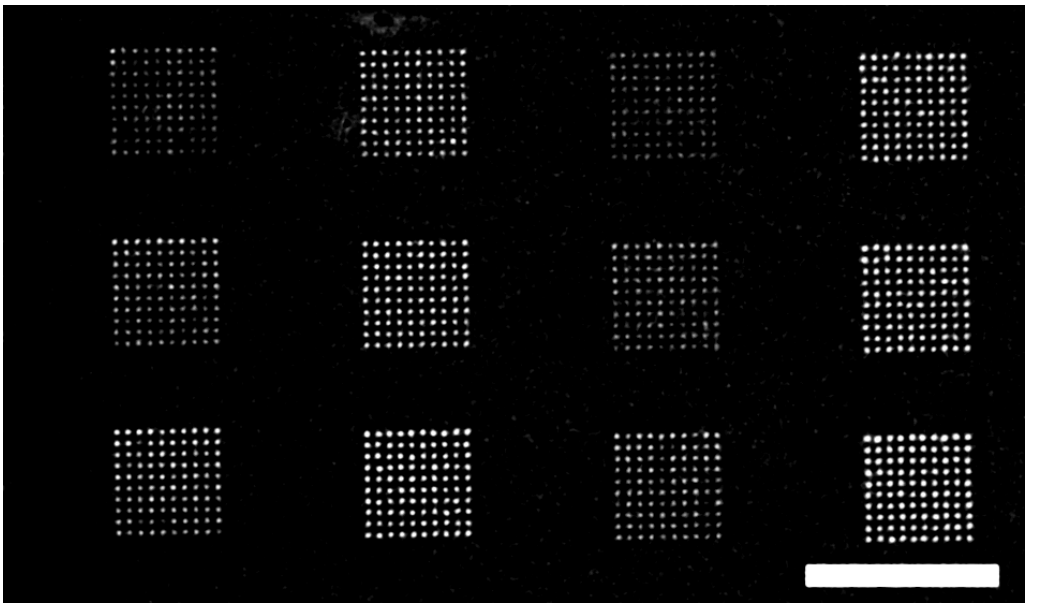

Figure 40: Fluorescence microscopy image showing the magnified area of Figure 39 namely tips 3-6. The scale bar equals 50 µm.

Figure 41 shows the word DNA which was also deposited with DPN as to show the capability of the technique. Image a) was taken directly after patterning, whereas b) shows the same area after washing and a dramatic decrease in fluorescent signal can be observed. This might be due to, on one hand, the little immobilization of oligonucleotide on the substrate or, on the other hand, due to bleaching of the fluorescent label by repeated exposure to light and to the laser of the DPN instrument, which cannot be switched off during lithography.

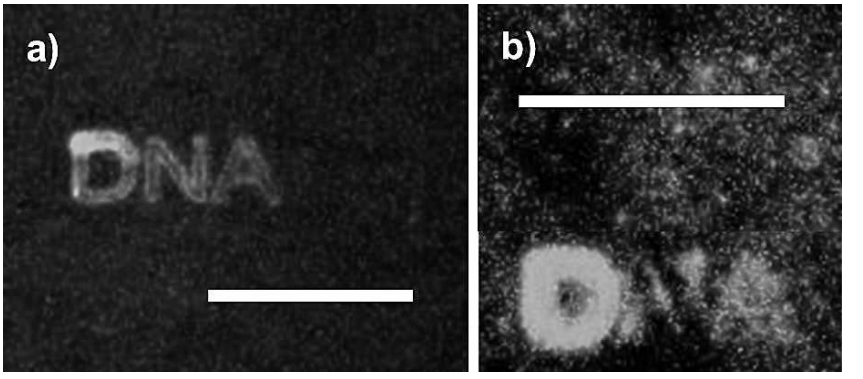

Figure 41: Fluorescence microscopy images of the letters DNA deposited with DPN. a) Shows the area before and b) after washing. The scale bars equal 30 µm.

Patterning of oligo "N3down" (thiol)

After proving that the patterning and immobilization of "RRSoja" was possible on SMPB modified glass, the next step was the immobilization of an oligonucleotide without fluorescent group, subsequent passivation of the surface and hybridization with a fluorescently marked complementary strand (in this case fluorescein). This way, two new error sources are introduced, the passivation and the hybridization step. On the other hand, since the fluorescent label is introduced in the last step, it is less likely that bleaching will occur.

Figure 42 shows fluorescence microscopy images of two areas of arrays from the patterning of "N3down". As already explained before, the patterning characteristics of the tips cause inhomogeneous ink deposition and arrays. Also, only little fluorescent signal was obtained.

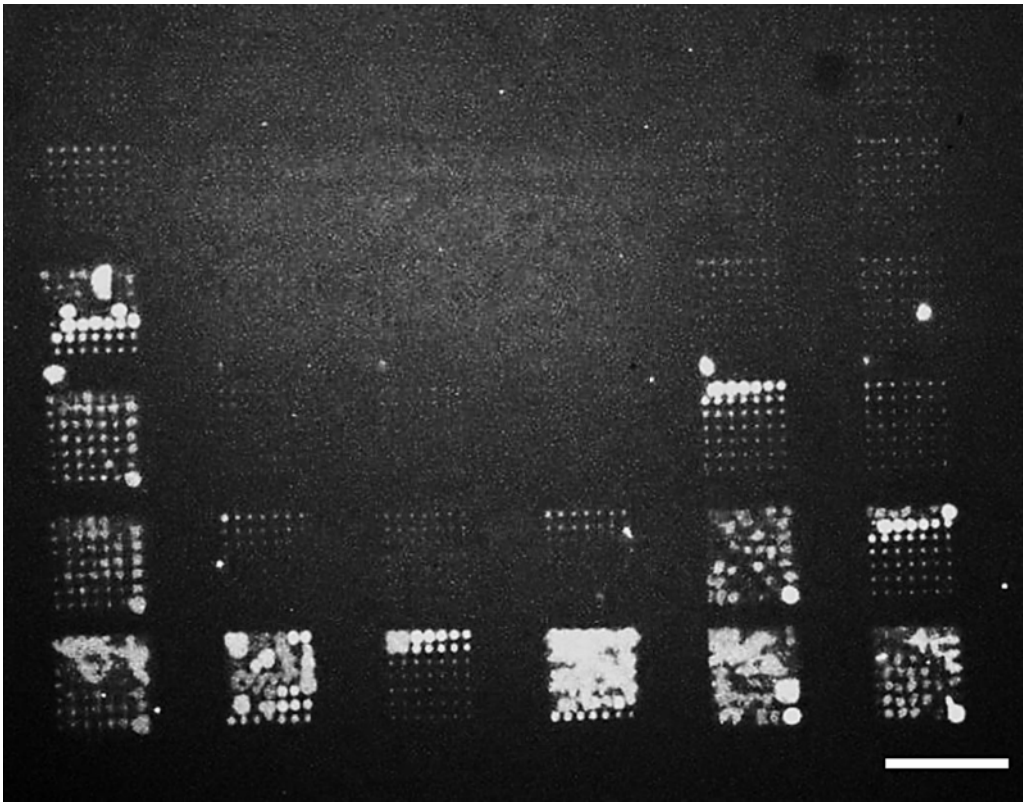

Figure 42: Fluorescence microscopy image of arrays of oligo „N3down" deposited on SMPB modified glass and hybridized with „N3up" (FAM). The scale bar equals 50 µm.

There is one mayor problem when using oligos with a thiol group, which is labile to oxidation and is usually protected with dithiothreitol (DTT),[83] which is bound to the oligo via a disulfide bond. In order to deprotect the oligo, it is passed through a column whereas the sample volumes are fixed and given by the column protocol. Therefore, the concentration of the oligo is not freely eligible but fixed. Nevertheless, it can be increased by means of an Eppendorf concentrator where the water is evaporated from the solution under vacuum. This procedure can be repeated only a few times because the salts from the PBS solution remain and thus the solution has a higher salt concentration every time the water is evaporated. The elevated salt concentration interferes in the writing process by DPN where crystals form on the tips, which makes this ink composition suitable to only a limited extent. The recommended concentration for deposition of DNA with Dip-pen Nanolithography is around 1 mM.[24] Nevertheless, deprotection of the oligonucleotide is necessary since the reaction of the protected thiol group or a disulfide group with maleimide is minimal and the immobilization of the oligo therefore insufficient.

2.3.2. Patterning on gold via DPN using PBS/glycerol (liquid ink)

Patterning of oligo "20down" (thiol)

In order to avoid the not satisfying surface functionalization of glass, the following experiments were performed on gold surfaces. This way, it is not necessary to deprotect the oligonucleotides from the DTT group because it has already been reported that also disulfides are immobilized on gold.[84]

In a first experiment, the oligonucleotide "20down" was deposited by DPN and after incubation overnight and passivation of the surface, the complementary strand "15up" (with a 10 nm gold particle at one end) was incubated on the substrate. Figure 43 shows the AFM topography image of the patterned area, where the top image is an AFM topography image. The bottom image represents the height profile taken from the evaluation of the topography image, proving the presence of the 10 nm big gold particles (see peaks of approx. 10 nm height).

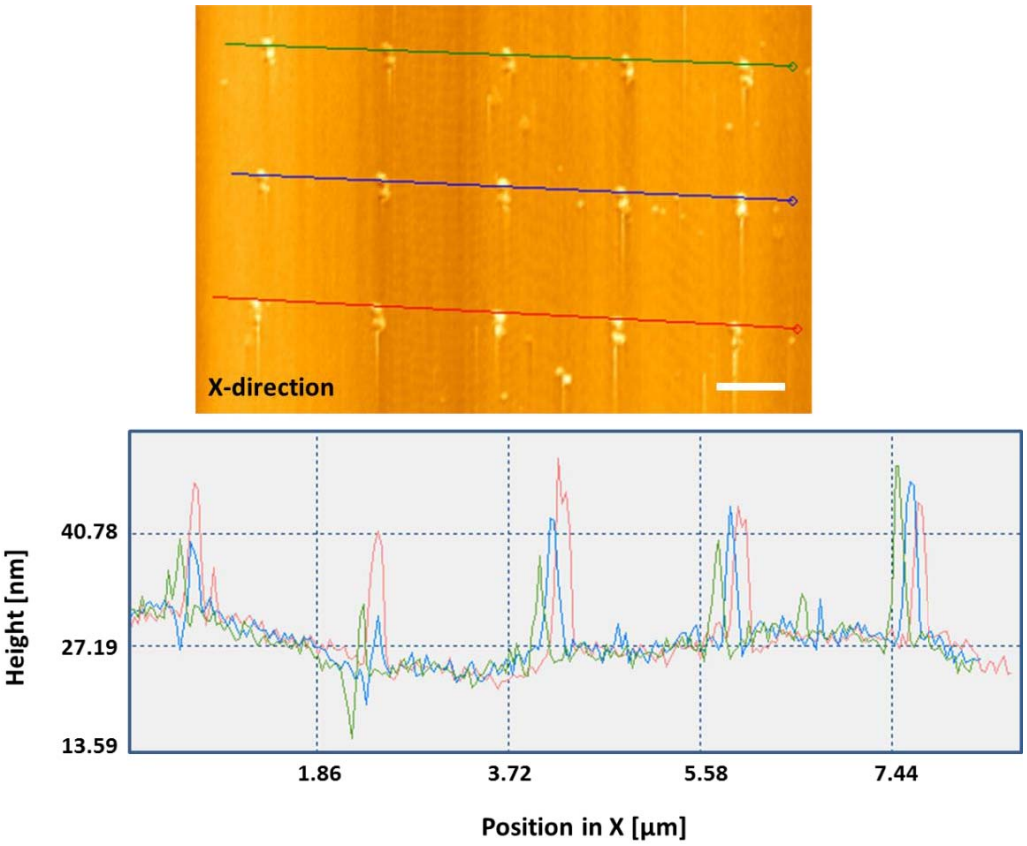

Figure 43: AFM topography image (above) and line analysis: The white features on the top image and the corresponding height change (peaks in the image below) prove the presence of the gold particles (10 nm) and thus successful hybridization. The scale bar equals 1 µm.

Since the pattern is obtained by deposition of small liquid drops, the operation mode of the Dip-pen AFM is the constant height mode. This means that before patterning, the 12 tips have to be leveled with respect to the relative sample surface. By motor movement, they are then brought in a distance to the surface which is constant throughout the patterning routine. The patterning itself is performed by small up and down movements of the piezo elements. This means, the patterning is done without laser feedback and thus without automatic force control, what may result in the production of holes instead of ink deposition. The reason therefore can be insufficient leveling on one hand or, on the other hand, too close contact to the surface. The point of contact has to be determined by eye and the tips are therefore touching the sample relatively hard. While this was no problem when patterning on glass, on gold surfaces it is very difficult to avoid making holes without laser feedback

because, in contrast to glass, gold is a very soft material. Furthermore, the tips have to have a high spring constant as to not bend with the liquid drop or, during retracting the tips from the surface, get stuck there due to the meniscus of the liquid. Figure 44 a) shows the SEM image of a so called "bleeding dot". These dots are generated when the excess of ink is removed by briefly touching the surface with the tips and leaving a quite big droplet behind. This process has to be repeated until the created dot is sufficiently small to avoid smearing of the pattern from overflowing dots. The white arrow indicated where the tip of the cantilever touched the substrate. Furthermore, Figure 44 b shows part of a patterned area which consists of 14 x 14 dots and the white arrow indicates the patterning direction. It is clearly visible that the patterning force changed during the lithography process, being reflected in the holes getting lesser with progressive patterning. This problem has already been explained in Chapter 1 but summarized shortly: the control over the force exerted on the surface during patterning with liquid inks has to be controlled by eye. This means that factors like camera resolution, illumination and contrast and finally also the "sensitivity" of the own eye play an important role in the process of avoiding making holes during lithography. It is also important to point out that a difference as small as 5 µm of the cantilever being "too close" to the surface can make the difference between making or not making holes.

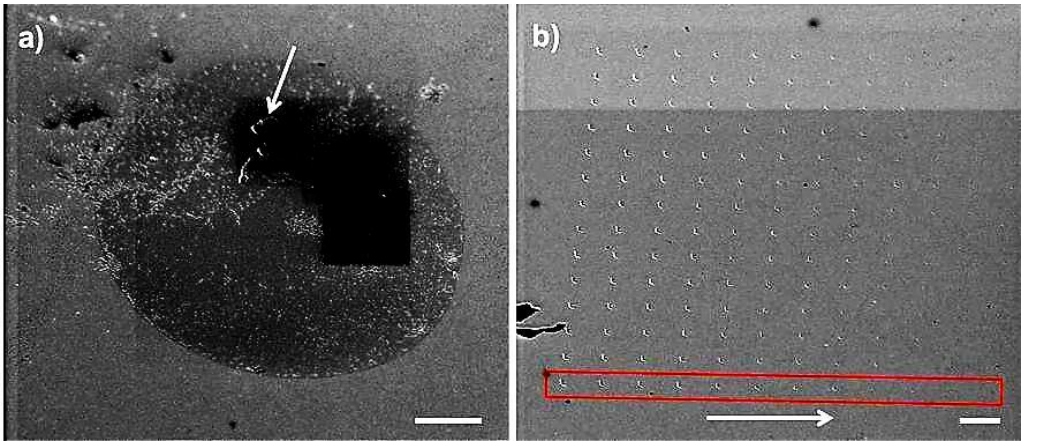

Figure 44: SEM images of oligo "20down". a) shows a so called "bleeding dot" and the white arrow indicates the holes which were made by the cantilever tip. The grey areas indicate pictures taken at higher magnification. b) A 14 x 14 array of holes where the white arrow indicates the writing direction and the red box the decreasing depth of holes which corresponds to decreasing pressure of the tips on the surface. The scale bars equal 2 µm.

Apart from only making holes, there were also some patterned areas where the pressure of the tips during lithography was gentle enough as to not create holes in the gold. Figure 45 shows such an area. In the images a) and b), a "bleeding dot" can be seen and the small white objects correspond to the gold nanoparticles of the complementary strand. Furthermore, it is also visible that the spot itself appears darker than the surrounding surface which is due to the solvent of the ink (PBS and glycerol). Images c and d correspond to an area inside in an array and no holes are visible.

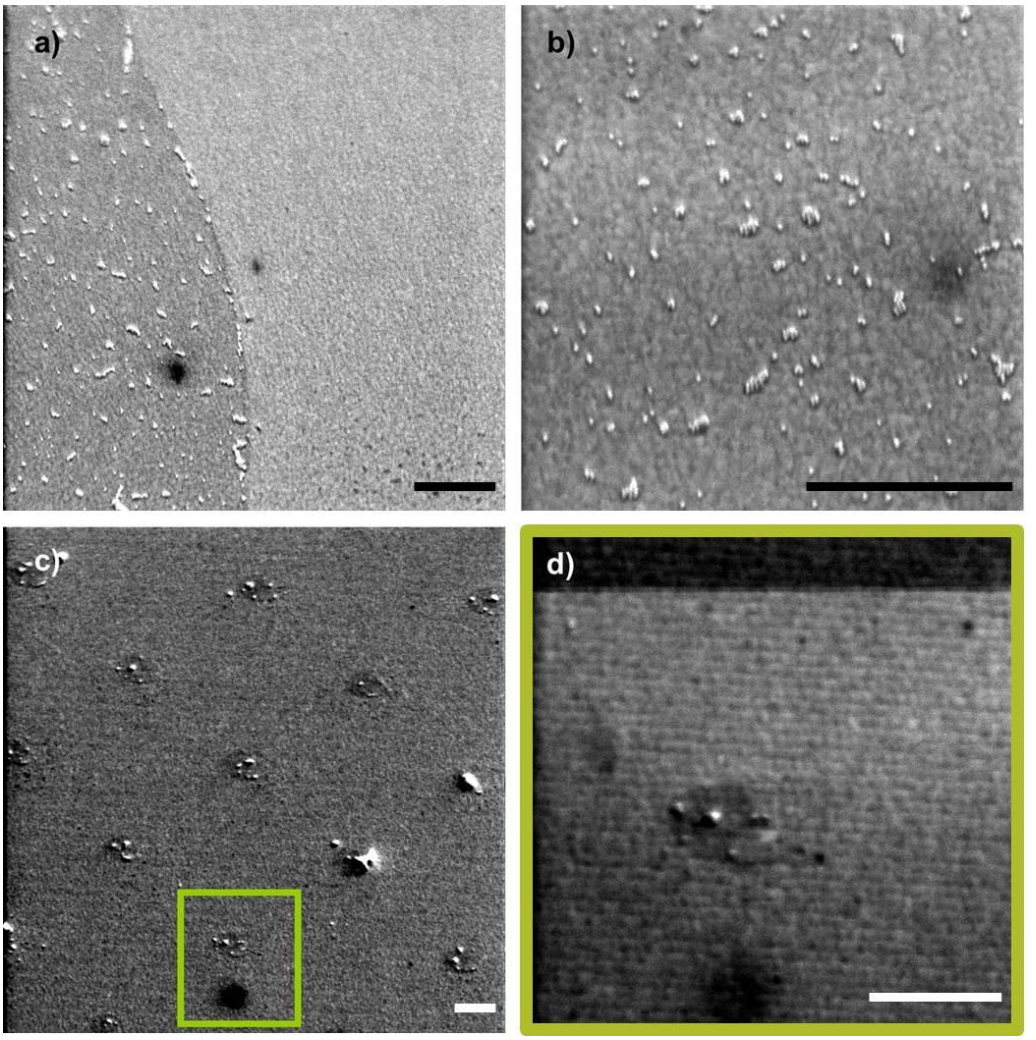

Figure 45: SEM images of oligo "20down" and subsequent hybridization with complementary oligo bearing a gold nanoparticle, visible as small white spots. a) part of a "bleeding dot" and b) zoom in on the "bleeding dot". c) Part of an array and inset d) zoom in on one spot of the array. The scale bars equal 500 nm.

Apparently, the complementary oligo only attached to the areas where "20down" was deposited (images a and c) and not to the intermediate passivated area. This confirms that the passivation method works well. Unfortunately, as can be observed in image d, there is only little complementary strand immobilized on the surface (only 1 gold particle in this specific dot). This is most likely due to the low concentration of oligo in the ink during patterning, so only few strands are present in the droplet and finally in the spot on the surface. This means that for the following experiments, the concentration has to be adjusted and made sure of before each experiment.

Patterning of oligo "N3down" (thiol)

It was possible to reduce the likeliness of making holes by an improved leveling routine. In Figure 46, the SEM image of a section of the patterned area without holes can be seen. The brighter spots represent the gold nanoparticles which have a diameter of 20 nm. The remaining gold area after patterning was passivated with ODT. Since there is a clear difference in nanoparticle density inside and outside of the spots, ODT seems a good passivating agent. The darker squares represent areas where the surface has been charged by the electrons used for scanning the sample, meaning that a picture has been taken before taking the overview image.

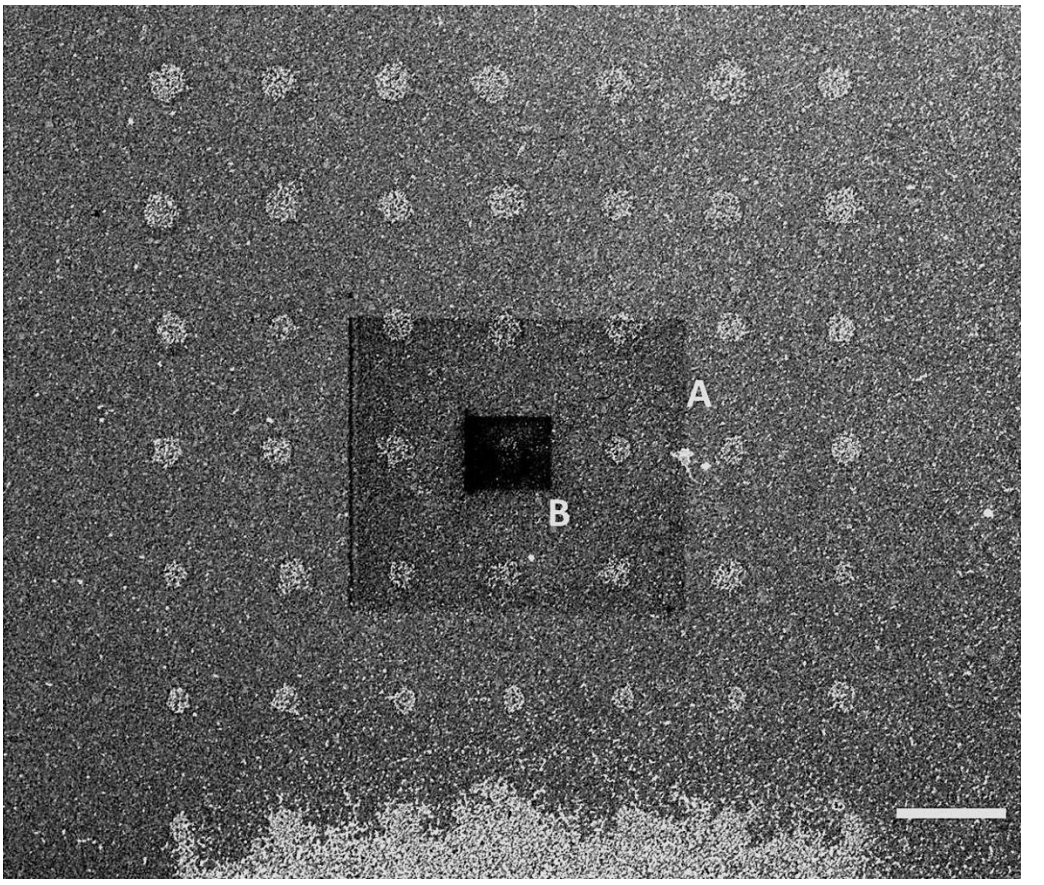

Figure 46: SEM image of an array of oligo "N3down" with subsequent passivation and hybridization with complementary oligo "N3up". The patterned area can be distinguished very well from the "background". The white color is due to the gold nanoparticles attached to the complementary strand. The letters A and B are enlarged areas visible in Figure 47. The scale bar equals 5 µm.

The areas are labeled A and B and can be appreciated in Figure 47 and Figure 48 as zoom. It is obvious that no holes have been made during lithography (especially in image B). It is also visible that there are more gold particles immobilized inside the pattern than outside, even though the "background signal" is quite high. An image analysis counting all the particles inside and outside the pattern resulted in the particle density inside the patterned areas being approximately 10 times higher than outside (76 particles / µm² inside the dots compared to 7 particles / µm² for the background).

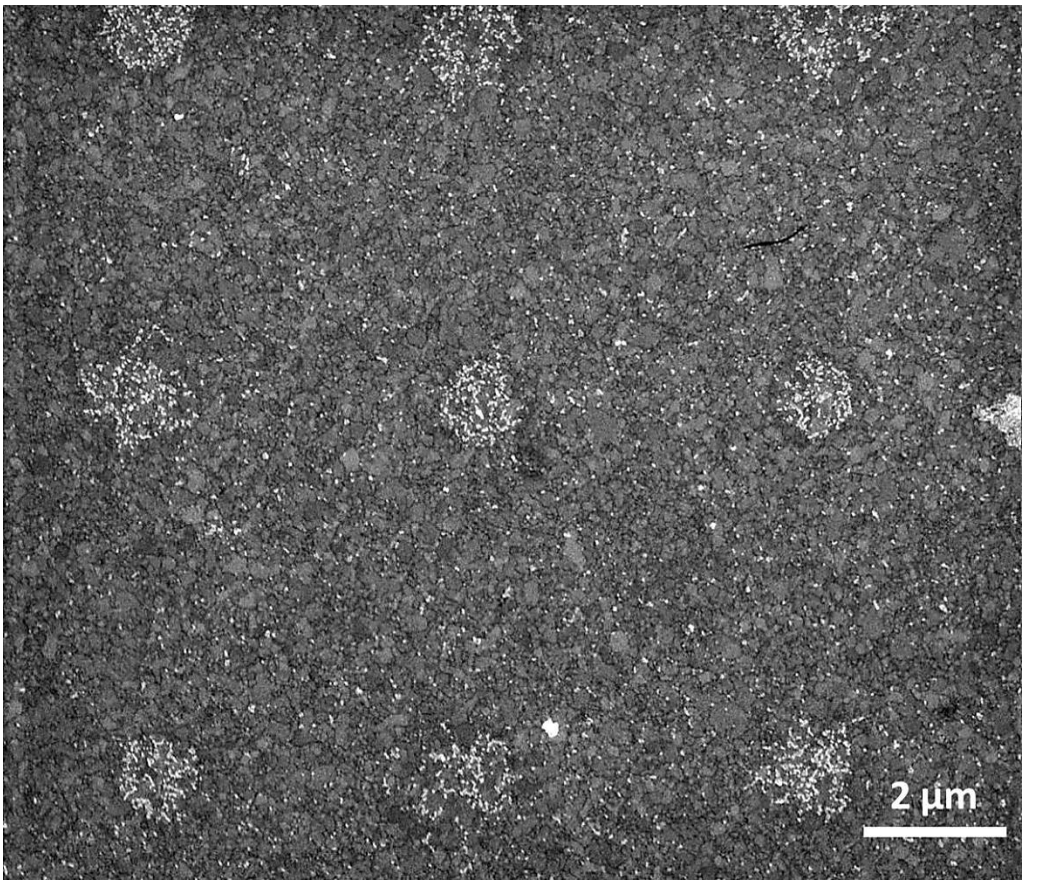

Figure 47: SEM images, enlarged area from Figure 46 area A. It can be observed that on one hand no holes were made and on the other, the concentration of the oligo in the deposited droplets is sufficiently high to ensure that more than a few oligo strands are immobilized. The scale bar equals 2 µm.

Despite these seemingly positive results, these parameters for lithography mostly result in the making of holes along with only little deposition, as can be seen in Figure 49. It furthermore becomes clear that an array having holes cannot be used for sensitivity measurements as a biosensor because there is no oligo deposited in the middle of the hole, only at the edges. This will yield in an inhomogeneous and erroneous signal.

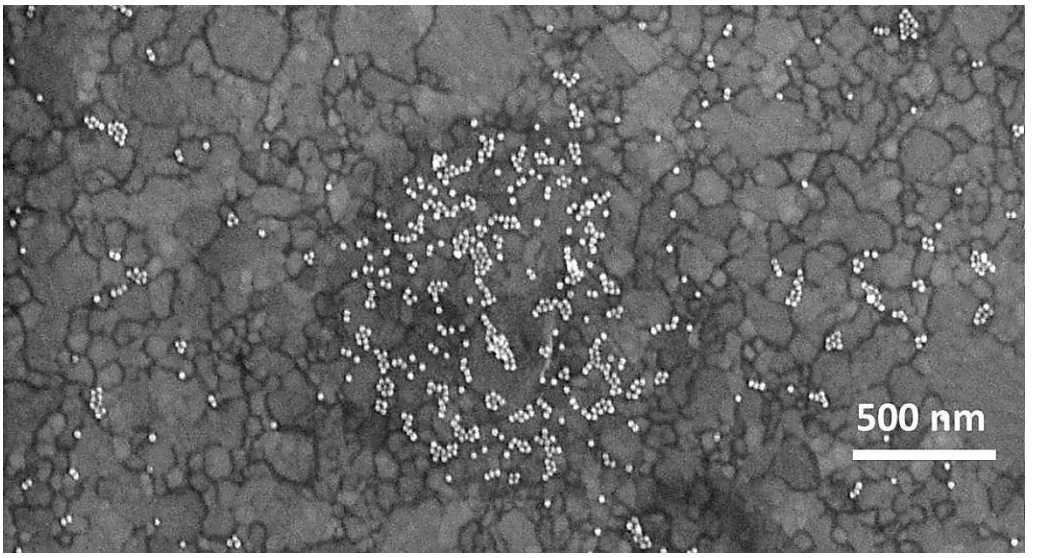

Figure 48: SEM images, enlarged area from Figure 46 area B. No hole can be seen inside the area with higher concentration of gold particles (white dots). The scale bar equals 500 nm.

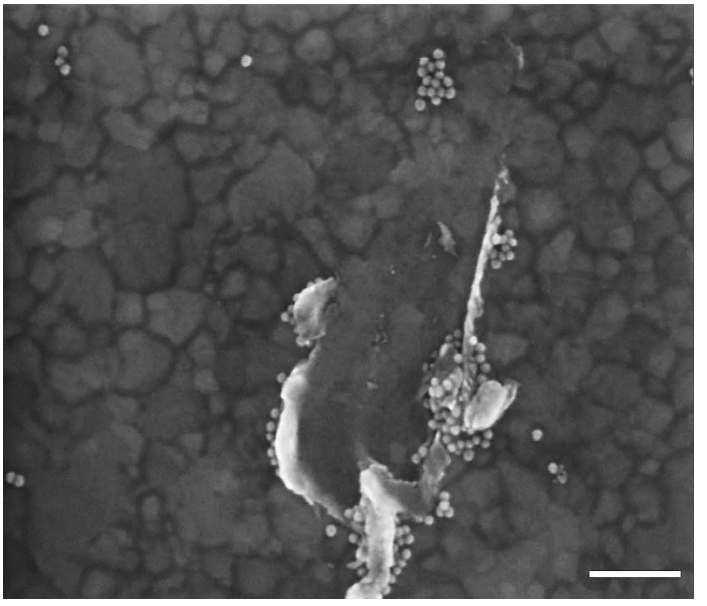

Figure 49: SEM images of a single dot in an array of dots, similar to the one shown in Figure 47. The difference is that this dot has a hole in the middle from the tip pressing too hard and only little complementary oligo is immobilized, meaning only little oligo deposited. The scale bar equals 200 nm.

2.3.3. Patterning on gold via DPN using "Just Add DNA" (liquid ink)

After launching a new DPN instrument which is working without laser but has greater travelling range and improved leveling routing, the following experiments were conducted with this new instrument. The patterning of oligo "S2down" was monitored during the lithography process via the built in microscope, which also allowed taking pictures after completing the patterning routine. Figure 50 shows a picture taken directly during lithography, in which the patterned area appears as quite homogeneous and with well resolved spots of liquid ink. The patterning parameters were 6 x 6 dots per array with a dwell time of 0.5 s and spot to spot distance of 10 µm. The spacing between the arrays was 20 µm in y-direction (writing direction) and 16 µm in x-direction (given by the spacing between the cantilevers being 66 µm). Furthermore, it can be appreciated that due to the improved deposition property of the tips, more homogeneous array sequences can be obtained with one tip and when comparing the tips amongst each other.

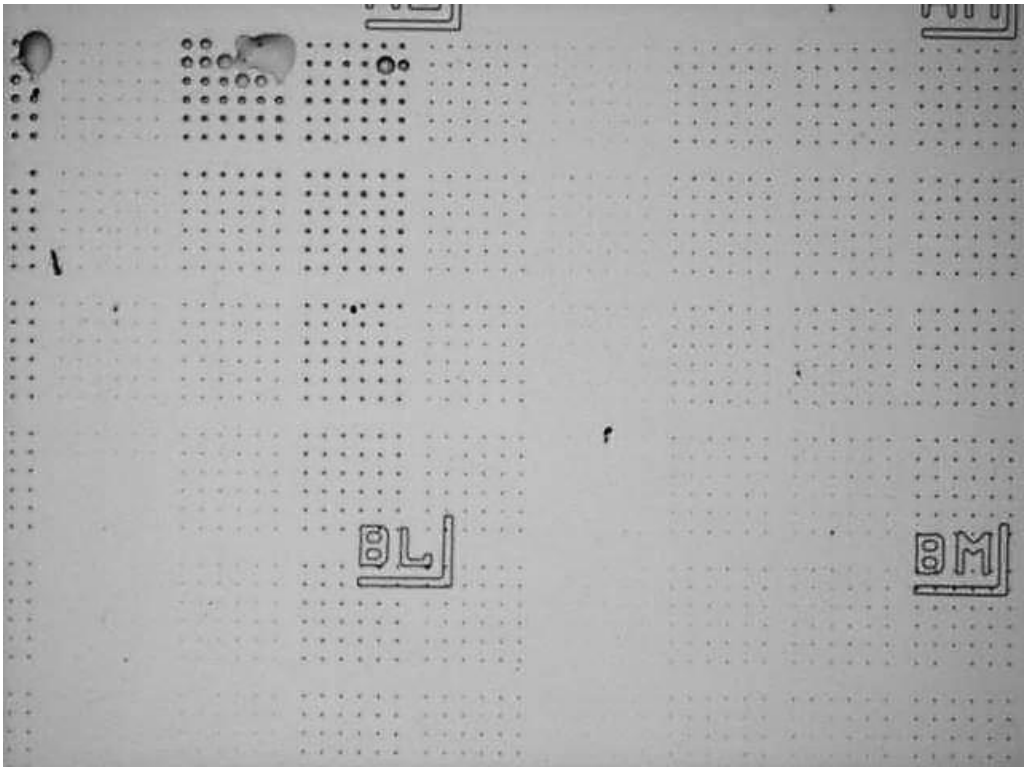

Figure 50: Brightfield microscopy image during the lithography process of oligo "S2down". The writing direction is from top to bottom.

In order to verify the deposition of ink and to evaluate what had been deposited, the substrate was incubated overnight and subsequently examined with SEM and AFM. Figure 51 shows several SEM images which were taken all over the patterned areas.

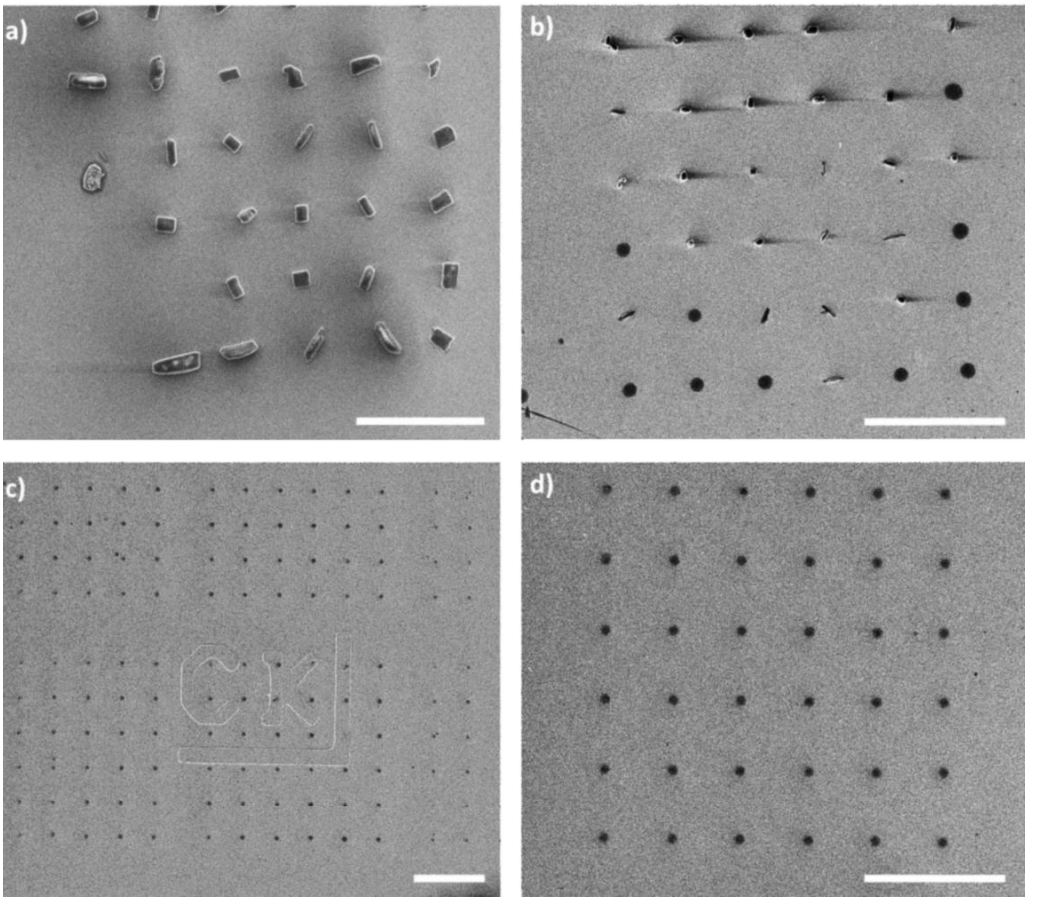

Figure 51: SEM images of the surface shown in Figure 50 after the ink has dried. Some areas of the sample suggest the formation of salt crystals, as shown in images a and b. Other areas, as shown in images c and d show no formation of salt crystals at all. The black spots result from the solvent of the ink.

Figure 52 shows the results of the AFM measurements of one array of the patterned area, with a) bright field microscopy image of the area; the red square indicates the scanned area which is shown in b), representing the topography image recorded in tapping mode. The white line shows where the height profile was taken as an example, which can be seen in c). It is obvious that the deposited material cannot consist only of oligonucleotides since the mean height of the dry dots

(118.20 nm ± 22.12 nm) is too high. It is assumed therefore, that the elevated height is due to salts from the solution.

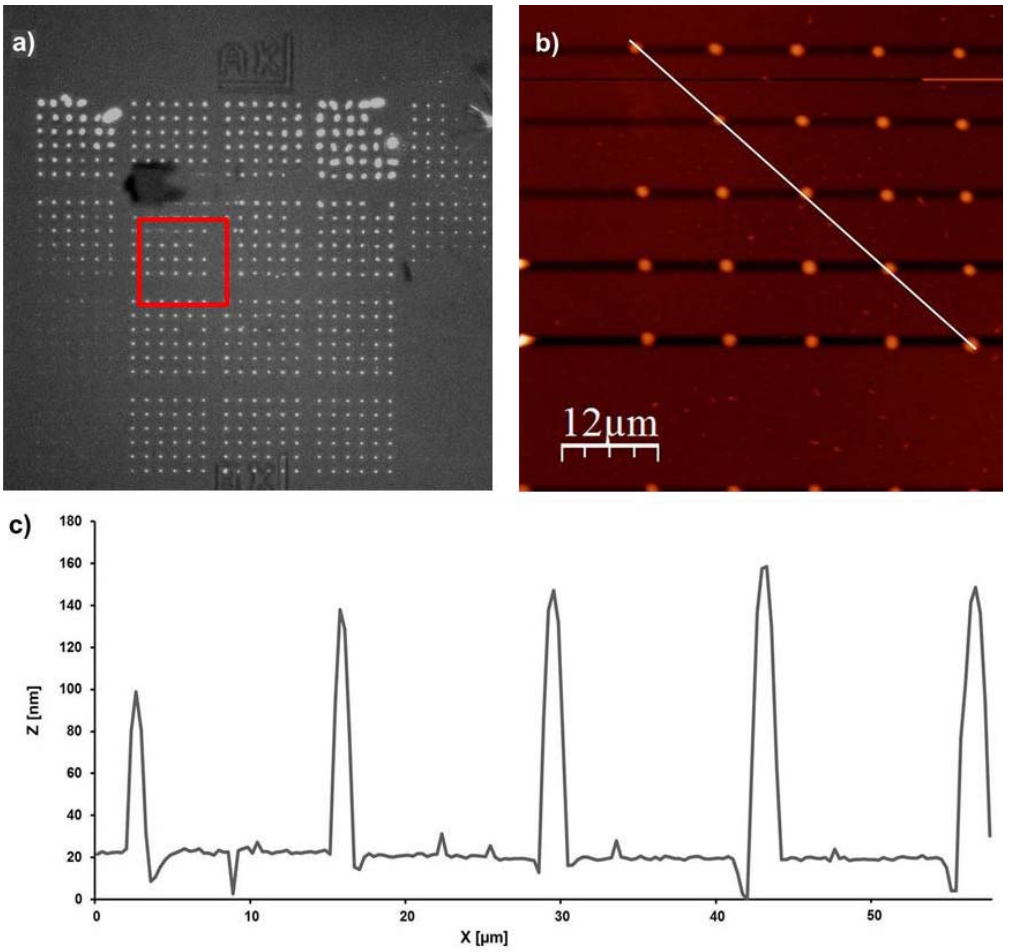

Figure 52: a) Bright field microscopy image of the scanned area. The red square indicates the scanned area, which is represented in b) as AFM topography image. The white line corresponds to the height profile, which is shown in c).

In order to remove the salt crystals, the sample was rinsed with Milli-Q water. Afterwards, it was examined with brightfield microscopy (data not shown here) and none of the before observed salt crystals could be detected. Since the surface appeared "clean", it was passivated and hybridized with a nanogold particle (10 nm) bearing complementary strand. Subsequent inspection of the sample with SEM revealed that no holes were made during the lithography process thanks to the new device (NLP2000, NanoInk Inc., USA) which allows for better leveling routine and surface

plane control and thus reduces the pressure of the tips on the surface (see Chapter 1). Even though this is a positive result and the goal of making no holes during lithography could be achieved, this fact, on the other hand, can also be a drawback: it was very difficult to locate the patterned areas even though alignment marks were of some help, precisely because no holes were made during patterning which could serve as orientation marks. Figure 53 shows the SEM images of the patterned area.

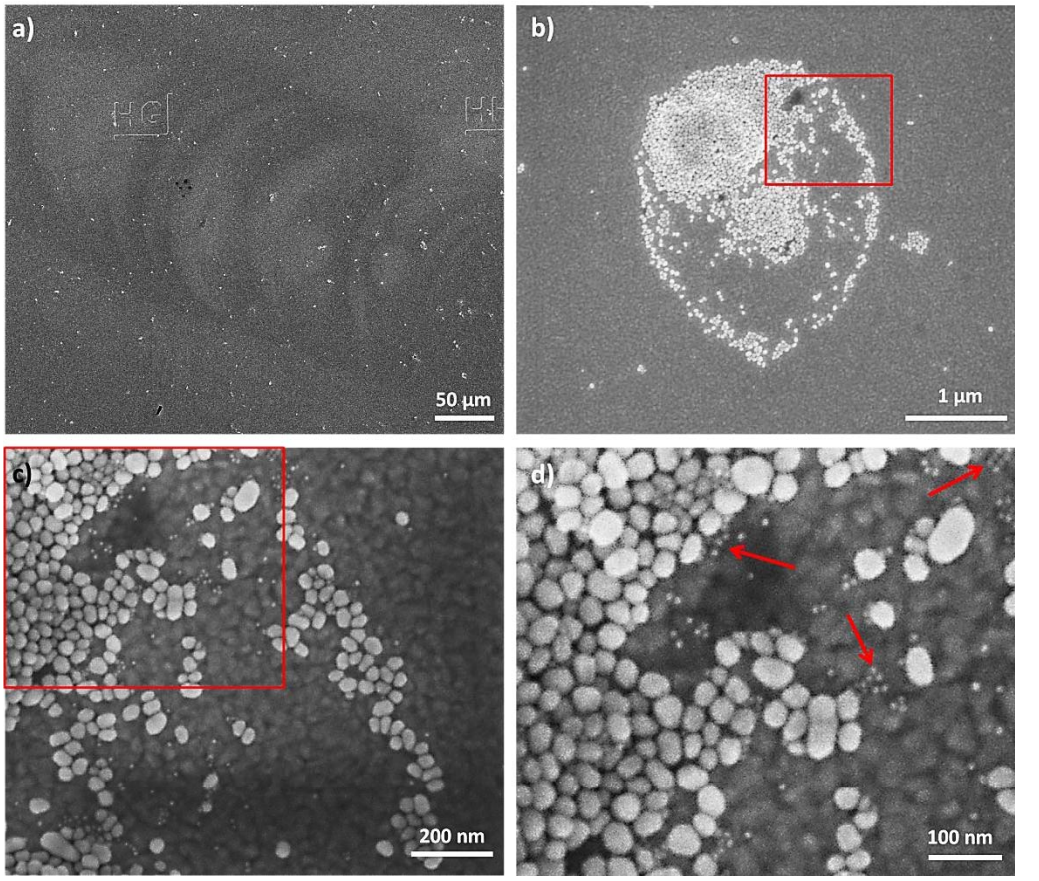

Figure 53: SEM images of the sample shown in Figure 50 - Figure 52, after hybridization with the complementary oligonucleotide strand, bearing a 10 nm gold nanoparticle. Image a) shows an overview over the area and no holes can be observed. Images b-d) represent a bleeding dot with a much bigger diameter than the dots in the pattern. Only in image d), the small 10 nm big gold particles can be seen. The bigger particles can come from the hybridization solution or from the smaller particles fusing to a bigger one.

It can be seen that the concentration of particles is elevated where big spots were located before or where merging of several dots had occurred. Almost no particles could be found on the other hand in the remaining areas. A reason might be

that the entire amount of oligonucleotide was deposited in the big drops ("bleeding dots", image b) and little or no oligo was left on the tip for the patterning of the remaining dots, which only consist of solvent and salts. It also becomes clear that the pattern has to be localized very well before zooming in for visualization of the gold particles since they are very small and cannot be seen at low magnifications (image a).

2.3.4. Patterning on gold via DPN using DMF/H_2O (molecular ink)

Following the already published protocol of depositing DNA as molecular ink on gold,[24] the solvent mixture of DMF and H_2O was prepared with 0.3 M $MgCl_2$. Despite mixing all ingredients thoroughly with a vortex mixer and using the ultrasonic bath, precipitation occurred and could not be avoided. Therefore, no further experiments were performed involving the solution of the oligonucleotide in the ink. Since no results could be obtained with this approach, it was discarded.

2.3.5. Patterning on glass with click chemistry

An immobilization method which has recently gained quite some interest for Dip-pen Nanolithography is the so called click chemistry. The advantage is a very stable functionalization of the substrate and a very selective anchoring only at the site where the ink has been deposited. In order to perform click chemistry on silicon oxide based substrates, they have to be modified chemically - in this case yielding alkyne groups on the substrate which will be able to react with an azide group and form the desired triazole.

Modification of the glass with (3-Glycidyloxypropyl)trimethoxysilane

Figure 54 shows the chosen functionalization strategy: Glass substrates were silanized with (3-glyxidyloxypropyl)trimethoxysilane (GPTMS) and directly afterwards used for the next reaction step, in order to ensure the functional reliability of the epoxy group. In the second step, the epoxy group is subjected to a ring-opening

reaction with propargylamine to give the alkyne group on the substrate and resulting in an aminoalcohol.

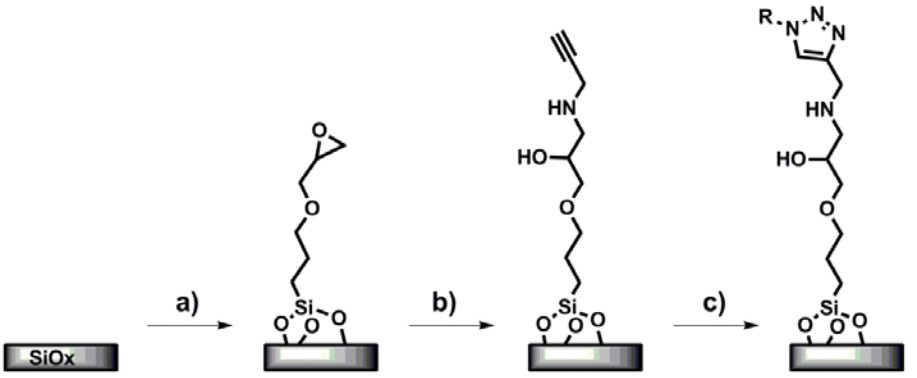

Figure 54: Functionalization strategy for silicon-oxide based substrates to enable surface click chemistry. a) Silanization step, including piranha cleaning and silanization with (3-glyxidoxypropyl)trimethoxysilane (GPTMS). b) Ring-opening of the epoxy group with propargylamine to yield an amino alcohol. c) Surface click reaction of immobilized alkyne with incoming azide R-N_3 to yield the 1,2,3-triazole.

Both functionalization steps can be considered clean since no side products are formed and no work-up is needed. On top of that, by using the epoxy group instead of a carboxyl moiety, no activation was necessary. In order to increase the stability of the platform for biological applications, the formation of an amino alcohol was preferred over the typical coupling via an amide group (peptide bond) because the latter is prone to being cleaved by proteases. The two-step surface functionalization was monitored by XPS. ToF-SIMS experiments were performed as complementary measurements because it was not possible to analyze the phosphorus signature (P 2p peak) with XPS measurements, as has been reported by Zhang *et al*.[85] Thus, the presence of DNA on the sample and negative controls was checked by ToF-SIMS experiments.

Surface characterization via XPS

Figure 55 gives an overview over the atomic composition of the surfaces and functionalization steps during the process of the fabrication of the click chemistry substrates. Glass stands for the bare but cleaned glass substrate, epoxy for the first functionalization step, alkyne for the second functionalization step and click for the surface on which the click reaction has been performed. All percentages increase and decrease as expected. The increase in nitrogen for the click reaction (last set of

columns) is due to the nucleobases (C and T) which contain nitrogen. The increase in oxygen is due to the nucleobases and also the DNA backbone, which has several oxygen atoms in its phosphate groups.

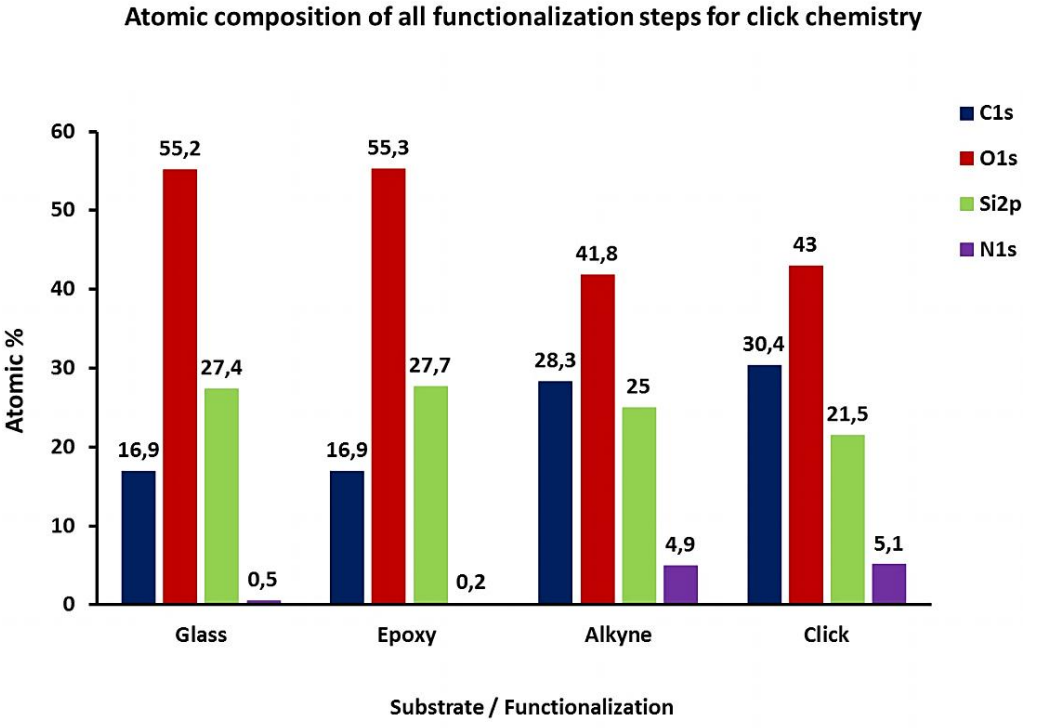

Figure 55: Atomic composition of all substrates and functionalization steps used for the click chemistry surfaces.

Figure 56 shows the results of the XPS analyses of high resolution spectra for C 1s. Image a) shows the overlay of C 1s signals of the different steps during the surface functionalization (see Figure 54). The initial weak carbon peak is thought to be a result of the facile contamination of the activated surface after piranha treatment. It can be seen that the signal intensity increases when the GPTMS is anchored on the surface and at the same time, the maximum is shifted to higher energies and the signal becomes more complex. This can also be seen for the step of alkyne immobilization. Image b) shows the deconvolution of the glass surface where two peaks are obtained and are attributed to surface contamination as mentioned above. Image c) shows the deconvolution of the epoxy terminated surface where the initially obtained peaks from the glass surface were kept and the curve was fitted with 3 new peaks which

correspond to 284.2 eV (Si-C, purple), 285.8 eV (C-C/C-H, green) and 287.7 eV (C-O from ether groups, red). Image d) shows the deconvolution of the alkyne terminated surface where peaks were identified at 284.1 eV (Si-C, purple) and 285.0 eV (C-C/C-H/C≡C, green), 286.3 eV (C-O from ether and alcohol, red) and 288.8 eV (C-N, blue). The shift of the C-O peak was expected since the newly created alcohol group has a lower binding energy (286 – 286.8 eV) compared to the ether group (286.3-288 eV).[86,87]

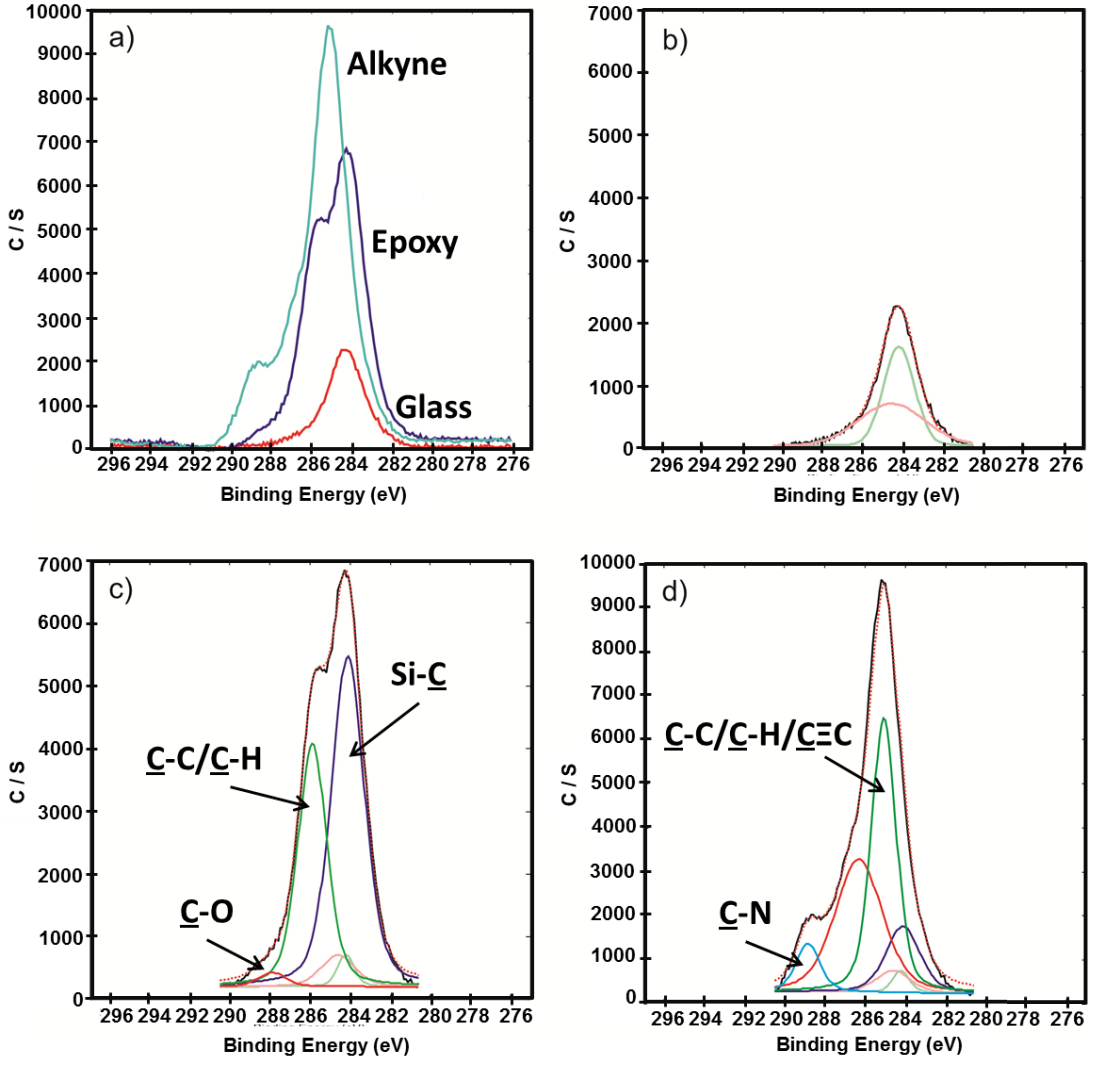

Figure 56: High resolution C 1s XPS spectra of (a) overlay of the three steps of the functionalization strategy; Curve fit and deconvolution of (b) glass surface, (c) epoxy surface and (d) alkyne surface indicating their atomic components or important changes, respectively.

Figure 57 shows the high resolution XPS spectra of N 1s with image a) being the overlay of all substrates, including the one where the click chemistry has been performed. It can be appreciated that on both, the glass and the epoxy surface, the N 1s signal is almost not existent. The alkyne surface shows an increase in signal and the deconvolution can be seen in image b), where the peak at 400.1 eV (blue) is attributed to the amino group.[88] Image c) shows the deconvolution of the peak obtained for the click reaction surface, where 2 new components were identified as N-N-C at 400.1 eV (green) and N N-N at 401.5 eV (pink).[89]

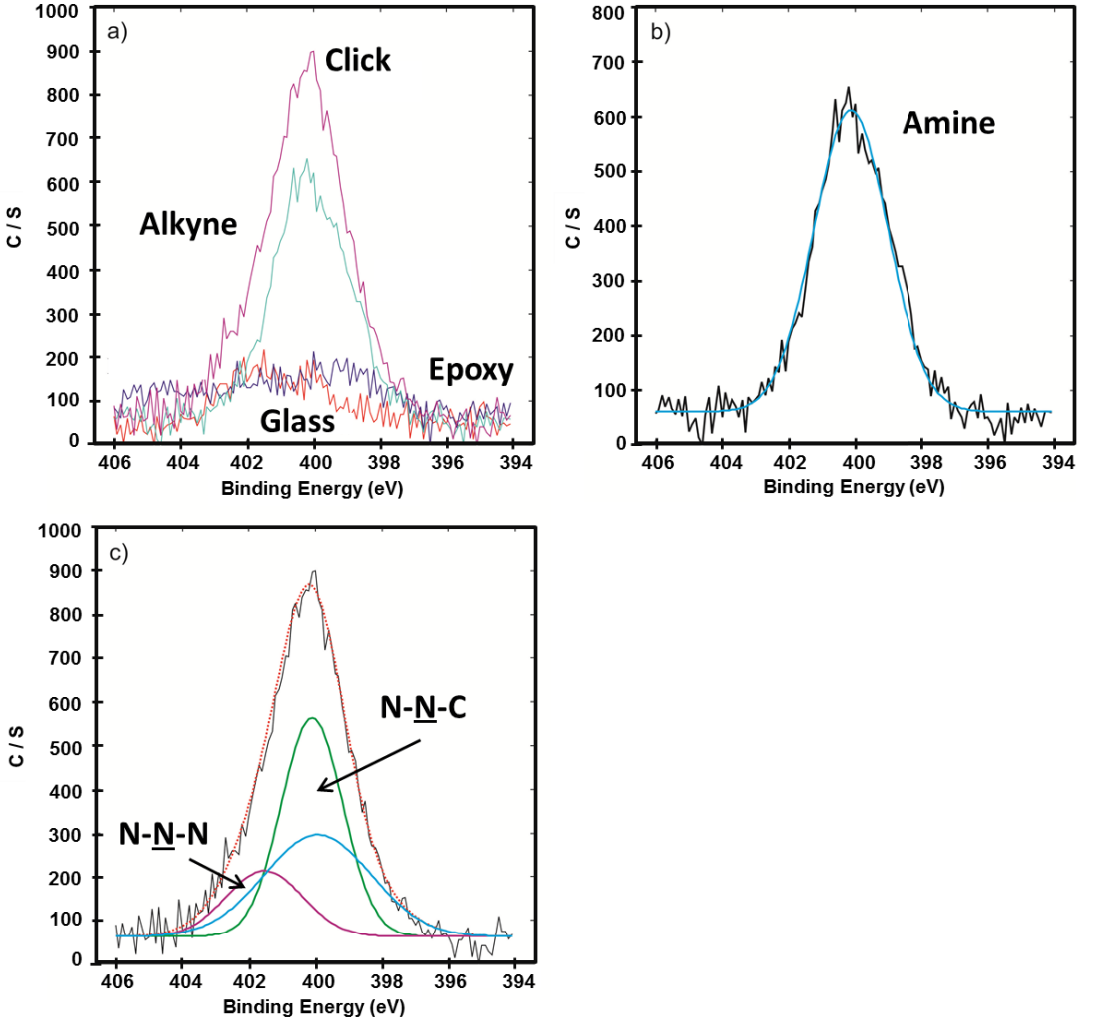

Figure 57: High resolution N 1s XPS spectra of (a) overlay of the three steps of the functionalization strategy and the click reaction substrate; Curve fit and deconvolution of (b) alkyne and (c) click reaction surface indicating their atomic components or important changes, respectively.

Figure 58 shows the high resolution spectra of (a) O 1s and (b) Si 2p. In both cases, the overlay of the three different steps of the surface functionalization (glass, epoxy and alkyne) can be seen.

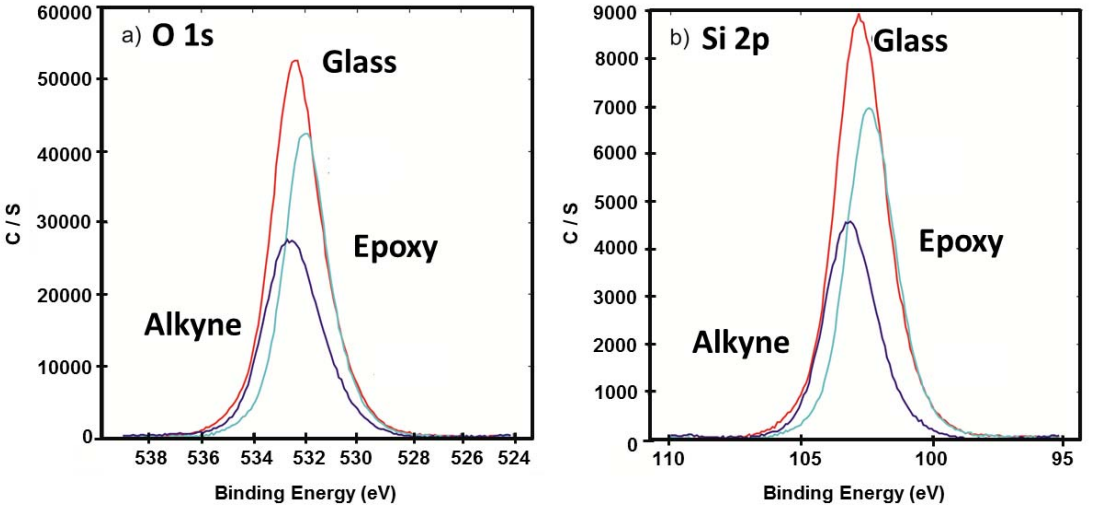

Figure 58: Overlay of the high resolution XPS spectra of (a) O 1s and (b) Si 2p for the different steps of the functionalization strategy.

Surface characterization via ToF-SIMS

After homogeneous incubation of the oligo-azide on a functionalized glass slide and subsequent hybridization with the complementary strand, ToF-SIMS experiments were performed as complementary measurements because it was not possible to analyze the phosphorus signature (P 2p peak) with XPS measurements, as has been reported by Zhang *et al.*[85] Thus, the presence of DNA on the sample and negative controls was checked by ToF-SIMS experiments.

Figure 59 shows the results of the ToF-SIMS experiments for the click reaction. Two substrates were incubated with the azide bearing CT oligo, one with catalyst (CT + cat) and one without catalyst (CT). Furthermore, two control surfaces were measured as well, namely bare glass and GA oligo without azide group but with catalyst (GA + cat). It is obvious that more oligonucleotide has been immobilized on the substrate for CT oligo with catalyst. Some CT oligo without catalyst has reacted with the alkyne group on the substrate but in a much lesser extent, as was expected from beforehand. There is still some GA oligo on the substrate, but this is rather due to

unspecific adsorption than because of reaction, since the GA oligo lacks the azide group. More extensive washing and sonication of the surface will overcome this problem.

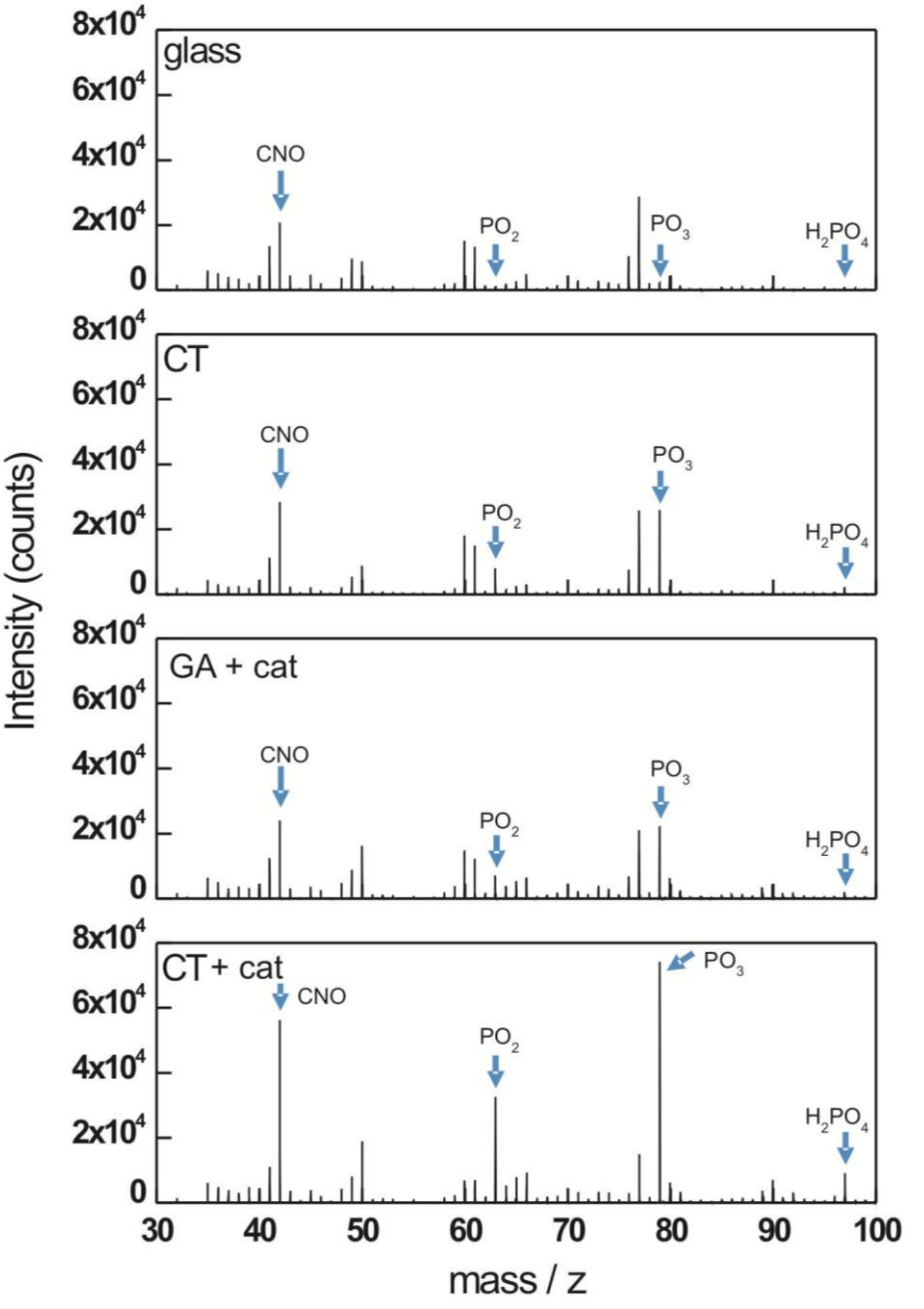

Figure 59: ToF-SIMS measurements of the surface click reaction. CT oligonucleotide was used with (CT + cat) and without catalyst (CT) and compared to negative controls: glass and GA oligo with cat (GA + cat), which lacks the azide group.

Patterning of oligos at the microscale

In order to test the utility of the substrates for click chemistry, a single stranded oligonucleotide with an azide anchor was printed on an alkyne modified glass slide by a robotic non-contact piezoelectric plotter (Nano-Plotter). Devaraj *et al.* already showed the immobilization of alkyne terminated oligos on an azide terminated homogeneous self-assembled monolayer on gold via click reaction.[58] In comparison, the patterning with the Nanoplotter yielded spots of around 250 µm in diameter (corresponding to drops of 0.4 nL in volume), which were printed in an array configuration (Figure 60 a). Solutions with and without catalyst (copper) were used, as well as negative controls (see Table 5).

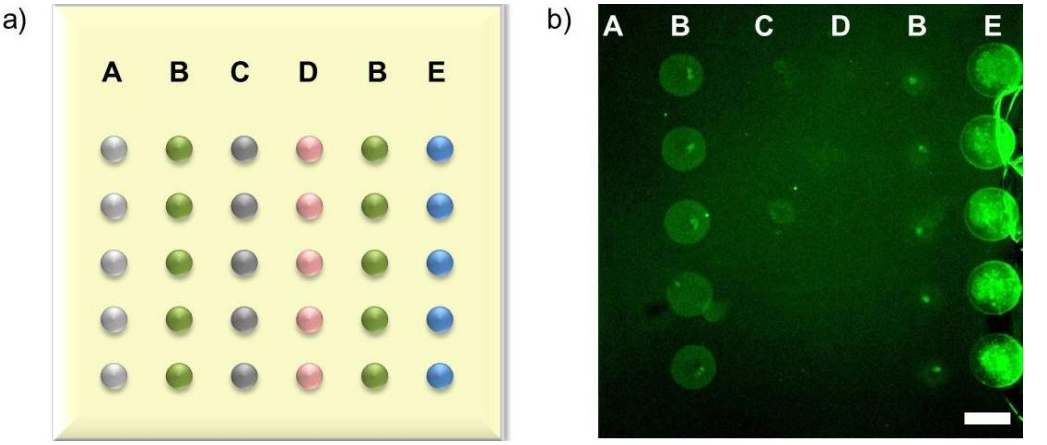

Figure 60: (a) Schematic layout of the patterned area. Letters A - E refer to the printed solutions, for explanation see Table 5. (b) Fluorescence microscope image of a functionalized glass substrate after patterning the azide terminated oligonucleotide and incubation with a complementary strand bearing Texas Red®. The scale bar equals 200 µm.

The size of the dots allowed for easy and fast observation of the patterning outcome with fluorescence microscopy since the complementary strand is equipped with a Texas-Red group. The substrate modification itself did not give rise to autofluorescence. Figure 60 b shows fluorescent signal for solutions B and E, which correspond to oligonucleotide with (E) and without Cu(I) (B), respectively. As expected, the solution with catalyst gives rise to a stronger fluorescent signal (E), since it is known that the presence of Cu(I) accelerates the cycloaddition reaction.[73,90] On the other hand, the oligonucleotide solution without catalyst (B, corresponding to the original Huisgen's reaction) also gives rise to a, even though weaker, fluorescent

signal and it is important to know that the reaction will also take place without the Cu(I) catalyst because the presence of Cu(I) can be critical[69,91] and, over time, degradation of the oligonucleotide will occur. This problem has already been reported[92,93] and can be reduced by using a Cu(I) binding ligand,[94] but not completely avoided. Negative controls did not give any signal after hybridization (solutions A, C and D). The stability of the surface functionalization was tested by extensive washing before and after patterning. After successful immobilization of the oligonucleotide via Nanoplotter spotting, the next experiment was performed using Dip-pen Nanolithography.

Patterning of oligo "CT" with DPN as molecular ink

The patterning of oligonucleotide as molecular ink was performed similar to an experiment from Chapter 3, where a biotin-azide was deposited on a functionalized glass substrate via DPN. Nevertheless, the deposition method using the oligo as a molecular ink doesn't seem to be adequate since no fluorescence could be detected after passivation and hybridization with the fluorescently marked complementary strand. This might be due to the poor solubility of the catalyst in water and the resulting phase separation, what leads to insufficient catalyst on the tip and the click reaction not being perfectly performed. Therefore, the following DPN experiments were performed with a liquid ink in order to ensure sufficient oligo and catalyst on the surface for a perfect click reaction.

Patterning of oligo "CT" with DPN as liquid ink

Similar to the patterning of the oligo "CT" with the Nanoplotter, here the ink was deposited as small drops which contain the oligo as well as the catalyst for the surface click reaction. Nevertheless, the deposited volume is smaller which can be seen from the resulting smaller dots. The estimated volume of deposition via DPN is in the range of femtoliters. Table 6 shows a comparison of the estimated probe surface densities of oligonucleotide "CT", obtained with the two different patterning methods (DPN and Nanoplotter).

Table 6: Estimated molecular densities of the deposited oligonucleotide "CT" for spots obtained with Dip-pen Nanolithography (DPN) and Nanoplotter.

	DPN	**Nanoplotter**
Concentration ink (µM)	51	11
Oligonucleotide molecules / L	3.1×10^{19}	6.6×10^{18}
Spot diameter (area)	5.5 µm (23.76 µm²)	250 µm (49087 µm²)
Drop volume (L)	$(10 / 100) \times 10^{-15}$	0.4×10^{-9}
Probe density (molecules/µm²)	1.3 x (**10^4** / **10^5**)	5.4 x **10^4**

Since the volume for the deposition with DPN was not determined exactly, the probe density values were calculated for drop volumes of 10 pL and 100 pL. These values are comparable to the one obtained with the Nanoplotter.

Peterson *et al.* reported that (using thiolated oligos on gold) probe densities below ~3 x 10^4 molecules/µm² proved to be better for rapid and reliable hybridization with the complementary oligonucleotide. For higher probe densities, probably repulsive electrostatic interactions will decrease the hybridization efficiency.[95] This means, that a packed monolayers of probe would be disadvantageous for the hybridization efficiency.

Figure 61 and Figure 62 show fluorescence images of a click chemistry array of DNA. Briefly, the oligo "CT" (51 µM solution) was covalently immobilized on a modified glass substrate and then hybridized with the fluorescently marked complementary strand (10 µM solution). It can be observed that the complementary strand is attached stably and selectively only to those areas where the oligo-azide was deposited. Also, "CT" is immobilized in a stable manner on the surface which could be shown by resisting several washing steps (MilliQ, DMSO, ethanol, buffered solutions). Figure 63 shows the intensity profile plot of one line of the array from Figure 62 (yellow inset are the respective dots) in order to estimate the size of the dots. The mean diameter is 5.49 µm ± 0.39 µm.

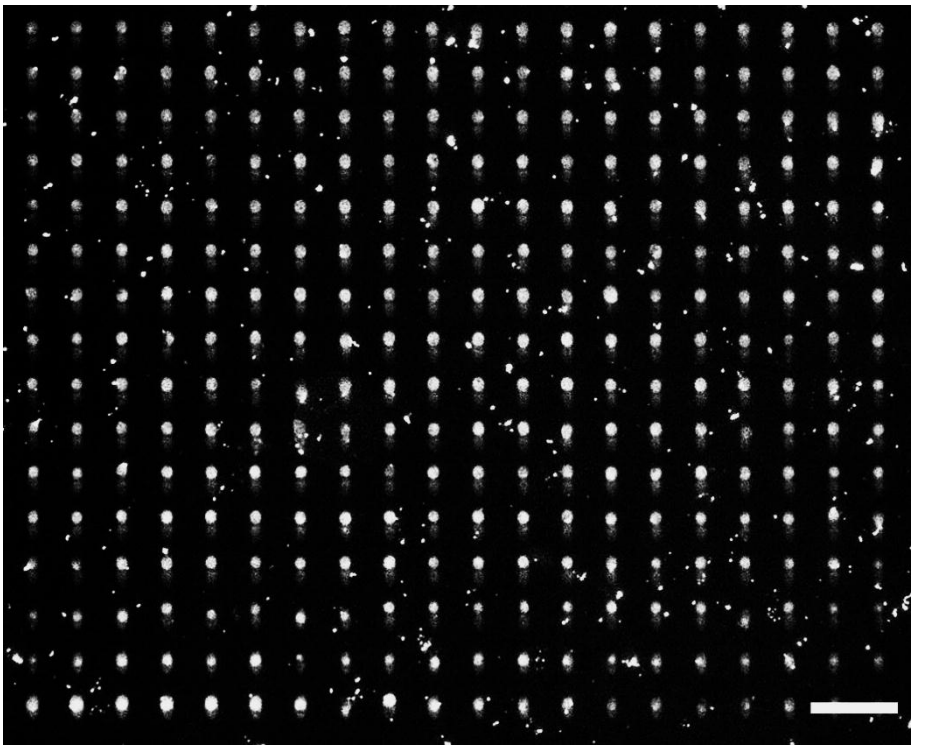

Figure 61: Fluorescence microscopy image of an oligo-azide deposited via Dip-pen Nanolithography. After patterning of the azide oligo, the surface was passivated with BSA and incubated with a fluorescently marked complementary strand. The scale bar equals 30 µm.

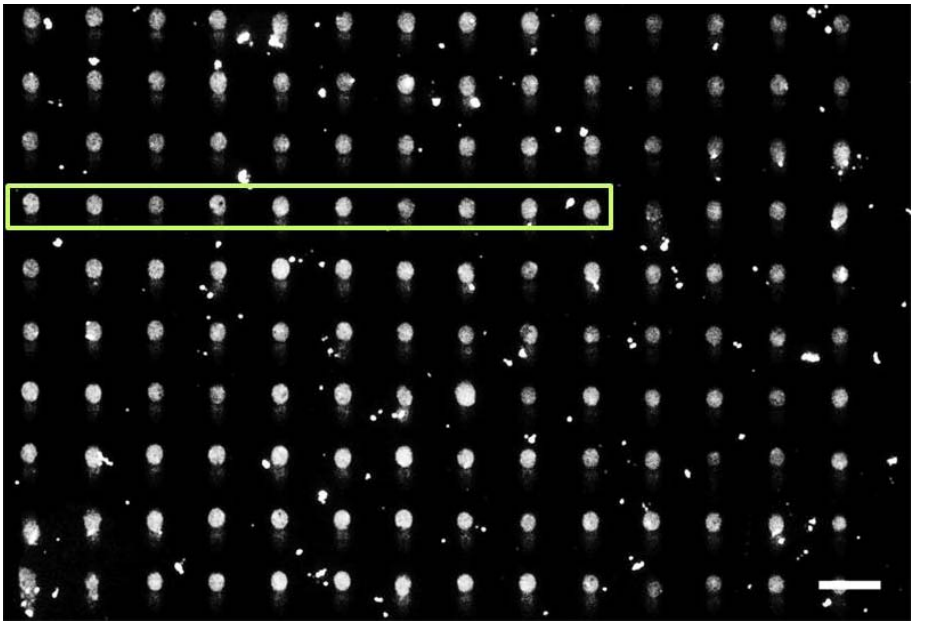

Figure 62: Fluorescence microscopy image of an oligo-azide deposited via Dip-pen Nanolithography. Zoom of Figure 61. The scale bar equals 15 µm.

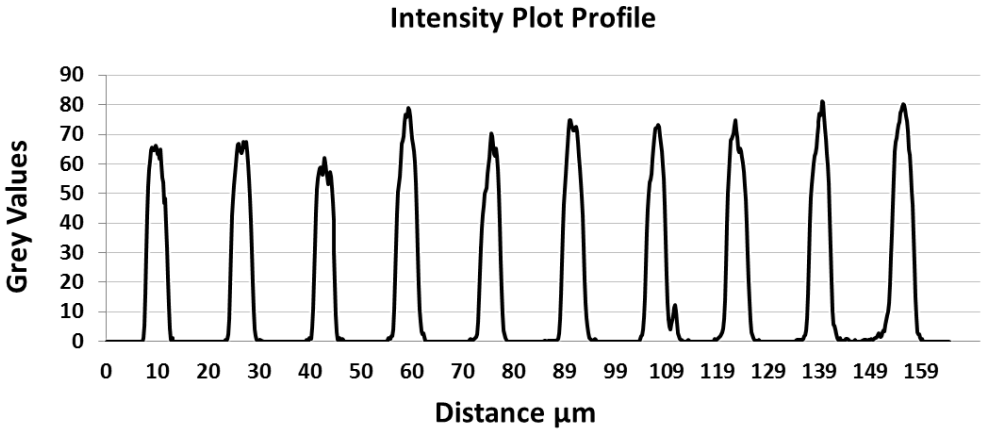

Figure 63: Intensity profile of the fluorescence of the dots of the array.

2.3.6. Assessment of the sensitivity of the sensor platform

In order to perform a concentration dependent calibration curve, the hybridized sample was placed as it was in a plate-reader scanner which is used to analyze standard ELISA experiments. In this case, no results were obtained because the dot size is too small for detection. Therefore, all measurements were performed with a standard fluorescence microscope, ensuring that no ambient light would falsify the fluorescence intensity. Figure 64 shows the arrays patterned for the assessment of the sensitivity. For evaluation of the values, one array was taken and the fluorescence intensity was determined for the 25 dots.

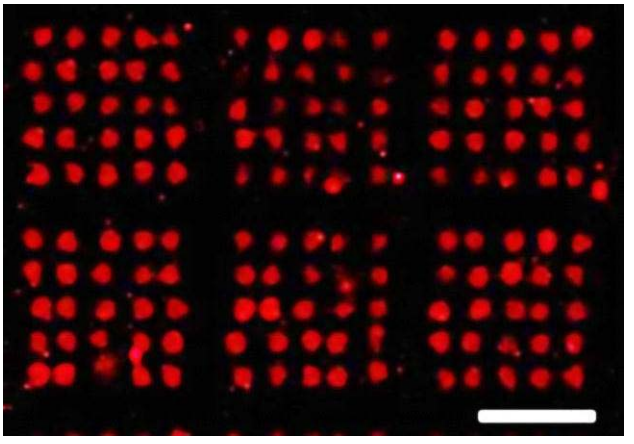

Figure 64: Fluorescence image of oligo arrays for the sensitivity assessment. The complementary oligo is equipped with the fluorophore Texas Red. The scale bar equals 50 µm.

The concentrations of complementary oligonucleotide for the calibration experiment ranged from 100 pM to 10 µM. The detection was performed by measuring the fluorescent signal of the platform after hybridization. Figure 65 shows fluorescence images of an array for different concentrations of complementary oligonucleotide, as well as the plot derived from evaluation of these images.

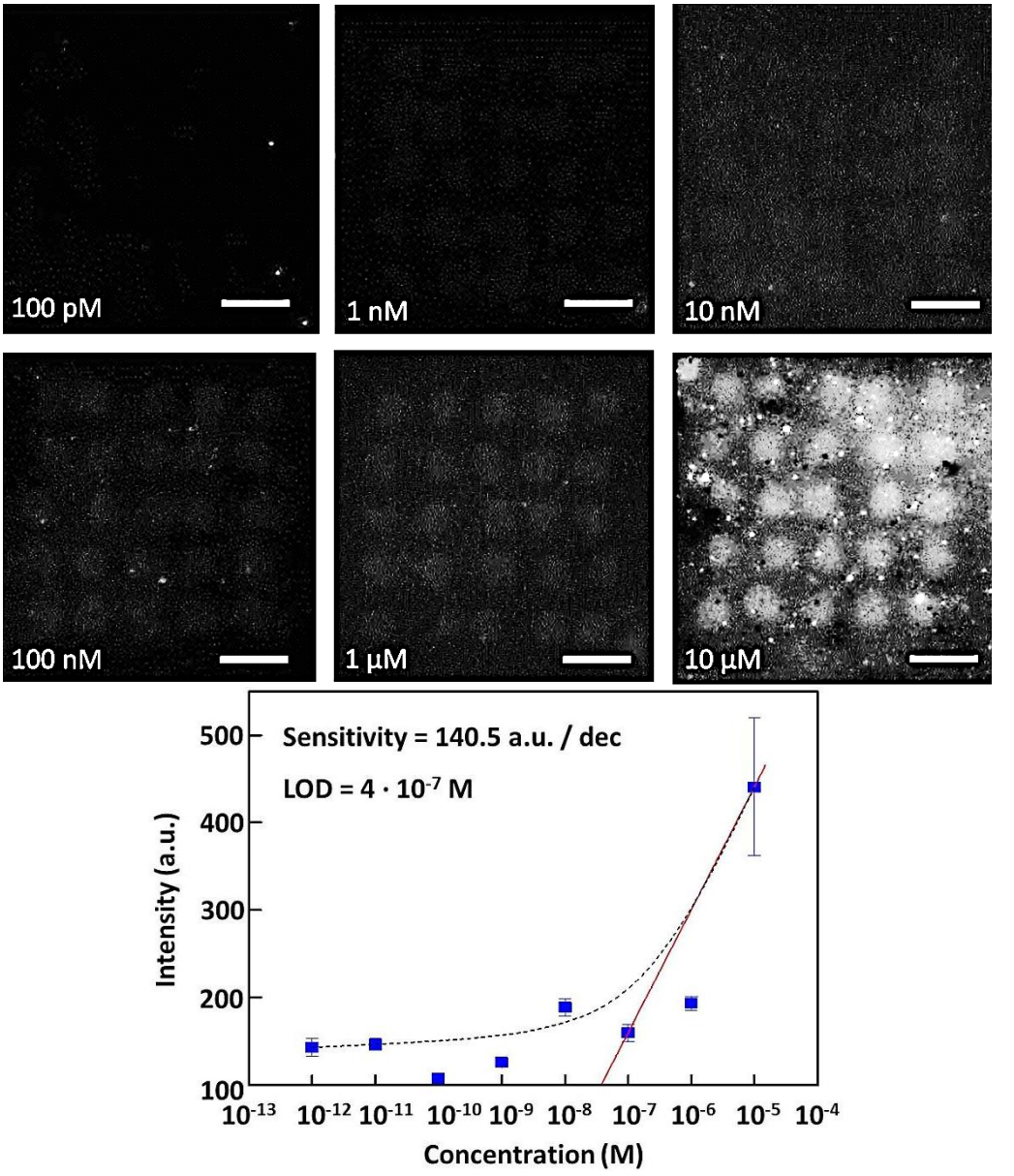

Figure 65: Fluorescence images and plot of the average normalized spot intensity of the hybridized complementary oligonucleotide bearing a fluorophore. The plot shows the average spot intensity of the 25 spots in each 5 x 5 array with error bars corresponding to the standard deviation. The blue line represents a second-order polynomial fit. Scale bars equal 20 µm.

Evaluation of the 25 spots of the 5 x 5 array for each concentration yielded a calculated limit of detection (LOD) of 4 x 10^{-7} M, which corresponds to 4 x 10^{3} µg/L. The LOD of the corresponding sensor with spot diameters of 200 µm is in the range of µg/L.[45] Nevertheless, both sensors cannot be compared directly because the detection methods are different. In our case, the fluorescently marked complementary strand was detected directly; in the case of the other sensor, the detection was by a competitive assay, and also, it was not the complementary strand which was detected but a protein which attaches to an immobilized hapten. The miniaturized sensors presented in the introductory section which reported sensationally low LOD (references 38 and 39) use atomic force microscopy and scanning electron microscopy as read out techniques which we did not choose on purpose because they are far from being fast and easy detection methods, even though they might result in a lower LOD.

Up to now, to the best of knowledge, there is no biosensor which is directly comparable to the one presented in this work. A similar approach was taken by Thompson *et al.*, who used Dip-pen Nanolithography to create a sensor "mesoarray" for the screening of protein-protein interactions.[48] By direct deposition of a protein, they achieved similar spot-sizes to the ones obtained for our sensor. Also, their reported concentrations for the analyte are in the µM range. So even though the overall sensitivity of the platform was not very high, this is a promising approach for other biosensor platforms based on oligonucleotides. The sensor platform itself is very stable due to the covalent attachment of the oligonucleotide and also withstands several dehybridization steps, as seen for the sensitivity assay. Also, the local confinement and the reproducibility of the pattern features on the substrate are very good.

Improvement of the sensitivity of the sensor might be obtained by decreasing the capture probe density and thus facilitate the hybridization process (see reference 95). This sensor platform can be even more attractive when multiplexed patterning is performed. Therefore, future work in this direction will include the multiplexed patterning of 3 different oligonucleotide sequences and subsequent hybridization with a cocktail of complementary strands in order to show the capacity of this platform.

2.4. CONCLUSIONS

The present work describes the development of a miniaturized oligonucleotide-based biosensor fabricated via Dip-pen Nanolithography.

To accomplish this goal, two types of substrates were tested, namely gold and glass along with several immobilization strategies.

Even though it was possible to deposit and successfully immobilize and hybridize thiolated oligonucleotides on gold, this approach was discarded because of the low reproducibility of top quality features and the almost inevitable problem of damaging the substrate.

The glass substrates are – per se – insensitive against damaging but have the disadvantage of needing to be chemically modified in order to enable covalent immobilization. Two modification methods were tested, whereas the click chemistry approach proved to be successful and produced reliable feature size, quality and stability. The versatility of this direct patterning approach has been shown by using two direct-writing techniques at the micro- and ”meso”scale. After successful fabrication of an array of oligo-dots, the biosensor capability was accessed by measuring different concentrations of fluorescently labeled complementary strand (100 pM – 10 μM).

The obtained limit of detection (4×10^{-7} M) was comparable to the one reported for a similar approach for fabrication of “mesoarrays”. Further improvement of the density of the capture probe and also the multiplexed patterning of several different oligonucleotide sequences can render this biosensor platform into a successful approach for the fabrication of miniaturized microarrays.

2.5. REFERENCES

[1] D. Grieshaber, R. MacKenzie, J. Vörös and E. Reimhult. *Electrochemical Biosensors – Sensor Principles and Architectures*. Sensors 2008. **8 (3)**: p. 1400-1458.

[2] J. Wang. *Electrochemical Glucose Biosensors*. Chemical Reviews 2008. **108 (2)**: p. 814-825.

[3] S. Haron and A.K. Ray. *Optical biodetection of cadmium and lead ions in water*. Medical Engineering & Physics 2006. **28 (10)**: p. 978-981.

[4] T.F. McGrath, C.T. Elliott and T.L. Fodey. *Biosensors for the analysis of microbiological and chemical contaminants in food.* Analytical and Bioanalytical Chemistry 2012. **403 (1)**: p. 75-92.

[5] A.C. Huet, C.Charlier, S. Weigel, S.B. Godefroy and P. Delahaut. *Validation of an optical surface plasmon resonance biosensor assay for scerrning (fluoro)quinolones in egg, fish and poultry.* Food additives & contaminants. Part A, Chemistry, analysis, control, exposure & risk assessment 2009. **26 (10)**: p. 1341-1347.

[6] G.A. Baxter, M.C. O'Connor, S.A. Haughey, S.R. Crooks and C.T. Elliott. *Evaluation of an immunobiosensor for the on-site testing of veterinary drug residues at an abattoir.* Analyst 1999. **124 (9)**: p. 1315-1319.

[7] N. Charaklias, H. Raja, M.L. Humphreys, N. Magan and C.A. Kendall. *The future of early disease detection? Application of electronic nose technology in otolaryngology.* The Journal of laryngology and otology 2010. **124 (8)**: p. 823-827.

[8] R. Seigneuric, L. Markey, D.S.A. Nuyten, C. Dubernet, C.T.A. Evelo, E. Finot and C. Garrido. *From Nanotechnology to Nanomedicine: Applications to Cancer Research*. Current Molecular Medicine 2010. **10 (7)**: p. 640-652.

[9] http://news.bbc.co.uk/2/hi/health/4564604.stm, accessed in June 2012.

[10] G.C. Rains, S.L. Utley and W.J. Lewis. *Behavioural monitoring of trained insects for chemical detection.* Biotechnology Progress 2006. **22 (1)**: p. 2-8.

[11] http://www.nytimes.com/2011/02/20/business/20proto.html, accessed in June 2012.

[12] A. Hulanicki, S. Glag and F. Ingman. *Chemical sensors definitions and classification*. Pure and Applied Chemistry 1991. **63 (9)**: p. 1247-1250.

[13] H. Harms, M.C. Wells and J. Roelof van der Meer. *Whole-cell living biosensors – are they ready for environmental application?* Applied Microbiology and Biotechnology 2006. **70 (3)**: p. 273-280.

[14] X. Zeng, Z. Shen and R. Mernaugh. *Recombinant antibodies and their use in biosensors.* Analytical and Bioanalytical Chemistry 2012. **402 (10)**: p. 3027-3038.

[15] P. Hollingen and P.J. Hudson. *Engineered antibody fragments and the rise of single domains.* Nature Biotechnology 2005. **23 (9)**: p- 1126-1136.

[16] J. Galbán, I. Sanz-Vicente, E. Ortega, M. del Barrio and S. de Marcos. *Reagentless fluorescent biosensors based on proteins for continuous monitoring systems.* Analytical and Bioanalytical Chemistry 2012. **402 (10)**: p. 3039-3054.

[17] T.A. Martin, C.T. Herman, F.T. Limpoco, M.C. Michael, G.K. Potts and R.C. Bailey. *Quantitative Photochemical Immobilization of Biomolecules on Planar and Corrugated Substrates: A Versatile Strategy for Creating Functional Biointerfaces*. ACS Applied Materials and Interfaces 2011. **3 (9)**: p. 3762-3771.

[18] R. Glatz and K. Bailey-Hill. *Mimicking nature's noses: From receptor deorphaning to olfactory biosensing.* Progress in Neurobiology 2011. **93 (2)**: p. 270-296.

[19] Y. Lei, W. Chen and A. Mulchandani. *Microbial biosensors*. Analytica Chimica Acta 2006. **568**: p. 200-210.

[20] O. Lee, A. Takesono, M. Tada, C.R. Tyler and T. Kudoh. *Biosensor zebrafish provide new insights into potential health effects of environmental estrogens*. Environmental Health Perspectives 2012. **120 (7)**: p. 990-996.

[21] F.R.R. Teles and L.P. Fonsecs. *Trends in DNA biosensors*. Talanta 2008. **77 (2)**: p. 606-623.

[22] B. Strehlitz, C. Reinemann, S. Linkorn and R. Stoltenburg. *Aptamers for pharmaceuticals and their application in environmental analytics.* Bioanalytical Reviews 2012. **4 (1)**: p. 1-30.

[23] C. Brioni and M. Moreno. *Applications of peptide nucleic acids (PNAs) and locked nucleic acids (LNAs) in biosensor development.* Analytical and Bioanalytical Chemistry 2012. **402 (10)**: p. 3071-3089.

[24] L.M. Demers, D.S. Ginger, S.-J. Park, Z. Li, S.-W. Chung and C.A. Mirkin. *Direct Patterning of Modified Oligonucleotides on Metals and Insulators by Dip-pen Nanolithography*. Science 2002. **296 (5574)**: p. 1836-1838.

[25] M. Alvira and R. Eritja. *Synthesis of oligonucleotides carrying 5'-5' linkages using copper-catalyzed cycloaddition reactions*. Chemistry and Biodiversity 2007. **4 (12)**: p. 27989-2809.

[26] R.B. Stoughton. *Applications of DNA Microarrays in Biology.* Annual Review of Biochemistry 2005. **74**: p. 53-82.

[27] T. Lettieri. *Recent Applications of DNA Microarray Technology to Toxicology and Exotoxicology.* Environmental Health Perspectives 2006. **114 (1)**: p. 4-9.

[28] P. Hong, W. Li and J. Li. *Applications of Aptasensors in Clinical Diagnostics.* Sensors 2012. **12 (2)**: p. 1181-1193.

[29] F. Mao, N. Mano and A. *Heller. Long tethers binding redox centers to polymer backbones enhance electron transport in enzyme "wiring" hydrogels*. Journal of the American Chemical Society 2003. **125 (16)**: p. 4951-4957.

[30] D. Avnir, T. Coradin, O. Lev and J. Livage. *Recent bio-applications of sol-gel materials.* Journal of Materials Chemistry 2006. **16 (11)**: p. 1013-1030.

[31] J.R. LaGraff and Q. Chu-LaGraff. *Scanning force microscopy and fluorescence microscopy of microcontact printed antibodies and antibody fragments.* Langmuir 2006. **22 (10)**: p. 4685-4693.

[32] R. Wacker, H. Schroder and C.M Niemeyer. *Performance of antibody microarrays fabricated by either dna-directed immobilization, direct spotting or streptavidin-biotin attachment: a comparative study*. Analytical Biochemistry 2004. **330 (2)**: p. 281-287.

[33] J. Labuda, A.M. Oliveira Brett, G. Evtugyn, M. Fojta, M. Mascini, M.Ozsoz, I. Plachetti, E. Palečec and J. Wang. *Electrochemical nucleic acid-based biosensors: Concepts, terms, and methodology (IUPAC Technical Report)*. Pure Applied Chemistry 2010. **82 (5)**: p. 1161-1187.

[34] E. Engvall and P. Perlmann. *Enzyme-linked immunosorbent assay (ELISA). Quantitative assay of immunoglobulin G.* Immunochemistry 1971. **8 (9)**: p. 871-874.

[35] M.J. Heller. *DNA MICROARRAY TECHNOLOGY: Devices, Systems and Applications.* Annual Revies of Biomedical Engineering 2002. **4**: p. 129-153.

[36] D.A. Lashkari, J.L. DeRisi, J.H. McCusker, A.F. Namath, C. Gentile, S.Y. Hwang, P.O. Brown and R.W. Davis. *Yeast microarrays for genome wide parallel genetic and gene expression analysis.* Proceedings of the National Academy of Sciences of the United States of America 1997. **94 (24)**: p. 13057-13062.

[37] H. Wolinsky. *The thousand-dollar genome. Genetic brinkmanship or personalized medicine?* EMBO reports 2007. **8 (10)**: p. 900-903.

[38] K-B. Lee, E-Y. Kim, C.A. Mirkin and S.M. Wolinsky. *The Use of Nanoarrays for Highly Sensitive and Selective Detection of Human Immunodeficiency Virus Type 1 in Plasma.* Nano Letters 2004. **4 (10)**: p. 1869-1872.

[39] S. Lee, S. Lee, Y-H. Ko, H. Jung, J.D. Kim, J.M. Song, J. Choo, S.K. Eo and S.H. Kang. *Quantitative analysis of human serum leptin using a nanoarray protein chip based on single-molecule sandwich immunoassay.* Talanta 2009. **78 (2)**: p. 608-612.

[40] E.J. Irvine, A. Hernandez-Santana, K. Faulds and D. Graham. *Fabricating protein immunoassays on nitrocellulose using Dip-pen lithography techniques.* Analyst 2011, **136 (14)**: p. 2925-2930.

[41] P. Buchegger, U. Sauer, H. Toth-Székély and C. Preininger. *Miniaturized Protein microarray with Internal Calibration as Point-of-Care Device for Diagnosis of Neonatal Sepsis.* Sensors 2012. **12 (2)**: p. 1494-1508.

[42] R.J. Stokes, J.A. Dougan and D. Graham. *Dip-pen nanolithography and SERRS as synergic techniques.* Chemical communications 2008. **44**: p. 5734-5736.

[43] A.J. Senesi, D.I. Rozkiewicz, D.N. Reinhoudt, and C.A. Mirkin. *Agarose-Assisted Dip-pen Nanolithography of Oligonucleotides and Proteins.* ACS Nano 2009. **3 (8)**: p. 2394-2402.

[44] D. Nyamjav and R.C. Holz. *Direct patterning of silanized-biomolecules on semiconductor surfaces*. Langmuir 2010. **26 (23)**: p. 18300-18302.

[45] N. Tort, J.P. Salvador, R. Eritja, M. Poch, E. Martinez, J. Samitier and M-P. Marco. *Fluorescence site-encoded DNA addressable hapten microarray for anabolic androgenic steroids*. TrAC Trends in Analytical Chemistry 2009. **28 (6)**: p. 718-728.

[46] S. Laschi, I. Palchetti, G. Marrazza and M. Mascini. *Enzyme-amplified electrochemical hybridization assay based on PNA, LNA and DNA probe-modified micro-magnetic beads.* Bioelectrochemistry 2009. **76 (1-2)**: p. 214-220.

[47] H. Jang, J. Kim, J-J. Choi, Y. Son and H. Park. *Peptide Nucleic Acid Array for Detection of Point Mutations in Hepatitis B Virus Associated with Antiviral Resistance.* Journal of Clinical Microbiology 2010. **48 (9)**: p. 3127-3131.

[48] D.G. Thomson, E.O. McKenna, A. Pitt and D. Graham. *Microscale mesoarrays created by Dip-pen nanolithography for screening of protein-protein interactions.* Biosensors and Bioelectronics 2011. **26 (12)**: p. 4667-4673.

[49] S. Ghatnekar-Nilsson, L. Dexlin, C. Wingren, L. Montelius and C.A.K. Borrebaeck. *Design of atto-vial based recombinant antibody arrays combined with planar wave-guide detection system.* Proteomics 2007. **7 (4)**: p. 540-547.

[50] R. Huisgen. *Centenary Lecture: 1,3-Dipolar Cycloadditions*. Proceedings of the Chemical Society 1961. p. 357-369.

[51] R. Huisgen. *1,3-Dipolar Cycloadditions: Past and Future.* Angewandte Chemie, International Edition 1963. **2 (10)**: p. 565-632.

[52] H.C. Kolb, M.G. Finn and K.B. Sharpless. *Click Chemistry: Diverse Chemical Function from a Few Good Reactions*. Angewandte Chemie, International Edition 2001. **40 (11)**: p. 2004-2021.

[53] C.W. Tornoe, C. Christensen and M. Meldal. *Peptidotriazoles on Solid Phase: [1,2,3]-Triazoles by Regiospecific Copper(I)-Catalyzed 1,3-Dipolar Cycloadditions of Terminal Alkynes to Azides*. The Journal of Organic Chemistry 2002. **67 (9)**: p. 3057-3064.

[54] V.V. Rostovtsev, L.G. Green, V.V. Fokin and K.B. Sharpless. *A Stepwise Huisgen Cycloaddition Process: Copper(I)-Catalyzed Regioselective "Ligation" of Azides and Terminal Alkynes*. Angewandte Chemie, International Edition 2002. **41 (14)**: p. 2596-2599.

[55] F. Himo, T. Lovell, R. Hilgraf, V.V. Rostovtsev, L. Noodleman, K.B. Sharpless and V.V. Vokin. *Copper(I)-Catalyzed Synthesis of Azoles. DFT Study Predicts Unprecedented Reactivity and Intermediates.* Journal of the American Chemical Society 2005. **127 (1)**: p. 210-216.

[56] S. Hohloch, C-Y. Su and B. Sarkar. *Copper(I) Complexes of Normal and Abnormal Carbenes and Their Use as Catalysts for the Huisgen [3+2] Cycloaddition between Azides and Alkynes.* European Journal of Inorganic Chemistry 2011. **20**: p. 3067-3075.

[57] J.P. Collman, N.K. Devaraj and C.E.D. Chidsey. *"Clicking" functionality onto electrode surfaces*. Langmuir 2004. **20 (4)**: p. 1051-1053.

[58] N.K. Devaraj, G.P. Miller, W. Ebina, B. Kakaradov, J.P. Collman, E.T. Kool and C.E.D. Chidsey. *Chemoselective Covalent Coupling of Oligonucleotide Probes to Self-Assembled Monolayers*. Journal of the American Chemical Society 2005. **127 (24)**: p. 8600-8601.

[59] Y. Zhang, S. Luo, Y. Tang, L. Yu, K.Y. Hou, J-P. Cheng, X. Zeng, P.G. Wang. *Carbohydrate-Protein Interactions by „Clicked" Carbohydrate Self-Assembled Monolayers.* Analytical Chemistry 2006. **78 (6)**: p. 2001-2008.

[60] T. Lummerstorfer and H. Hoffmann. *Click Chemistry on Surfaces: 1,3-Dipolar Cycloaddition Reactions of Azide-Terminated Monolayers on Silica.* The Journal of Physical Chemistry B 2004. **108 (13)**: p. 3963-3966.

[61] X.L. Sun, C.L. Stabler, C.S Cazalis and E.L. Chaikof. *Carbohydrate and Protein Immobilization onto Solid Surfaces by Sequential Diels-Alder and Azide-Alkyne Cycloadditions.* Bioconjugate Chemistry 2006. **17 (1)**: p. 52-57.

[62] R. A. Evans. *The Rise of Azide—Alkyne 1,3-Dipolar 'Click' Cycloaddition and Its Application to Polymer Science and Surface Modification.* Australian Journal of Chemistry 2007. **60 (6)**: p. 384-395.

[63] M. Bertoldo, G. Zampano, F. La Terra, V. Villari and V. Castelvetro. *Amphiphilic Amylose-g-poly(meth)acrylate Copolymers through "Click" onto Grafting Method.* Biomacromolecules 2011. **12 (2)**: p. 388-398.

[64] X. Huang, X-J. Huang, A-G. Yu, C. Wang, Z-W. Dai and Z-K. Xu. *"Click Chemistry" as a Facile Approach to the Synthesis of Polyphosphazene Glycopolymers.* Macromolecular Chemistry and Physics 2011. **212 (3)**: p. 272-277.

[65] X. Liu, H-N. Zheng, Y-Z. Ma, Q. Yan and S-J. Xiao. *Microwave irradiated click reactions on silicon surfaces via derivertization of covalently grafted poly(PEGMA) brushes*. Journal of Colloid and Interface Science 2011. **358 (1)**: p. 116-122.

[66] A. Koschella, M. Hartlieb and T. Heinze. *A 'click-chemistry' approach to cellulose-based hydrogels*. Carbohydrate Polymers 2011. **86 (1)**: p. 154-161.

[67] P. Dutta, S. Sawoo, N. Ray, O. Bouloussa and A. Sarkar. *Engineering Bioactive Surfaces with Fischer Carbene Complex: Protein A on Self-Assembled Monolayer for Antibody Sensing*. Bioconjugate Chemistry 2011. **22 (6)**: p. 1202-1209.

[68] H. Nandivada, H-Y. Chen, L. Bondarenko and J. Lahann. *Reactive Polymer Coatings that „Click"*. Angewandte Chemie, International Edition 2006. **45 (20)**: p. 3360-3363.

[69] D.I. Rozkiewicz, D. Janczewski, W. Verboom, B.J. Ravoo and D.N. Reinhoudt. *„Click" Chemistry by Microcontact Printing.* Angewandte Chemie, International Edition 2006. **45 (32)**: p. 5292-5296.

[70] F.A. Scaramuzzo, A. Gonzalez-Campo, C-C. Wu, A.H. Velders, V. Subramaniam, G. Doddi, P. Mencarelli, M. Barteri, P. Jonkheijm and J. Huskens. *Pyrylium monolayers as amino-reactive platform*. Chemical Communications 2010. **46**: p. 4193-4195.

[71] J.J. Gassensmith, P.M. Erne, W.F. Paxton, C. Valente and J.F. Stoddart. *Microcontact Click Printing for Templating Ultrathin Films of Metal-Organic Frameworks*. Langmuir 2011. **27 (4)**: p. 1341-1345.

[72] P-C. Lin, S-H. Ueng, M-C. Tseng, J-L. Ko, K-T. Huang, S-C. Yu, A.K. Adak, Y-J. Chen and C-C. Lin. *Site-Specific Protein Modification through CuI-Catalyzed 1,2,3-Triazole Formation and Its Implementation in Protein Microarray Fabrication*. Angewandte Chemie, International Edition 2006. **45 (26)**: p. 4286-4290.

[73] D.A. Long, K. Unal, R.C. Pratt, M. Malkoch and J. Frommer. *Localized "Click" Chemistry Through Dip-pen Nanolithography.* Advanced Materials 2007. **19 (24)**: p. 4471-4473.

[74] W.F. Paxton, J.M. Spruell and J.F. Stoddart. *Heterogeneous Catalysis of a Copper-Coated Atomic Force Microscopy Tip for Direct-Write Click Chemistry.* Journal of the American Chemical Society 2009. **131 (19)**: p. 6692-6694.

[75] H.Y. Chen, M. Hirtz, X. Deng, T. Laue, H. Fuchs and J. Lahann. *Substrate-Independent Dip-pen Nanolithography Based on Reactive Coatings.* Journal of the American Chemical Society 2010. **132 (51)**: p. 18023-18025.

[76] "Azides are energy-rich molecules, […] can be heat and shock sensitive and can decompose with little input of external energy." taken from the website http://www.stanford.edu/dept/EHS/prod/researchlab/lab/safety_sheets/08-203.pdf ; accessed in July 2011.

[77] S. Bräse, C. Gil, K. Knepper and V. Zimmermann. *Organic Azides: An Exploding Diversity of a Unique Class of Compounds.* Angewandte Chemie, International Edition 2005. **44 (33)**: p. 5188-5240.

[78] L.S. Penn, T.F. Hunter, Y. Lee and R.P. Quirk. *Grafting Rates of Amine-Functionalized Polystyrenes onto Epoxidized Silica Surfaces*. Macromolecules 2000. **33 (4)**: p. 1105-1107.

[79] T.C. Hang and A. Guiseppi-Elie. *Frequency dependent and surface characterization of DNA immobilization and hybridization.* Biosensensors and Bioelectronics 2004. **19 (11)**: p. 1537-1548.

[80] N.Y. Lee and B.H. Chung. *Novel Poly(dimethylsiloxane) Bonding Strategy via Room Temperature "Chemical Gluing"*. Langmuir 2009. **25 (6)**: p. 3861-3866.

[81] E. Soto-Cantu, B.S. Lokitz, J.P. Hinestrosa, C. Deodhar, J.M. Messman, J.F. Ankner and S.M. Kilbey. *Versatility of Alkyne-Modified Poly(Glycidyl Methacrylate) Layers for Click Reactions.* Langmuir 2011. **27 (10)**: p. 5986-5996.

[82] http://www5.gelifesciences.com/aptrix/upp00919.nsf/Content/984222A5DCDFA6E9C125726700341D DC/$file/17-0854-01PL_Rev-B_2007_WEB.pdf; accessed in July 2011.

[83] W.W. Cleland. *Dithiothreitol,* a *New Protective Reagent for SH Groups.* Biochemistry 1964. **3 (4)**: p. 480-482.

[84] G. Nelles, H. Schönherr, M. Jaschke, H. Wolf, M. Schaub, J. Küther, W. Tremel, E. Bamberg, H. Ringsdorf and H.-J. Butt. *Two-Dimensional Structure of Disulfides and Thiols on Gold(111)*. Langmuir 1998. **14 (4)**: p. 808-815.

[85] X. Zhang, S. Kumar, J. Chen and A.V. Teplyakov. *Covalent attachment of shape-restricted DNA molecules on amine-functionalized Si(111) surface.* Surface Science 2009. **603 (16)**: p. 2445-2457.

[86] L. Britcher, T.J. Barnes, H.J. Griesser and C.A. Prestidge. *PEGylation of porous silicon using click chemistry.* Langmuir 2008. **24 (15)**: p. 7625-7627.

[87] J.F. Moulder, W.F. Stickle, P.E. Sobol, K.D Bomben, in *Handbook of X-ray photoelectron spectroscopy: a reference book of standard spectra for identification and interpretation of XPS-data*, (Eds: J.F. Moulder, J. Chastain), PHYSICAL ELECTRONICS, 1995, p.41 and 43, published by Perkin-Elmer Corporation, Minnesota, USA.

[88] T. Ramanathan, F.T. Fisher, R.S. Ruoff and L.C. Brinson. *Amino-Functionalized Carbon Nanotubes for Binding to Polymers and Biological Systems.* Chemistry of Materials 2005. **17 (6)**: p. 1290-1295.

[89] X. Liu, H-N. Zheng, Y-Z. Ma, Q. Yan and S-J. Xiao. *Microwave irradiated click reactions on silicon surfaces via derivertization of covalently grafted poly(PEGMA) brushes.* Journal of Colloid and Interface Science 2011. **358 (1)**: p. 116-122.

[90] J.F. Lutz. *1,3-Dipolar Cycloadditions of Azides and Alkynes: A Universal Ligation Tool in Polymer and Materials Science*. Angewandte Chemie, International Edition 2007. **46 (7)**: p. 1018-1025.

[91] R. Manova, T.A. van Beek and H. Zuilhof. *Surface Functionalization by Strain-Promoted Alkyne-Azide Click Reactions.* Angewandte Chemie, International Edition 2011. **50 (24)**: p. 5428-5430.

[92] M.W. Kanan, M.M. Rozenman, K. Sakurai, T.M. Snyder and D.R. Lui. *Reaction discovery enabled by DNA-templated synthesis and in vitro selection*. Nature 2004. **431**: p. 545-549.

[93] R. Kumar, A. El-Sagheer, J. Tumpane, P. Lincoln, L.M. Wilhelmsson, T. Brown. *Template-Directed Oligonucleotide Strand Ligation, Covalent Intramolecular DNA Circularization and Catenation Using Click Chemistry.* Journal of the American Chemical Society 2007. **129 (21)**: p. 6859-6864.

[94] T.R. Chan, R. Hilgraf, K.B. Sharpless and V.V. Fokin. *Polytriazoles as Copper(I)-Stabilizing Ligands in Catalysis.* Organic Letters 2004. **6 (17)**: p. 2853-2855.

[95] A.W. Peterson, R.J. Heaton and R.M Georgiadis. *The effect of surface probe density on DNA hybridization.* Nucleic Acids Research 2001. **29 (24)**: p. 5163-5168.

Chapter 3.

Large-area patterning of gold and glass substrates with Dip-pen Nanolithography and their application in cell differentiation experiments

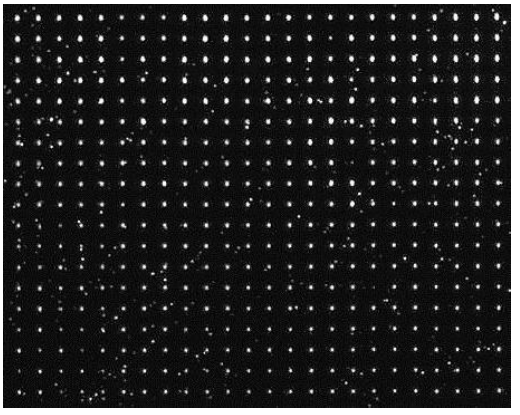

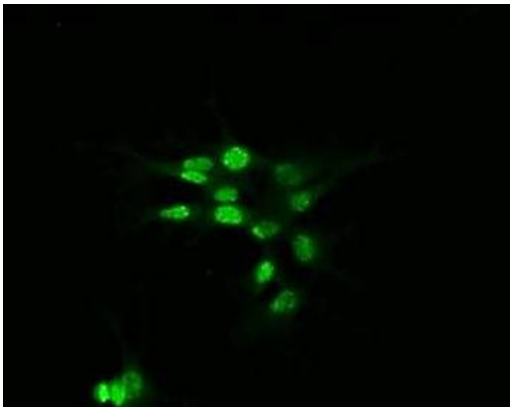

3.1. INTRODUCTION

In the past two decades, the emerging nanotechnologies gave access to the field of nanomedicine, which amongst other include approaches to biosensing[1], basic cell biology, tissue engineering and regenerative medicine, in order to address various diseases[2]. The role of micro- and nano-technology in these areas is evident since already existing fabrication technologies could not provide access to nanoscale structures. The reason behind the relevance of such nanoscale structures is the body's cells: cell adhesion is a crucial process for anchorage dependent cells. *In vitro* experiments have proved that in order to be viable, spread and proliferate, these cells need to attach to adhesive surfaces.[3] The cell receptors that play a role in attachment and signal transduction are at the micro- and nano-length scale themselves[4], as well as the intracellular proteins that enable the cells to exert forces onto the substrate[5]. In literature, there are many examples of cells being influenced by chemical or topographical cues as micro- or nano-features, wherein the cell alignment, polarization, migration, proliferation and gene expression is altered[6]. Recent studies have shown that the geometrical order of the micro- or nano-pattern is important[7] and controls cell proliferation and even differentiation.

The human body consists of many different cell types. Nevertheless, they all come from but one single cell type which is created during the process of fertilization, when the ovum fuses with the sperm cell and a foetus will develop from it. In order to go from just this single cell type to the fully developed embryo, a complex program is undergone with many cycles of cell division and differentiation as well as directed cell migration. The main actors in this complicated play are the so called stem cells. Stem cells have been a hot topic in the last few years and there were many publications and press releases about their promising application in regenerative medicine[8]. They are undeveloped cells and possess the ability of self-renewal, differentiation and tissue regeneration. Figure 66 shows the differentiation pathways of stem cells, where the zygote, the fertilized egg, is the starting point. The zygote has the ability to differentiate into all types of cells further down the pathway and is called *totipotent*. In the blastocyst stage, there are already two different types of cells, which are both

*pluripoten*t. The extra-embryonic cell layer called trophoblast, which later forms the placenta and the so called inner cell mass (ICM) which gives rise to the embryo. A cell from the trophoblast cannot differentiate into a cell from the ICM and vice versa; they can only stay in their own "lineage". The ICM then continues to differentiate into the three germ layers ectoderm, mesoderm and endoderm; the cells from the ICM are called embryonic stem cells (ESCs), which are also *pluripotent* and can differentiate into every cell type found in the body[9]. Although ESCs are the ideal model for regenerative medicine, they are very controversial considering the ethical issue of extraction of cells from embryos. However, there are also stem cells in the adult body, which can be found mainly in renewing tissues like bone marrow, umbilical cord blood, adipose and neural tissue. They are called *multipotent* and are not able to differentiate into whatever type of cell, but only into several phenotypes (along the lineage).

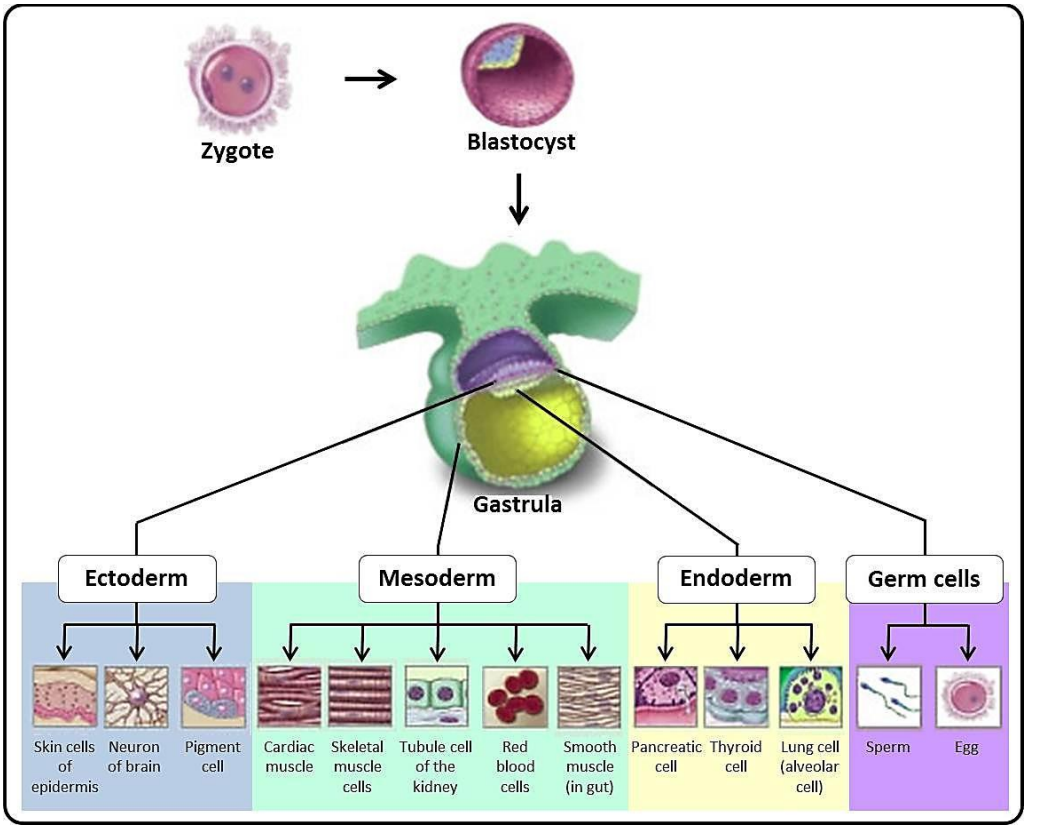

Figure 66: Cell differentiation pathways from zygote to specialized cell types. Image adapted from reference 10.

A well-known cell line is the mesenchymal stem cell line (MSCs) which upon exposing to appropriate stimuli can be differentiated into either osteoblasts, myoblasts or neurons.[11] The advantage of this cell type (non-ESC) is that they can be obtained from adult tissue and could be used in stem cell therapy (re-implantation of stem cells in an individual after *in-vitro* differentiation). Adult stem cells are already used in the acceleration of bone or tendon healing, the repair of cartilage damage, replacement of damaged heart-muscle cells or, which is the most common application, the restoration of blood cells for patients with leukaemia[12].

Opposing the theory of potential benefits of stem cells, in practice there are still many unsolved problems concerning effective stem cell culture. Like every other cell type, stem cells are sensitive to many different signaling cues coming from their microenvironment.[13,14] Figure 67 shows a schematic overview over those microenvironmental signals which are modulating stem cell proliferation, influencing symmetric versus asymmetric division, controlling differentiation, and protecting stem cells from physiologic stress.[15,16] These signals influence the cellular response and therefore the stem cell fate. In addition to the cell-cell interactions and the influence of physical forces or the control of cell shape, there are two very important factors which have been and still are closely studied.

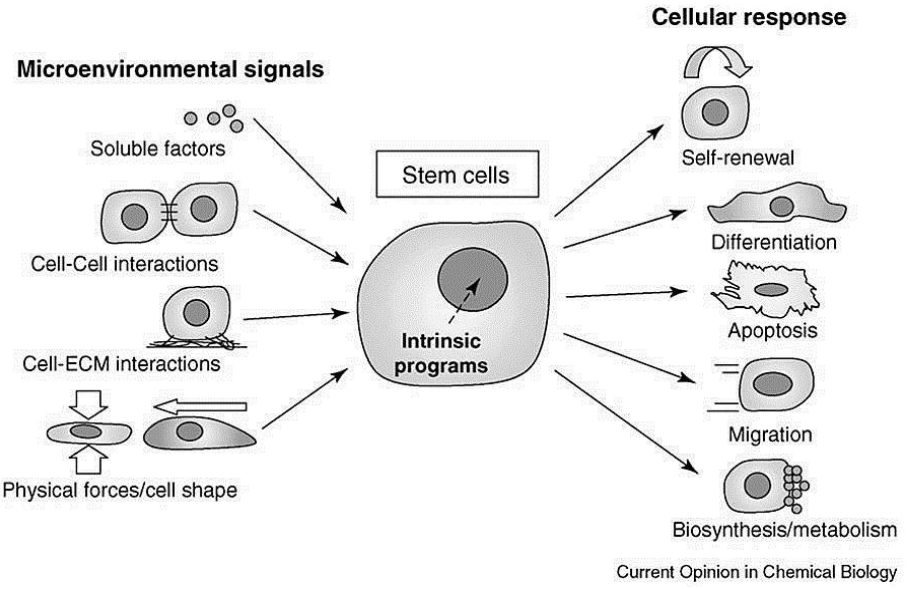

Figure 67: Signals from the microenvironment determine the stem cell fate. ECM = Extra-cellular matrix. Image taken from reference 17.

Much effort is put into controlling the interactions of cells with the so called soluble factors as well as with the substrate or extra-cellular matrix (ECM). A very impressive example therefore was given by the group of Discher, who demonstrated the influence of the substrate rigidity on cell differentiation.[18] Both parameters (the soluble factors and the interactions with the substrate/ECM) are not only of high importance for stem cells but for all cells in general. Generally, a viable stem cell culture is assumed to need a high amount of control over these cues in order to achieve homogeneous cell populations (meaning that for example 100% of the cells undergo self-renewal or differentiation or whatever they are supposed to do). The homogeneity of the cell population can be influenced by administrating soluble exogenous stimuli (biochemical factors which are usually presented as media supplements) or by controlling the extracellular environment which is presented to the cells and consists of ECM proteins.[17] As stated by Underhill and Bhatia, in order to decouple the complex spatiotemporal cues that cells experience *in vivo,* microfabrication tools have been applied to *in vitro* cell culture models, amongst which for example cell multiwell plate assays are frequently applied.[17] The drawback of this method is that, when parallelized, it is time consuming and expensive due to the high quantities of growth factors required, which up to now are usually administered in solution.

ECM proteins which are usually applied in stem cell experiments are fibronectin, laminin and collagen,[13,19] which are either physisorbed on the surface or intended to be bound covalently without loss of their biological activity. Instead of using the whole protein, small motifs can be immobilized which are known to have an influence on cell adhesion by interacting with the transmembrane proteins called integrins, namely the amino acid sequence arginine-glycine-aspartate (RGD)[20]. The molecules used as soluble factors are so called growth factors, usually being a cytokine or a steroid hormone which stimulates cell growth, proliferation and also differentiation. There are several big families of growth factors which include amongst other: Fibroblast Growth Factor (FGF), Transforming Growth Factor (TGF), Hedgehog signaling pathway and Wnt signaling pathway.

From the sub-family of transforming growth factors β (TGF β), the bone morphogenetic proteins (BMPs) have gained interest lately, especially BMP-2, which

has already been used *in vivo* for oral surgery.[21,22] Concerning cell differentiation, BMP-2 has been established as highly effective inducer of bone formation and regeneration,[23,24,25] where it acts as trigger and makes cells differentiate towards the osteoblastic regime. Originally, BMP-2 has been used in solution; but due to its high solubility in body fluids it can get easily lost by diffusion, leading to a reduction of the time during which its signaling cascade is stimulated and finally resulting in a compromised effectiveness.[26,27] The solution, which suggests itself to this problem, is the immobilization of BMP-2 on the substrate. This is further favored by the fact that BMP-2 doesn't have to be internalized by the cell to activate its signaling cascade. In any case, the mode of BMP-2 receptor oligomerization determines different BMP-2 signal pathways.

A model cell line for studying the influence of BMP-2 in cell differentiation is the so called C2C12 myoblast cell line, which has a very limited differentiation pathway (see Figure 68). BMP-2 can be considered as a trigger for this cell line because when present, cells will differentiate into osteoblasts and in its absence to myoblasts.[28]

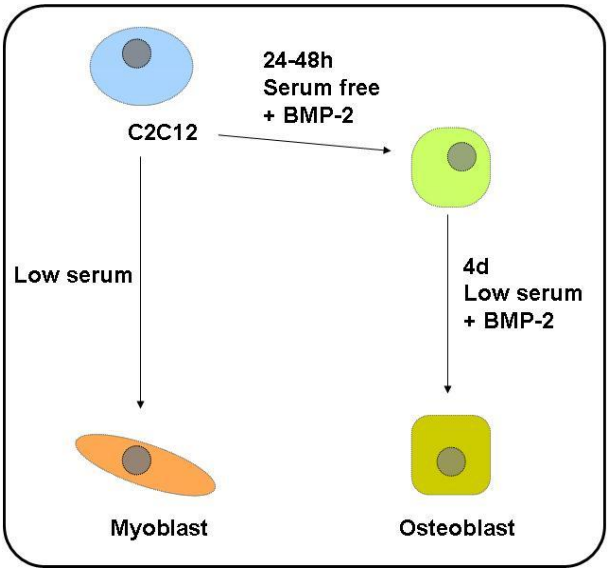

Figure 68: Differentiation pathway of C2C12 myoblastic cells with and without BMP-2. Image adapted from reference 29.

As already mentioned above, standard culture protocols usually lead to inhomogeneous cell populations composed of differentiated and undifferentiated cells. In order to take full advantage of their therapeutic potential, the ultimate challenge when working in the area of stem cell differentiation is the generation or maintaining of a population of cells with a homogeneous phenotype. An attempt on trying to avoid uncontrolled exogenous stimuli as far as possible is the immobilization of the factors on a surface and their presentation to the cell in a controlled way. A clear difference in differentiation behavior could be shown when comparing factors in solution to factors immobilized on the surface.[29] Promising results for more homogeneous cell populations have been obtained recently when using chemically modified substrates.[30,31,32]

There are many different methods with which molecules relevant for cell differentiation can be patterned and immobilized on a substrate. More detailed information can be found in the review of our group, where examples are given for the different molecules which can be immobilized.[6] Further examples include the use of a Nanoplotter[29] or an Inkjet printer[33] to immobilize BMP-2 on chemically modified glass slides. For Dip-pen Nanolithography, there are already many different applications, however, only few results are published where DPN was used for cell differentiation experiments.[31,32] Up to now, the drawbacks of this method were the missing of an automation feature and the limited area size. But in order to create surfaces for cell culture, certain claims have to be met such as large surface area of pattern (for embryonic stem cells in culture at least 500 μm in length and width)[34] and biological compatibility of substrates and ink.

Important factors for successful protein immobilization: stability, functionality and directionality

An important pre-condition for successful factor immobilization is the complete control over orientation and density of the factor on the surface. If the factor immobilization on the substrate yields denatured proteins (strong and irreversible immobilization of cytokines is likely to diminish their functionality) or the cell simply is not able to recognize the binding site due to very dense surface packing or wrong orientation, this leads to false results. There are several possibilities how a protein can

be immobilized on a substrate, but not all of them leave the protein active for cell recognition, as was shown by Kashiwagi *et al.*[35].

Instead of physical adsorption[36,37] or direct chemical linking,[38,39,40,41] our group takes advantage of the well-known biorecognition mechanism of the biotin-streptavidin pair in order to achieve a reliable and reproducible factor immobilization. Only chemical grafting strategies ensure a stable link between biomolecule and surface and avoid uncontrolled desorption under physiological conditions.[42] The only critical step before attaching the protein to the substrate is a biotinylation step, which has to ensure that the protein remains biologically active. The stable and controlled immobilization of BMP-2 on the surface is performed in order to avoid uncontrolled exogenous stimuli as far as possible and increase the homogeneity of the cell phenotype. Furthermore, the immobilized molecule is less likely to be lost by media exchange steps in long term experiments and the necessary dose is less. In our group it has already been shown that the attachment of biotinylated BMP-2 to a surface still induces stem cell differentiation in C2C12 cells towards osteoblasts.[43] Furthermore, by using the biotin-streptavidin-biotin sandwich, the proteins are given a sort of directionality away from the surface. And ultimately, due to the strong biotin-streptavidin bond (the strongest known protein-ligand interaction, almost of covalent strength)[44] the loss of the immobilized protein under physiological conditions is very likely to be eliminated.

The **aim of this chapter** is the fabrication of patterned substrates with Dip-pen Nanolithography (DPN) and their subsequent use for cell differentiation experiments. The C2C12 cell line was used as a model because it is only sensitive to the cue coming from one protein (in this case bone morphogenetic protein-2, BMP-2). For the fabrication of the substrates a sufficiently large area which is homogeneously patterned is a key issue. In a first step, the large scale approach with DPN was tested by depositing mercaptohexadecanoic acid (MHA) on gold. In a second step, a relevant molecule allowing for easy immobilization of the BMP-2 was chosen, namely biotin-thiol. The patterning of the biotin-thiol with DPN was successfully performed by using a carrier for enhanced ink flow. The carrier used for the experiments was

1,2-dioleoyl-*sn*-glycero-3-phosphocholine (DOPC), which is easily controllable. Furthermore, chemically modified glass substrates were patterned with a biotin molecule as well (biotin-azide). On these substrates, it was possible to create a large homogeneously patterned area of biotin moieties which were derivatized with streptavidin and biotinylated BMP-2 as well. For cell differentiation experiments, several gold substrates were homogeneously patterned over a large-area with biotin-PEG-thiol using DOPC. Evaluation of the cells on these substrates showed promising first results.

3.2. EXPERIMENTAL SECTION

PART A: FABRICATION OF SUBSTRATES FOR CELL EXPERIMENTS

3.2.1. Immobilization of 16-mercaptohexadecanoic acid on gold

All gold surfaces (~25 nm gold with an underlying 10 nm adhesion layer of titanium; NanoInk Inc. USA) were used as provided without prior treatment. A 5 mM solution of 16-mercaptohexadecanoic acid (MHA; Aldrich, Spain) in acetonitrile (Sigma Aldrich, Spain) was used as ink for all following experiments. The cantilevers (NanoInk Inc., USA) were immersed into the solution for 10 s and dipped shortly into pure ethanol (Panreac Química S.A.U., Spain). This procedure was repeated two more times and the cantilevers were then gently dried under a stream of nitrogen.

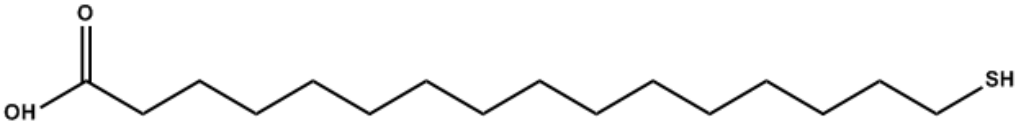

Figure 69: Molecular structure of 16-mercaptohexadecanoic acid (MHA).

Determining optimal patterning conditions

In a first step, a calibration of the ink was performed in order to correlate the dwell time with the diameter of the created spots. Therefore, a set of different dots was written on the surface (NLP2000; NanoInk Inc., USA) and the diameter was determined afterwards by AFM measurements (DPN5000; NanoInk Inc., USA). Typical dwell times used in this calibration step include 8 s, 6 s, 4 s, 2 s, 0.6 s, 0.3 s and 0.1 s.

In order to perform the patterning with the DPN instrument (NLP2000, NanoInk Inc., USA), the tips have to be leveled with respect to the substrate. Therefore, the substrate is slowly and carefully brought into contact with the tips (the tips are fixed, the substrate is moved), more precisely with the two outermost tips. The difference in

the touching angle is determined automatically by a leveling routing implemented in the instrument. After correcting the tip leveling, the plane leveling (explanation provided in Chapter 1.3.2.) has to be performed around the area where the pattern will be created afterwards. Plane leveling includes 3 touching points on the substrate distributed in a triangle and helps determining any inclination of the substrate in x and/or y and thus influences the touching force of the tips.

Further calibration experiments included the patterning of MHA using different tips (F-type and M-type), pattern shapes, spacing and area coverage, as well as adjusting the humidity for good patterning results (50 - 70% RH). Parameters of the patterns included dwell times of 0.6 - 0.1 s, dot spacing of 0.5 µm and 0.3 µm, and usually several 10 x 10 dot arrays (2 - 4 in x and 4 in y).

The optimal relative humidity was determined as 65% RH and used for all further experiments. The optimal cantilevers for patterning, which were used for all further experiments, were the 1-D cantilever array (F-type) containing 24 Si_3N_4 tips and with a spring constant of 0.053 N/m (quite soft cantilevers) and a tip-to-tip pitch of 35 µm.

In the following, small areas with arrays were expanded to larger areas with arrays and finally a large area with a homogeneous pattern. These experiments were performed gradually in order to check if the dwell times were the correct ones and also, if the leveling procedures were supporting a large-area pattern. Furthermore, it was important to make sure, that the tips won't run out of ink during the experiment and the integrity of the patterned area was not compromised. Table 7 shows the pattern parameters for the three experiments, where for the preliminary experiment (1) only one set of arrays was written (see Figure 70). In the second experiment (2), this set of arrays was repeated over 250 µm distance and for the final experiment (3), the arrays were merged together in order to yield a homogeneously patterned area. Remark: for all experiments, the number of dots and the repetition of arrays given represent the pattern written by only one of the 24 tips, but all tips perform equally. Nevertheless, the total area reflects the area covered by the pattern from all 24 tips.

Table 7: Pattern parameters for all experiments.

No.	Dot spacing	Dots per array	Repetition of arrays	Array spacing	Dwell times [s]	Total area [mm²]
(1)	0.5 µm	10 x 10	2 in x, 4 in y	2 µm	0.1 / 0.2 / 0.6	0.022
(2)	0.5 µm	10 x 10	(3 in x, 4 in y) 5 times in y	2 µm / 5 µm	0.1 / 0.2 / 0.6	0.185
(3)	1 µm	34 x 200	-	-	0.2	0.167

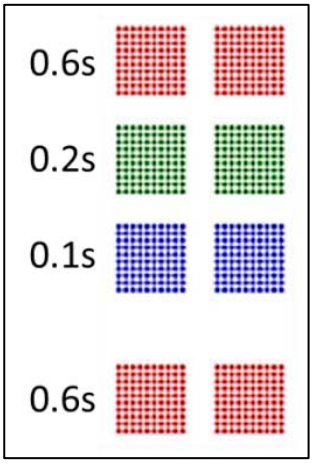

Figure 70: Pattern layout as taken from InkCad software (NanoInk Inc., USA). The 0.6 s arrays were included because they yield bigger dot size (above 100 nm diameter) and are better visible in order to locate the pattern area. The pattern is visualized for reasons of simplicity for only 1 of the 24 tips, but all tips perform equally.

After patterning, the remaining free gold surface was passivated for 40 min at room temperature in a 1 mM solution of (1-mercapto-11-undecyl)tri(ethylene glycol) (PEG-thiol; Sigma Aldrich, USA) in ethanol and subsequently rinsed with ethanol and dried with pressurized air. In order to increase the height difference and make detection with AFM easier, the sample was incubated with two antibodies (primary and secondary; custom-made, nondisclosed information) for 1 h at room temperature and subsequently rinsed with PBS and a little Milli-Q water and dried with pressurized nitrogen.

3.2.2. Immobilization of biotin-PEG-thiol on gold

In this section, three different methods for the deposition of biotin-PEG-thiol (see Figure 71) were applied: microcontact printing, Dip-pen with molecular ink and Dip-pen with liquid ink.

The biotin-PEG-thiol used was a generous gift from the group of Prof. Albericio (IRB, Barcelona, Spain).[45]

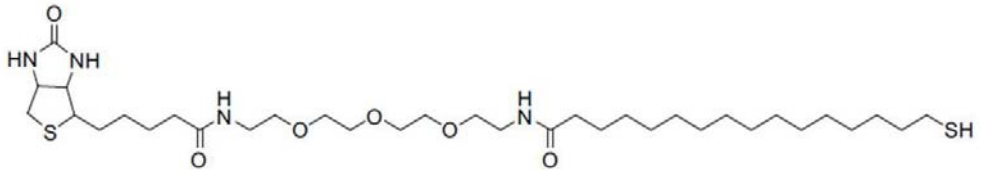

Figure 71: Molecular structure of biotin-PEG-thiol used for all further experiments on gold.

Gold surfaces were rinsed successively with THF, acetone, ethanol and Milli-Q water and subsequently immersed in piranha acid for 30 min. Afterwards they were rinsed thoroughly with Milli-Q water and dried with pressurized air. ***Caution: piranha acid is a strong oxidizer and a strong acid. It should be handled with extreme care as it reacts violently with most organic materials!***

3.2.2.1. Patterning via Microcontact printing

Fabrication of a polydimethylsiloxane (PDMS) stamp

A polydimethylsiloxane (PDMS) stamp was fabricated following reported standard procedures.[46,47] Therefore, a silicon oxide master with 5 µm broad holes was cleaned in a 1:1 mixture of isopropanol and ethanol, subsequently immersed during 1 h in piranha acid (3:7 H_2O_2:H_2SO_4), rinsed with copious amounts of water and dried with pressurized air. Directly afterwards, the master was put into a vacuum desiccator along with a few drops of silane (Perfluorooctyl-trichlorosilane; Aldrich, Spain), the chamber was evacuated and the master thus silanized for 30 min at room temperature.[48] After curing the master at 80ºC for 1 h, it was rinsed with heptane and dried. Polydimethylsiloxane (PDMS, Sylgard 184; Dow Corning, Belgium) was

prepared by mixing the elastomer base with 10 wt% curing agent and poured over the previously silanized master. The PDMS was cured at 90ºC for 1 h, cooled down and peeled off the master. Since the PDMS stamp is an inverse replica of the master, the features of the stamp are 5 μm posts with an approximate height of 800 nm.

Microcontact printing (μCP) of biotin-PEG-thiol on gold

For microcontact printing (μCP), the PDMS stamps (5 μm diameter posts and 5 μm broad lines) were cleaned in absolute ethanol, and incubated in a solution of biotin-PEG-thiol (1 mM) in ethanol for 30 min at room temperature. The stamps were then dried carefully with pressurized air, placed on the gold surface and left in contact for 1 min. After 12 h, the surface was rinsed with absolute ethanol. In order to avoid unspecific adsorption of proteins, the remaining free gold of the patterned substrates was backfilled with a 2 mM solution of PEG-thiol (Aldrich, Spain) in absolute ethanol for 2 h at room temperature (never overnight in order to avoid the substitution of the biotin-PEG-thiol by PEG-thiol which will occur otherwise!), rinsed with ethanol, dried with pressurized air and transferred immediately into a sterile environment. For a more detailed explanation of the μCP-technique see appendix F.

Immobilization of streptavidin

From this point on, the samples were handled in sterile environment and all solutions were either already sterile or sterilized before. Samples were incubated with 100 μM/mL streptavidin (SAV) or streptavidin Texas Red® (both from Cultek, Spain) in PBS for 1 h at room temperature, subsequently rinsed with PBS and stored in PBS at 4ºC until further use.

Biotinylation of BMP-2 and Western Blot Analysis

Carrier free recombinant human BMP-2 (rhBMP-2/CF; R&D Systems, USA) was reconstituted with 100 μL of 4 mM HCl (Panreac Química S.A.U., Spain), diluted with 100 μL sterile PBS (Sigma Aldrich, Spain) to a concentration of 50 μg/mL and subsequently incubated under stirring with 174 μL biotin-NHS (Sigma Aldrich, Spain) in PBS (10 μg/mL) at room temperature for 1.5 h as previously described.[49,50] The resulting biotinylated BMP-2 was purified by centrifugation using ZebaTM Spin Desalting Columns (Thermo Scientific, Spain) of 0.5 mL volume. The final concentration was approx. 1 nmol/mL.

Table 8: Buffers used for the western blot analysis.

3X sample buffer

Reagent	Amount
Glycerol	10 mL
B-Mercaptoethanol	5 mL
Sodium Dodecyl Sulphate (SDS)	2.3 g
Tris(hydroxymethyl)aminomethane (Tris)	0.76 g
Bromophenol blue	1 mg
Milli-Q water	70 mL

Bring to pH=6.8 with HCl, then add Milli-Q water for a final volume of 100 mL.

Z-buffer

Reagent	Amount
Magnesium chloride ($MgCl_2 \cdot 6H_2O$)	22.33 g
Triton X-100	10 mL
Tween 20	5 mL
Bovine Serum Albumin (BSA)	10 g
Fetal Bovine Serum (FBS)	50 mL

Bring to a final volume of 1L with Milli-Q water.

Successful biotinylation of BMP-2 was confirmed by western blot analysis using an avidin-peroxidase conjugate (see Figure 72; Sigma Aldrich, Spain). Therefore, 20 µL of biotinylated BMP-2 in PBS was added to 4 µL of "sample buffer" (see Table 8) and the mixture was heated to 100°C for 3 min. The same procedure was performed with 20 µL of the original rhBMP-2/CF (4 nmol/mL) in 4 mM HCl. Both samples were then resolved by SDS-PAGE together with 2 µL of the reference marker and electrotransferred onto a nitrocellulose membrane. The membrane was blocked against unspecific adsorption by incubation with "Z-buffer" (see Table 8). Incubation of the membrane with avidin-peroxidase was carried out overnight at 4°C at a dilution of 1:500 in Z-buffer (original stock solution avidin-peroxidase 1 mg/mL). The protein bands were finally visualized by incubating the membrane with a solution of luminol (1 mL solution A + 25 µL of solution B) and using an automatic X-ray film processor. For a more detailed explanation of the Western Blot technique see appendix G.

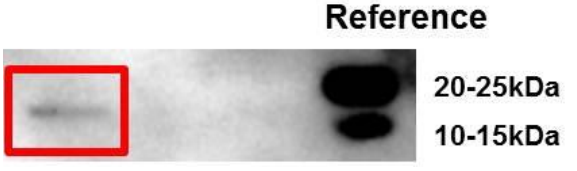

Figure 72: Western Blot analysis of biotinylated BMP-2 (left side, marked in red). Right side: reference molecules. The big band detected at ~20 kDa indicates that the contribution to the overall protein weight of the biotin molecules attached to the BMP-2 is negligible in this case.

Immobilization of biotinylated BMP-2

14 µL of biotinylated BMP-2 in PBS were incubated on the substrates for 1 h at room temperature (sterile atmosphere) and subsequently rinsed with PBS. At this point, the samples were ready for cell culture and transferred into culture well plates.

Immunofluorescence of biotinylated BMP-2

The presence of immobilized BMP-2 on the substrate was verified with immunofluorescence. Therefore, the substrate was incubated overnight at 4ºC with goat anti-human BMP-2/4 polyclonal antibody (10 µg/mL; R&D Systems, USA) in PBS with 1% BSA. After rinsing with PBS with 1% BSA (Sigma Aldrich, Spain), the sample was incubated with the secondary antibody donkey anti-goat Alexa 488 (2 mg/mL; Merk Sharp & Dohme, Spain) at a dilution of 1:500 in PBS with 1% BSA for 1 h at room temperature. Afterwards, the sample was rinsed with PBS with 1% BSA, very little Milli-Q water and carefully dried with pressurized air. The patterned area was then visualized with fluorescence microscopy using an Eclipse E1000 upright microscope (Nikon, Netherlands) equipped with a charge-coupled-device (CCD) camera and working with a green excitation G-2A long-pass emission filter. Pictures were processed with the freeware image analysis ImageJ (NIH, http://rsb.info.nih.gov/ij/).

3.2.2.2. Patterning via Dip-pen Nanolithography as molecular ink

Biotin-PEG-thiol was dissolved acetonitrile to yield a 5 mM solution. All cantilevers were cleaned and activated for 10 min in an ozone cleaner (UV/Ozone ProCleaner™ Plus, BioForce Nanosciences Inc, USA), directly afterwards immersed into the ink solution for 5 min and subsequently dried carefully with pressurized nitrogen. This process was repeated twice more before the tips were used, in order to load them with sufficient material. The tips used for the experiment were A-type chips (NanoInk Inc., USA) with only one single Si_3N_4 tip in order to calibrate the ink. Writing was performed at a humidity of 50% RH.

In order to check if the ink could be deposited, a 1 µm² square was written at a scanning speed of 1 Hz; directly after writing, the area was scanned in contact mode

with the same tip at a velocity of 5 Hz. At a higher scanning rate, the ink flow is minimized and thus deposition almost avoided. Calibration pattern were written in order to evaluate the ink deposition characteristics at different writing speeds and dwell times. Writing speed for lines included 0.02; 0.05; 0.1 and 0.3 µm/s. Dwell times for dots included 5, 10, 20, 30 and 40 s. The respective areas were scanned after lithography at elevated scanning rates (2-3Hz).

3.2.2.3. Patterning via Dip-pen Nanolithography as liquid ink

At first, two precursor inks were prepared: on one hand, biotin-PEG-thiol (see Figure 71 for the structure) was dissolved in ethanol to yield concentrations of 5 mg/mL and 8 mg/mL, respectively. On the other hand, the lipid 1,2-Dioleoyl-*sn*-glycero-3-phosphocholine (DOPC, see Figure 73; Avanti Polar Lipids Inc., Germany) was dissolved in chloroform (Sigma Aldrich, Spain) to yield a final concentration of 1 µM. The "final ink" consisted of 80 mol% DOPC and 20 mol% biotin-PEG-thiol solution and was sonicated for 15 min after mixing and directly before every use.

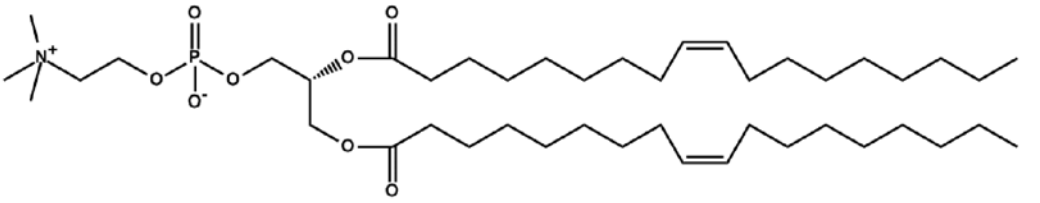

Figure 73: Molecular structure of 1,2-Dioleoyl-*sn*-glycero-3-phosphocholine (DOPC).

Patterning of biotin-PEG-thiol using DOPC as a carrier

Approximately 4 µL of the "final ink" were filled into an empty inkwell which was then placed, along with the gold substrate, into the NLP2000 chamber (NanoInk Inc., USA). A 1-D cantilever array containing 12 Si_3N_4 tips (M-ED type, NanoInk Inc., USA) was cleaned with oxygen plasma, 10 sccm at 100 mTorr with 30 W for 5 min. The tips were subsequently immersed in the ink for 15 min at a relative humidity of 70%. After inking, the RH was decreased to 35% and the tips were brought over the gold surface for patterning. The RH was adjusted during lithography. From the original 35% it was raised in steps of 5% when the ink flow seemed to worsen

(Explanation: with increasing humidity the lipids become more fluid and can flow from the tips to the surface more easily). Table 9 lists the parameters for the different patterns that were written. The first entry refers to a trial pattern over a smaller area in order to test the pattern characteristics. In general, the Z-clearance parameter was set to 50 µm. Further explanation to the pattern design is given in section 3.3.3.3 (results and discussion section), like the fragmentation of the dots into arrays for y-direction in order to minimize inhomogeneity in the pattern.

Table 9: Pattern parameters for the deposition of biotin-thiol using DOPC as a carrier.

Dots per tip in x / y (repetitions)	**Dot spacing in x and y [µm]**	**Dwell time [s]**	**Total No. dots for 12 tips**	**Total area [mm²]**
12 / 200	5.5	0.4	28800	0.86
3 *(3x)* / 5 *(11x)*	22	0.1	5940	2.79
3 *(3x)* / 5 *(14x)*	22	0.1 / 0.3	7560	3.57
3 *(2x)* / 5 *(15x)*	22	0.1 / 0.2 / 0.3	5400	2.54
3 *(2x)* / 5 *(14x)*	22	0.2	5040	2.37

After completing the patterning, the substrate was incubated overnight at 40% RH in order to minimize possible lipid spreading due to changes in the ambient humidity in the laboratory. The samples were then inspected with darkfield microscopy in order to check the quality of the lipid pattern and afterwards thoroughly rinsed with a solution of 1% Triton-X (Sigma Aldrich, Spain) in Milli-Q in order to remove the lipids and leave only the biotin-thiol which, by then, has bound to the gold. Finally, the gold surface was rinsed with Milli-Q water and dried with pressurized air. At this point, the substrates were used either for inspection of the created pattern with fluorescence microscopy by incubating with fluorescently marked streptavidin or, and this was the final goal, for cell culture experiments, wherefore they were stored until use in a dry and cool place under argon.

Immobilization of streptavidin and fluorescence imaging

The successful covalent attachment of biotin-PEG-thiol and the pattern quality were verified by incubation with fluorescently labeled streptavidin. Therefore, some of the patterned gold surfaces were incubated with a solution of 2% BSA in PBS for

30 min at room temperature, rinsed with PBS and then incubated with a solution of streptavidin-Cy3 (1:200; Invitrogen, Germany) in PBS at room temperature for 30 min. After rinsing the samples with PBS and very little Milli-Q, they were dried with pressurized air and inspected with fluorescence microscopy.

Immobilization of streptavidin and BMP-2 for cell experiments

For cell culture experiments, the remaining free gold between the patterned areas was passivated against unspecific protein adsorption by incubating the samples for 2 h at room temperature in a 2 mM solution of PEG-thiol (Aldrich, Spain) in ethanol. Afterwards, the samples were rinsed with copious amounts of ethanol, dried in a nitrogen stream and directly transferred into a sterile environment. Derivatization of the surfaces with streptavidin and biotinylated BMP-2 was performed as described above except that all reagents were sterile.

3.2.3. Immobilization of biotin on glass

In this section, three different methods for the immobilization of biotin on glass were tested: biotin-amine on epoxy modified glass; a biotinylated lipid directly on glass and finally biotin-azide on alkyne modified glass.

All glass slides were cleaned in piranha acid (3:1 v/v solution of H_2SO_4 and H_2O_2) for 30 min, rinsed with Milli-Q water and dried with pressurized air.

3.2.3.1. Patterning of biotin-amine on epoxy modified glass

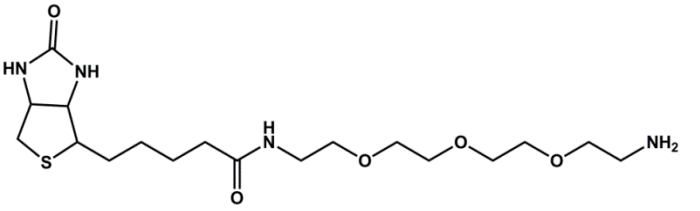

Figure 74: Molecular structure of biotin-PEO_3-amine.

Modification of the glass with (3-Glycidyloxypropyl)trimethoxysilane

After treatment of the samples with piranha acid, they were immersed in a solution of (3-Glycidyloxypropyl)trimethoxysilane (GPTMS; Aldrich, Spain) in toluene (1% v/v; Panreac Química S.A.U., Spain) for 8 h at room temperature, afterwards rinsed with acetone and dried with pressurized air.

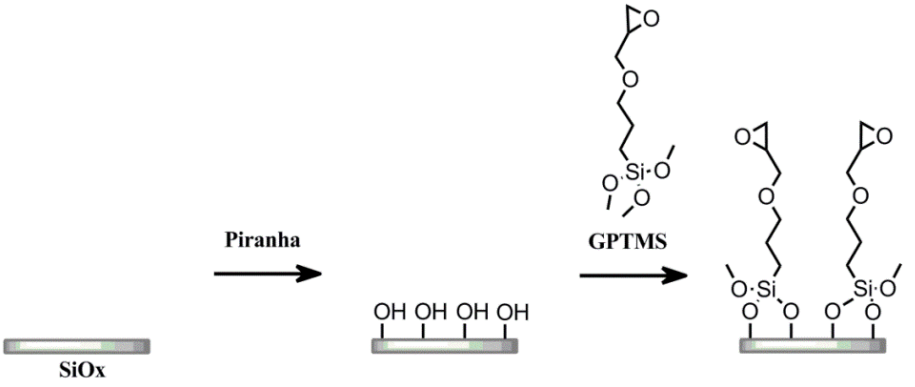

Figure 75: Reaction scheme of the functionalization of glass with GPTMS.

Patterning of biotin-amine

At first, two precursor inks were prepared: on one hand, biotin-PEO_3-amine (Figure 74; Cultek S.L., Spain) was dissolved in ethanol to yield a concentration of 5 mg/mL. On the other hand, the lipid 1,2-Dioleoyl-*sn*-glycero-3-phosphocholine (DOPC, see Figure 73) was dissolved in chloroform (Sigma Aldrich, Spain) to yield a final concentration of 1 µM. The "final ink" consisted of 80 vol% DOPC and 20 vol% biotin-amine solution and was sonicated for 15 min after mixing and directly before every use. Approximately 4 µL of the "final ink" were filled into an empty inkwell (M-type, NanoInk Inc., USA) which was then placed, along with the gold substrate, into the NLP2000 chamber (NanoInk Inc., USA). Writing was done on an NLP2000 instrument (NanoInk Inc., USA) using a 1-D cantilever array containing 12 Si_3N_4 tips (M-ED type, NanoInk Inc., USA), which was cleaned with oxygen plasma, 10 sccm at 100 mTorr with 30 W for 5 min (Plasmalab System 100, Oxford Instruments GmbH, Germany). The ink was then transferred into inkwells and inking of the tips was performed at 70% RH. Afterwards, the humidity was brought to 30%, the epoxy-modified surface was inserted into the machine and patterning was performed at 30% RH.

3.2.3.2. Patterning of a biotinylated lipid directly on glass

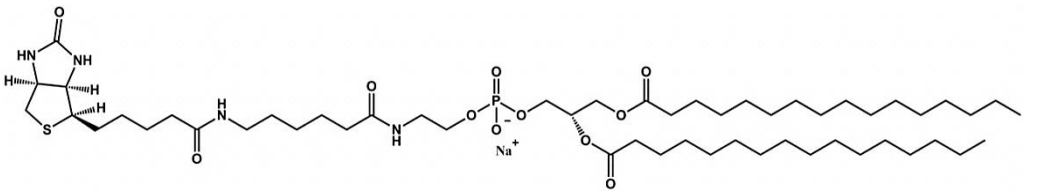

Figure 76: Molecular structure of biotinyl Cap PE.

The ink consisted of 10 g/L 1,2-Dioleoyl-sn-glycero-3-phosphocholine DOPC (Figure 73) in chloroform with 8 mol% of 1,2-dipalmitoyl-sn-glycero-3-phosphoethanolamine-N-(cap biotinyl) (sodium salt) (biotinyl Cap PE, Figure 76; Avanti Polar Lipids Inc., Germany). Writing was done on an NLP2000 instrument (NanoInk Inc., USA) using a 1-D cantilever array containing 12 Si_3N_4 tips (M-ED type, NanoInk Inc., USA), which was cleaned with oxygen plasma, 10 sccm at 100 mTorr with 30 W for 5 min. The biotinylated lipid was patterned directly on the piranha cleaned glass without chemical modification. Therefore, the ink was coated on the tips at 70% RH using inkwells. After bringing the humidity to 35%, the patterning was performed. The parameter Z-clearance was set to 70 µm.

3.2.3.3. Patterning of biotin-azide on alkyne modified glass for surface click chemistry

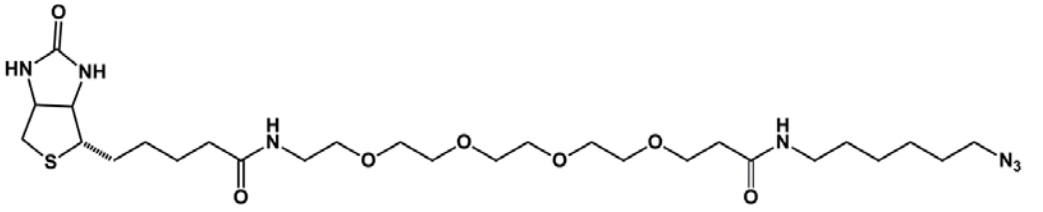

Figure 77: Molecular structure of biotin-azide.

Modification of the glass with (3-Glycidyloxypropyl)trimethoxysilane

Glass slides were cleaned as described above and then immersed in a solution of (3-Glycidyloxypropyl)trimethoxysilane (GPTMS) in toluene (1% v/v) for 8 h at room

temperature, afterwards rinsed with acetone and dried with pressurized air. Immediately afterwards, the epoxy ring-opening was performed by immersing the substrates in a solution of propargylamine in acetonitrile (2% v/v) for 8 h at 45ºC (see Figure 78). The samples were taken out of the solution, sonicated in ethanol for 5 min, rinsed thoroughly with ethanol and Milli-Q water and dried with pressurized air. If the samples were not used directly, they were stored at 4ºC under argon atmosphere.

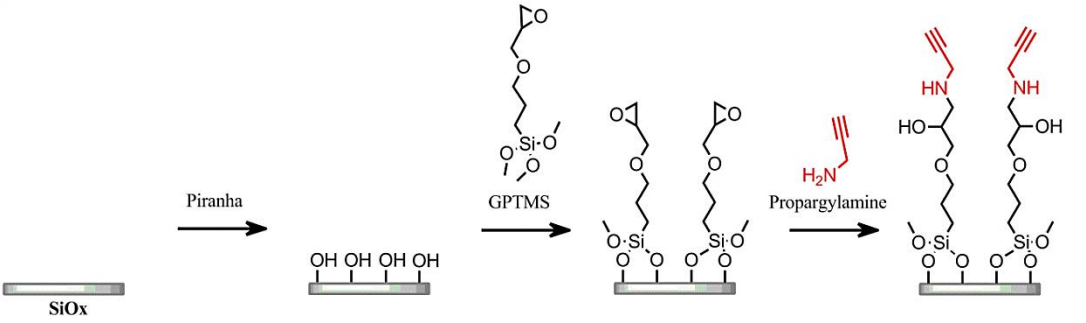

Figure 78: Reaction scheme of the functionalization of glass with GPTMS and propargylamine.

Patterning of biotin-azide

The patterning was performed in collaboration with the group of Prof. Fuchs at the KIT in Karlsruhe, Germany. Patterning of the biotin-azide was done on a DPN5000 system (NanoInk Inc., USA). A 1-D cantilever array containing 26 Si_3N_4 (F-type, NanoInk Inc., USA) was cleaned with oxygen plasma, 10 sccm at 100 mTorr with 30 W for 5 min. The cantilevers were subsequently immersed for 10 min in a solution of biotin azide (PEG4 carboxamide-6-azidohexanyl biotin, 2 mg/mL) with 20 mM sodium ascorbate and 10 mM $CuSO_4$. After inking, the cantilever arrays were blow-dried with pressurized nitrogen. Writing of the Alexa Fluor® 555 patterns was performed in feedback mode with a velocity of 1 µm/s at 74.8% relative humidity and 26.4ºC. The biotin azide dot patterns were generated with a dwell time of 2 s per dot at 74.0% relative humidity and 26.4°C.

After the DPN process for the biotin pattern the sample was blocked with a PBS solution containing 0.5% BSA for 15 min, then washed with PBS three times and incubated for another 15 min with PBS containing 1 vol% Streptavidin-Cy3 (Sigma-Aldrich GmbH, Germany). After that, the sample was washed again three times with

PBS, rinsed with Milli-Q water and blow-dried with nitrogen before inspection with fluorescent Microscopy.

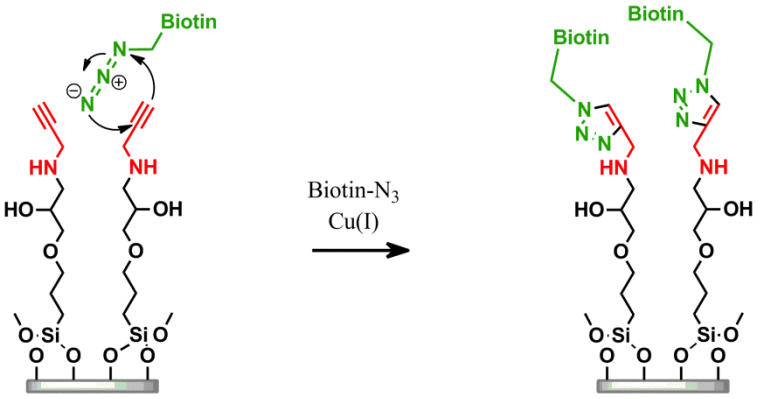

Figure 79: Surface click reaction of immobilized alkyne (in red) with incoming azide R-N_3 (in green) to yield the 1,2,3-triazole.

Patterning parameters for cell experiments

The patterning was performed as described above, with the exception that an NLP2000 (NanoInk Inc., USA) was used for the experiments. Writing of the biotin azide patterns was performed in feedback mode with a dwell time of 2 s per dot at 70% relative humidity and 29ºC. The parameters of the pattern were (per cantilever) 2 dots in x-direction and 75 dots in y-direction with a dot-dot distance of 17.5 µm.

Immobilization of streptavidin

After lithography, the samples were rinsed with Milli-Q and ethanol and thus sterilized at the same time. After drying the samples with pressurized air, they were transferred into sterile environment. All solutions used from this point on were either already sterile or sterilized before. Samples were incubated with 100 µM/mL streptavidin (SAV) or streptavidin Texas Red® in PBS for 1 h at room temperature, subsequently rinsed with PBS and stored in PBS at 4ºC until further use.

Immobilization of biotinylated BMP-2

14 µL of biotinylated BMP-2 in PBS were incubated on the substrates for 1 h at room temperature under sterile atmosphere and subsequently rinsed with PBS. At this point, the samples were ready for cell culture and transferred into culture well plates.

PART B: CELL DIFFERENTIATION EXPERIMENTS

The samples which did not contain BMP-2 have a homogeneous layer / pattern of streptavidin (SAV) presented to the cells, since the last incubation step with BMP-2 was not performed. They serve as control samples since no differentiation should be induced in the absence of BMP-2. The same applies for the surfaces with biotin or gold, where no differentiation should occur.

Cell culture

C2C12 mouse myoblast cells (kindly provided from Prof. Francesc Ventura, Hospital de Bellvitge, Spain) from passage 4 were expanded for 1 day at 37 ºC and 10% CO_2 in growth medium prior to the experiments. The growth medium consisted of: Dulbecco's Modified Eagle Medium liquid high glucose (D-MEM) supplemented with 10% fetal bovine serum (FBS), 1% L-glutamine, 1% penicillin-streptomycin and 1% sodium pyruvate (all from Invitrogen S.A., Spain). After treating the cells for 1 min with Trypsin (Invitrogen S.A., Spain), the cells were centrifuged, resuspended and seeded on the different samples.

Immunostaining of the cells for osterix

The expression of osterix (OSX) was evaluated after 24 h of cell culture in order to determine whether the cells had started to differentiation into osteoblasts or not (further explanation is given below).

Therefore, the non-adherent cells were removed by gentle washing of the samples with PBS. The remaining attached cells were fixed with a solution of 4% paraformaldehyde (Merck Sharp & Dohme, Germany) in PBS for 30 min and rinsed 3x with PBS. Afterwards, the cells were permeabilized with a solution of 0.1% saponin (Fluka, Spain) in PBS with 1% BSA for 10 min at room temperature. Subsequently, the rabbit anti mouse antibody for OSX (200 µg/mL; Santa Cruz Biotechnology Inc., Germany) was diluted 1:150 in PBS with 1% BSA and the samples were incubated for 1 h at room temperature. After rinsing twice with PBS, the samples were incubated for 1 h at room temperature in a solution of secondary antibody Alexa Fluor® 568 goat anti-rabbit IgG (2 mg/mL, diluted 1:400) and Hoechst

(10 mg/mL, diluted 1:1000; both from Invitrogen S.A., Spain) in PBS with 1% BSA. After incubation, the samples were carefully rinsed with PBS and mounted with Fluoromount (Sigma Aldrich, Spain). The samples were examined with fluorescence microscopy, using a green excitation G-2A long pass emission filter for OSX and a UV emission filter for Hoechst (stains the cell nuclei). For cell counting, Image J software was used.

3.2.4. Gold surfaces - Microcontact printing

Cells were seeded on the substrates at a density of 30.000 cells/cm^2. Table 10 gives on overview over all surfaces used in the experiment. Additional control experiments included plain gold and homogeneous biotin surfaces. All surfaces were prepared triplicate.

Table 10: µCP-Substrates for C2C12 differentiation experiments.

	homogeneous	**5 µm round**	**5 µm lines**
+ BMP-2	Homo BMP-2	5-R BMP-2	5-L BMP-2
- BMP-2	Homo SAV	5-R SAV	5-L SAV

3.2.5. Gold surfaces - DPN with DOPC

Cells were seeded on the substrates at a density of 35.000 cells/cm^2. Since the experimental set-up is the same as for the µCP surfaces (biotin-streptavidin-biotin BMP-2), no further control experiments were conducted. The samples included three types of surfaces: with BMP-2 and without (corresponding to a pattern of streptavidin). Additionally, BMP-2 in solution was used as control sample. Figure 80 gives an overview over the three sample types used for cell differentiation experiments.

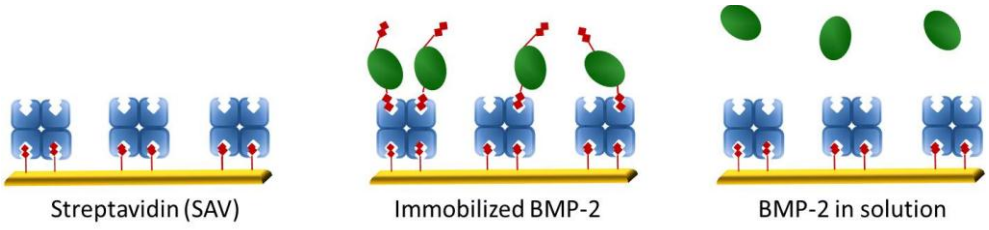

Figure 80: The three different sample types used for cell differentiation experiments.

Conditions for "BMP-2 in solution": 24 h of cell culture in culture medium and subsequently 24 h of cell culture with 300 ng/mL BMP-2 (CF BMP-2 without biotin-anchor as indicated in Figure 80). All surfaces were prepared triplicate.

3.2.6. Glass surfaces - DPN with surface click chemistry

Cells were seeded on the substrates at a density of 30.000 cells/cm^2. The samples included two types of surfaces: with BMP-2 and without BMP-2 (corresponding to a pattern of streptavidin). All surfaces were prepared triplicate. Figure 81 gives an overview over the two sample types used for cell differentiation experiments.

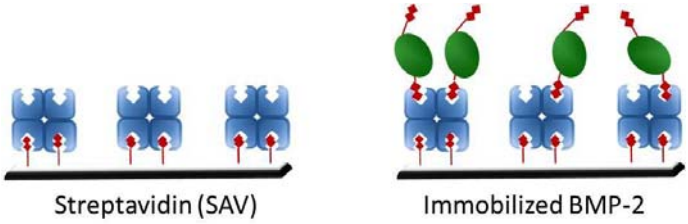

Figure 81: The two different sample types used for cell differentiation experiments.

3.2.7. Statistical analysis of the cell culture experiments

Statistical analysis was performed on all used substrates taking into account the several parameters like pattern (homogeneous, patterned with μCP and with DPN) and functionalization (with and without BMP-2). Therefore, a research hypothesis has to

be established in a first step, which comprises two different questions concerning the differentiation percentage (differentiation-%):

1) Are there significant differences in the differentiation-% due to the functionalization?

2) Are there significant differences between patterns for a differentiation-% > 90% and > 100%?

The Normality of the samples was determined by the Kolmogorov-Smirnov test and the Variance in Homogeneity by the Levene test (data not shown). Further tests included in the analysis were the Dunnett's T3 test, the no parametric Kruskall-Wallis test and the Mann-Whitney test. Significant levels were established at $\alpha=0.05$.

At least 80 cells were considered per substrate (at different locations) and all substrates were prepared triplicate.

3.3. RESULTS AND DISCUSSION

The present section is separated into two parts: Part A deals with the fabrication of substrates for cell culture using different patterning techniques. Part B deals with the application of some of the successfully patterned substrates and their application in cell differentiation experiments. This chapter was divided in such a way in order to be able to compare easily all the obtained results for the cell experiments among each other and also with related results which have been published by others.

PART A: FABRICATION OF SUBSTRATES FOR CELL EXPERIMENTS

3.3.1. Immobilization of 16-mercaptohexadecanoic acid on gold

In order to perform cell experiments on a surface, the area of the pattern has to be sufficiently large (at least 500 x 500 μm^2).[34] The homogeneous patterning of big areas with DPN has been a challenge so far, especially when the molecule of interest cannot be vapor coated on a 2D array (see Chapter 1.1) and only multi-pen arrays can be used. Homogeneous dot-like patterning can be achieved by adjusting the dot diameter and dot-dot distances so that the pattern of one tip merges with the pattern of the neighboring tip and no separate arrays are created. Figure 82 shows an example of how several tips can create a homogeneously patterned area. In a), no merge was desired and the respective pattern of each tip is clearly visible (patterning direction is from bottom to top). In b), the patterning parameters were adjusted and there are no gaps in the pattern, all dots are spaced equally.

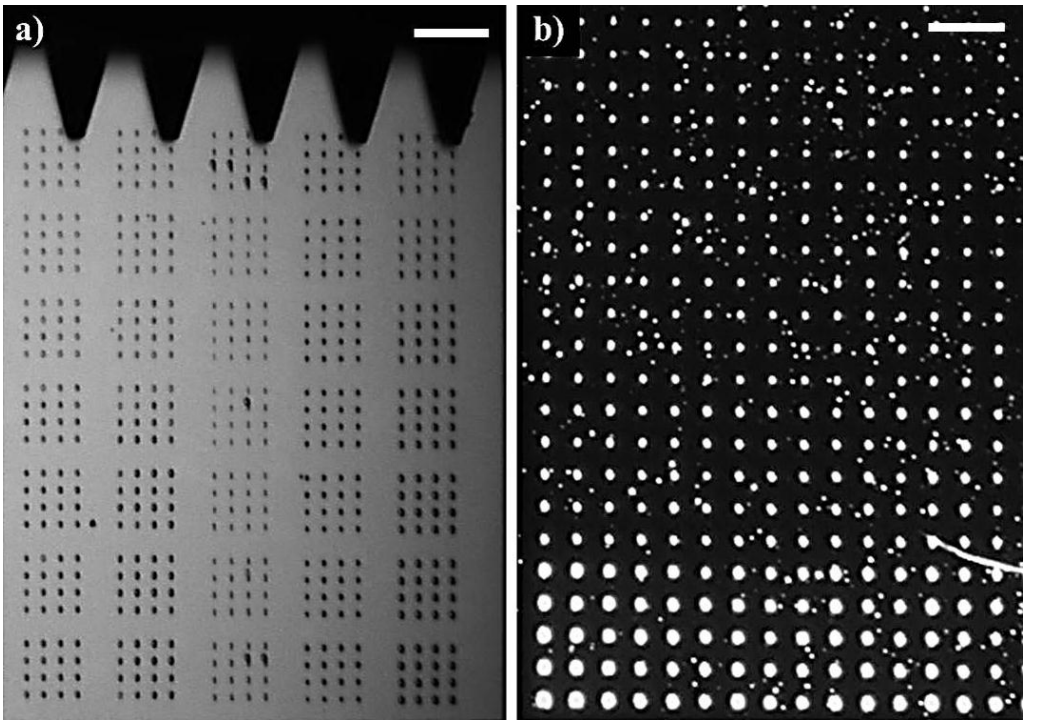

Figure 82: DOPC on gold a) Brightfield microscopy image of a set of arrays without merging the pattern of the single tips. b) Darkfield microscopy image of the homogeneously merged pattern of 5 tips (each tip wrote 3 dots in x-direction). The scale bars equal 50 µm.

For the validation of the hypothesis that a sufficiently large area can be patterned with DPN using multi-pens, 16-mercaptohexadecanoid acid (MHA) was deposited on gold substrates with the NLP2000 instrument. In this case, the NScriptor/DPN5000 is not the adequate instrument due to its limitations in automation and patterning range (see Chapter 1). Before starting the actual patterning process, experiments were performed in order to determine the optimal cantilever type and patterning conditions. Figure 83 shows the calibration pattern for several different dwell times (dt). The calculated dot diameter for the different dwell times (dt) are: (312 ± 10) nm for 8 s; (250 ± 8) nm for 6 s; (215 ± 6) nm for 4 s; (206 ± 5) nm for 2 s (see Figure 84). For the dt of 0.5 s and 0.1 s, no measurements could be performed because no pattern was visible.

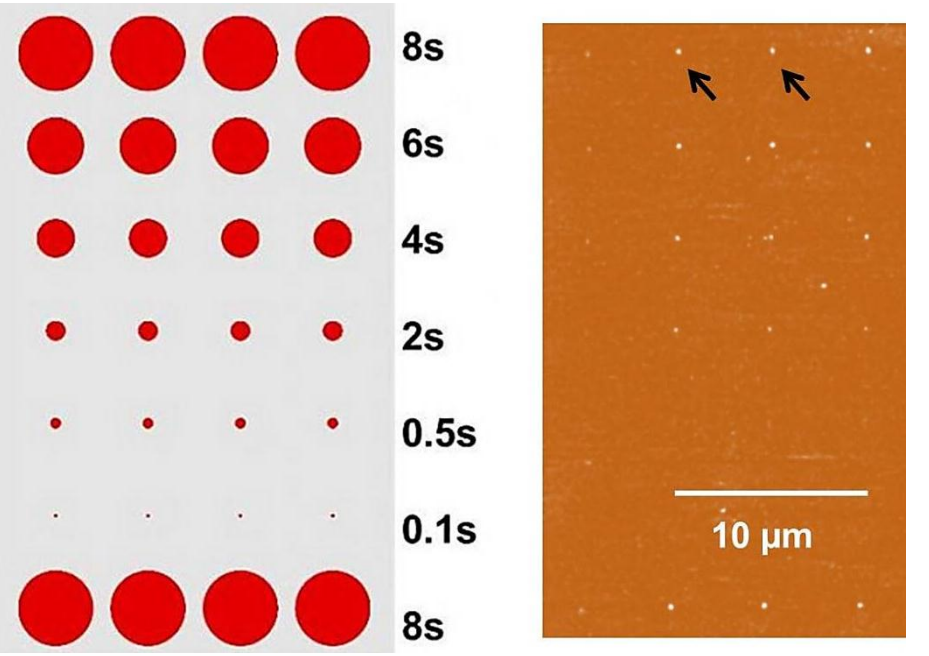

Figure 83: Calibration of the optimal dwell time of MHA (T=25ºC, RH=60%); the left image is taken from InkCad software (NanoInk Inc., USA); the right image is a lateral force mode (LFM) AFM image.

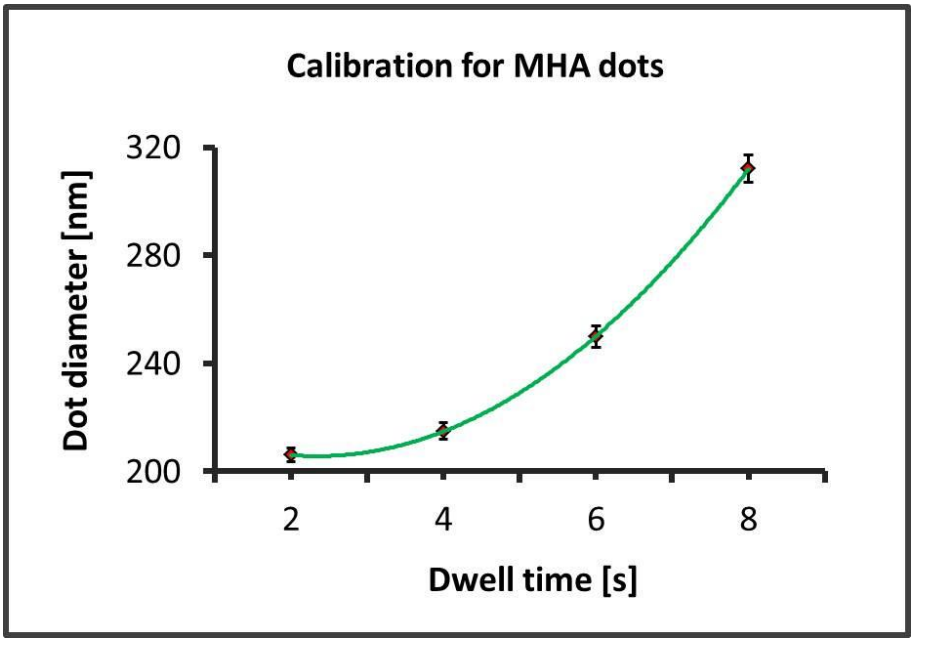

Figure 84: Calibration pattern of dots for MHA, obtained from the image shown in Figure 83. The green line represents a second-order polynomial fit.

In order to have a reasonable patterning time for an area of around 1 mm^2, the dwell time has to be adequate to meet two oppositional needs: on one hand, a short dwell time is required for reducing the total patterning time to a reasonable time, not exceeding 4 h (for the final experiment, the number of dots written by each tip will be 6800). On the other hand, a sufficiently homogeneous MHA layer is to be deposited on the substrate, which is not guaranteed at very short dwell times. Several experiments were conducted to ensure the reproducibility of a spot diameter of smaller than 100 nm.

Figure 85 shows the final experiments to define the approximate dot diameter for dwell times of 0.1 s and 0.2 s (see Figure 70 for pattern layout; dimensions of the pattern: 11 µm in x and 27 µm in y-direction). Determined diameter for a dwell time of 0.2 s is between 64 nm and 71 nm and for 0.1 s between 35 nm and 45 nm.

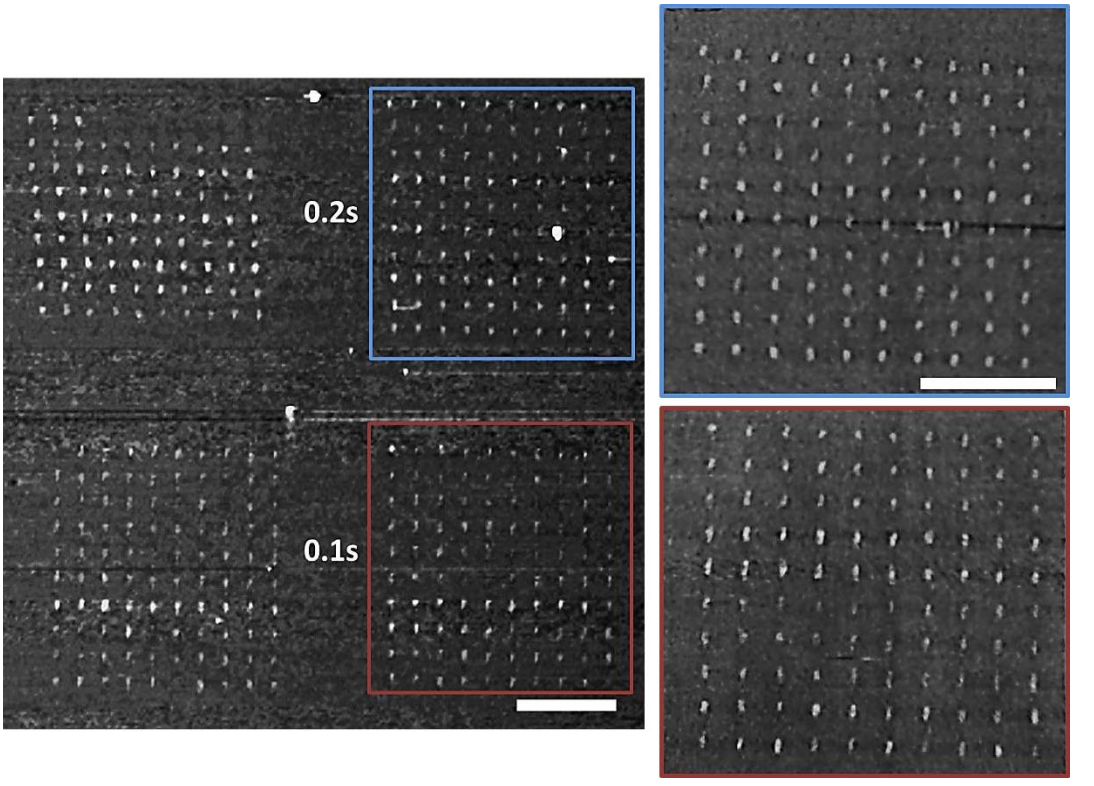

Figure 85: Lateral force microscopy (LFM) images of patterned areas with dots of dwell times 0.1 s (bottom) and 0.2 s (top). The insets give an enhanced view of the marked areas. The scale bars equal 2 µm.

After determining the pattern parameters, the obtained results for a small region were translated to a larger region in order to have a sufficiently big area for cell culture experiments (areas of minimum size 200 µm x 600 µm). *Remark: The homogeneity in x direction is assumed due to the fabrication process of the tip array.*

In a first step, the homogeneity of small array areas in a big area was tested by a set of arrays (17.5 µm in x and 27 µm in y-direction), which was repeated 4 more times, finally covering a total length of 227 µm in y-direction. The length of the pattern in x-direction is 839 µm, using 24 tips. Figure 86 shows several lateral force mode images (numbers 740 – 900, approximate size of each image is 90 x 90 µm²) which were taken at positions all over the whole patterned area and correspond to different tips. The white inset shows the pattern set-up and is scaled as to fit the AFM scans. After evaluating all LFM images, the homogeneity of the features both in x and y-direction proved satisfying.

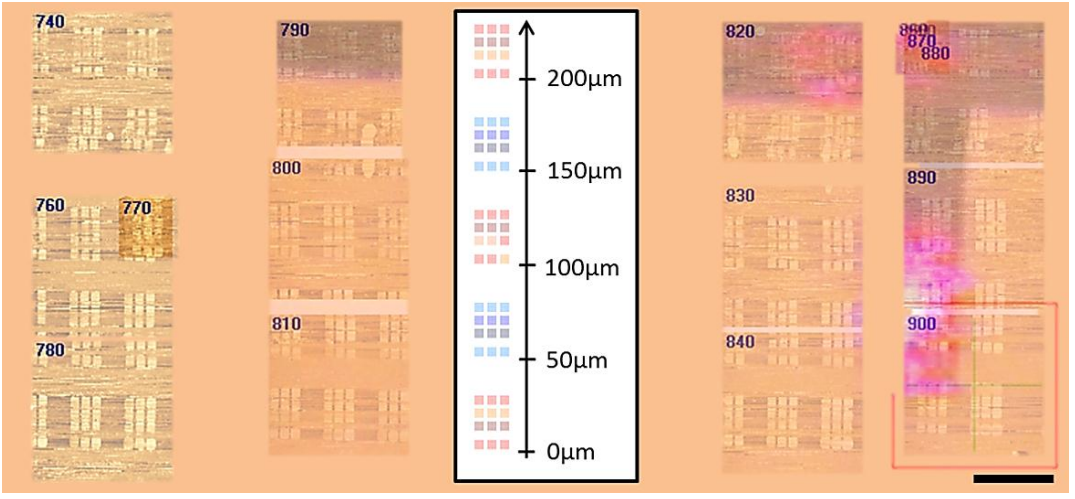

Figure 86: Stitching of LFM images consisting of scans in different areas of the big array pattern for verification of homogeneity in y-direction. The red square in the lower right corner indicated the maximum scanner area which is 90 x 90 µm². The inset is taken from NanoInk Inc. software and used to visualize the programmed pattern. The scale bar equals 50 µm.

After proving that it is possible to pattern a large area by adjusting the conditions, the following experiment was patterning a large area with a homogeneous array. Here, the pattern written by one tip merges with the one of the neighboring in order to yield a completely homogeneously patterned area. Each tip wrote 6800 dots (34 dots in x and 200 dots in y). A surface area of 199 µm x 815 µm (0.167 mm²) was

patterned with MHA dots having a diameter of less than 100 nm and a spacing of 1 µm, using a dwell time of 0.2 s. The surface was subsequently passivated with a PEG-thiol against unspecific protein adhesion and incubated with an antibody, that binds electrostatically to the carboxyl group (-COOH) of the surface bound MHA. Incubation with a secondary antibody (against the first one) yields an approximate overall Z-height of about 9 nm. Evaluation of the topographical data of the AFM measurements (contact mode) showed a definite height increase compared to the not bio-modified surfaces. Figure 87 shows two topography images obtained by AFM (tapping mode due to the higher sensitivity in Z height measurement). The mean spot diameter was below 100 nm. With these experiments, it could be shown that by using multi-pens, the patterning over a large area at very small feature size is indeed realizable.

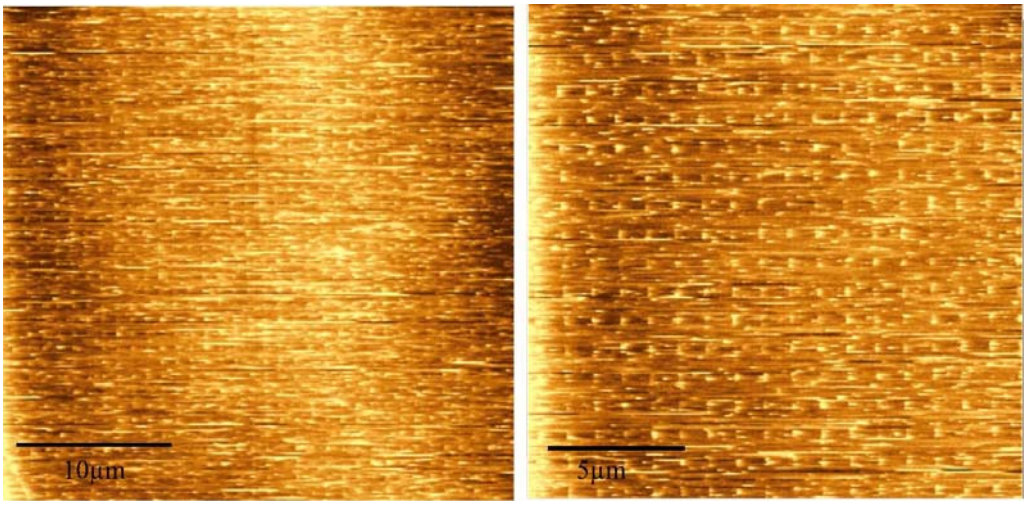

Figure 87: AFM topography images of two areas in the homogeneous pattern.

After proving that it is possible to homogeneously pattern an area which is large enough for cell experiments, the next step was finding a substitute for MHA which enables easy modification of the molecule on the surface and can thus serve as a platform for biomolecule anchoring. A molecule which complies with such characteristics is the so called biotin-thiol.[45] By simply derivatizing it with streptavidin, there are still two free binding pockets for a second derivatization step with any molecule that can be biotinylated. Promising results with this approach have already been obtained in our group previously.[51] For the following experiments, the

transforming growth factor bone morphogenetic protein-2 (BMP-2) was selected and attached to a surface functionalized with streptavidin. This was achieved by biotinylating the BMP-2.

3.3.2. Immobilization of biotin-PEG-thiol on gold

The methods used for the deposition of biotin-PEG-thiol on gold are Microcontact printing and Dip-pen Nanolithography, whereas for the latter technique two different approaches were used: a molecular ink and a liquid ink.

3.3.2.1. Patterning via microcontact printing

Before fabricating the nano-patterned substrates, all experiments were performed at the micrometer scale in order to test the feasibility of the whole experimental set-up. By doing so, it will be possible to directly compare the patterning at the micro scale (which, up to date, is predominantly used) with patterning at the nano scale. Furthermore, detection with conventional fluorescence microscopy is easier at the micro scale and does not have the risk of pattern features being too small for the resolution limit of the microscope (around 500 nm diameter).

Figure 88 shows the experimental set-up for the cell differentiation experiments onto micropatterns: patterning of biotin-thiol molecules (small red sticks attached to the surface), passivation with BSA/PEG-thiol (not shown here), incubation with streptavidin (blue blocks) and final incubation with the biotinylated BMP-2 (BMP-2 green with red sticks of biotin).

The substrates with immobilized biotin-PEG-thiol were the following: 5 μm round pattern and 5 μm line pattern, both prepared by microcontact printing (μCP). Furthermore, a monolayer of biotin-PEG-thiol was prepared by saturating the gold surface with molecules and subsequently incubating with an excess of streptavidin. This type of substrates is further referred to as “homogeneous”.

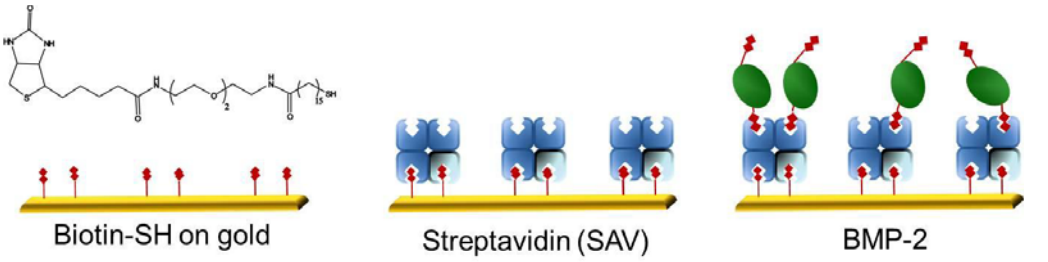

Figure 88: Experimental set-up of the μCP experiments for cell differentiation.

The quality of the obtained pattern of biotin-PEG-thiol on gold was assessed by fluorescence microscopy together with the selective binding of streptavidin to the biotin pattern. Also, the immobilization and co-localization of BMP-2 was evaluated. Figure 89 and Figure 90 show the pattern (round and lines) after the first derivatization with fluorescently labeled streptavidin (left side, red image, fluorophore is Texas Red) and after immunofluorescent detection of the biotinylated BMP-2 with a fluorescently labeled secondary antibody (middle, green image, Alexa 488). The spots have a diameter of 5 μm, perfectly reproducing the features of the μCP stamp and the co-localization of both fluorescent images can be appreciated on the right side.

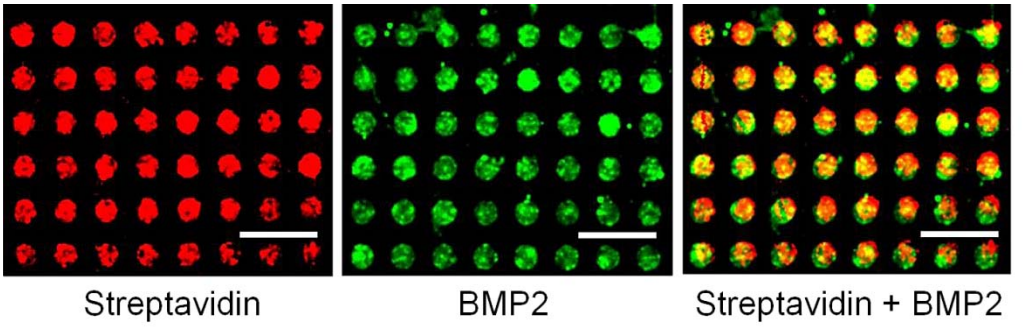

Figure 89: Fluorescence microscopy images for the 5 μm round pattern: (left side) streptavidin-Texas Red immobilized on biotin-PEG-thiol; (middle) biotinylated BMP-2 over streptavidin, detected with immunofluorescence; (right side) co-localization of both fluorescence microscopy images. The scale bars equal 20 μm.

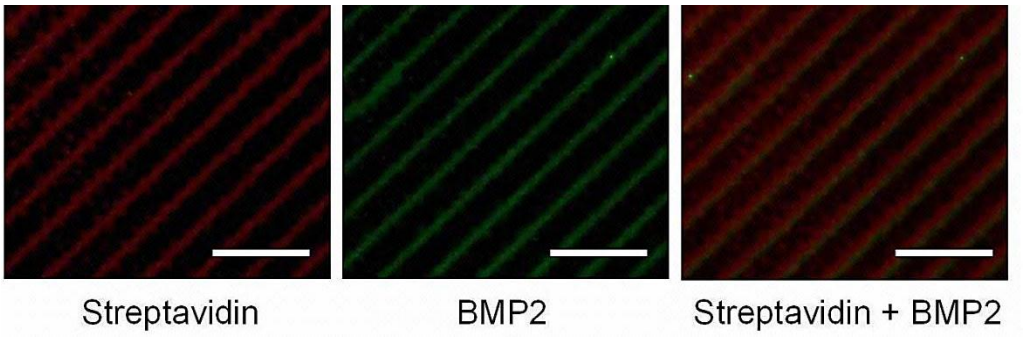

Figure 90: Fluorescence microscopy images for the 5 µm line pattern: (left side) streptavidin-Texas Red immobilized on biotin-PEG-thiol; (middle) biotinylated BMP-2 over streptavidin, detected with immunofluorescence; (right side) co-localization of both fluorescence microscopy images. The scale bars equal 50 µm.

After proving that it was possible to anchor the biotinylated BMP-2 in a stable and selective manner on the surface where it resists washing steps, cell differentiation experiments were performed as to test the influence of the immobilized BMP-2 on C2C12 myoblastic cells: see section 3.3.7.

3.3.2.2. Patterning via Dip-pen Nanolithography as molecular ink

In order to change the pattern from the micro to the nano scale, biotin-PEG-thiol was deposited in a similar manner as presented in section 3.3.1. for MHA. Figure 91 shows the lateral force mode (LFM) image of a calibration pattern written with biotin-PEG-thiol ink.

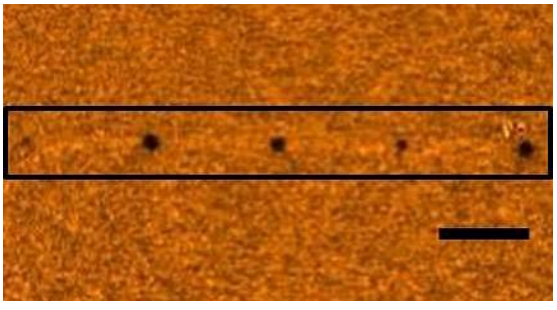

Figure 91: Lateral force mode (LFM) image of biotin-PEG-thiol deposited on gold via DPN. The black square indicated the area of the dots. The dwell times – from left to right – are 5 s, 40 s, 20 s, 10 s and 30 s. The scale bar equals 1 µm.

The spots marked in the black square indicate that the deposition of biotin-thiol via DPN was possible. Nevertheless, no reliable and reproducible results could be obtained with this approach. This might be due to the poor solubility of the biotin-PEG-thiol in the solvents tested for deposition (ethanol, methanol and acetonitrile) which leads to only few molecules on the tip or, on the other hand, to an energy barrier which favors the molecules remaining on the tip instead of flowing towards the surface.

Figure 92 shows the two calibration curves for dots deposited with MHA (blue line) and biotin-PEG-thiol (red line). It is obvious that the slope of the red line is very low, when compared to the blue. This means that the dot diameter increases only very slow with increasing dwell time. This also means that, in order to get bigger dots, the dwell time has to be increased dramatically and the overall patterning time will become too long. This finding is in good correspondence with a work published by Rakickas *et al.* who reported that, using a biotin-disulfide as ink on gold substrates, spot diameters of 200 nm were achieved with dwell times of 60 s.[52] For an array with 6800 dots (as shown above with MHA, see section 3.3.1.), it would take 113 h, corresponding to almost 5 days for one substrate.

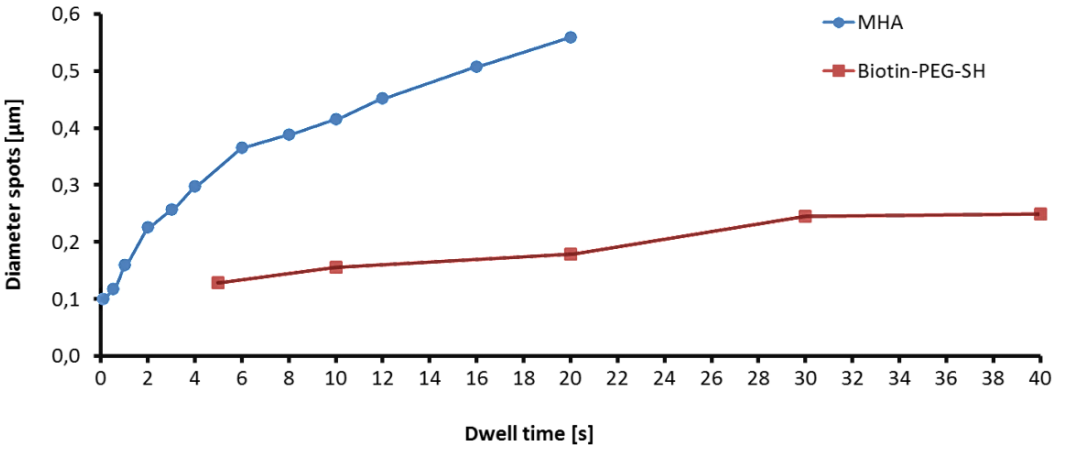

Figure 92: Calibration curve for biotin-PEG-thiol (red line). The values were obtained by measuring the calibration pattern dots with the InkCad software. As a reference, the calibration for MHA is given (blue line).

Due to the facts of no reproducibility and disadvantageous deposition characteristics, this approach was regarded not suitable for the fabrication of substrates for cell experiments.

A solution for the bad deposition characteristics of the biotin-PEG-thiol can be found in the use of a so called “carrier material”. Carriers usually have a well-controlled behavior concerning lithography and can be deposited easily.

3.3.2.3. Patterning via Dip-pen Nanolithography as liquid ink

In order to overcome possible energy barriers which can have a negative effect on the ink flow from the tip to the surface, a carrier can be used to facilitate the ink flow. Several different carriers have been used successfully for Dip-pen Nanolithography (DPN): agarose[53] and polyethyleneglycol (PEG)[54]. Special attention has also been paid to lipids, which have been successfully used for the immobilization of biomolecules on a surface and are very well known for the delivery of drugs and other active ingredients by encapsulation.[55,56] Furthermore, a patent application states their suitability as carrier for patterning.[57]

When using 1,2-dioleoyl-*sn*-glycero-3-phosphocholine (DOPC) as a lipid, acetonitrile cannot be used as solvent due to solubility problems, as well as PBS, where the lipid is very likely to form micelles. Therefore, ethanol was used as a solvent for the biotin-PEG-thiol. DOPC in particular was chosen because it can be controlled easily by adjusting the relative humidity and the group of Professor Fuchs had plenty of experience in the deposition of DOPC with DPN.[58,59,60]

The first experiments aimed at determining the optimal patterning conditions like the relative humidity (RH) for inking and lithography. After being able to pattern reliably homogenous dot arrays (see Figure 93 for a section of the whole pattern) over larger areas (see Table 11 for pattern specifications), the pattern was examined for the presence of biotin. Therefore, the sample was directly incubated with fluorescently labeled streptavidin and examined under a microscope. Figure 94 shows that the biotin-PEG-thiol could be successfully deposited on the gold surface.

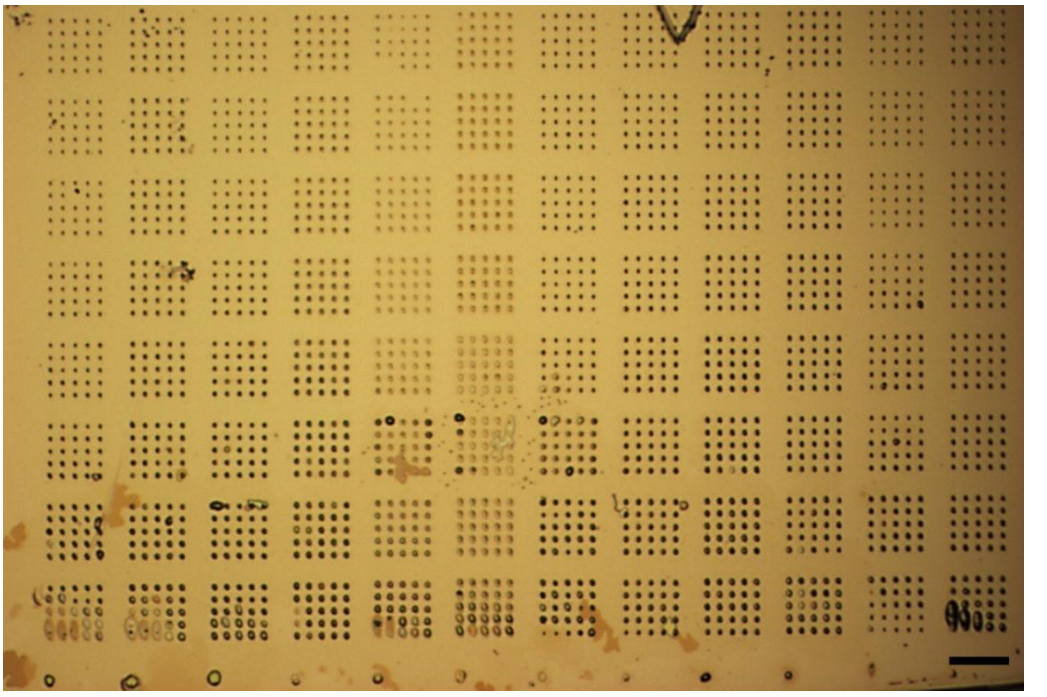

Figure 93: Brightfield microscopy image of DOPC dots on gold. DOPC is used as a carrier to facilitate the deposition of biotin-thiol. The pattern of all 12 tips is shown; each tip wrote one array of dots per line. Writing direction is from bottom to top and the scale bar equals 50 µm.

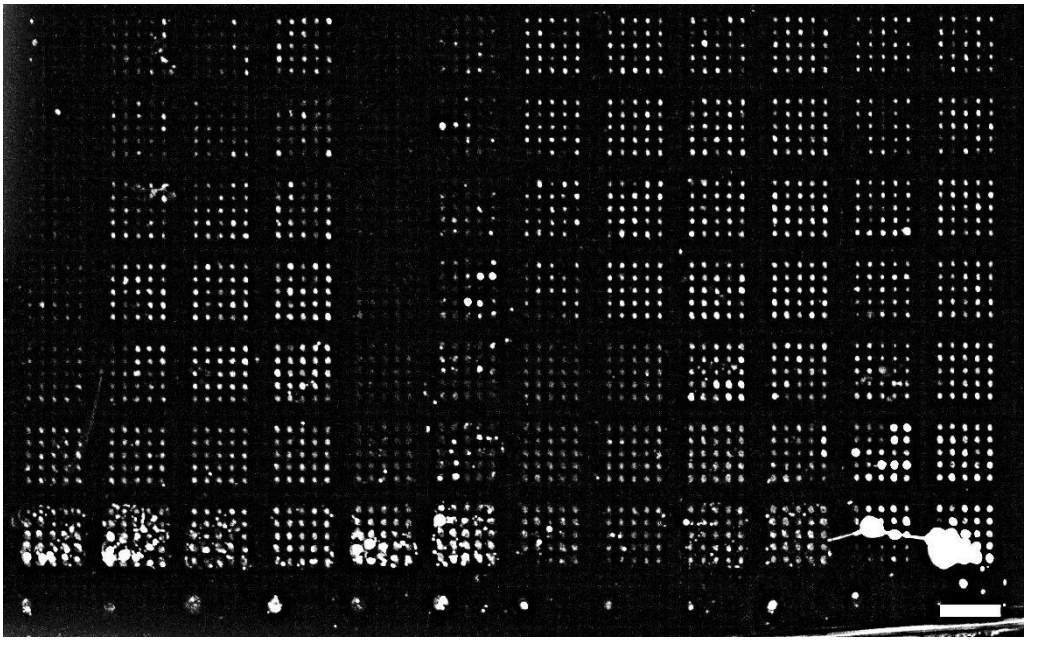

Figure 94: Fluorescence microscopy image of streptavidin-Texas Red which specifically bound to the biotin, which was deposited using DOPC as a carrier. The scale bar equals 50 µm.

Table 11: Details of the test pattern of biotin-PEG-thiol deposited on gold using DOPC.

Dimensions x-y (mm²)	Area (mm²)	Dots	Dots/mm²	Patterning time
745 x 1055	0.786	5100	6489	~ 75 min

After verification that the biotin was deposited along with the lipid carrier DOPC, the concentration of biotin-thiol in the ink was increased from an initial 5 µg/mL to 8 µg/mL in order to ensure that sufficient biotin will be present. Furthermore, even though DOPC is biocompatible and might be used in cell culture, it was beneficial to remove it from the surface for further experiments, in order to avoid the likely smearing of lipids under the shear flow of the washing steps.

For this purpose, Triton X-100 (a detergent) was used and all surfaces were rinsed with a 0.1% solution of Triton X-100 in Milli-Q after an incubation of 12 h at low RH. The incubation step was included in order to assure that the biotin-thiol had sufficient time to bind to the gold and will not be removed during the washing step. The suitability of this approach was tested by passivation one of the surfaces with BSA and subsequent incubation with fluorescently labeled streptavidin. The resulting fluorescent pattern was perfectly visible in fluorescence microscopy and no smearing of the pattern could be detected. The lipid could be removed from the surface and the biotin-PEG-thiol was still in its place. The washing procedure was therefore included for all further experiments.

With the deposition parameters adjusted and the proof that biotin-PEG-thiol could be immobilized correctly, the next step was the expansion of the pattern as already explained in section 3.3.1. Therefore, a large area was patterned in order to evaluate the pattern homogeneity and the limitations of the DOPC ink. Figure 95 explains how this expansion can be obtained. After completing the pattern in y-direction, the whole set of cantilevers is shifted a specific distance to the left or right, where the patterning is continued. If all distances are calculated well, the resulting pattern will be homogeneous.

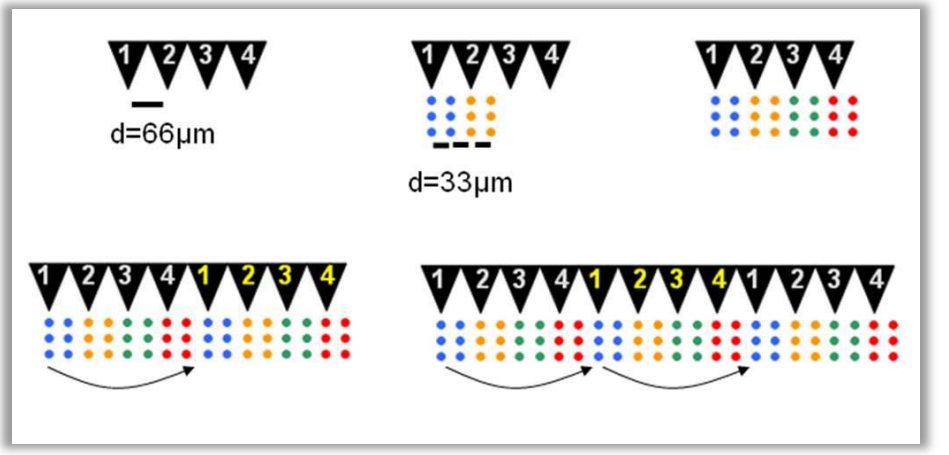

Figure 95: Schematic explication of the pattern expansion in x-direction by moving all cantilevers to the right (arrow). (Distance between tips is 66 µm, between spots 33 µm.)

Applying this strategy, a pattern is obtained (Figure 96). The patterning process started on the bottom left side, continued to the top and then, the whole cantilever array was moved to the right and the patterning started again from bottom to the top. The numbers indicate the different tips (12 cantilevers on the chip). In order to be able to better distinguish between the first area (blue numbers) and the second (green numbers), the first area has double the y-spacing between the dots.

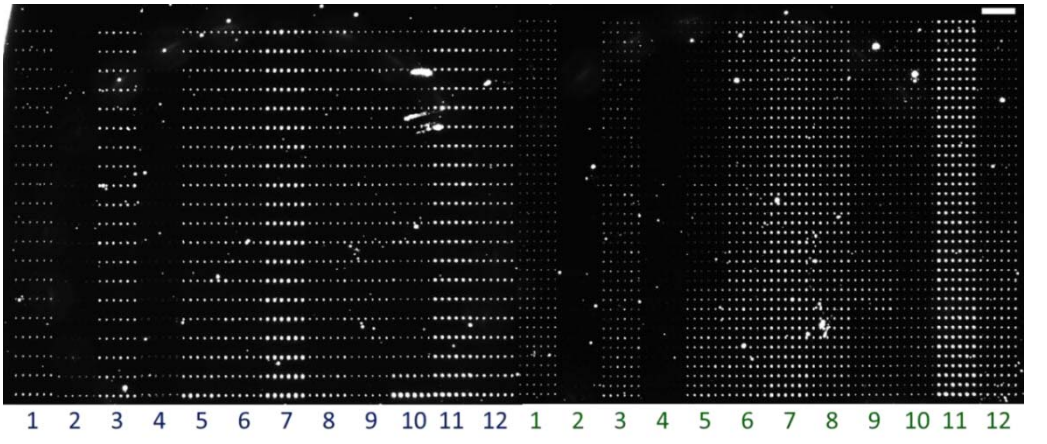

Figure 96: Darkfield microscopy image of DOPC with biotin-thiol on gold after patterning. The numbers indicate the different cantilevers; the writing direction is from bottom to top. Blue numbers indicate where the first area was patterned and the green where the whole cantilever array was moved to the right and the pattern area thus amplified. The scale bar equals 50 µm.

The resulting pattern is more or less homogeneous for the blue numbers. For the green numbers, a slight gradient in y-direction can be seen, especially for tips number 5 and 12, which were slowly running out of ink. In order to increase the overall homogeneity of the patterned area, changes were made to the patterning routine as indicated in Figure 97. The image on the left side shows the pattern of the first tip (red dots). The red arrows correspond to the way each tip makes during lithography, meaning that the tip will fist pattern the left column of dots (blue number 1), move to the right and then pattern the right column (green number 1). For all further experiments, the tip described the way as indicated in the image on the right side, where each column is written in fractions in order to minimize the gradient.

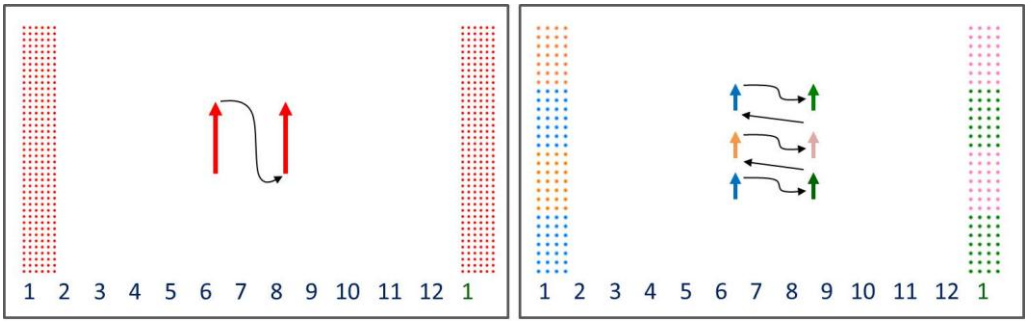

Figure 97: Schematic set-up of the improved patterning conditions (right side) for a big area pattern with one or two shifts in order to amplify the area in y-direction. Numbers indicate the different cantilevers; blue is the first patterning area, green the second after the shift. For simplification, the pattern of only one cantilever is shown but all cantilevers perform equally.

Even though there are a lot more movements, the pattern quality does not suffer and the homogeneity could be improved, as can be observed in Figure 98. The quality of the gold surface was quite low which is indicated by the scratches, which are highly visible in darkfield microscopy. The holes in the pattern could have been caused by dirt which is taken up by the tip but gotten rid of again during patterning. Further improvement of the pattern homogeneity was achieved by testing different dot densities of the pattern. For high dot densities, the pattern is less likely to be homogeneous since the cantilevers can run out of ink faster. Table 12 shows a comparison of the arrays of Figure 98 and Figure 99. An example for a high-density surface is shown in Figure 99.

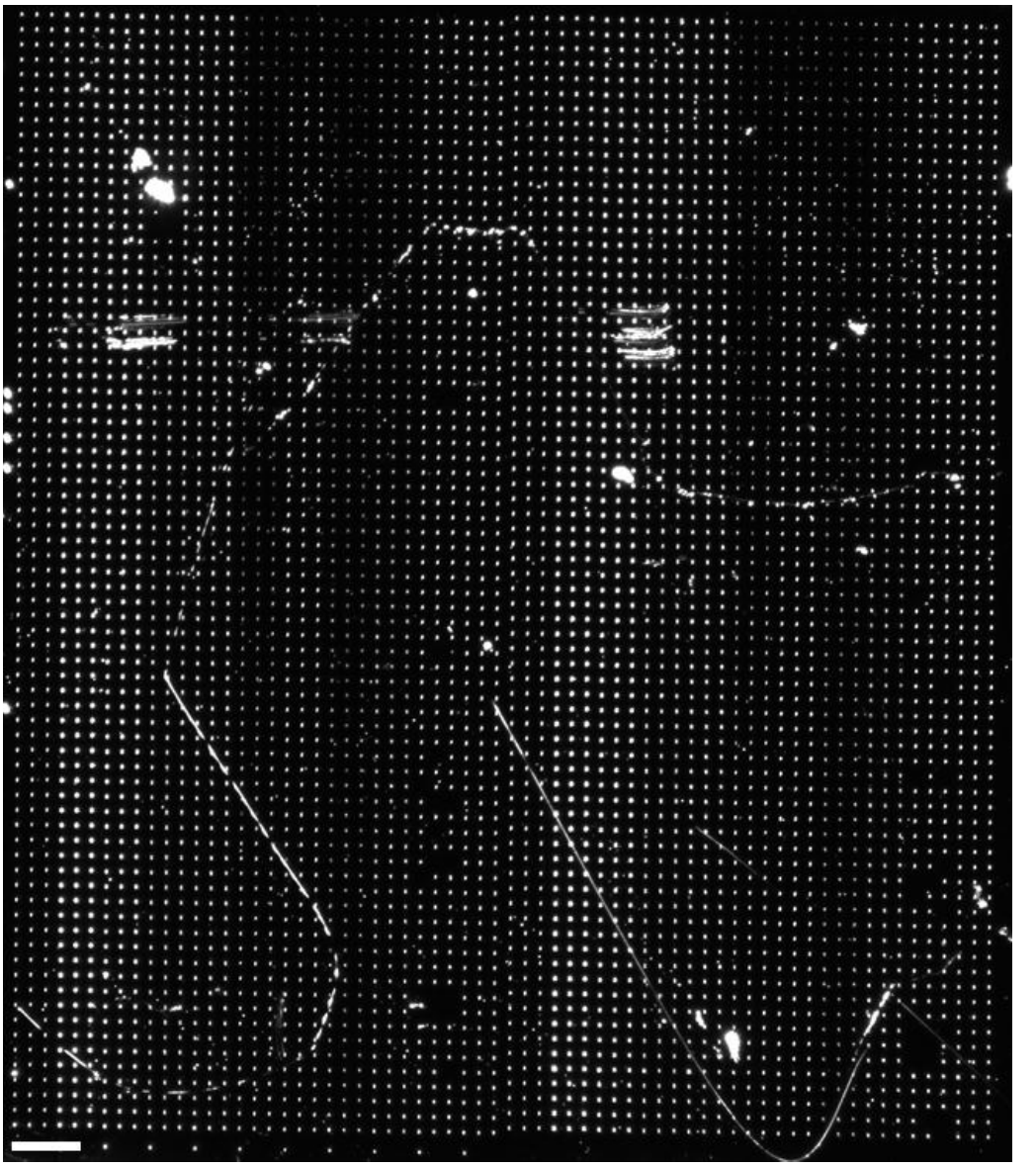

Figure 98: Darkfield microscopy image of a pattern of DOPC with biotin-PEG-thiol on gold. The homogeneity of the pattern was increased by changing the patterning routine towards stepwise patterning of small fractions. The scale bar equals 100 µm.

Table 12: Comparison of the features of a low-density and a high-density array of DOPC.

Array	Pattern dimensions (x-y)	No. of dots	Dots / mm²
Low-density (Figure 98)	1452 x 1628 µm²	4950	2094
High-density (Figure 99)	660 x 1573 µm²	8784	8460

The patterning direction is from bottom to top and it is clearly visible that the amount of ink which is deposited is decreasing during the lithographic process.

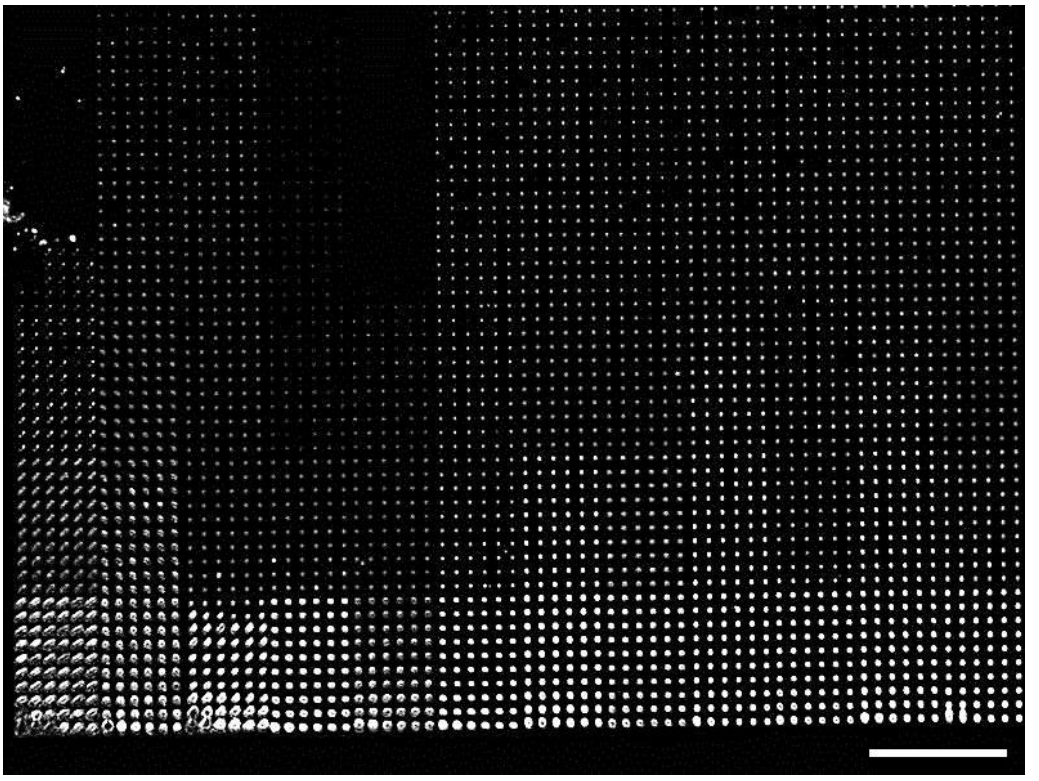

Figure 99: Darkfield microscopy image of a half a pattern of DOPC with biotin-PEG-thiol deposited on gold. The high dot density/mm² leads to inhomogeneity in Y-direction (the writing direction, which is from bottom to top). The scale bar equals 100 µm.

Figure 100 shows a table with different values for the dot density and different pattern sizes. After evaluation of all patterns by darkfield microscopy, concerning the homogeneity and integrity of the complete patterned area, the optimal dot density value was determined for around 4000 dots/mm² (red encircled data points in the graph). This decision was taken due to personal evaluation of all created pattern with microscopy, considering the highest density possible (the smallest dot-dot distance) without losing pattern quality. This approximate density was used for all further experiments.

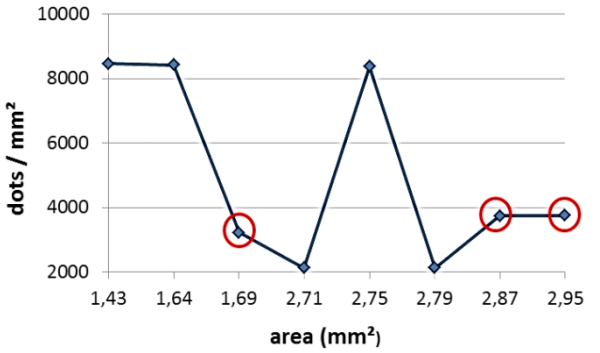

area (mm²)	dots	dots/mm²
1,43	12096	8459
1,64	13824	8429
1,69	5445	3222
2,71	5760	2125
2,75	23040	8378
2,79	5940	2129
2,87	10752	3746
2,95	11088	3759

Figure 100: Graph and table for different dot densities. The dot density was calculated with the pattern area and the total number of dots written. The red circles indicate the – as determined – optimal dot densities for further experiments.

In order to estimate the approximate quantity of deposited DOPC and biotin-PEG-thiol, the mean dot size for the arrays was determined as 4.01 ± 0.90 µm (mean dot area 53.20 ± 23.89 µm²; determined from 100 random dots in the array). Furthermore, a recently published work determined the mass transfer of DOPC doing Dip-pen Nanolithography.[61] Following these calculations, we take into account that dot areas > 65 µm² have a mass transfer of 1.59 ± 0.10 pg ink/dot and dot areas < 65 µm² have a mass transfer of 0.08 ± 0.02 pg ink/dot, since the dots are bigger at the beginning of the array and get smaller during patterning because of ink loss (for the calculated dots, 72% are bigger than 65 µm² and 28% smaller). The estimated number of molecules is therefore 2.48 x 10^8 (for bigger dots) and 1.25 x 10^7 (for smaller dots). Thus it can be deduced that for bigger dots 411.82 amol of biotin-PEG-thiol are deposited and for smaller dots 20.72 amol. These values are only estimated since the humidity during deposition varied and ranged from 35 % to 55% and was therefore not fixed as for the work of the group of Prof. Fuchs.

Further combination of the obtained values for number of molecules deposited and dot areas obtained from the images leads to the estimation of biotin-PEG-thiol molecules per surface area: around 2.5 x 10^6 molecules/µm² for all dots, which corresponds to 4.1 amol/µm² biotin-PEG-thiol (in more detail: 3.1 x 10^5 molecules/µm² for small droplets and 2.7 x 10^6 molecules/µm² for big droplets).

In order to be able to calculate if a monolayer of biotin-PEG-thiol was formed in the spots, the stearic acid molecule was chosen as approach. This comparison is based on the structural similarity which both molecules present due to their aliphatic chain and they should very likely arrange themselves in a similar way. If we estimate that one molecule of stearic acid (M = 284 g/mol) occupies 21 Å² (taken from reference 62) we can calculate that there is a density of 4.76 x 10^6 molecules/µm² for the stearic acid. For the biotin-PEG-thiol, the values for large droplets correspond to a closed monolayer whereas the values for the smaller droplets correspond to a spaced-out monolayer.

After the fabrication of several equally patterned substrates, they were incubated overnight, rinsed with the detergent solution, passivated with PEG-thiol and then derivatized first with streptavidin (SAV) and subsequently with biotinylated BMP-2 (half of the substrates, the other half was used as negative control with only SAV). Then, they were applied for cell differentiation experiments with C2C12 cells, see section 3.3.7.

The next step was taking the patterning of biotin from gold to glass. All experiments involving cells are preferably performed on glass substrates due to possible quenching for fluorescence staining or loss of contrast when using colorimetric staining. Obviously, glass substrates are also easier to use for conventional light microscopy since they are completely transparent.

3.3.3. Immobilization of biotin on glass

In this section, three different methods for the immobilization of biotin on glass were tested: biotin-amine on epoxy modified glass; a biotinylated lipid directly on glass and finally biotin-azide on alkyne modified glass.

3.3.3.1. Patterning of biotin-amine on epoxy modified glass

To transfer the patterning of a biotin molecule from gold onto glass and yet maintain its local and covalent anchoring, the glass surface has to be functionalized previously. The modification chosen was an epoxysilane due to its stability during the functionalization step and also during the patterning step. At the same time, the opening of the epoxy ring with an incoming amino group is an easy and fast reaction which doesn't require any activation or other treatment, like for example when carboxyl groups are used. The biotin molecule therefore has to have an amine group instead of a thiol as used for gold. The often used maleimide group together with a biotin-thiol was disregarded due to problems experienced earlier on (Chapter 2.3.1.).

The patterning of biotin-amine was performed as described for the biotin-thiol using the DOPC lipid. Figure 101 shows a brightfield image of the patterning process of biotin-amine on epoxy-modified glass. The arrows indicate areas where the patterned liquid drops are not staying in their place but rather spreading out, causing the pattern to smear and merge. This happens due to the epoxy group rendering the surface very hydrophilic which leads the lipid ink to spread out instead of staying locally defined. Even though the humidity was decreased dramatically, this effect could not be avoided and is even more visible with fluorescence microscopy, after binding streptavidin-Texas Red to the immobilized biotin (see Figure 102).

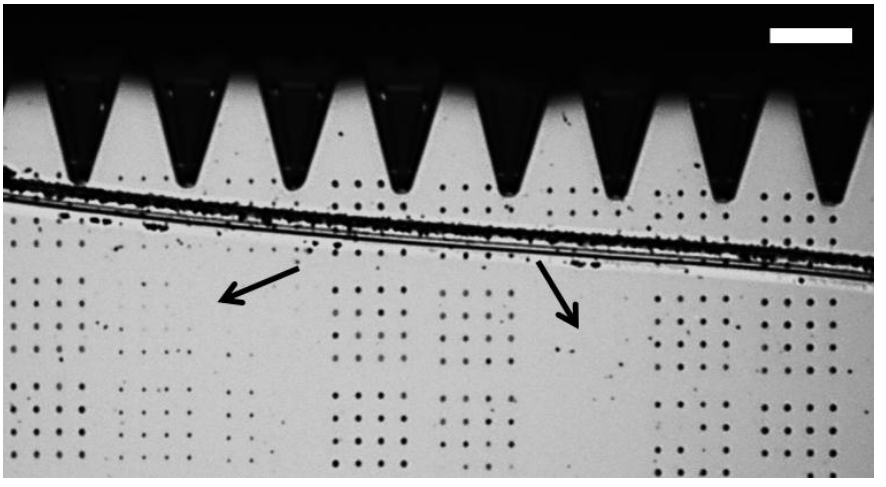

Figure 101: Brightfield microscopy image of the patterning process of biotin-amine on epoxy-modified glass, using DOPC as a carrier. Writing direction is upwards. The arrows indicate where the pattern is spreading. The scale bar equals 50 µm.

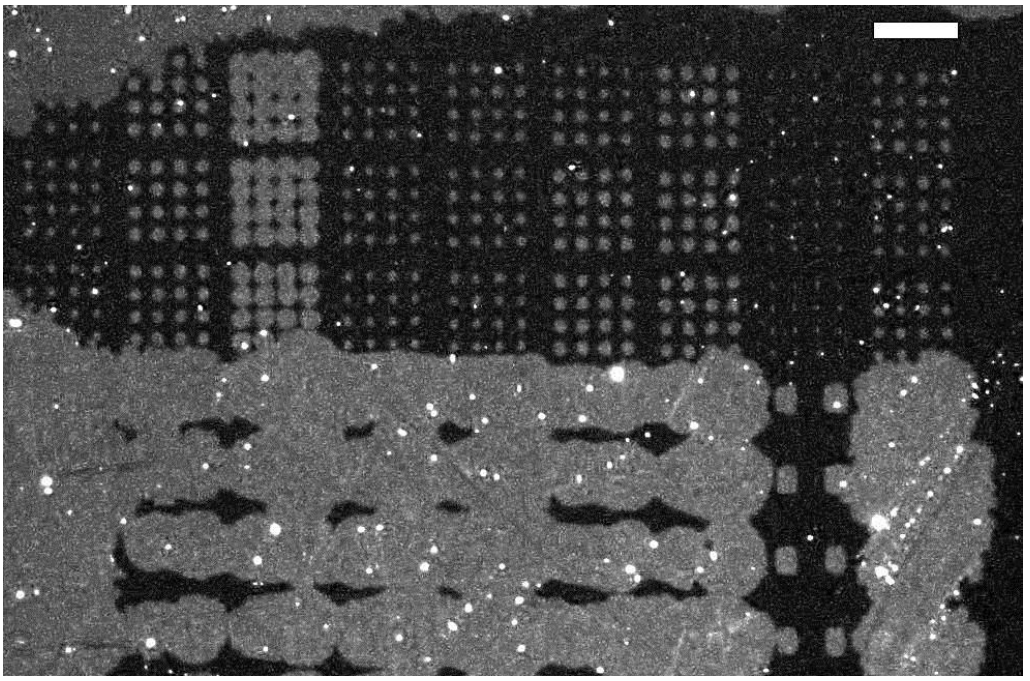

Figure 102: Fluorescence microscopy image of streptavidin-Texas Red bound to biotin-amine, which was covalently immobilized on an epoxy-modified glass surface. In the lower part of the image, ink spreading can be observed, leading to the destruction of the individual pattern. The scale bar equals 50 μm.

Since it was not possible to obtain a locally confined pattern due to ink spreading, this approach was not suitable for the fabrication of substrates for cell experiments.

3.3.3.2. Patterning of a biotinylated lipid directly on glass

A different approach for obtaining a biotin moiety on a glass substrate is the direct patterning of a biotinylated lipid on not modified glass, which was considered a good alternative in terms of hydrophilicity of the substrate and the problems experienced during patterning. Therefore, the lipid "biotinyl Cap PE" (see Figure 76) was patterned on glass and incubated with SAV-TR. Even though the patterning step itself seemed to give very good results, after passivation with BSA and incubation with fluorescently labeled streptavidin (SAV), the pattern was smeared from the shear flow which is caused during the washing steps. Figure 103 shows two fluorescence

microscopy images of the same area before and after the washing steps: A) was taken directly after patterning, taking advantage of the mixed-in FITC fluorophore in the ink. The separate lines in the letters are clearly distinguishable. This isn't the case anymore after passivation and incubation with SAV (image B).

Even though the washing steps have been performed very carefully, they caused the lipids to smear over the surface. Lipids have been used by other groups for cell experiments,[58,63] but for the following reasons, this approach was not considered suitable and not employed further: the integrity of the patterned area is of vital importance for the cell experiments and several washing steps have to be performed until the final protein is immobilized on the surface. Furthermore, the biotin moiety will not be linked covalently to the substrate, which was considered important.

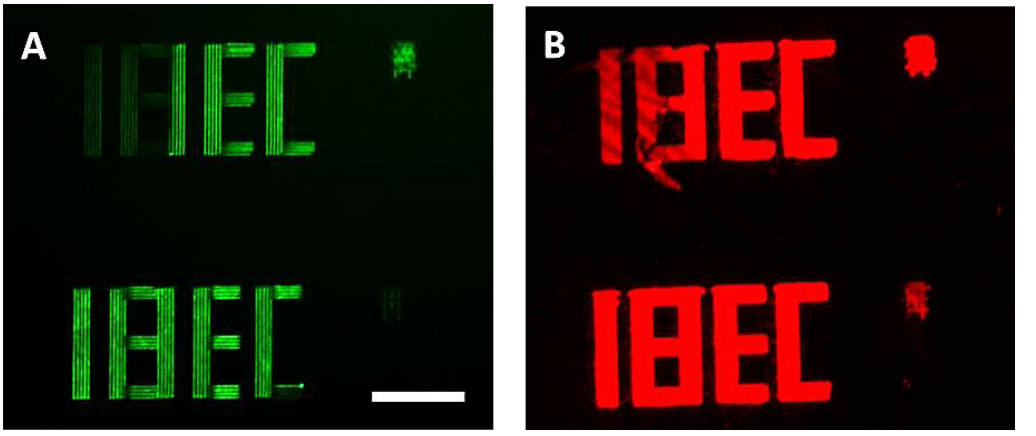

Figure 103: A) Fluorescence image of biotinyl CAP PE patterned on glass. The green Fluorescence comes from mixed-in FITC fluorophore. B) The same area after passivation with BSA and incubation with SAV-TR. The scale bar equals 25 µm.

3.3.3.3. Patterning of biotin-azide on alkyne modified glass for surface click chemistry

The advantages of click chemistry for immobilization of a compound on the surface have already been highlighted in Chapter 2. Related to this work is the use of a polymer as substrate for click chemistry along with a biotin-azide ink, where promising results have been obtained for the patterning with DPN.[64] A polymer might

not be the optimal solution for a substrate; therefore, this approach uses an alkyne functionalization directly on glass without polymer in-between, furthermore also taking advantage of the already existing functionalization step of glass with GPTMS (this surface functionalization strategy has been published in collaboration with the group of Prof. Fuchs)[65]. Instead of using a biotin-amine ink for the epoxy ring opening, propargylamine is used to yield a homogeneous layer of alkyne groups as surface functionalization. Apart from being stable at ambient conditions and allowing for longer term storage, this group also eliminates the problems which were experienced with highly hydrophilic surfaces and therefore makes the patterning step more reliable and less sensitive to a high ambient humidity.

After proving via XPS measurements (see Chapter 2.3.5.) that the functionalization step has been successful, Dip-pen experiments were performed with a biotin-azide ink. Figure 104 shows the fluorescence microscopy image of fluorescently labeled streptavidin (SAV), which bound exclusively to the biotin-azide pattern. This pattern was obtained after adjusting patterning parameters like relative humidity and dwell time and could be reproduced without problems.

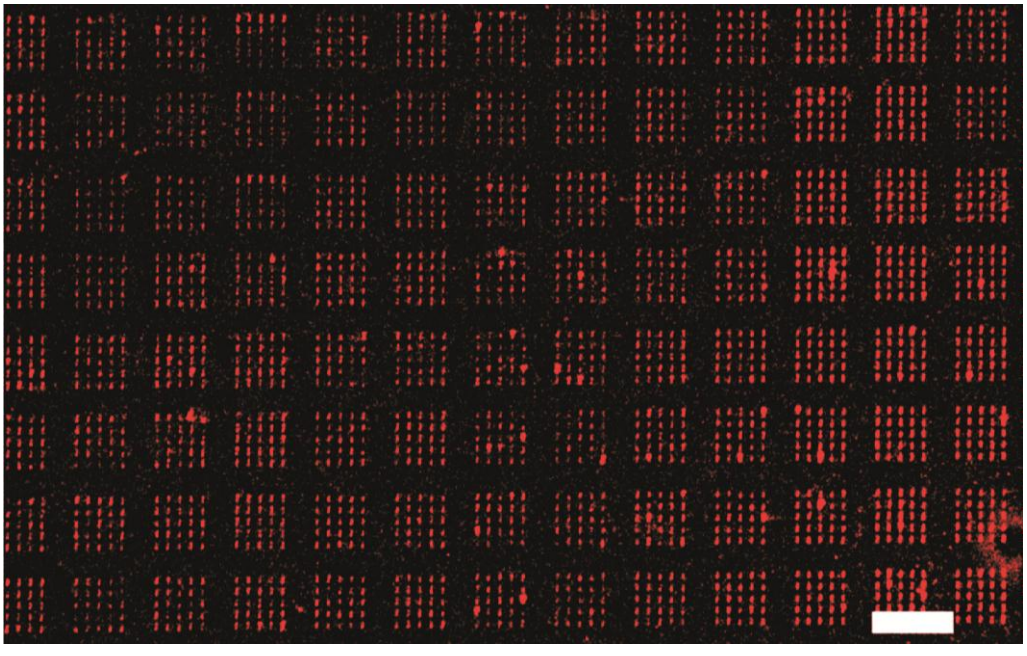

Figure 104: Fluorescence microscopy image of streptavidin-Cy3 which is specifically bound only to the areas patterned with immobilized biotin-azide on alkyne modified glass. The scale bar equals 50 µm.

Furthermore, the biotin functionalization proved to be very stable towards repeated washing steps and even denaturing conditions like boiling water and rinsing with detergents. This procedure was performed in order to remove bound SAV and functionalize again, so as to test the ability to reuse the platform. The pattern was perfectly visible which suggests that the biotin-azide molecule is anchored covalently on the surface and was not destroyed by this treatment, making this platform ideal for recovery and multiple using.

For cell culture experiments, a homogeneous pattern was written over a large area (see the fluorescence image of the pattern in Figure 105). As passivation, BSA was chosen because it is commonly used for passivation for short term cell experiments.

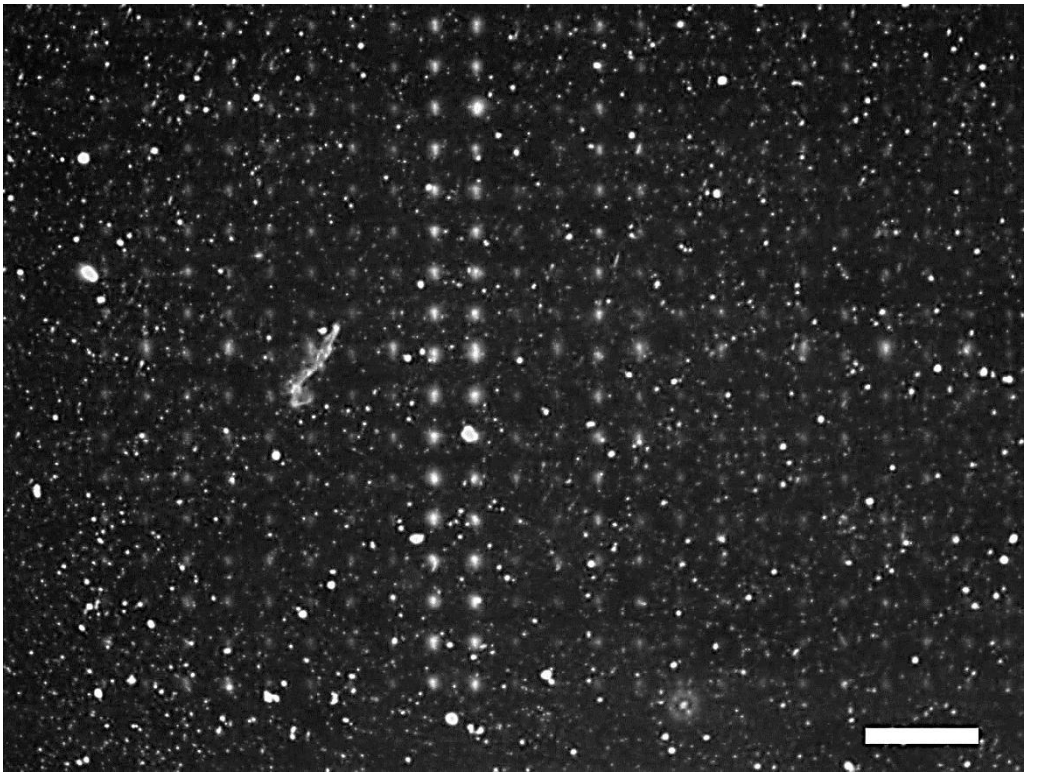

Figure 105: Fluorescence microscopy image of the patterned area for cell differentiation studies. The scale bar equals 50 µm.

This section will not be mentioned in the results for the cell experiments because no positive results could be obtained: After 24 h of culture, the cells were

fixed on the substrates and stained for the protein OSX. When examined with fluorescence microscopy (no data shown here due to failure of the experiment), it became obvious that the passivation strategy (BSA in this case) had not worked out. Cells were found everywhere and not only restricted to the patterned area, as seen for the gold surfaces and passivation with PEG-thiol. These results are unfortunate but reproducible, as seen with our collaboration at the KIT. Presently, they are trying to develop a good passivation strategy in order to be able to successfully perform cell experiments on these surfaces. Strangely, the passivation works fine for both streptavidin-Texas Red functionalization and hybridization of oligonucleotides (see Chapter 2), so it has to be the cells who interact with the BSA on the substrate in a way that makes it not useful for passivation with click chemistry substrates.

PART B: CELL DIFFERENTIATION EXPERIMENTS

3.3.4. Osterix as early differentiation marker

As explained in the introductory section, the protein immobilized on the substrates (bone morphogenetic protein-2, BMP-2) makes the C2C12 cells differentiate into osteoblasts (Figure 68). Quantification of osteogenic differentiation was performed by staining for a so called "early differentiation" marker. It has been reported that osterix (OSX) is induced rapidly in C2C12 cells by BMP-2 during the first 24 h of administration,[66] making it an ideal candidate for fast assessment of cell differentiation. The quantification of OSX positive cells (i.e. cells starting to have differentiated towards osteoblasts) was based on the criteria defined by Polak *et al.*,[67] who reported that OSX was activated and translocated from the cell cytosol into the nucleus during preosteoblast stages of osteoblastic lineage differentiation. Therefore, all cells with a void nucleus are counted as negative and all cells with a homogeneous coloring or a pronounced green nucleus are counted as positive for differentiation towards the osteoblastic regime (see Figure 106).

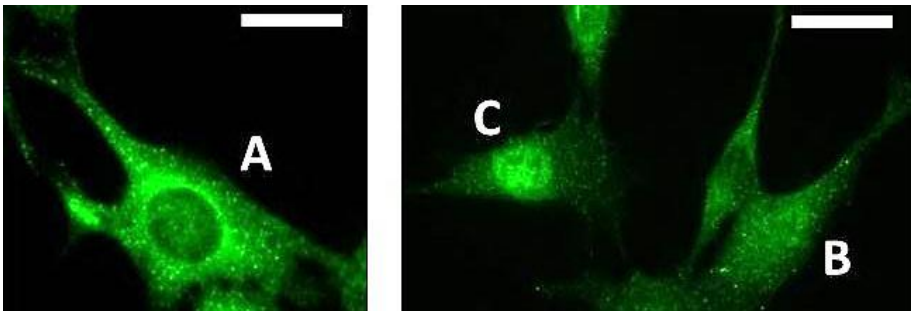

Figure 106: Osterix staining of C2C12 myoblastic cells. The cell on the left side (A) shows an empty nucleus and is considered negative for differentiation. On the other hand, the cells on the right side are positive for differentiation because they are homogeneously green (B) or have a brighter green nucleus (C). The scale bars equal 25 µm.

Osterix is a marker for early cell differentiation, as mentioned before, because changes are induced already after 24 h. In order to completely assess the differentiation of C2C12 cells in dependence of immobilized BMP-2, more experiments would have to be performed, evaluating the marker alkaline phosphatase, which is also very important in differentiation towards osteoblasts. The staining for this protein is usually performed after 6 days of cell culture via a colorimetric assay. Just to mention that it has been performed but due to the gold on the substrates, a very bad contrast was obtained and no quantification could be performed.

3.3.5. Preservation of the biological activity of immobilized BMP-2

In order to check if the immobilized BMP-2 was still biologically active, C2C12 cells were cultured on the substrates from conventional micropatterning (homo, 5-R and 5-L; see Table 13) with and without immobilized BMP-2 ("+" and "-"). The differentiation of the cells was determined by quantifying the number of osterix (OSX) positive cells, as explained in Figure 106. It could be proven that the BMP-2 immobilized on the substrates wasn't compromised because more cells are differentiated on the substrates with BMP-2 than on the ones without (see Figure 107) and the differences between the respective substrates with and without BMP-2 were significant (indicated by the asterisk).

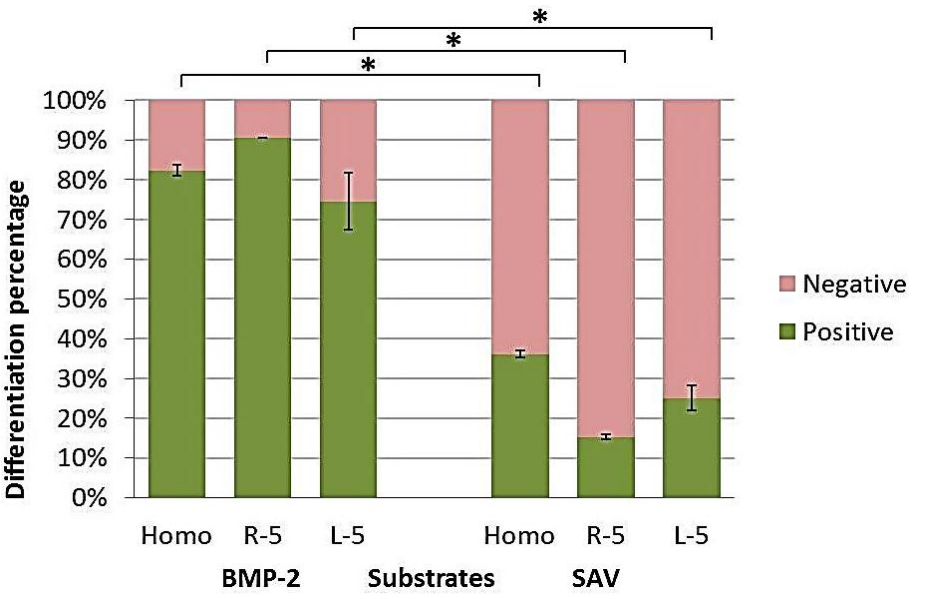

Figure 107: Graph representing the differentiation percentage of C2C12 cells stained for osterix. Cells identified as positive (green) have started to differentiate, negative cells (red) didn't. The asterisk indicates significant differences.

Furthermore, the differentiation percentage of cells on the substrates 5-R is comparable to the one reported for experiments with BMP-2 in solution (~90%)[68]. The immobilization method used here (directional immobilization) has yielded higher values differentiation when compared to randomly immobilized[29] BMP-2 (~75%-91% compared to 20%-24% for BMP-2 immobilized in cellular microarrays). Similar percentages of differentiation have also been obtained by our group when using directed immobilization of BMP-2 on poly(methyl methacrylate) functionalized substrates.[43]

3.3.6. Substrates used for cell differentiation experiments

Table 13 gives an overview over the substrates which were used for cell differentiation experiments discussed in the following section. The denomination is used in order to refer to the particular substrate and facilitate its identification.

Table 13: Summary of the substrates used for cell differentiation experiments and their characteristics.

Denomination	homo	5-R	5-L	dots
Method	Immersion	µ-CP	µ-CP	Dip-pen
Feature size	Monolayer	5 µm round	5 µm lines	4 µm dots
Spacing	-	5 µm	5 µm	22 µm

In order to avoid attachment of single cells to a spot / line, the pattern features were made sufficiently small. It has been shown that cells stayed on a single island for features with a diameter of > 20 µm. In contrast, on smaller features cells tended to spread across multiple islands.[69] The spacing for the substrate dots was predetermined by the cantilever spacing (66 µm): in order to create a homogeneous pattern, the spacing has to be a fraction of the cantilever spacing. Negative controls were included and consisted of substrates without BMP-2 (i.e. presenting streptavidin to the cells).

3.3.7. Cell differentiation experiments

In the following, representative fluorescence microscopy pictures of cells on the different substrates (homo, 5-R, 5-L, dots) are shown, with and without BMP-2. First of all, the pictures are described qualitatively and differences between the respective substrates are presented. Then, in a more quantitative way, the statistics of the obtained results will be presented and discussed.

Figure 108 shows the fluorescence images of C2C12 cells on 5-L substrates (linear features). The cells are mostly aligning along the features (direction indicated by the white arrow) and present a rather elongated shape. On the left side, the substrates with BMP-2 (5-L(+)) are shown and on the right side, the substrates without BMP-2 (5-L(-)), presenting streptavidin to the cells. There are slightly less cells on the substrates without BMP-2. Also visible is the number of cells with an empty nucleus on the upper left image, even though it contains immobilized BMP-2.

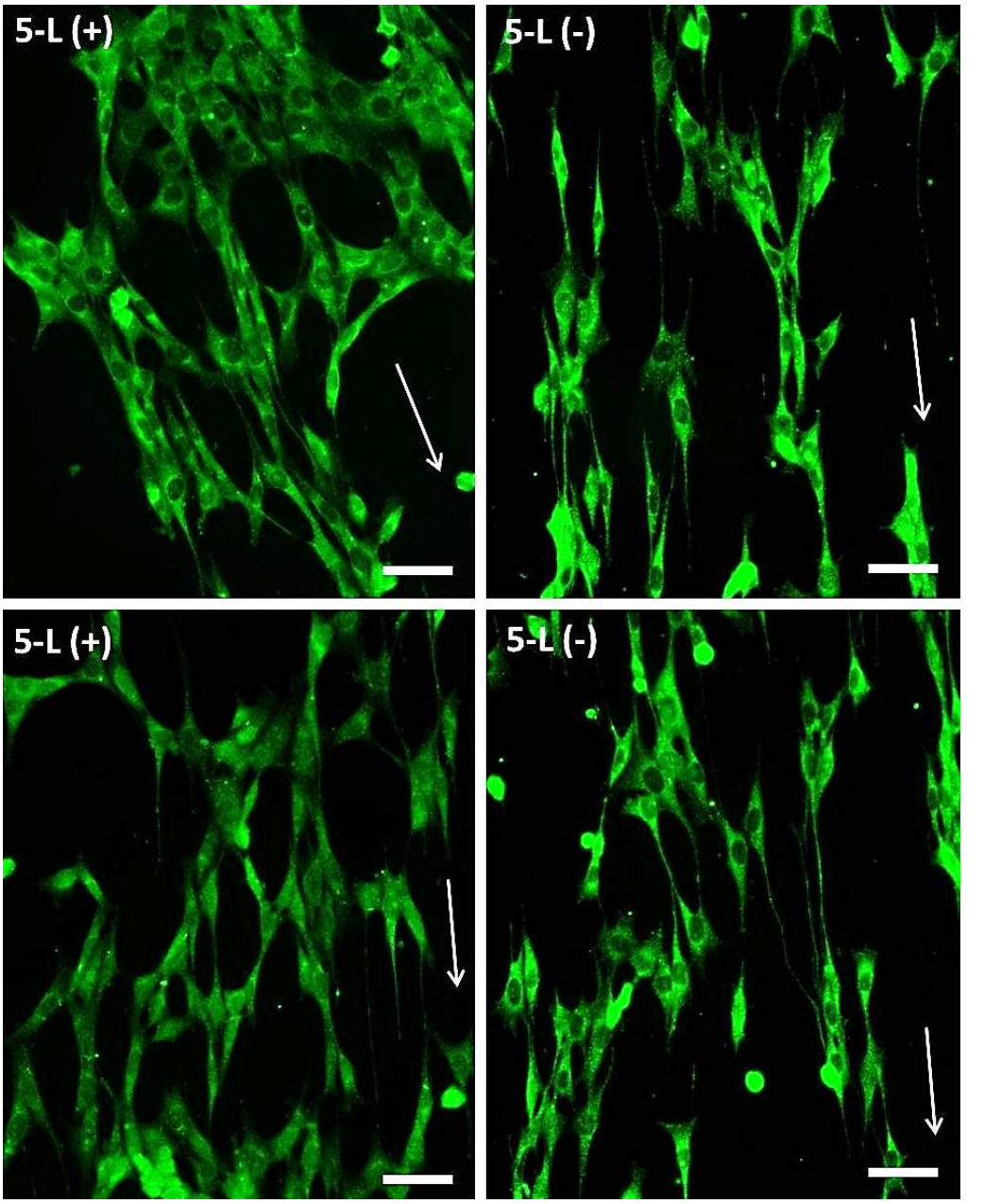

Figure 108: Fluorescence images of C2C12 myoblastic cells on 5-L substrates (5 µm line pattern) with and without BMP-2 (+ / -). OSX was fluorescently marked after 24 h of cell culture for quantification of the cell differentiation towards osteoblastic cells. The white arrows indicate the line direction. The scale bars equal 50 µm.

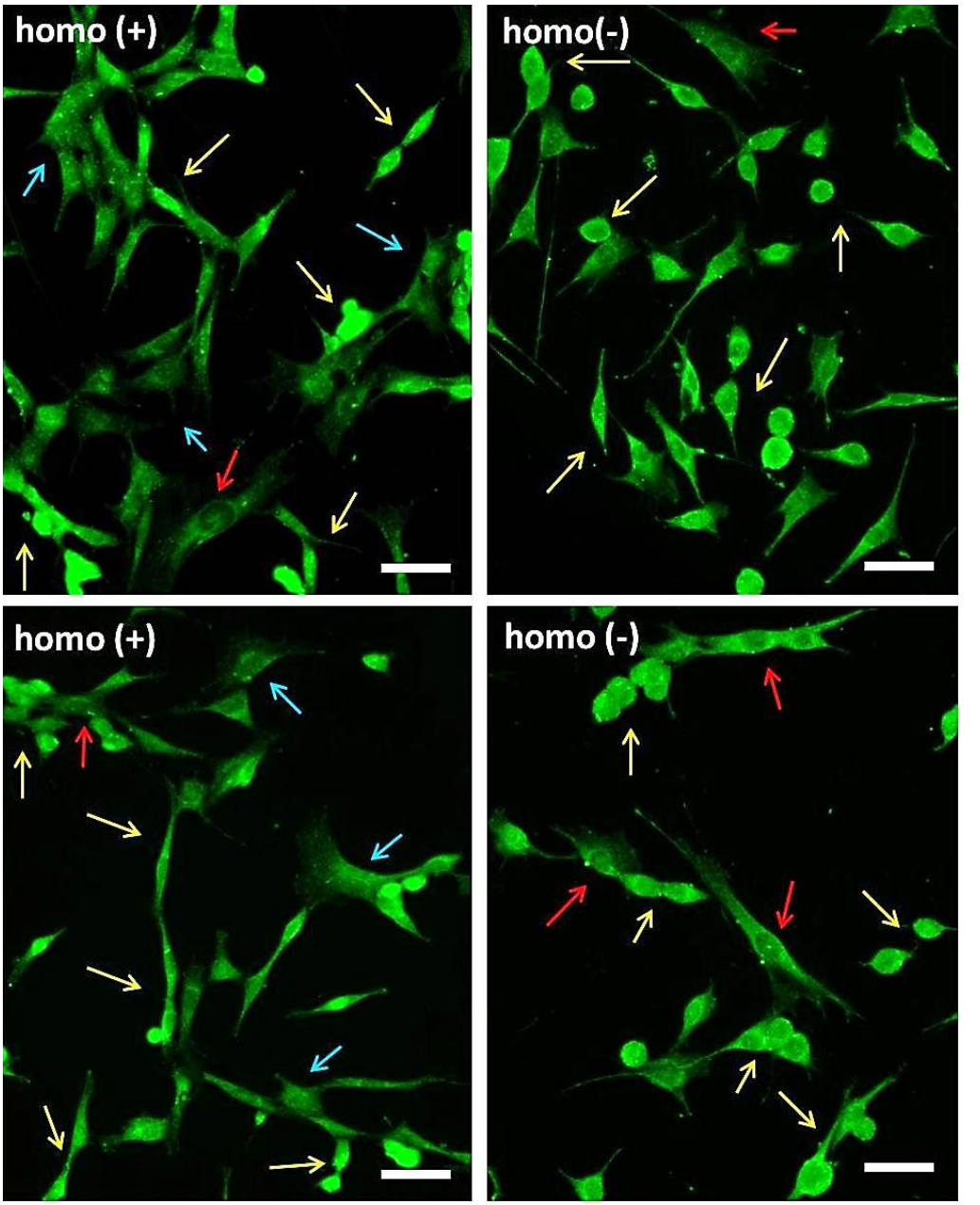

Figure 109: Fluorescence images of C2C12 myoblastic cells on homogeneous substrates with and without BMP-2 (+ / -). OSX was fluorescently marked after 24 h of cell culture in order to quantify the cell differentiation towards osteoblastic cells. The arrows indicate: red – negative cells; blue – positive cells; yellow – not well spread. The scale bars equal 50 µm.

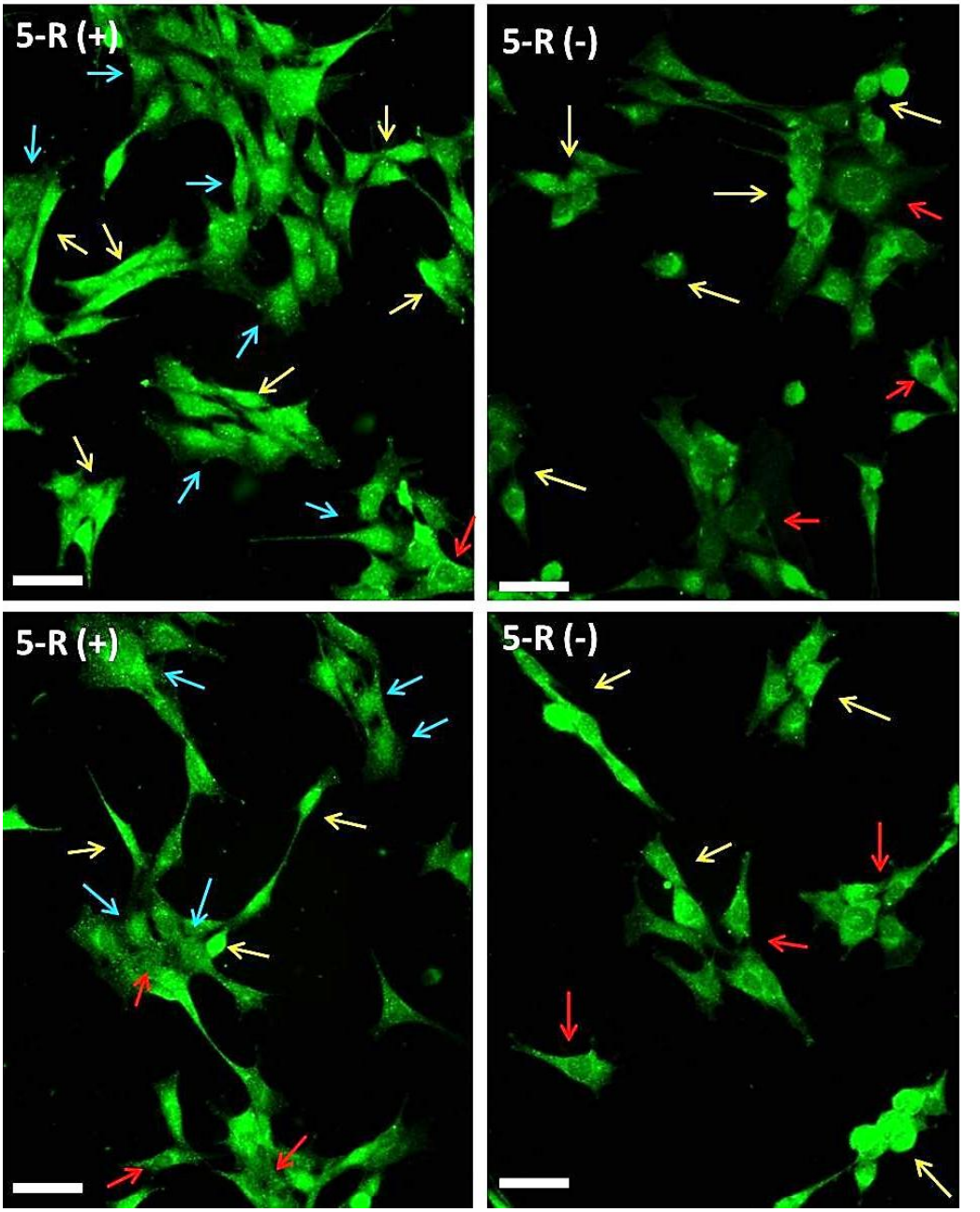

Figure 110: Fluorescence images of C2C12 myoblastic cells on 5-R substrates (5 µm round pattern from µCP) with and without BMP-2 (+ / -). The protein OSX was fluorescently marked after 24 h of cell culture in order to quantify the cell differentiation towards osteoblastic cells. The arrows indicate: red – negative cells; blue – positive cells (pronounced nucleus); yellow – not well spread cells. The scale bars equal 50 µm.

Figure 109 shows the fluorescence images of C2C12 cells on homogeneous substrates. The arrows in the pictures indicate not well spread cells (yellow), "negative" cells (red arrows, empty nuclei) and cells regarded "positive" for differentiation (blue arrows, homogeneous green color). It can be seen that there are quite a lot of cells which are small and roundish in shape, meaning they are not well spread (yellow arrows). For the substrates with BMP-2 (homo (+)), there are some positive cells and scattered negative cells. The substrates without BMP-2 (homo (-)) show even more roundish cells (yellow arrows) and no positive cells (blue arrows).

Figure 110 shows the fluorescence images of C2C12 cells on 5-R substrates (round features). Also here, the colored arrows indicate the different "cell types" encountered on the substrates. On the substrates with BMP-2 (left side, 5-R (+)), only few cells are not well adhered and spread (yellow arrows) and the majority of the cells show a complete green cell body or even a slightly pronounced green nucleus (blue arrows). Also, some cells with an empty nucleus (red arrows) can be found, but significantly less when compared to the substrates without BMP-2 (right side, 5-R (-)). On these substrates there are, apart from the negative cells (red arrows), also some poorly adhered cells (yellow arrows).

Figure 111 shows the fluorescence images of C2C12 cells on "dots" substrates (fabricated with Dip-pen Nanolithography). The images shown are only from substrates with BMP-2 present because on the substrates without BMP-2 (i.e. with streptavidin and with streptavidin + BMP-2 in solution), almost no cells at all were found adhered to the substrate. Images A and B show different areas from the patterned region. *Remark: In comparison to the substrates 5-L, homo and 5-R, where the whole substrate is modified, here, only a small area has the pattern. The rest of the substrate is passivated against cell adhesion and no cells can attach.* Images B and D are overexposed versions of A and C in order to visualize the underlying streptavidin-Texas Red pattern. While in image A, there are cells which are perfectly differentiated (predominantly green nuclei), image C shows cells with empty nuclei, which are negative for differentiation. This fact reflects the inhomogeneity of cell types on the substrate. The red inset shows a close-up of image A with the differentiated cells.

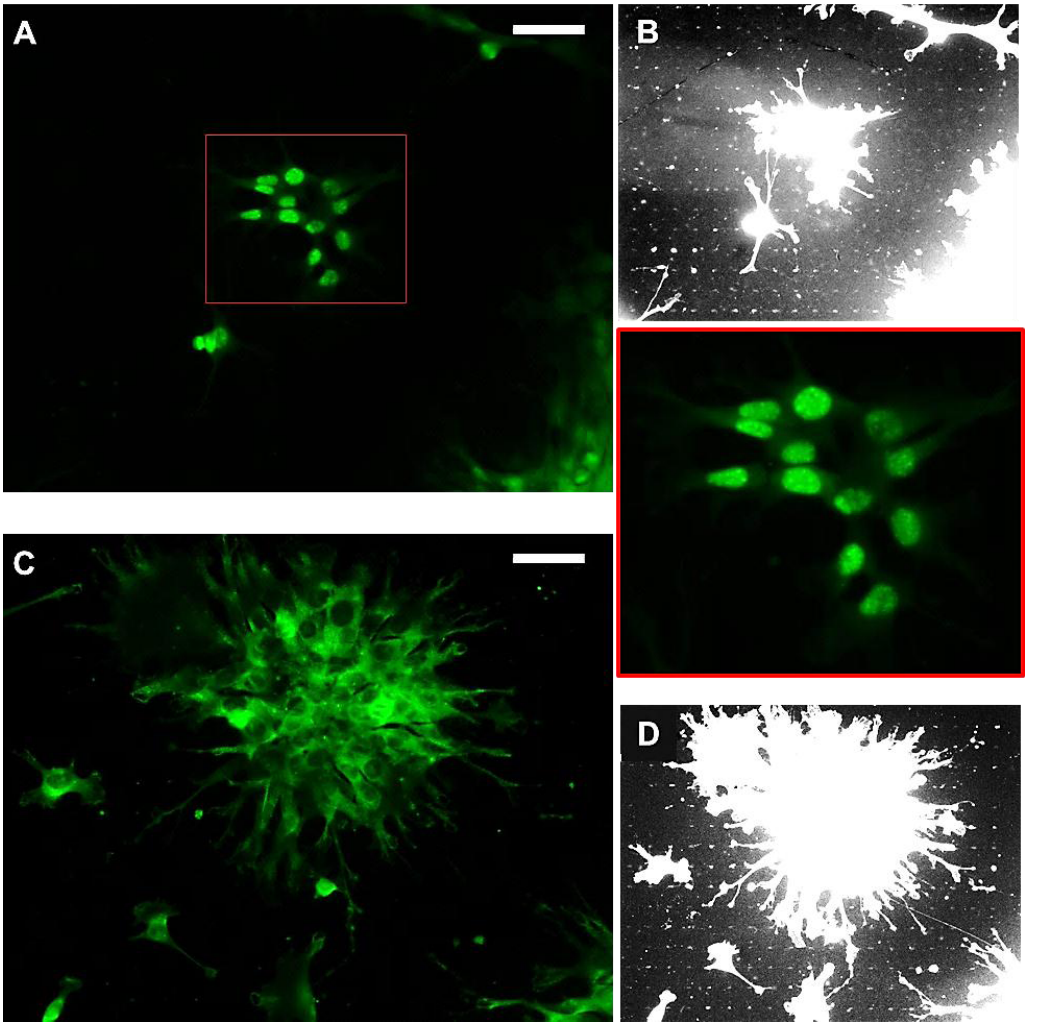

Figure 111: Fluorescence images of C2C12 myoblastic cells on substrates with BMP-2 created by DPN. The protein OSX was fluorescently marked after 24 h of cell culture in order to quantify the cell differentiation towards osteoblastic cells. Images B (D) and A (C) are identical, whereas the first ones are overexposed in order to visualize the underlying streptavidin-Texas Red pattern. The scale bars equal 50 µm.

On the basis of evaluated images for all substrates, the differentiation percentage was calculated and is shown as graph in Figure 112. The asterisk indicates significant differences between the compared substrates (obtained by analysis of variance evaluation (ANOVA)). As can be seen, there are significant differences between all BMP-2 containing substrates (left side) and their respective substrates without BMP-2 (right side). The green and the blue color stand for differentiated cells ("positive"), whereas cells with a predominantly green nucleus (blue columns) were

distinguished from cells with an "all-over" green coloring (green columns). The red columns stand for "negative" cells which present an empty nucleus. Precise values for all substrates along with the standard deviation are given in Table 14.

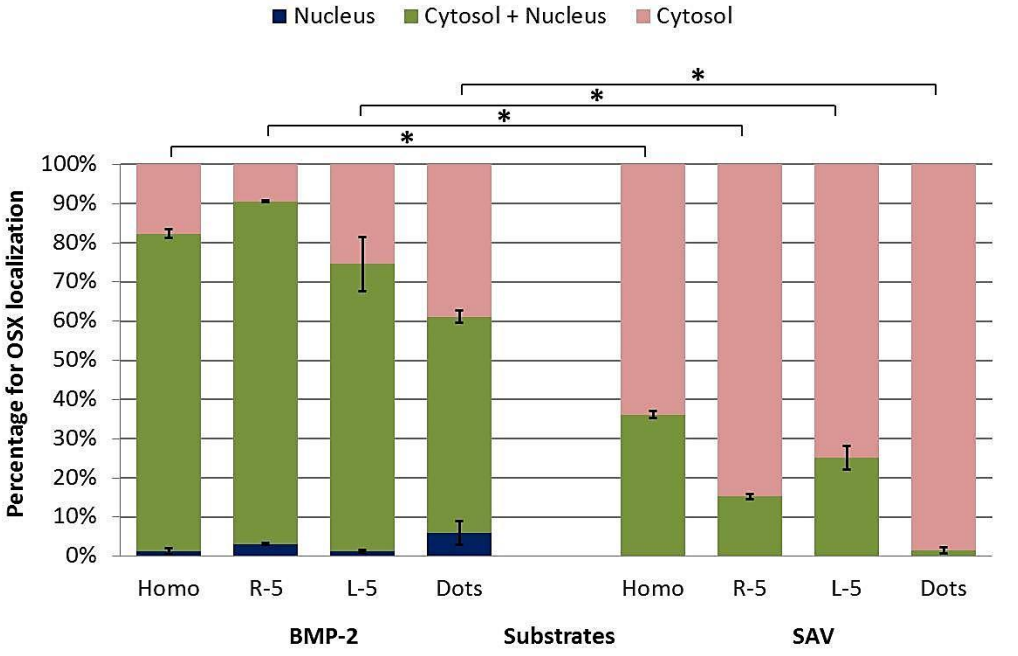

Figure 112: Graph representing the percentage of OSX in the cytosol (red), cytosol and nucleus (green) and mostly in the nucleus (blue). The left side shows the substrates with BMP-2 and the right side (without the blue columns) the substrates without BMP-2 (= streptavidin).

Table 14: Values for the differentiation percentage of C2C12 cells towards osteoblasts.

Substrate (+ BMP-2)	**5-L**	**Homo**	**5-R**	**dots**
Differentiation %	74.59 ±14.35	82.32 ± 2.68	90.61 ± 0.02	61.31 ± 2.91

For comparison, reported differentiation percentages when working with BMP-2 in solution are around 90%.[68] The substrates corresponding to this value are the substrates with round features (5-R).

Following, the findings are discussed more in detail and explained with or compared to the state of the art.

Substrates with streptavidin (without BMP-2) in comparison to substrates with BMP-2

In general, fewer cells were found adhered and spread on the substrates **without BMP-2**, meaning with streptavidin presented to the cells. This can be explained by the fact that streptavidin slows down cell adhesion to the surface, acting as an anti-adhesive matrix towards both proteins and cells.[70] Cell adhesion was found to be initiated after 18 h. Since the staining for osterix was performed after 24 h in cell culture, the cells had only little time to adhere and spread.

For the substrates **"dots" without BMP-2** (i.e. dots with streptavidin and dots with BMP-2 in solution), almost no cells were found adhered to the substrates. This might be attributed to the combination of the two facts that, firstly, streptavidin slows down cell adhesion and, secondly, the overall surface area for cell adhesion was very small (see Table 15) and gave little possibility for adhesion.

Table 15: Comparison of the pattern parameters for Microcontact printed substrates (5-R) and Dip-pen (dots).

Substrate	Pattern size	Feature density
5-R	1 cm²	10000 spots / mm²
dots	2.37 mm²	2126 dots / mm²

Substrates with BMP-2

On the substrates with the **linear features (5-L)**, the cells align along the lines and the general homogeneity of the cell population (differentiated or not) was very low. This can be seen, for example, in the upper left image of Figure 108, where many cells with an empty nucleus are found despite being on top of the linear BMP-2 pattern. Furthermore, the cell differentiation percentage was quite low (only 74.59 % ± 14.35 % instead of 90 % when compared to in solution). This finding might be explained by the linear features being counterproductive for the differentiation of C2C12 cells into osteoblasts because it corresponds more to the natural shape of a myoblast. Tay *et al.* showed that they could steer mesenchymal stem cell (MSC) differentiation towards myoblasts without the use of any exogenous stimuli like growth factors, by just using surfaces with fibronectin lines

(20 µm width), to which the cells aligned.[71] Their justification for the linear pattern is the mimicry of the *in vivo* cell organization in the myocardium.

The differences in the differentiation percentage of the C2C12 cells for the remaining three substrates (homo, 5-R and dots) can all be attributed to the differences in surface density of BMP-2. It is well known, that the influence of immobilized cytokines on cell differentiation is dependent on the density.

The values for BMP-2 surface densities were estimated and are presented in Table 16. The estimations started from the biotin-PEG-thiol underlying layer. It was assumed that both, the substrates homo and 5-R have a monolayer of biotin-PEG-thiol. For the substrates dots, the estimated value from section 3.3.2.3. was taken into account.

Assuming furthermore, that even if there was no complete monolayer (substrates dots), the size of the protein streptavidin (4.5 x 4.5 x 5.3 nm^3)[72] will be able to overcome possible "holes" in the monolayer. Since a sufficient amount of streptavidin was provided during incubation, the calculated values are based on a monolayer of streptavidin for all substrates.

We hypothesize that each molecule of streptavidin will bind 1 molecule of BMP-2 since their dimensions are very similar (BMP-2[73]: 7 x 3.5 x 2.5 nm^3). Therefore, the density of BMP-2 depends only on the amount of BMP-2 provided during incubation. The local values indicate the density of BMP-2 on the pattern features. Since the homogeneous substrate doesn't have any areas where BMP-2 could not bind and a random but homogeneous distribution is assumed for the whole surface, the local and the overall densities are the same. The patterned substrates, on the other hand, exhibit regions without streptavidin (the passivated areas), where BMP-2 cannot bind. Therefore, the overall area for BMP-2 attachment is smaller. This area was calculated taking into account the pattern parameters and is reflected in the overall surface coverage of BMP-2. The resulting values for the overall density of BMP-2 show a decrease in the density from the substrates homo to 5-R to dots. An interesting point to highlight here is that the assembly of BMP-2 on the substrates homo is

random, whereas on the substrates 5-R and dots, the assembly is guided by the pattern features and most accurately localized.

The terms local and overall density are also depicted in Figure 113, whereas local density is indicated in red, referring to the density of BMP-2 molecules in 1 pattern feature. Overall density refers to the amount of BMP-2 on the whole substrate. Since the substrates "homo" don't have pattern features, both densities are the same.

Table 16: Different surface densities of BMP-2 on the substrates homo, 5-R and dots: The local density reflects the density found in each dot of the pattern. The overall density reflects the BMP-2 density with respect to the whole substrate.

Substrate	**Homo**	**5-R**	**Dots**
Local surface coverage BMP-2	35.52%	100%	100%
Local BMP-2 density (pmol/cm²)	**4.44**	**12.5**	**12.5**
Overall surface coverage BMP-2	35.52%	28.27%	2.63%
Overall BMP-2 density (pmol/cm²)	**4.44**	**3.53**	**0.33**

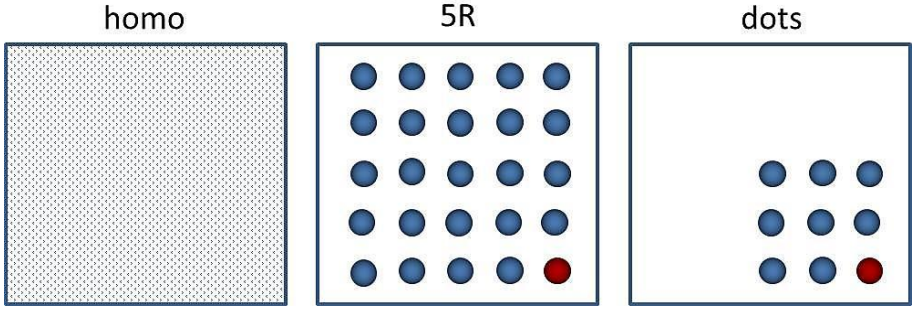

Figure 113: Schematic figure representing the BMP-2 densities of the substrates homo, 5-R and dots. The red color indicates the local density of BMP-2, which in case of the substrate homo is the same as the overall density because there is no pattern. Also reflected: the patterned area on the substrate dots is much smaller than on the other substrates.

The lower differentiation percentage of cells on the substrates **homo** (~82%) when compared to the substrates **5-R** (~91%) can most likely be attributed to the lower local BMP-2 surface density. Ligand density is known to play an important role

in stem cell differentiation.[74] Also, it has been reported that the concentration of BMP-2, when administered in solution, has an effect on the cell differentiation percentage.[75,76] Since BMP-2 doesn't have to be internalized in order to trigger the differentiation towards osteoblasts, it can be assumed that a lower density of BMP-2 on the surface has a similar effect as a lower concentration of BMP-2 in solution, i.e. a lower differentiation percentage of cells who are in the osteoblastic regime. Furthermore, it has been shown in our group that by applying a gradient platform with steadily increasing BMP-2 concentration, differences in cell differentiation are obtained.[43]

On the other hand, it is also known that oligomerization of BMP receptors can influence the activation of downstream BMP signaling pathways.[77,78] Even though BMP-2 receptors naturally exist in the cell membrane in multiple forms of pre-assembled oligomers, about 90% of them are receptor monomers.[79] If a region with high-density BMP-2 (like in the 5-R spots) encounters one or more receptors, the occupancy of this receptor can be improved dramatically. In contrast to BMP-2 in solution, immobilization leads to its local density being much higher; furthermore, the complete detachment of the receptor from the BMP-2 can be avoided by its restricted diffusion (immobilized on the surface).[80] Interaction of BMP-2 with a single receptor, in turn, can lead to receptor oligomerization[81] and thus increase the overall signaling.

This might be reflected in the distribution of BMP-2 on both substrate types: on the substrates homo, the BMP-2 distribution is random; in contrast, on the substrates 5-R, high density BMP-2 areas are locally defined by the pattern areas. The differentiation percentage for the substrates 5-R corresponds to what has been found for cell differentiation in solution (90%), leading to the conclusion that this type of substrates could replace cell experiments with BMP-2 in solution in order to avoid loss of BMP-2 when the cell culture medium is exchanged.

The lower differentiation percentages found for DPN **dots** substrates in comparison to conventional microcontact printed **5-R** substrates might be attributed to the different overall density of BMP-2, since both, the local density in one "spot feature" of the array, as well as the feature size are comparable. The only difference in the arrays is the spacing between the features which in turn leads to a much smaller

overall density (Table 16). In order to further evaluate the differences in differentiation for all substrates containing BMP-2 and to see, a frequency analysis was performed.

Frequency analysis of the substrates with BMP-2

A frequency analysis is based on the individual analyzed images (at least 18 images per sample) and their respective differentiation rates. This means that each of the images taken into account are evaluated for their respective differentiation percentages and, in the case of 90% differentiation, classified as yes (>90%) or no (<90%).

The left side of Figure 114 represents the percentage of images which have a differentiation higher than 90% (in green). The obtained value of over 50% for the substrates 5-R means that more than 50% of the images evaluated show a differentiation of 90% or more.

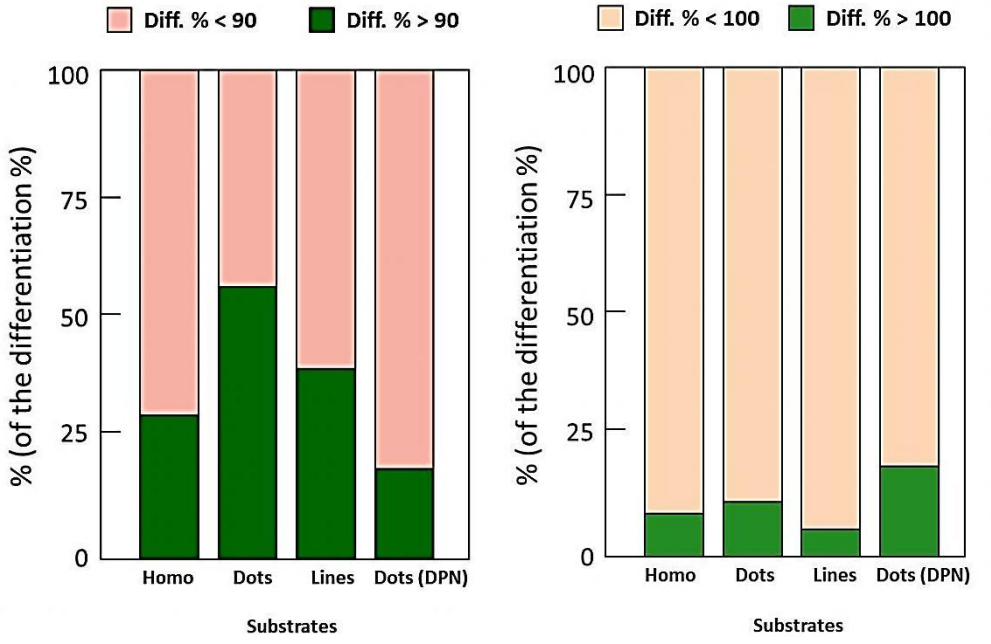

Figure 114: Frequency analysis for the differentiation-%. Left side: differentiation-% above 90%. Right side: differentiation-% equals 100%.

On the other hand, for a differentiation of 100%, the best results are obtained for the substrate dots (DPN). This means that even though the overall cell differentiation is lower, all the cells which have been identified as positive for differentiation, are

completely differentiated (all of them show a green nucleus and not only an overall green color which indicates beginning differentiation). This result, although still not completely explained, may be related with either a feature spacing favorable in terms of BMP-2 receptor arrangement or with a better performance of the DPN technique in terms of pattern homogeneity in comparison with conventional microcontact printing.

In summary, even though the differentiation of cells for the substrates fabricated with DPN is not as high as reported in solution, this approach is very promising and has a lot of potential. The advantage of using DPN for the fabrication of substrates for cell culture lies in the easy modification of the pattern parameters like spacing and spot size, which in turn control the factor density on the substrate. Whereas for microcontact printing a new stamp or even a new master has to be fabricated for each pattern modification, these parameters can be varied directly before the lithography for DPN. Also, multiplexing is easily possible, meaning that various proteins can be immobilized locally defined next to each other. Another interesting possibility is the fabrication of protein gradients at the micro-scale. Nano-scale "gradients" have already been applied to cell polarization experiments.[82] Again, the gradient parameters would be easily adjusted. The only limiting parameter so far has been the total size of the pattern. In this work, it has been shown that it is possible to accomplish fabrication of sufficiently large areas for cell experiments, both at the micro- and the nano-scale.

3.4. CONCLUSIONS

In this chapter, it has been shown that Dip-pen Nanolithography could be applied successfully for the patterning of glass and gold surfaces and their subsequent application for cell differentiation studies.

Several ways of ink deposition have been evaluated for gold and glass substrates in order to obtain reproducible, stable and locally confined biotin-moieties on the surface. For the gold substrates, this was achieved by depositing an ink containing a lipid as a carrier for the actual molecule of interest, the biotin-PEG-thiol. For the glass substrates, a new functionalization strategy was developed in order to enable surface click chemistry with a biotin-azide. Both substrates stand out due to their easy patterning and robustness of the covalently immobilized biotin, which constitutes a universal coupling strategy for any biotinylated molecule.

Due to a problem with the passivation step on the glass substrates, no evaluation could be performed for the cell differentiation experiments. For the gold substrates, cell differentiation experiments on C2C12 cells yielded positive results for osteoblast differentiation induced by the BMP-2 factor. Substrates created with Dip-pen Nanolithography (dots) showed cell differentiation percentages comparable to substrates patterned with conventional techniques such as microcontact printing and similar to traditional experiments where the BMP-2 protein is added in solution. This is a very promising result and encourages further studies with this type of surfaces, especially because they allow insight into how cell differentiation might be dependent on the density of a protein.

3.5. REFERENCES

[1] K-B. Lee, E-Y. Kim. C.A. Mirkin and S.M. Wolinsky. *The Use of Nanoarrays for Highly Sensitive and Selective Detection of Human Immunodeficiency Virus Type 1 in Plasma.* Nano Letters 2004. **4 (10)**: p. 1869-1872.

[2] D.T. Harris, M. Badowski, N. Ahmad and M.A. Gaballa. *The potential of cord blood stem cells for use in regenerative medicine.* Expert Opinion on Biological Therapy 2007. **7 (9)**: p. 1311-1322.

[3] R.G. Flemming, C.J. Murphy, G.A. Abrams, S.L. Goodman and P.F. Nealey. *Effects of synthetic micro- and nano-structured surfaces on cell behavior.* Biomaterials 1999. **20 (6)**: p. 573-588.

[4] J. Tagaki, B.M. Petre, T. Walz and T.A. Springer. *Global Conformational Rearrangements in Integrin Extracellular Domains in Outside-In and Inside-Out Signaling.* Cell 2002. **110 (5)**: p. 599-611.

[5] S.K. Mitra, D.A. Hanson and D.D. Schlaepfer. *Focal adhesion kinase: in command and control of cell motility.* Nature Review Molecular Cell Biology 2005. **6 (1)**: p. 56-68.

[6] E. Martinez, A. Lagunas, C.A. Mills, S. Rodriguez-Segui, M. Estevez, S. Oberhansl, J. Comelles and J. Samitier. *Stem cell differentiation by functionalized micro- and nano-structured surfaces.* Nanomedicine 2009. **4 (1)**: p. 65-82.

[7] E.A. Cavalcanti, P. Tomakidi, M. Bezler and J.P. Spatz. *Geometric organization of the extracellular matrix in the control of integrin-mediated adhesion and cell function in osteoblasts.* Progress in Orthodontics 2005. **6 (2)**: p. 232-237.

[8] B.E. Tuch. *Stem cells – a clinical update.* Australian Family Physician 2006. **35 (9)**: p. 719-721.

[9] J.A. Thomson, J. Itskovitz-Eldor, S.S. Shapiro, M.A. Waknitz, J.J. Swiergiel, V.S. Marshall and J.M. Jones. *Embryonic Stem Cell Lines Derived from Human Blastocysts*. Science 1998. **282 (5391)**:p. 1145-1147.

[10] Taken from http://thefutureofthings.com/articles/57/shedding-light-on-blindness.html; accessed June 2012.

[11] M.F. Pittenger, A.M. Mackay, S.C. Beck, R.K. Jaiswal, R. Douglas, J.D. Mosca, M.A. Moorman, D.W. Simonetti, S. Craig and D.R. Marshak. *Multilineage potential of adult human mesenchymal stem cells.* Science 1999. **584 (5411)**: p. 143-147.

[12] Taken from http://learn.genetics.utah.edu/content/tech/stemcells/sctoday/; accessed June 2012.

[13] C.J. Flaim, S. Chien and S.N. Bhatia. *An extracellular matrix microarray for probing cellular differentiation.* Nature Methods 2005. **2 (2)**: p. 119–125.

[14] A. Wilson and A. Trumpp. *Bone-marrow haematopoietic-stem-cell niches.* Nature Reviews: Immunology 2006. **6 (2)**: p. 93-106.

[15] D.T. Scadden. *The stem-cell niche as an entity of action.* Nature 2006. **441 (7097)**: p. 1075-1079.

[16] E. Fuchs, T. Tumbar and G. Guasch. *Socializing with the neighbors: stem cells and their niche.* Cell 2004. **116 (6)**: p. 769-778.

[17] G.H. Underhill and S.N. Bhatia. *High-throughput analysis of signals regulating stem cell fate and function.* Current Opinion in Chemical Biology 2007. **11 (4)**: p. 357-366.

[18] A.J. Engler, S. Sen, H.L. Sweeney and D.E. Discher. *Matrix elasticity directs stem cell lineage specification.* Cell 2006. **126 (4)**: p. 677-689.

[19] C. Kuschel, H. Steuer, A.N. Maurer, B. Kanzok, R. Stoop and B. Angres. *Cell adhesion profiling using extracellular matrix protein microarrays.* Biotechniques 2006. **40 (4)**: p. 523–531.

[20] M. Kantlehner, P. Schaffner, D. Finsinger, J. Meyer, A. Jonczyk, B. Diefenbach, B. Nies, G. Hölzemann, S.L. Goodman and H. Kessler. *Surface Coating with Cyclic RGD Peptides Stimulates Osteoblast Adhesion and Proliferation as well as Bone Formation.* Chembiochem 2000. **1 (2)**: p. 107-114.

[21] H.G. Moghadam, M.R. Urist, G.K. Sandor and C.M. Clokie. *Successful mandibular reconstruction using a BMP bioimplant*. Journal of Craniofacial Surgery 2001. **12 (2)**: p. 119–127.

[22] U.M.E. Wikesjö, M. Qahash, Y-H. Huang, A. Xiropaidis, G. Polimeni and C. Susin. *Bone morphogenetic proteins for periodontal and alveolar indications; biological observations – clinical implications*. Orthodontics & Craniofacial Research 2009. **12 (3)**: p. 263–270.

[23] D. Chen, M. Zhao and G.R. Mundy. *Bone morphogenetic proteins.* Growth Factors 2004. **22 (4)**: p. 233-241.

[24] V.Rosen. *BMP-2 signaling in bone development and repair.* Cytokine & Growth Factor Reviews 2009. **20 (5-6)**: p. 475-480.

[25] Y.Y. Yu, S. Lieu, C. Lu and C. Colnot. *Bone morphogenetic protein 2 stimulates endochondral ossification by regulating periosteal cell fate during bone repair.* Bone 2010. **47 (1)**: p. 65-73.

[26] E. Yamachika, H. Tsujigiwa, N. Shirasu, T. Ueno, Y. Sakata, J. Fukunaga, N. Mizukawa, M. Yamada and T. Sugahara. *Immobilized recombinant human bone morphogenetic protein-2 enhances the phosphorylation of receptor activated Smads.* Journal of Biomedical Materials Research Part A 2009. **88 (3)**: p. 599-607.

[27] Y. Zhao, J. Zhang, X. Wang, B. Chen, Z. Xiao, C. Shi, Z. Wei, X. Hou, Q. Wang and J. Dai. *The osteogenic effect of bone morphogenetic protein-2 on the collagen scaffold conjugated with antibodies.* Journal of Controlled Release 2010. **141 (1)**: p. 30-37.

[28] H.M. Ryoo, M.H. Lee and Y.J. Kim. *Critical molecular switches involved in BMP-2 induced osteogenic differentiation of mesenchymal cells.* Gene 2006. **366 (1)**: p. 51-57.

[29] S.A. Rodriguez Segui, University of Barcelona, PhD thesis 2009. *Development of cellular microarrays for stem cell culture and early stage differentiation evaluation.*

[30] J.M. Curran, R. Chen and J.A. Hunt. *The guidance of human mesenchymal stem cell differentiation in vitro by controlled modifications to the cell substrate.* Biomaterials 2006. **27 (27)**: p. 4783-4793.

[31] J.M. Curran, R. Stokes, E. Irvine, D. Graham, N.A. Amro, R.G. Sanedrin, H. Jamil and J.A. Hunt. *Introducing dip pen nanolithography as a tool for controlling stem cell behaviour: unlocking the potential of the next generation of smart materials in regenerative medicine.* Lab on a Chip 2010. **10 (13)**: p. 1662-1670.

[32] J.M. Curran, R. Chen, R. Stokes, E. Irvine, D. Graham, E. Grubbins, D. Delaney, N. Amro, R. Sanedrin, H. Jamil and J. Hunt. *Nanoscale definition of substrate materials to direct human adult stem cells towards tissue specific populations*. Journal of Material Science: Materials in Medicine 2010. **21 (3)**: p. 1021-1029.

[33] J.A. Phillippi, E. Miller, L. Weiss, J. Huard, A. Waggoner and P. Campbell. *Microenvironments engineered by inkjet bioprinting spatially direct adult stem cells toward muscle- and bone-like subpopulations.* Stem cells 2008. **26 (1)**: p. 127-134.

[34] R. Derda, L. Li, B.P. Orner, R.L. Lewis, J.A. Thomson and L.L. Kiessling. *Defined substrates for human embryonic stem cell growth identified from surface arrays.* ACS Chemical Biology 2007. **2 (5)**: p. 347-355.

[35] K. Kashiwagi, T. Tsuji and K. Shiba. *Directional BMP-2 for functionalization of titanium surfaces.* Biomaterials 2009. **30 (6)**: p. 1166-1175.

[36] J.D. Boerckel, Y.M. Kolambkar, K.M. Dupont, B.A. Uhrig, E.A. Phelps, H.Y. Stevens, A.J. Garcia and R.E. Guldberg. *Effects of protein dose and delivery system on BMP-mediated bone regeneration.* Biomaterials 2011. **32 (22)**: p. 5241-5251.

[37] H. Schliephake, A. Aref, D. Scharnweber, S. Bierbaum, S. Roessler and A. Sewing. *Effect of immobilized bone morphogenetic protein-2 coating of titanium implants on peri-implant bone formation.* Clinical Oral Implants Research 2005. **16 (5)**: p. 563-569.

[38] V. Karageorgiou, L. Meinel, S. Hofmann, A. Malhotra, V. Volloch and D. Kaplan. *Bone morphogenetic protein-2 decorated silk fibroin films induce osteogenic differentiation of human bone marrow stromal cells*. Journal of Biomedical Material Research Part A 2004. **71A (3)**: p. 528-537.

[39] Y.J. Park, K.H. Kim, J.Y. Lee, Y. Ku, S.J. Lee, B.M. Min and C.P. Chung. *Immobilization of bone morphogenetic protein-2 on a nanofibrous chitosan membrane for enhanced guided bone regeneration.* Biotechnology and Applied Biochemistry 2006. **43 (Pt 1)**: p. 17-24.

[40] C. Lorenz, A. Hoffmann, G. Gross, H. Windhagen, P. Dellinger, K. Möhwald, W. Dempwolf and H. Menzel. *Coating of titanium implant materials with thin polymeric films for binding the signaling protein BMP-2*. Macromolecular Bioscience 2011. **11(2)**: p. 234-244.

[41] T.L. Pohl, J.H. Boergermann, G.K. Schwaerzer, P. Knaus and E.A. Cavalcanti-Adam. *Surface immobilization of bone morphogenetic protein 2 via a self-assembled monolayer formation induces cell differentiation.* Acta Biomaterialia 2012. **8 (2)**: p. 772-780.

[42] S.M. Kang, B. Kong, E. Oh, J.S. Choi and I.S. Choi. *Osteoinductive conjugation of bone morphogenetic protein-2 onto titanium/titanium oxide surfaces coated with non-biofouling poly(poly(ethylene glycol)methacrylate).* Colloids and Surfaces B: Biointerfaces 2010. **75 (1)**: p. 385-389.

[43] A. Lagunas, J. Comelles, S. Oberhansl, V. Hortigüela, E. Martinez and J. Samitier. *Continuous bone morphogenetic protein-2 gradient for screening concentration studies: detailed effects in C2C12 cell differentiation.* In preparation.

[44] O.H. Laitinen, V.P. Hytonen, H.R. Nordlund and M.S. Kulomaa. *Genetically engineered avidins and streptavidins.* Cell and Molecular Life Science 2006. **63 (24)**: p. 2992–3017.

[45] E. Prats-Alfonso, F. Garcia-Martin, N. Bayo, L.J. Cruz, M. Pla-Roca, J. Samitier, A. Errachid and F. Albericio. *Facile solid-phase synthesis of biotinylated alkyl thiols.* Tetrahedron 2006. **62**: p. 6876-6881.

[46] J.L. Wilbur, A. Kumar, E. Kim and G.M. Whitesides. *Microfabrication by microcontact printing of self-assembled monolayers.* Advanced Materials 1994. **6 (7-8)**: p. 600-604.

[47] Y. Xia and G.M. Whitesides. *Soft lithography*. Angewandte Chemie, International Edition 1998. **37 (5)**: p. 550-575.

[48] A.Y. Fadeev and T.J. McCarthy. *Self-assembly is Not the Only Reaction Possible between Alkyltrichlorosilanes and Surfaces: Monomolecular and Oligomeric Covalently Attached Layers of Dichloro- and Trichloroalkylsilanes on Silicon.* Langmuir 2000. **16 (18)**: p. 7268-7274.

[49] C.F. Lai and S.L. Cheng. *Alphavbeta integrins play an essential role in BMP-2 induction of osteoblast differentiation.* Journal of Bone and Mineral Research 2005. **20 (2)**: p. 330-340.

[50] H. Uludag, J. Golden, R. Palmer and J.M. Wozney. *Biotinated bone morphogenetic protein-2: In vivo and in vitro activity.* Biotechnology and Bioengineering 1999. **65 (6)**: p. 668-672.

[51] A. Lagunas, J. Comelles, E. Martinez and J. Samitier. *Universal chemical gradient platforms using poly(methylmethacrylate) based on the biotin-streptavidin interaction for biological applications.* Langmuir 2010. **26 (17)**: p. 14154-14161.

[52] T. Takickas, M. Gavutis, A. Reichel, J. Piehler, B. Liedberg and R. Valiokas. *Protein-Protein Interactions in Reversibly Assembled Nanopatterns.* Nano Letters 2008. **8 (10)**: p. 3369-3375.

[53] A.J. Senesi, D.I. Rozkiewicz, D.N. Reinhoudt and C.A. Mirkin. *Agarose-assisted Dip-pen nanolithography of oligonucleotides and proteins.* ACS Nano 2009. **3 (8)**: p. 2394-2402.

[54] L. Huang, A.B. Braunschweig, W. Shim, L.Qin, J.K. Lim, S.J. Hurst, F. Huo, C. Xue, J-W. Jang and C.A. Mirkin. *Matrix-Assisted Dip-pen Nanolithography and Polymer Pen Lithography.* Small 2010. **6 (10)**: p. 1077-1081.

[55] P. Severino, T. Andreani, A.S. Macedo, J.F. Fangueiro, M.H.A. Santana, A.M. Silva and E.B. Souto. *Current State-of-Art and New Trends on Lipid Nanoparticles (SLN and NLC) for Oral Drug Delivery.* Journal of Drug Delivery 2012. **Volume 2012**. Article ID: 750891.

[56] H. Harshad, M. Das and S. Jain. *Solid lipid nanoparticles: an oral bioavailability enhacer vehicle.* Expert Opinion on Drug Delivery 2011. **8 (11)**: p. 1407-1424.

[57] C.A. Mirkin, L. Huang, L. Lenhert and R.A. Vega. *Patterning with compositions comprising lipids as biocompatible matrix for biomolecules when using Dip-pen nanolithography (DPN) to form microarrays.* Patent number WO 2008156732, 24th of December 2008.

[58] S. Sekula, J. Fuchs, S. Weg-Remers, P. Nagel, S. Schuppler, J. Fragala, N. Theilacker, M. Franzreb, C. Wingren, P. Ellmark, C.A. Borrebaeck, C.A. Mirkin, H. Fuchs and S. Lenhert. *Multiplexed lipid Dip-pen nanolithography on subcellular scales for the templating of functional proteins and cell culture.* Small 2008. **4 (10)**: p. 1875-1893.

[59] S. Lenhert, F. Brinkmann, T. Laue, S. Walheim, C. Vannahme, S. Klinkhammer, M. Xu, S. Sekula, T. Mappes, T. Schimmel and H. Fuchs. *Lipid multilayer gratings*. Nature Nanotechnology 2010. **5 (4)**: p. 275-279.

[60] S. Sekula-Neuner, J. Maier, E. Oppong, A.C. Cato, M. Hirtz and H. Fuchs. *Allergen arrays for antibody screening and immune cell activation profiling generated by parallel lipid Dip-pen nanolithography.* Small 2012. **8 (4)**: p. 585-591.

[61] S. Biswas, M. Hirtz and H. Fuchs. *Measurement of Mass Transfer during Dip-pen Nanolithography with Phospholipids.* Small 2011. **7 (14)**: p. 2081-2086.

[62] Taken from http://www.philasim.org/newmanual/exp21.pdf; accessed in July 2012.

[63] A.E. Kusi-Appiah, N. Vafai, P.J. Cranfill, M.W. Davidson and S. Lenhert. *Lipid multilayer microarrays for in vitro liposomal drug delivery and screening*. Biomaterials 2012. **33 (16)**: p. 4187-5194.

[64] H.Y. Chen, M. Hirtz, X. Deng, T. Laue, H. Fuchs and J. Lahann. *Substrate-independent Dip-pen Nanolithography based on reactive coatings.* Journal of the American Chemical Society 2010. **132 (51)**: p. 18023-18025.

[65] S. Oberhansl, M. Hirtz, A. Lagunas, R. Eritja, E. Martinez, H. Fuchs and J. Samitier. *Facile modification of silica substrates provides a platform for direct writing surface click chemistry*. Small 2012. **8 (4)**: p. 541-545.

[66] M. Hayashi, S. Maeda, H. Aburatani, K. Kitamura, H. Miyoshi, K. Miyazono and T. Imamura. *Pitx2 prevents osteoblastic transdifferentiation of myoblasts by bone morphogenetic proteins.* Journal of Biological Chemistry 2008. **283 (1)**: p. 565-571.

[67] G. Tai, I. Christodoulou, A.E. Bishop and J.M Polak. *Use of green fluorescent fusion protein to track activation of the transcription factor osterix during early osteoblast differentiation.* Biochemical and Biophysical Research Communications 2005. **333 (4)**: p. 1116-1122.

[68] T. Katagiri, A. Yamaguchi, M. Komaki, E. Abe, N. Takahashi, T. Ikeda, V. Rosen, J.M Wozney, A. Fujisawa-Sehara and T. Suda. *Bone morphogenetic protein-2 converts the differentiation pathway of C2C12 myoblasts into the osteoblast lineage.* The Journal of Cell Biology 1994. **127 (6)**: p. 1755-1766.

[69] C.S. Chen, J.L, Alonso, E. Ostuni, G.M. Whitesides and D.E. Ingber. *Cell shape provides global control of focal adhesion assembly.* Biochemical and Biophysical Research Communications 2003. **307 (2)**: p. 355-361.

[70] M. Lehnhert, M. Gorbahn, M. Klein, B. Al-Nawas, I. Köper, W. Knoll and M. Veith. *Streptavidin-coated TiO_2 surfaces are biologically inert: Protein adsorption and osteoblast adhesion studies.* Journal of Biomedical Materials Research A, 2012. **100A (2)**: p. 388-395.

[71] C.Y. Tay, M. Pal, H. Yu, W.S. Leong, N.S. Tan, K.W. Ng, S. Venkatraman, F. Boey, D.T. Leong and L.P. Tan. *Bio-inspired Micropatterned Platform to Steer Stem Cell Differentiation*. Small 2011. **7 (10)**: p. 1416-1421.

[72] W. Knoll, M. Zizelsperger, T. Liebermann, S. Arnold, A. Badia, M. Liley, D. Piscevic, F-J. Schmitt and J. Spinke. *Streptavidin arrays as supramolecular architectures in surface-plasmon optical sensor formats.* Colloids and Surfaces A: Physicochemical and Engineering Aspects 2000. **161 (1)**: p. 115-137.

[73] M. Laub, T. Seul, E. Schmachtenberg and H.P. Jennissen. *Molecular modeling of bone morphogenic protein-2 (BMP-2) by 3D-rapid prototyping.* Materialwissenschaften und Werkstofftechnik 2001. **32**: p. 926-930.

[74] W. Luo, E.W.L. Chan and M.N. Yousaf. *Tailored Electroactive and Quantitative Ligand Density Microarrays Applied to Stem Cell Differentiation.* Journal of the American Chemical Society 2010. **132 (8)**: p. 2614-2621.

[75] J. van den Dolder, A.J.E. de Ruijter, P.H.M. Spauwen and J.A. Jansen. *Observations on the effect of BMP-2 on rat bone marrow cells cultured on titanium substrates of different roughness.* Biomaterials 2003. **24 (11)**: p. 1853-1860.

[76] I. Song, B-S. Kim, C-S. Kim and G-I. Im. *Effects of BMP-2 and vitamin D_3on the osteogenic differentiation of adipose stem cells.* Biochemical and Biophysical Research Communications 2011. **408 (1)**: p. 126-131.

[77] A. Nohe, E. Keating, T.M. Underhill, P. Knaus and N.O. Petersen. *Effect of the distribution and clustering of type I A BMP receptor (ALK3) with the type II BMP receptor on the activation of signalling pathways.* Journal of Cell Science 2003. **116 (16)**: p. 3277-3284.

[78] S. Hassel, S. Schmitt, A. Hartung, M. Roth, A. Nohe, N. Peterson, M. Ehrlich, Y.I. Henis, W. Sebald and P. Knaus. *Initiation of Smad-Dependent and Smad-Independent Signaling via Distinct BMP-Receptor Complexes.* The Journal of Bone & Joint Surgery 2003. **85 (3)**: p. 44-51.

[79] K. Heinecke, A. Seher, W. Schmitz, T.D. Mueller, W.Sebald and J. Nickel. *Receptor oligomerization and beyond: a case study in bone morphogenetic proteins.* BMC Biology 2009. **7**: p. 59.

[80] T. Crouzier, L. Fourel, T. Boudou, C. Albigès-Rizo and C. Picart. *Presentation of BMP-2 from a Soft Biopolymeric Film Unveils its Activity on Cell Adhesion and Migration*. Advanced Materials 2011. **23 (12)**: p. H111-H118.

[81] T. Kirsch, J. Nickel and W. Sebald. *BMP-2 antagonists emerge from alterations in the low-affinity binding epitope for receptor BMPR-II.* The EMBO Journal 2000. **19 (13)**: p. 3314-3324.

[82] D.K. Hoover, E.W.L Chan and M.N Yousaf. *Asymmetric Peptide Nanoarray Surfaces for Stidies of Single Cell Polarization.* Journal of the American Chemical Society 2008. **130 (11)**: p. 3280-3281.

General Conclusions

In **Chapter 1**, a general problem encountered in Dip-pen Nanolithography was addressed: the leveling of the multi-cantilever array tips with respect to the substrate before lithography. This step is crucial in order to ensure a homogeneous ink deposition. Up to now, this process has to be performed "by eye" and is not quantitative. In order to facilitate and improve the tip leveling, a device has been developed and implemented which has piezoelectric sensors in the back of the cantilever. These sensors give a permanent feedback of the touching force and a custom-made software calculates the correction angle. Furthermore, the permanent feedback of the force also allowed to detect the touching point of the tips much earlier than when using a visual approach. Furthermore, by the increased sensitivity of the touching, soft substrates as gold are not damaged during lithography.

In **Chapter 2**, Dip-pen Nanolithography was used for the miniaturization of an oligonucleotide-based biosensor platform. The stable and reproducible immobilization of oligonucleotides on glass substrates was achieved by taking advantage of surface click chemistry, which is a fast and selective way to form a covalent bond between two molecules. The stability of the platform was tested by extensive washing steps. Finally, the sensitivity of the biosensor platform was assessed by hybridizing with different concentrations of complementary oligonucleotide strand. Even though the overall sensitivity of the platform was not very high, this is a promising approach for other biosensor platforms based on oligonucleotides because of its stability and reproducibility.

In **Chapter 3**, the viability of using Dip-pen Nanolithography for the fabrication of patterned substrates for cell experiments was evaluated. Cell experiments require a sufficiently large area, which was one of the challenges when using a nanofabrication method for an area a 1 mm^2. Biotin-PEG-thiol could be deposited successfully on gold over an area of >1 mm^2, although in the end, the feature size was not at the nanoscale. By using the lipid DOPC as a carrier to facilitate ink flow, features of ~4 μm were achieved. Advantage was taken of an established functionalization process of the

biotin with streptavidin and biotinylated BMP-2. The BMP-2 modified substrates could be successfully applied in C2C12 cell differentiation experiments. Differentiation percentages comparable to those achieved by conventional patterning techniques such as microcontact printing were achieved. This type of substrates is promising because of the easily adaptable parameters and thus allows the investigation of factor density dependency of cell differentiation.

Publications and conference communications

Author's journal articles:

- Continuous bone morphogenetic protein-2 gradient for screening concentration studies: detailed effects in C2C12 cell differentiation
  A. Lagunas, J. Comelles, **S. Oberhansl**, V. Hortigüela, E. Martinez and J. Samitier.
  In preparation

- The EUMINAfab Project – report on the collaboration IBEC-KIT: Facile modification of silica substrates provides a platform for direct writing surface click chemistry
  S. Oberhansl, M. Hirtz, A. Lagunas, R. Eritja, E. Martinez, H. Fuchs and J. Samitier.
  CMM Magazine 2012. 5 (1): pp. 55-58.

- Facile modification of silica substrates provides a platform for direct writing surface click chemistry.
  S. Oberhansl, M. Hirtz, A. Lagunas, R. Eritja, E. Martinez, H. Fuchs and J. Samitier.
  Small 2012. 8 (4): pp. 541-545.

- Stem cell differentiation by functionalized micro- and nanostructured surfaces.
  E. Martinez, A. Lagunas, C.A. Mills, S. Rodríguez-Seguí, M. Estévez, **S. Oberhansl**, J. Comelles and J. Samitier. "
  Nanomedicine 2009. 4(1): pp. 65-82.

- Design and production of micro and nanostructured polymer substrates for cell culture applications.
  E. Martinez, C.A. Mills, A. Lagunas, M. Estévez, S. Rodríguez-Seguí, J. Comelles, **S. Oberhansl** and J. Samitier. "
  NanoSpain Newsletter 2008.

Congress communications:

- *4th IBEC Symposium on Bioengineering and Nanomedicine*

Title: "Facile modification of silica substrates provides a platform for direct writing surface click chemistry"

Authors: **S. Oberhansl**, M. Hirtz, A. Lagunas, R. Eritja, E. Martinez, H. Fuchs and J. Samitier

Contribution: Poster

Place: Barcelona (Spain)

Date: 18th October 2011

- *TechConnect World 2010 Conference and Expo*

Title: "Preparation of nanopatterned substrates via Dip-pen Nanolithography for stem cell applications"

Authors: **S. Oberhansl**, A. Lagunas, E. Martinez, H. Jamil and J. Samitier

Contribution: Oral presentation

Place: Anaheim, California (United States)

Date: 21st - 25th June 2010

- *3rd IBEC Symposium on Bioengineering and Nanomedicine*

Title: "Design and Fabrication of Smart Surfaces for Cell Studies and Biosensor Applications"

Authors: A. Lagunas, L. Diéguez, M. Estévez, **S. Oberhansl**, J. Comelles, T. Galan, R. Vado, E. Martinez and J. Samitier

Contribution: Poster

Place: Barcelona (Spain)

Date: 1st – 2nd June 2010

- *NanoSpain2010*

Title: "DNA Biosensors Based on Polypyrrole Nanowires"

Authors: T. Galán, **S. Oberhansl**, E. Martínez, J. Samitier

Contribution: Poster

Place: Barcelona (Spain)

Date: 23rd – 26th March 2010

- *TNT 2009 Trends in Nanotechnology*

Title: "DNA Biosensors Based on Polypyrrole Nanowires"

Authors: T. Galán, **S. Oberhansl**, E. Martínez, J. Samitier

Contribution: Poster

Place: Barcelona (Spain)

Date: 7th – 11th September 2009

- *ESF-EMBO Conference on Biological Surfaces and Interfaces*

Title: "Nanobiosensor multi-analyte platform for simultaneous detection of three different steroid hormones"

Authors: **S. Oberhansl**, J. Comelles, N. Tort, A. Lagunas, M.-P. Marco, E. Martinez and J. Samitier

Contribution: Poster

Place: Sant Feliu de Guixols (Spain)

Date: 27th June – 02nd July 2009

- *2nd ESF/UB European Summer School in Nanomedicine 2009*

Title: "DNA BIOSENSORS BASED ON POLYPYRROLE NANOWIRES"

Authors: T. Galán, **S. Oberhansl**, E. Martínez, J. Samitier

Contribution: Poster

Place: Lisboa (Portugal)

Date: 12th – 16th June 2009

- *2nd IBEC Symposium on Bioengineering and Nanomedicine*

Title: "Nanobiosensor multi-analyte platform for simultaneous detection of three different steroid hormones"

Authors: **S. Oberhansl**, J. Comelles, N. Tort, A. Lagunas, M.-P. Marco, E. Martinez and J. Samitier

Contribution: Poster

Place: Barcelona (Spain)

Date: 14th – 15th April 2009

- *2nd IBEC Symposium on Bioengineering and Nanomedicine*

Title: "DNA Biosensors Based on Polypyrrole Nanowires"

Authors: T. Galán, **S. Oberhansl**, M. Mir, E. Martínez, J. Samitier

Contribution: Poster

Place: Barcelona (Spain)

Date: 14th – 15th April 2009

- *Nanolitho08 – 2nd Spanish Workshop on Nanolithography,*

Title: "Protein nanopatterned surfaces by means of Dip-pen nanolithography"

Authors: **S. Oberhansl**, X. Sisquella, E. Martínez and J. Samitier

Contribution: Poster

Place: Bellaterra, Barcelona (Spain)

Date: 10th – 13th November 2008

- *NanoSMat2008 – 3rd International Conference on Surfaces, Coatings and Nanostructured Materials*

Title: "Protein nanopatterned surfaces by means of Dip-pen nanolithography"

Authors: **S. Oberhansl**, X. Sisquella, E. Martínez and J. Samitier

Contribution: Poster

Place: Barcelona (Spain)

Date: 21st – 24th October 2008

- *XXIV Trobades Científiques de la Mediterrània*

Title: "Protein nanopatterned surfaces by means of Dip-pen nanolithography"

Authors: **S. Oberhansl**, X. Sisquella, E. Martínez and J. Samitier

Contribution: Oral presentation (semiplenary)

Place: Maó, Menorca (Spain)

Date: 06th – 08th October 2008

Appendices

In this section, techniques for fabrication or characterization are presented in detail, which were used for the thesis work but were only shortly mentioned in the Experimental section.

Appendix A - Atomic Force Microscope (AFM)

The AFM was invented in 1989 by Binnig, Quate and Gerber[1] and belongs to the scanning probe microscopy (SPM) techniques. The precursor of the AFM, the scanning tunneling microscope (STM) has been invented in the early 1980s by Binnig and Rohrer (IBM Research in Zürich, Switzerland), which was rewarded with a Nobel Prize in Physics in 1986. For imaging of a substrate, the cantilever tip is brought into close proximity or contact and scanned over the surface. The curvature of the tip determines the lateral resolution of the surface features: typical values for the curvature are 10-20 nm which results in a lateral resolution of 0.1-10 nm. This allows for imaging of single atoms and makes this technique, along with the STM the microscopy technique with the highest resolution. Its imaging resolution is more than 1000 times better than the optical diffraction limit and it is one of the most important tools for imaging, measuring and manipulating matter at the nanoscale.

When a cantilever is approached towards a surface, there are atomic forces which start to act on the cantilever, depending on the distance tip-surface (see Figure 115). In general, the Lennard-Jones Potential describes the different stages of forces which act on the tip, like Van-der-Waals forces (VdW, long-range and attracting), capillary forces and the strongly repulsive forces (short range).

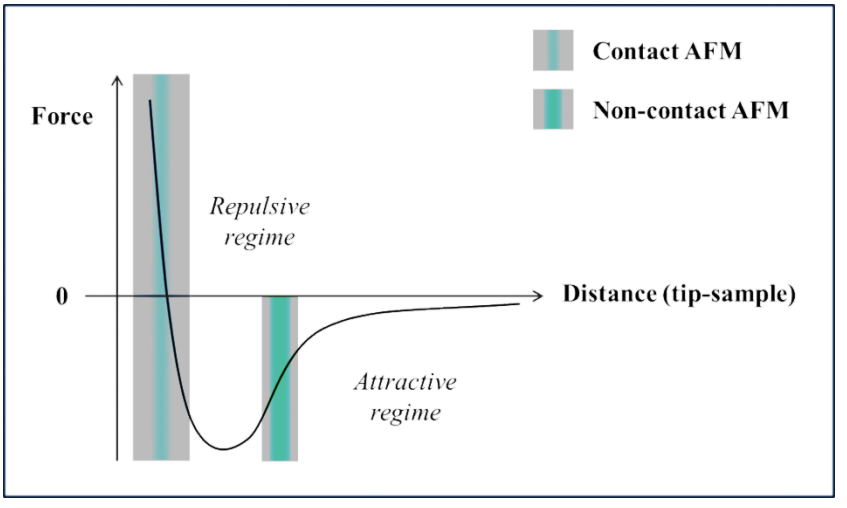

Figure 115: Lennard-Jones Potential describes the variation of interatomic force depending on the distance of the tip to the sample.

Figure 116 shows the general set-up of an AFM, where laser light is reflected off the back of a cantilever and collected by a photodetector (an arrangement of 2-4 photodiodes). Displacement of the cantilever results in a shift of the laser beam from the center of the diode array (set as 0 signal in the beginning) and one of the photodiodes collecting more light, which in turn produces an output signal proportional to the displacement of the cantilever. The detection is as low as cantilever deflections of < 10 nm and is only limited by the so called thermal noise. Piezoelements for all 3 directions allow, coupled to a feedback system, for precise control over positioning and movement of the cantilever with respect to the surface.

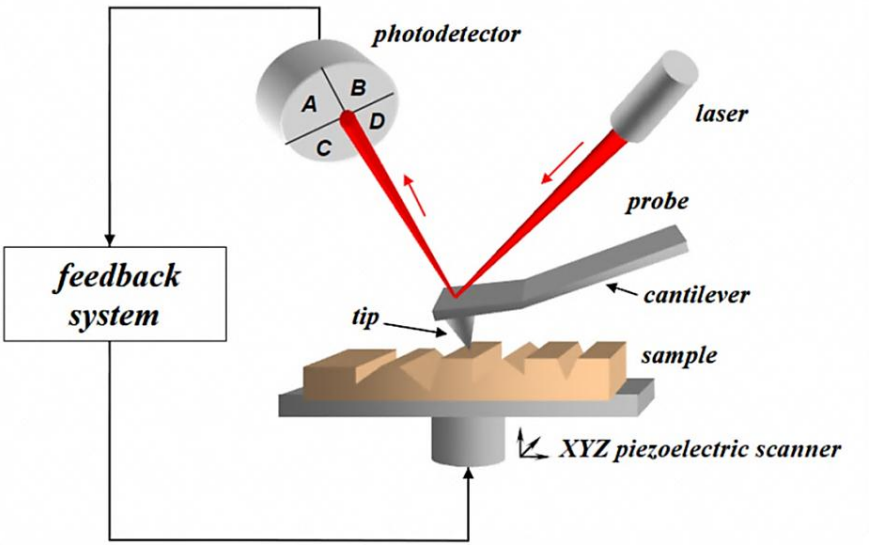

Figure 116: Schematic set-up of the basic compounds of an atomic force microscope (AFM).

The most important modes for imaging are:

Contact mode: There are two different ways of contact mode measurements, but for both of them, the tip is in permanent mechanical contact with the surface. Constant height mode: This is the original method of measuring with an AFM. No adjustment of the cantilever in z-direction (up/down) is performed. The cantilever which scans over the surface will bend and twist with respect to the surface structure and the laser which is reflected from the cantilever back gives the feedback and topography information. This method is suitable for flat and hard substrates, since soft substrates can be damaged during scanning. On the other hand, if the substrate is very rough, the wearing of the tip is very high due to the mechanical contact and sometimes

the tips might break due to encounter of obstacles. Top measurement velocities are up to 10 lines per second.

Constant force mode: In contrast to the constant height mode, the z-height of the cantilever is adjusted permanently during the scanning in order to provide a constant force between tip and substrate. This leads to the CF mode being slower because the regulating cycles need time to adjust, yielding a top velocity of 3-4 lines per second. This method is less destructive since the force on the substrate can be controlled. Nevertheless, there are still forces exerted on the sample which might damage very sensitive samples. In this mode, additional information can be obtained from the surface (lateral force microscopy, LFM). Depending on the friction between tip and substrate, the cantilever will be twisted laterally, meaning that areas with different friction can be distinguished on a substrate. This leads to information about the composition of the substrate additionally to the topographical information. Differences in viscosity, elasticity, adhesion, capillary forces, surface chemistry or electrostatic interactions can give rise to the surface having differences in the frictional attributes. There are even cases, where no topographical information can be obtained, but just the information from LFM, for example when the height of the molecules is the same but the chemical composition is different, as indicated in Figure 117.

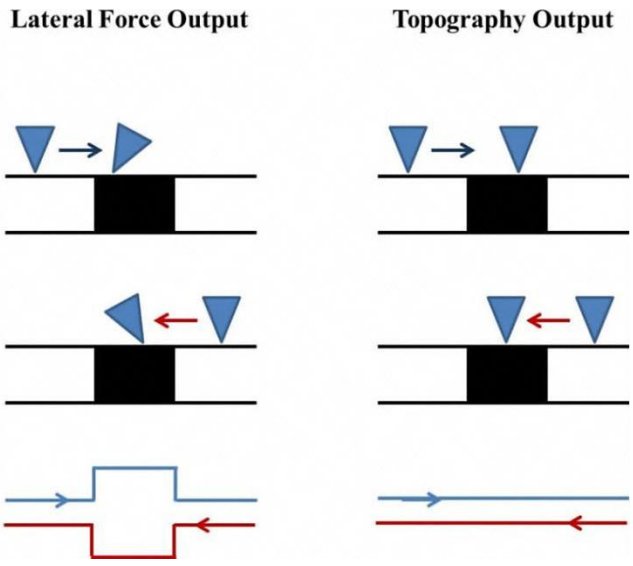

Figure 117: AFM imaging modes – LFM (left side) and topography (right side). LFM provides additional information regarding the surface properties, even when no signal can be obtained for the topography.

Tapping mode: In this mode, the cantilever is oscillated up and down near its resonance frequency by an additional small piezoelectric element. The amplitude of its oscillation is between 100-200 nm. When the tip comes near to the surface there are forces which act on it (see Figure 115), changing the resonance frequency of the system and therefore changing the oscillation amplitude and the phase. Since the tapping mode does not rely on mechanical contact with the sample, very little to no damage is done to both tip and the sample and the same area can be scanned for a very long time. This mode is also suitable for underwater measurements, making it especially interesting for biological samples or living cells.

Applications of AFM:

Force spectroscopy: Instead of scanning a surface for information about topography or chemical composition, in this case, the mechanical properties of molecules are studied. Therefore, the cantilever is pushed into the sample and subsequently retracted again, yielding so called force-distance curves (see Figure 118).

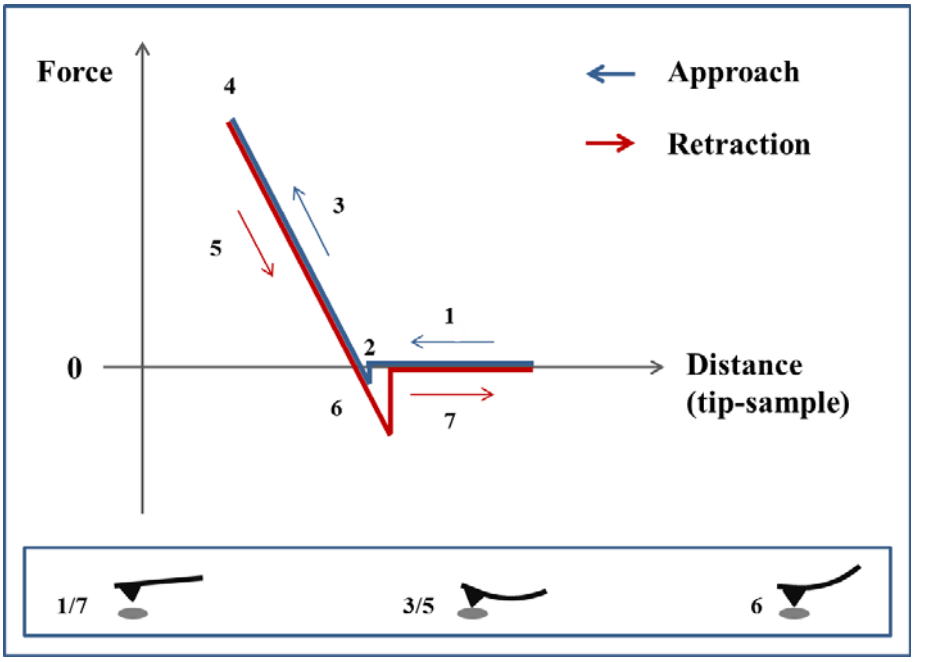

Figure 118: Typical force-distance curve: (1) approach; (2) jump to contact at very close distances; (3) applying force, cantilever bends upward; (4) turning point; (5) cantilever gets "unbend" as withdrawn from the sample; (6) the tips is "stuck" to the sample, the cantilever bends downward until it is suddenly detached; (7) no force is exerted on the cantilever anymore.

This technique is used for the measurement of polymer elasticity, especially biopolymers such as RNA and DNA. Especially interesting are the forces which act during the sequential unfolding of proteins or DNA. Furthermore, it is possible to quantify the binding forces resulting from the interactions between antibody-antigen, protein-protein, protein-living cell.

Dip-pen Nanolithography (DPN): The AFM is used to deposit molecules from the tip onto the substrate. There are two types of inks which use different AFM modes for lithography: Molecular inks are usually deposited in constant force mode, taking advantage of the laser feedback in order to control the force during lithography. Liquid inks, on the other hand, use the constant height mode and without laser control. This is due to the liquid character of the ink, which can also be present on the cantilever back and disturb the deflection of the laser to the point that no readout is possible anymore. The drawback hereby is that there is no control over force exerted on the surface, which is especially problematic when working with soft substrates.

Appendix B - Scanning Electron Microscopy (SEM)

The SEM is a type of electron microscope which uses a beam of electrons (instead of light as with conventional microscopy) to scan the surface in a raster scan pattern. These electrons interact with the atoms present in the sample surface thus producing signals which contain information about the topography of the sample, as well as its chemical composition and other properties such as electrical conductivity. Figure 119 shows the simplified set-up of a Scanning Electron Microscope. The electron beam is emitted by an electron source, which typically consist of a tungsten filament cathode, where the electron beam is emitted thermionically, having an energy ranging from 0.2 eV to 40 keV. It is focused by one or two condensing lenses to a spot of about 0.4 nm to 5 nm and afterwards passes through a set of magnetic coils which control the deflection of the beam in x- and y-direction so that it scans in a raster movement over the rectangular sample area.

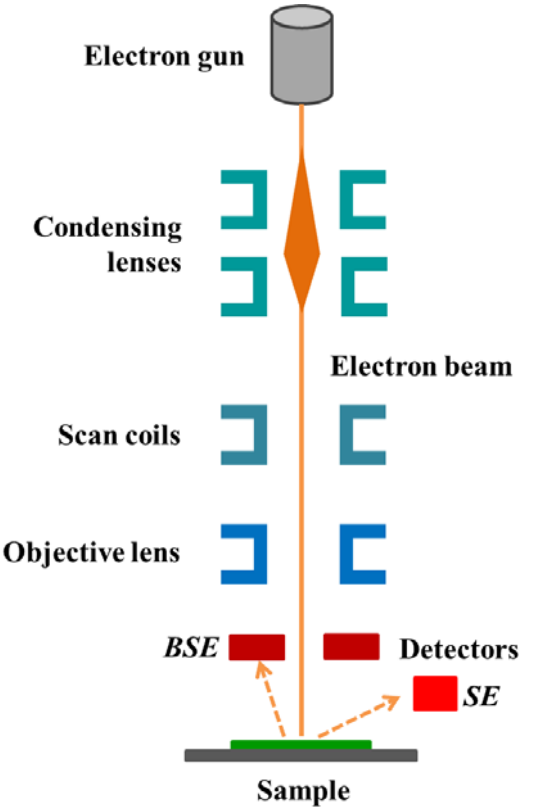

Figure 119: Schematic set-up of a Scanning electron microscope. The detectors indicated are the so called Back-scattered Electron detector (BSE) and the Secondary Electron detector (SE).

Detection methods:

The types of signals obtained by the SEM include secondary electrons, back-scattered electrons, characteristic X-rays and light (cathode luminescence). As most frequently used detection method, the secondary electrons (SE) are generated by interaction of the electrons from the beam with the atoms of the surface. The SE have only little energy (a few eV) and are obtained from the first few nm of the surface and thus reproduce the sample topography. The back-scattered electrons (BSE) are also used frequently for imaging and typically have an energy of several keV from being backscattered. These electrons give information about the materials of the surface: heavy elements (high atomic number) backscatter electrons more strongly than light elements (low atomic number) and therefore appear brighter in the image. This allows the detection of areas with different chemical composition by their contrast. The characteristic X-rays allow the characterization of the sample concerning its elemental composition. Methods used hereby include the Energy Dispersive X-ray Analysis (EDX), where the energy of the X-ray quant is evaluated. These X-rays are obtained when the electron beam removes an inner shell electron from the sample, causing a higher energy electron to fill the shell and give off energy.

Resolution:

The maximal magnification factor is 1000000:1, whereas with light-microscopy it is limited to 2000:1. In general, the spatial resolution depends on the size of the electron spot, which in turn depends on the wavelength of the electrons as well as on the electro-optical system that produces the scanning beam. Depending on the instrument, the resolution can range between less than 1 nm and 20 nm.

Environmental SEM (ESEM):

The first commercial ESEM was developed in the late 1980s. It finally allowed the samples to be observed at low-pressure gaseous environments (0.1 – 6.7 kPa) and high relative humidity (up to 100 %). The ESEM is especially useful for non-metallic materials and biological materials and coating with carbon or gold is not necessary. This is a great advantage since coating can be difficult to reverse, may conceal small features or may reduce the value of the obtained data.

Appendix C - X-Ray Photoelectron Spectroscopy (XPS)

X-ray Photoelectron Spectroscopy (XPS), also known as Electron Spectroscopy for Chemical Analysis (ESCA) is a quantitative spectroscopic technique for determining the elemental composition, empiric formula, chemical state and electronic state of all the elements which are present in a material, without destroying it during the measurement. This method uses energy rich X-rays which are obtained from an Al-Kα or Mg-Kα source in order to knock out electrons from the inner orbitals of the elements present in the surface (top 1 – 10 nm usually). By determining the kinetic energy of the photoelectron it is possible to calculate its binding energy, which is characteristic for the atom or, more precisely, the orbital from which the electron originates. Figure 120 shows the schematic set-up of an XPS, where the characteristic hemispherical analyzer is indicated, which is used to separate the photoelectrons from the sample according to their kinetic energy. Since its top part is negatively charges, the electrons are bent downwards towards the detector. Modern instruments are able to perform simultaneous detection of electrons of all kinetic energies due to a multichannel analyzer. An example for an XPS spectrum is given in the inset and shows the obtained peaks (counts versus binding energy of the electrons which is derived from the kinetic energy).

The spectra are obtained determining the kinetic energy and calculating backwards to obtain their binding energy, using the following equation

$$E_{binding} = E_{photon} - (E_{kinetic} - \phi_{spectrometer}),$$

where $E_{binding}$ is the binding energy, E_{photon} is the energy of the X-ray photons being used, $E_{kinetic}$ is the measured kinetic enery and $\phi_{spectrometer}$ is the work function of the spectrometer.

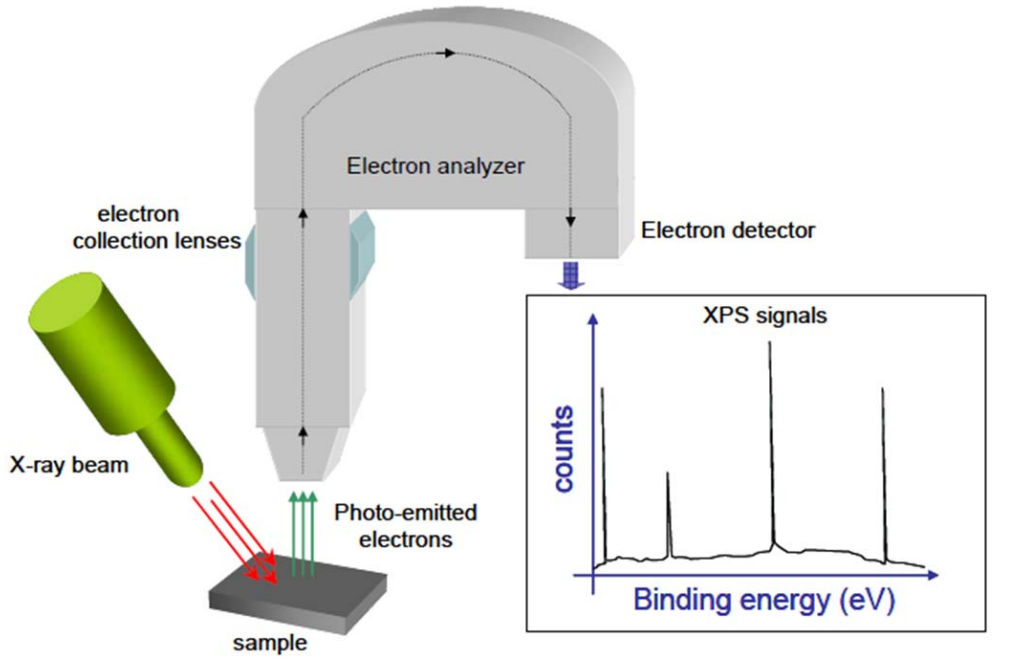

Figure 120: Simplified schematic set-up of an X-ray photoelectron spectrometer (XPS).

Each element produces a specific set of peaks at characteristic binding energy values which directly identify each element on or in the surface of the material being analyzed. Apart from a wide-scan spectrum where all the elements found during the surface scan are listed, a high resolution spectrum of a particularly interesting element provides detailed information about the electronic configuration of the atom (C-C, C-O, C-N, C=C, etc…) where the photoelectron originated from, for example in which bond configuration a carbon atom is present. Therefore, a deconvolution of the single curve into several different curves has to be performed with suitable software. Furthermore, by calculating the area under the curve, it is possible to quantify the amount of an element / electronic state present in the sample.

XPS is routinely used to analyze inorganic compounds, metal alloys, ion modified materials, semiconductors, polymers, ceramics, bones, medical implants, biomaterials and many others.[2] For the present work, XPS was used to check the surface functionalization steps by calculating the differences of surface composition as well as performing the deconvolution and fitting of the high resolution spectra in order to check with all present electronic states of the elements.

Appendix D - Time-of-Flight Secondary Ion Mass Spectrometry (ToF-SIMS)

Secondary Ion Mass Spectrometry (SIMS) belongs to the analytical techniques which are used for surface science and materials science in order to analyze the composition of solid surfaces or thin films. Therefore, the surface of the specimen is sputtered with a focused primary ion beam (see bottom inset of Figure 121) and the emerging secondary ions are measured with a mass spectrometer in order to determine the elemental, isotopic or molecular composition of the surface from which they originate. SIMS is the most sensitive technique for surface analysis and able to detect elements present on the surface in the range of parts per billion (ppb). The mayor drawback of this method is that during the measurements, there is a loss of material from the surface as well as a change in composition and morphology of the sample from the incoming primary ions.

Typically, a SIMS consists of the following components (see Figure 121): An ion gun creating the primary ion beam, an ion column for accelerating and focusing the beam onto the sample, a high vacuum chamber holding the sample and the secondary ion extraction lenses, the mass analyzer which separates the ion according to their mass to charge ratio (see upper inset) and finally, the ion detection unit.

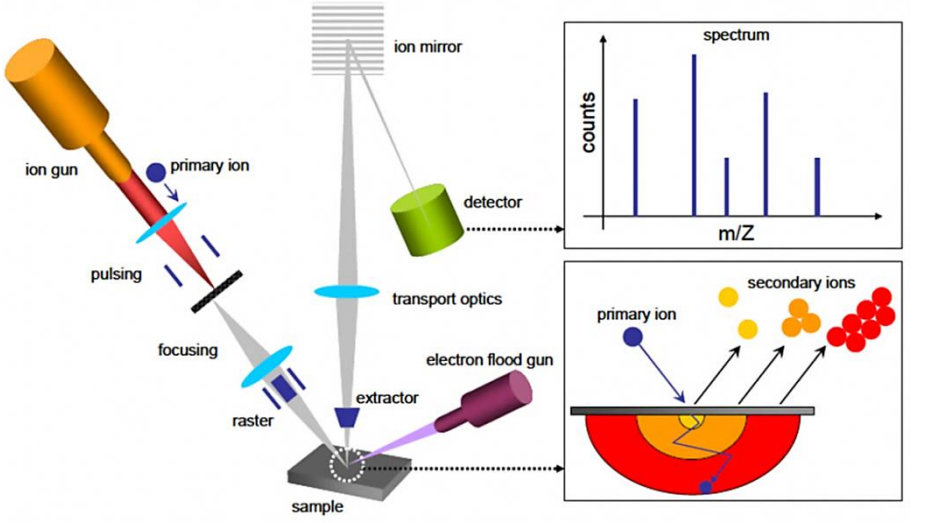

Figure 121: Schematic set-up of a Time-of-Flight Secondary Ion Mass Spectrometer.

Depending on the SIMS type, there are three basic **analyzers** available: sector, quadrupole and **time-of-flight** (ToF). The ToF analyzer separates the ions in a field-free drift path according to their velocity. Since all ions possess the same kinetic energy, the velocity and therefore the time of flight varies according to their mass. It requires pulsed secondary ion generation using either a pulsed primary ion gun or a pulsed secondary ion extraction. It is the only analyzer type which is able to detect all generated secondary ions simultaneously and is the standard analyzer for static SIMS instruments.

SIMS can be run in different modes: The depth-profile mode allows the characterization of the sample composition from the surface downwards. The resolution of depth is around a few nm and the maximum penetration depth up to a few µm. The lateral resolution depends strongly on the instrument but ranges between 50 nm to 1 µm. This way, a 3D mapping of the surface components can be obtained which helps understanding processes occurring at the surface and a few µm below the surface, on the inside of the sample.

Appendix E - Nano Plotter ™

The Nano Plotter used for this work belongs to the robotic non-contact piezoelectric printing devices from GeSIM (Germany) for microarray fabrication. The ink solution is spotted by non-contact microdispensing, applying voltage to the tip. Typically a sample volume of 0.4 nL yields spot sizes of 250 µm, depending on the ink composition and the surface properties.

The instrument is equipped with a workplate for placing and, if desired, cooling down the substrates, an area for a 384 wellplate for the sample uptake, a washing station for the tip (before, during and after spotting) and a stroboscope coupled with a camera for quality control of the ink droplets. A typical spotting cycle is represented in Figure 122. The red square in the testing/spotting cycle indicates the functioning of the piezoelectric crystal for droplet formation and the light source indicated the quality control via stroboscope.

Typical applications include the spotting of DNA, proteins, cells, polymers and gels. For more details we here refer to the GeSIM homepage.[3]

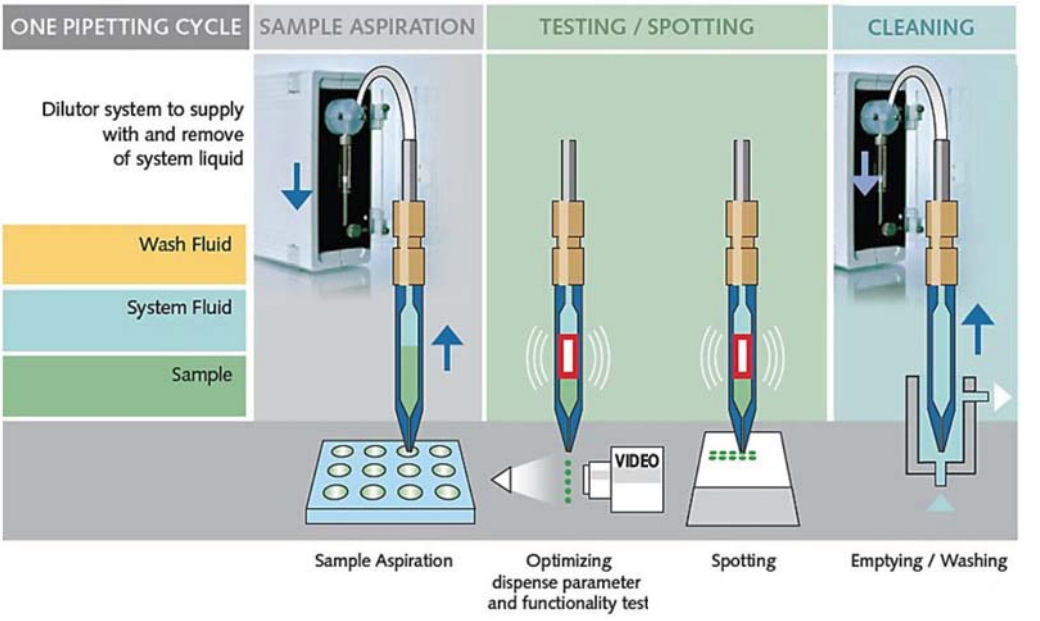

Figure 122: Nano plotter™ non-contact printing pipetting cycle. Image adapted from the GeSIM Nano Plotter brochure.[3]

Appendix F - Microcontact Printing (µCP)

Microcontact printing is a soft lithography technique which uses a polydimethylsiloxane (PDMS) stamp with a relief pattern (3D) to transfer molecules onto a substrate through formal contact. These molecules range from organic compounds like alkanethiols to biologically relevant molecules like DNA or proteins. µ CP was developed by Whitesides and Kumar in 1993, originally for patterning of self-assembled alkanethiols monolayers on gold.[4]

The stamps used for µ CP are made of a silicone elastomer – PDMS – which molds with very high fidelity to a 3D relief template called master. PDMS is a liquid prepolymer at room temperature due to its low melting point (about 50°C) and glass transition temperature (about 120°C). A stamp is usually replicated from a silicon or silicon nitride master which was fabricated by deep reactive ion etching (DRIE) and has the inverse features which are desired for the stamp. Before applying the liquid PDMS to the master, it has to be silanized with a fluorosilane in order to avoid the PDMS sticking to the fine structures of the master and thus the destruction of the stamp features when separating master and PDMS. After preparing the master, the prepolymer is mixed with the curing agent at a determined ratio, poured onto the master and cured by heat in order to crosslink the polymer. After cooling down, the PDMS is carefully peeled off the master and cut into adequate size (see Figure 123).

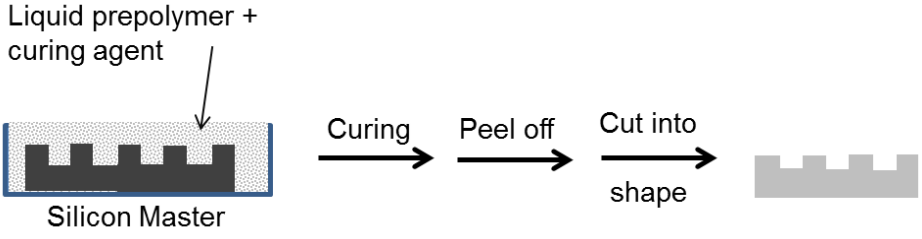

Figure 123: Schematic fabrication of a PDMS stamp

For printing (see Figure 124), the PDMS stamp is then submerged during several minutes in the desired ink which can consist of organic solvents like ethanol or methanol or buffered solutions like PBS. Afterwards, the excess ink is removed by gentle drying of the stamp surface in a nitrogen stream. The stamp is subsequently

placed onto the substrate; pressure is applied carefully so that the stamp is in full contact with the surface and finally, the stamp is removed to yield the pattern on the surface.

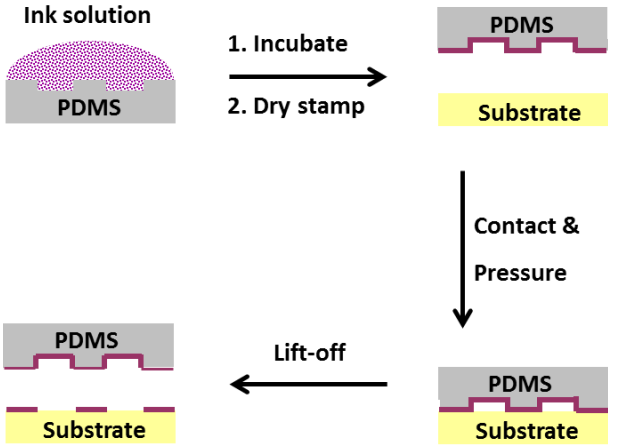

Figure 124: Schematic process of Microcontact Printing

The use of an elastomeric stamp presents several advantages. After a cleaning step, the stamp can be reused several times; PDMS is durable, nontoxic, chemically inert and environmentally safe; it is optically transparent down to 300 nm (UV-VIS region) and has a low thermal expansion; its surface properties can be altered from the natural hydrophobic state to a short-time hydrophilic state by exposure to plasma; several stamps can be obtained from one master; large scale micro-scale patterns can be created easily and with little effort; no special environment is necessary (no cleanroom etc). However, the main disadvantages are stamp deformation during the surface contact, ink loss by diffusion from the stamp itself since the ink slightly penetrates the PDMS surface and shrinking and swelling of the stamp depending on the solvent.

Depending on the ink and the substrate, there are several different applications of μCP: Micromachining[5], where an alkanethiols is patterned on a metal substrate and subsequently used as an etch resist to protect the metal. Only areas without alkanethiols are etched away. Furthermore, by the patterning of proteins, advancement has been made in the areas of biosensors,[6] cell biology research[7] and tissue engineering[8]. It was also possible to deposit DNA.[9]

Appendix G - Western Blot Analysis

Is a widely used technique for the detection of proteins which can be separated either by their 3D-structure or, when denatured before e.g. by heating, by the length of the polypeptide chain. The separation is achieved by gel electrophoresis (see Figure 125). Afterwards, the separated proteins are transferred to a membrane (usually nitrocellulose or polyvinylidene difluoride - PVDF), where they are detected by antibodies.

Gel electrophoresis

The most commonly applied electrophoresis uses polyacrylamide gel along with buffers loaded with sodium dodecyl sulfate (SDS), which is then abbreviated SDS-PAGE (PAGE = polyacrylamide gel electrophoresis). The proteins are treated with strong denaturing agents in order to remove any secondary or tertiary structure and thus allow separation by molecular weight. Then, the proteins become covered by the negatively charged SDS and move towards the positively charged electrode through the acrylamide mesh of the gel, in one dimension only for most of the blots. This allows the separation of the proteins by size since smaller molecules can move faster through the mesh that bigger ones. Furthermore, the concentration of acrylamide determines the resolution of the gel, whereas the higher the concentration of acrylamide, the better the resolution of lower molecular weight proteins and the lower the concentration, the better the resolution for higher molecular weight proteins.

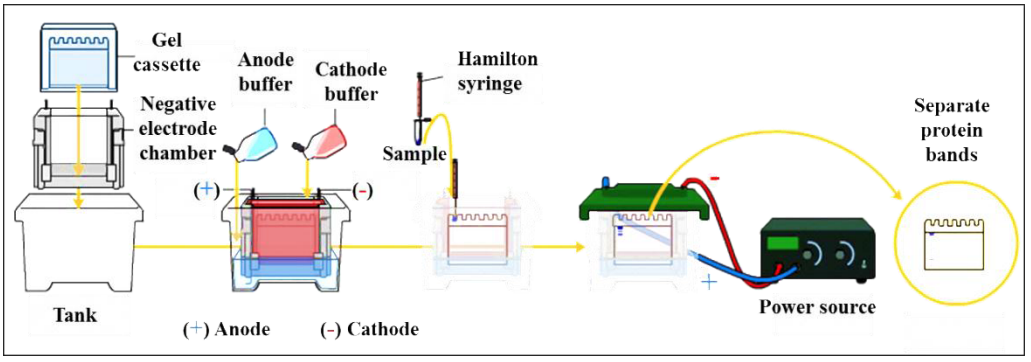

Figure 125: Schematic set-up of a SDS gel electrophoresis. The yellow circle is the gel with the resolved protein bands.

The samples are loaded into the small wells in the gel and usually one line is reserved for a so called marker or ladder, which is a commercially available mixture of proteins with well-defined molecular weights in order to have a reference for which distance in the gel corresponds to which weight. Upon staining, this marker forms visible, colored bands. After loading the samples, voltage is applied along the gel and the proteins migrate into it with different speeds. These different rates of migration (called electrophoretic mobility) cause separation into band within each of the wells = lanes.

Detection

While the proteins are still in the polyacrylamide gel, it is not possible to mark them fluorescently for detection. Therefore, the protein bands are moved from within the gel onto a membrane (typically nitrocellulose or PVDF). The transfer of the proteins to the gel is achieved by electroblotting, where a membrane is placed below the gel and an electric current is used to pull the proteins from the gel into the membrane (see Figure 126), retaining the organization which the proteins had in the gel. These kinds of membranes are chosen because of their non-specific protein binding properties, which means that they bind equally well all types of proteins, which is based upon hydrophobic interactions, as well as interactions between the protein and the membrane.

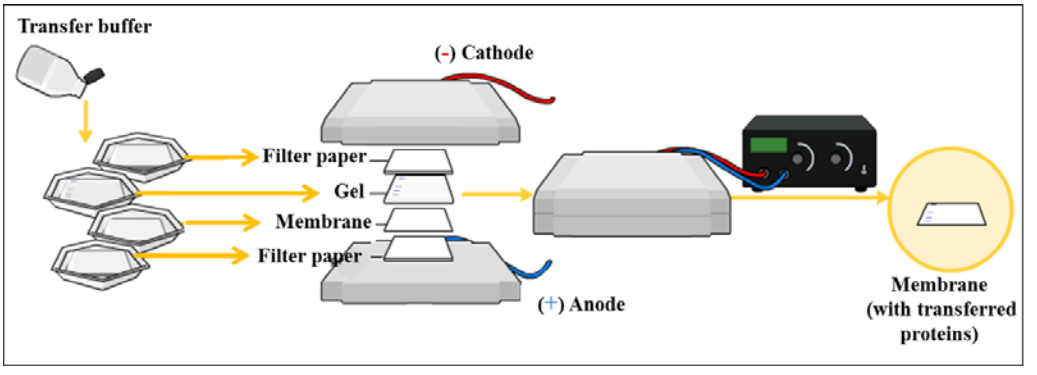

Figure 126: Transfer of the resolved protein bands from the PA gel to the membrane. If the proteins are hydrophobic, a PVDF membrane is used instead of a nitrocellulose membrane.

Before detecting the proteins with antibodies the membrane has to be blocked (it binds all proteins equally well and antibodies also fall into this class of proteins).

Blocking is obtained by saturating the free membrane with proteins from a dilute solution of bovine serum albumin (BSA, 3-5%) or non-fat dry milk in a buffered solution along with a small percentage of detergents such as Tween 20 or Triton X-100.

For detection, the protein of interest in the membrane is detected with a modified antibody which is linked to a reporter enzyme. This enzyme, upon exposure to an appropriate substrate, drives a colorimetric reaction and produces a color, which usually happens in a two-step process. Therefore, the membrane is incubated first with a primary antibody against the desired protein and in a second step with a secondary antibody, which is usually liked to biotin or a reporter enzyme like alkaline phosphatase (ALP) or horseradish peroxidase (HRP). This way, the signal of the primary antibody is enhanced.

In the case of the HRP, a chemiluminescent substrate is cleaved by the HRP producing luminescence in a proportion to the amount of the protein. A sheet of photographic film is placed against the membrane and exposed to the light from the reaction, thus creating an image.

Typical examples of Western blot analysis for medical applications.

- The confirmatory HIV test where proteins from HIV-infected cells are separated and blotted on a membrane. Then, the serum to be tested is applied in the primary antibody incubation step and as second step, a secondary anti-human antibody is added, which is linked to an enzyme signal. The stained bands thus indicate the proteins to which the patient´s serum contains the antibodies.

- The definitive test for Bovine spongiform encephalopathy (BSE).

- Some forms of Lyme disease testing can employ western blotting.

- Can be used for the confirmatory test of Hepatitis B infection

REFERENCES

[1] G. Binnig, C.F. Quate and C. Gerber. *Atomic Force Microscope.* Physical Review Letters 1986. **56 (9)**: p. 930-933.

[2] R.E. Van Grieken and A.A. Markowicz, in *Handbook of X-ray spectrometry: Methods and techniques.* Practical Spectroscopy Series 1993, **Vol. 14**: p. xiv and 704.

[3] http://www.gesim.de/en/nano-plotter/nano-plotter.html, accessed in July 2012.

[4] A. Kumar and G.M. Whitesides. *Features of gold having micrometer to centimeter dimensions can be formed through a combination of stamping with an elastomeric stamp and an alkanethiol ''ink'' followed by chemical etching.* Applied Physics Letters 1993. **63 (14)**: p. 2000–2004.

[5] J.L. Wilbur, A. Kumar, H.A. Biebuyck, E. Kim and G.M. Whitesides. *Microcontact printing of self-assembled monolayers: applications in microfabrication.* Nanotechnology 1996. **7 (4)**: p. 452-457.

[6] P.M. St. John, R. Davis, N. Cady, J. Czajka, C.A. Batt and H.G. Craighead. *Diffraction-Based Cell Detection Using a Microcontact Printed Antibody Grating.* Analytical Chemistry 1998. **70 (6)**: p. 1108-1111.

[7] C.S. Chen, M. Mrksich, S. Huang, G.M. Whitesides, D.E. Ingber. *Geometric control of cell life and death.* Science 1997. **276 (5317)**: p. 1425-1428.

[8] S.N. Bhatia, U.J. Balis, M.L. Yarmush and M. Toner. *Effect of cell-cell interactions in preservation of cellular phenotype: cocultivation of hepatocytes and nonparenchymal cells.* The FASEB Journal, 1999. **13 (14)**: p. 1883-1900.

[9] S.A. Lange, V. Benes, D.P. Kern, J.K.H. Hörber and A. Bernard. *Microcontact Printing of DNA Molecules*. Analytical Chemistry 2004. **76 (6)**: p. 1641-1647.

Resumen en castellano

Construcción de nanoplataformas biomoleculares versátiles via Nanolitografía Dip-pen y su aplicación en bio-sensing y diferenciación celular

Introducción General

La humanidad siempre ha sido curiosa. Después de descubrir casi todo lo relacionado con el espectro visible, los siguientes desafíos se encaminaron hacia cosas invisibles a simple vista. El poder de resolución del ojo humano ronda las 100 µm, que corresponde al ancho de un cabello humano.[1] Hoy en día, es posible investigar los objetos más pequeños, hasta de un tamaño de 0.5 Å o, dentro de una rutina de laboratorio, objetos de entre 1-20 nm. En la escala adjunta (Figura 1), encontramos varios ejemplos de la vida cotidiana con sus correspondientes tamaños.

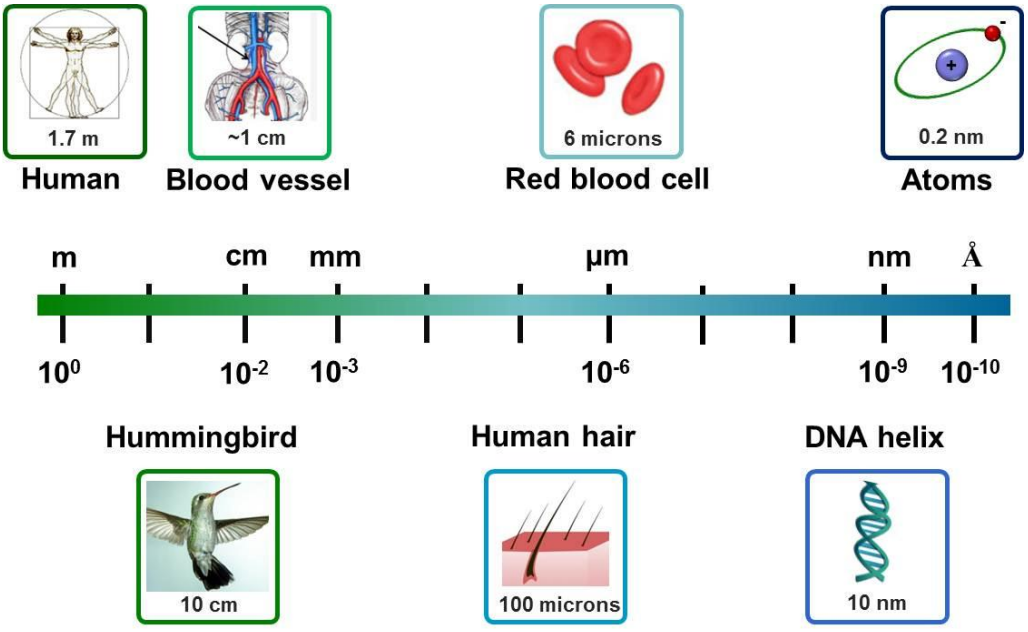

Figura 1: Diagrama de escala de longitudes poniendo en contexto la escala nanométrica.

Modificación de la superficie a escala micro- y nano

Las modificaciones de las superficies en general se realizan según dos técnicas diferenciadas: *structuring* y *patterning*. La superficie *structuring* engloba cambios en los rasgos topográficos de la superficie; la superficie *patterning*, por otra parte, consiste en modificaciones químicas de la superficie mientras la topografía permanece normalmente inalterada.

Origen de la Nanotecnología

Dos famosos científicos que están fuertemente relacionados y sentaron los fundamentos de la nanotecnología son Richard P. Feynman [2] y Gordon E. Moore [3]. Ambos pueden ser considerados como visionarios de su tiempo, ya que revelaron que la tendencia del futuro sería la miniaturización hacia el nanorango, con el objetivo de resolver necesidades de la sociedad.

Los métodos de micro- y nanofabricación se pueden dividir en dos aproximaciones diferentes: top-down y bottom-up

La aproximación **top-down** empieza normalmente desde una pieza mayor de material e intenta hacerla más pequeña mediante tratamiento físico o químico.[4] La aproximación **bottom-up** se aprovecha de las interacciones moleculares debido a las cuales las moléculas se fijan en la superficie de un modo determinado y controlable. Esta auto-organización se llama autoensamblaje (SAM)[9] y puede ser observada en sistemas con uno o más componentes.

Bioreconocimiento molecular

Las estrategias de nanofabricación "bottom-up" se aprovechan normalmente de este mecanismo para idear nanoestructuras que están basadas en fuertes interacciones biológicas. Un ejemplo es la pareja streptavidina-biotina que tiene una de las interacciones biológicas más fuertes que existen en la naturaleza.[5] Otro mecanismo de bioreconociemiento es el del ADN o de los oligonucleótidos, que se caracteriza como rápido, estable y altamente selectivo.

Esta tesis titulada **"Construcción de nanoplataformas biomoleculares versátiles via Nanolitografía Dip-pen y su aplicación en bio-sensing y diferenciación celular"**, tiene como objetivo contribuir al campo de la Nanolitografía. Para ello, este trabajo de investigación emplea una relativamente nueva técnica de nanofabricación, llamada Nanolitografía por Dip-pen (DPN) para realizar el "pattering" directo de moléculas biológicamente relevantes a escala nano y micro, tanto para aplicaciones de biosensor como para estudios de diferenciación celular. Varios métodos de inmovilización covalente para superficie de oro y vidrio fueron evaluados para las respectivas aplicaciones con el fin de asegurar la mayor estabilidad

y reproducibilidad posible en el proceso de la litografía, así como la compatibilidad biológica, especialmente importante para los experimentos celulares. Se evaluaron varios métodos para inmovilización covalente para asegurar máxima estabilidad y reproducibilidad en cuanto al proceso de litografía, y también en cuanto a compatibilidad biológica que es importante a la hora de hacer cultivo celular.

Capítulo 1. Desarrollo de micropalancas con sensores piezoresistivos para Nanolitografía Dip-pen

1.1. INTRODUCCIÓN

En el año 1986, el premio Nobel de Física se concedió a dos científicos llamados Binning y Rohrer, por el invento de un método de microscópía novedosa (scanning probe microscopy). En poco tiempo se hizo muy famoso el microscopio de fuerzas atómicas (AFM), que tiene como ventajas: resolución atómica, medidas en aire y en líquido, la posibilidad de manipulación directa y medidas de fuerzas inter- e intramoleculares por debajo del rango de pico Newton. Por otro lado, el mayor problema operando con el AFM en aire, es la formación de un menisco de agua entre la punta y la superficie, dependiendo de la humedad ambiental (alta humedad = menisco grande; baja humedad = menisco pequeño).[6]

Algunos años después, al grupo de Chad Mirkin se le ocurrió la idea de aprovechar este casi inevitable problema del menisco con el fin de depositar intencionadamente moléculas desde la punta de una micropalanca "químicamente modificada" sobre una superficie.[7] 1-octadecanethiol (ODT) fue la primera sustancia en ser depositada a propósito con una punta de AFM sobre sustrato de oro. Así comenzó la llamada nanolitografía Dip-pen (DPN), basada en la técnica del AFM.

Probablemente, DPN no habría sido una técnica tan exitosa si sólo una punta hubiese sido utilizada para el "pattering". Sin embargo, existen diferentes tipos de los llamados multi-pen arrays, que permiten la paralelización, y, así, el pattering a una escala mas amplia y rápida. El último avance hacia la paralelización se dio con la introducción del nano print array 2D, que contiene 55000 micropalancas idénticas, haciendo así posible un patrón nanométrico de varios mm^2 en un corto periodo de tiempo.[8]

Muy recientemente, se ha descubierto que DPN puede ser también utilizado para depositar pequeñas gotas de un líquido. Esto ha despejado el camino para tintas

consistentes en polímeros[9,10,11,12] o que contienen moléculas biológicamente sensibles como proteínas, péptidos, virus o ADN, donde garantizar la integridad y actividad biológica es de vital importancia. La gran variedad de tintas da lugar a un amplio espectro de aplicaciones para DPN [13] Estos campos de aplicación pueden ser categorizados en tres principales sectores: nanoingeniería, biomateriales y el proceso de DPN en sí mismo.

1.1.1. Tintas para DPN – tintas moleculares y líquidas

Tintas moleculares: Están normalmente compuestas por pequeñas moléculas orgánicas, que se depositan sobre la punta tanto por vaporización[14] o bien disolviendo la molécula en un solvente orgánico como etanol, acetonitrilo o similar. Estas moléculas deben ser estables al secado o denaturalización. El depósito de este tipo de tintas depende del menisco de agua y, por lo tanto, de la humedad ambiental. El modo de trabajar es el de **fuerza constante**, que significa que la fuerza sobre el substrato se mantiene constante durante de la litografía, cosa que se consigue con el feedback del laser.

Tintas líquidas: Las tintas líquidas incluyen cualquier material líquido a la hora de ser depositado o cualquier molécula que no pueda ser depositada en seco sobre las puntas, como por ejemplo hidrogeles, lípidos o simplemente biomoléculas [15,16,171819] que tienen que ser mantenidas en una solución buffer con el fin de prevenir su desnaturalización. El modo de trabajar es el de **altura constante**, que significa que durante la litografía, las puntas están a una altura fija. Eso también significa que, si la altura del substrato cambia, las puntas pueden perder el contacto, o, en el caso contrario, presionar con demasiada fuerza a la superficie. En este caso no se puede utilizar el feedback del laser ya que la tinta liquida puede interaccionar con el haz del laser y causar difracción.

1.1.2. Instrumentos para DPN

Los primeros instrumentos de DPN comercialmente disponibles son los llamados **NScriptor**, que consistían en un AFM convencional con un software específicamente diseñado para simplificar el diseño del "pattern". El DPN basado en AFM encuentra sus límites cuando se necesita un área más grande de patrón (rango de litografía 90x90 μm^2, después se tiene que desplazar a mano) o cuando el proceso de "patterning" se automatiza (si las puntas se tienen que llenar con tinta otra vez, se tiene que hacer a mano).

Un instrumento DPN diferente, que no está basado en el AFM, ha sido introducido por la misma compañía. Este instrumento (**NLP2000**) permite el uso de tintas líquidas y aplicaciones biológicas. El rango de litografía es de cm^2 y los procesos se pueden automatizar. Además permite incrementar la distancia que hay entre puntas y substrato durante de la litografía que puede ser necesario cuando se trabaja con tintas liquidas.

1.1.3. Trabajando con multi-pen arrays

Siempre cuando se use un multi-pen array, la nivelación de las puntas es un factor crucial y debe ser adaptada para ambos instrumentos (NScriptor y NLP). No hay una rutina automática de nivelación para este proceso, y debe hacerse manualmente y a ojo, ayudándose de la cámara microscópica que está implementado en el instrumento. En el caso de una litografía controlada por laser feedback, la nivelación debe hacerse antes del "patterning" y las puntas deben siempre ser niveladas a ojo, porque con el láser no es posible leer dos puntas al mismo tiempo.

La nivelación de la punta es tan importante en ambos casos (modo de trabajo de fuerza constante o altura constante) porque sólo con puntas perfectamente niveladas con respecto a la superficie se podrá obtener una litografía homogénea, debido a que la fuerza de contacto de las puntas es la misma para todas.

1.2. RESULTADOS Y DISCUSIÓN

1.2.1. Nivelación manual mejorada de multi-tip arrays

Como se ha mencionado antes, todavía no existe ninguna automatización de la nivelación de las puntas aunque éste es uno de los factores cruciales a la hora de hacer el patterning. La nivelación debe hacerse a ojo y determinando la distancia de las dos puntas más exteriores a la superficie, se determina el ángulo de nivelación. Una mayor precisión se alcanzó usando el zoom máximo, que permite una detección más temprana de la reflexión de las micropalancas cuando tocan la superficie: mejora de corrección de ángulo de 0.8°. Aunque se ha podido conseguir una mejora de la nivelación, siguen existiendo los problemas que este proceso no está automatizado, que las puntas ejercen demasiada fuerza al substrato y que esta fuerza no se puede cuantificar.

1.2.2. Nivelación multi-pen con puntas piezoresistivas

Gracias al nuevo dispositivo con puntas piezoresistivas, se puede determinar antes el momento de contracto entre las puntas y el sustrato. En comparación con el procedimiento manual, se consiguió una mejora de 18 μm. Eso significa que, en vez de hacer agujeros en el substrato a la hora de hacer la litografía en substratos blandos, las puntas están tocando con la fuerza justa. Además, la nivelación de puntas se consigue de una manera más fácil porque el software calcula automáticamente el ángulo de corrección.

Para comprobar que se puede hacer litografía con este dispositivo, se depositó MHA en un substrato de oro. Después de hacer el “etching” quimico, que levanta el oro donde no está protegido con MHA, se pudo ver que hacía falta hacer ajustes para tener una litografía optimizada. Comparado con los arrays multi-pen que se pueden comprar, las puntas del dispositivo fabricado están más alejadas del borde delantero del micropalanca y este borde está tocando el substrato a la hora de la litografía. Pero con simplemente corregir el ángulo entre substrato y dispositivo, se consiguió depositar la tinta sin problemas, como se puede ver en Figura 3.

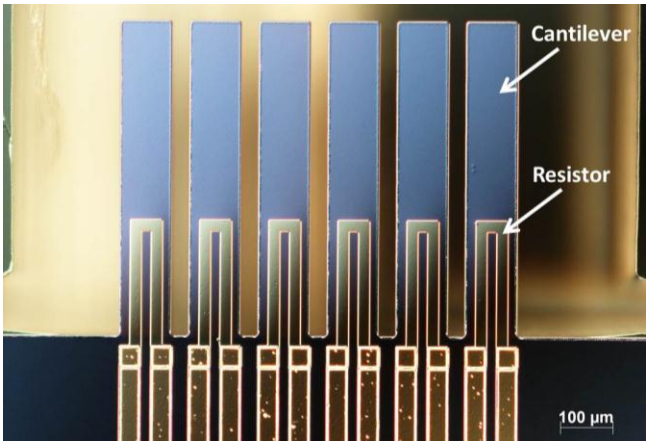

Figura 2: Vista superior de las micropalancas con el resistor integrado que sirve para detectar la deflexión de las puntas cuando tocan el substrato. Imagen de cortesía de NTB Buchs, Suiza.

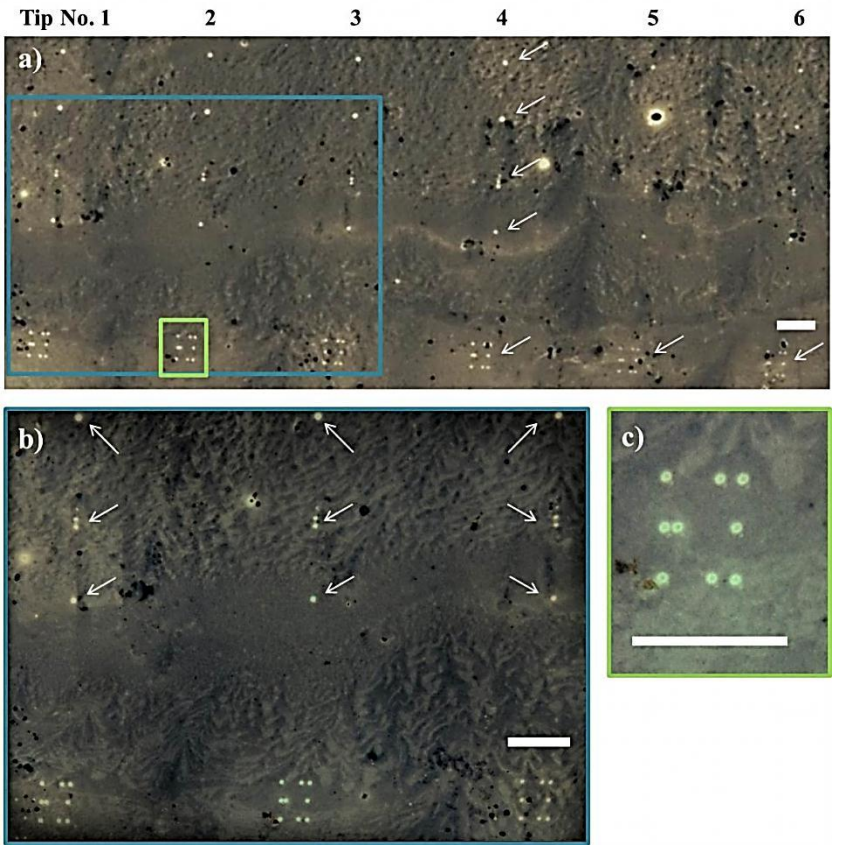

Figura 3: Imagen de microscopía de campo claro de un patrón de MHA en oro; donde el oro que no estaba protegido por MHA, este ha sido removido químicamente via etching. Las flechas indican las áreas donde hay patrón. Las imágenes b y c son áreas ampliadas de la imagen a. La escala corresponde a 30 µm.

Con el dispositivo se consiguió depositar tintas moleculares y líquidas pero las características de las puntas se tienen que modificar para facilitar un mejor depósito. De todas maneras se pudo incluir en el instrumento Nscriptor con éxito y los resultados de la nivelación son prometedores.

1.3. CONCLUSIÓN

En este capítulo se ha trabajado en la mejora de la técnica de litografía Dip-pen, que está en constante desarrollo. Se han implementado varias mejoras a la rutina de nivelación en el caso del uso de multi-pen arrays. Para ello se ha presentado un dispositivo piezoeléctrico. Después de implementar el dispositivo en el instrumento NScriptor y ajustar algunos parámetros, se pudo escribir con éxito en substratos de oro con las tintas MHA y streptavidin-Texas Red. Además se consiguió una sensibilidad más alta a la hora de hacer el contacto entre las puntas y la superficie.

Capítulo 2. Inmovilización de oligonucleótidos via Nanolitografía Dip-pen para la construcción de una plataforma biosensora

2.1. INTRODUCCIÓN

Los sensores juegan un papel importante en nuestra vida diaria. Un sensor es un mecanismo que mide una cantidad física y la convierte en una señal que puede ser fácilmente comprendida por el operador de ese mecanismo. Un tipo especial de sensor es el biosensor, que es un mecanismo analítico formado por a) un elemento biológicamente sensible que específicamente se une al analito b) una arquitectura interfaz c) un transductor o elemento detector, que transforma la interacción "analito – elemento biológico" en una señal cuantificable y, finalmente, d) una interfaz que permite la interpretación de la señal obtenida.[20]

Un biosensor puede ser **clasificado** de acuerdo a tres diferentes factores a) el receptor, b) la técnica de inmovilización utilizada por el receptor o c) el transductor.[21] Según su principio de interacción, los biosensores se pueden clasificar en calorimétricos, potenciométricos, amperométricos, piezoeléctricos y ópticos.

Los **elementos de reconocimiento** más comunes en biosensores incluyen células enteras, [22] anticuerpos[23], fragmentos de antígenos[24] o enzimas[25]. Por otra parte també se han utilizado receptores celulares, [26], tejidos[27] y microorganismos[28]. Los elementos de reconocimiento más utilizados son los anticuerpos debido a su alta especificidad al unirse al antígeno. Sin embargo, su inmovilización en la superficie puede causar la pérdida de la actividad biológica. Otro grupo de elementos de reconocimiento son los ácidos nucleicos, que tienen varias ventajas como por ejemplo alta estabilidad y el hecho que se pueden denaturalizar fácilmente y así el sensor se puede reutilizar.[29]

Los **ácidos nucleicos** engloban DNA, RNA, oligonucleótidos monocatenarios, aptámeros[30] y ácidos nucleicos análogos[31] tales como PNA y LNA. Los ácidos nucleicos tienen varias ventajas. No requieren una solución tampón, lo cual significa que no pierden su actividad biológica cuando se disuelven en agua o disolventes orgánicos. Además, una vez inmovilizados en la superficie su almacenaje es menos complicado y la incorporación de un grupo químico final para anclaje es relativamente sencilla y 100% controlable.

Para asegurar una **inmovilización** estable del elemento de reconocimiento en la superficie del sensor, normalmente es preferible la unión covalente sobre la simple adsorción. Frecuentemente, se usan grupos carboxyl-, amino- o ester-, o la pareja de biotina-streptavidina, donde los dos primeros grupos requieren una activación adicional. Para enzimas sensibles se utilizan técnicas vía hidrogel[32] o sol-gel[33]. También se emplean técnicas de "patterning" como impresión por microcontacto[34] o "spotting" [35]. Los métodos de inmovilización para ácidos nucleicos se explican en más detalle en la referencia 36. También se menciona un nuevo método usando "click chemistry".

Ventajas de la miniaturización de biosensores

El método de detección más común en biosensores es la inmunodetección, que se aplica en la fabricación de microarrays genómicos[37] y proteicos[38]. Un aspecto importante para estas técnicas es el "site-encoding" que significa que de cada posición en el microarray se puede deducir la composición.

Incluso siendo posible detectar millones de secuencias genéticas a partir de la técnica de microarrays genómicos, no hay posibilidad de secuenciar una cadena simple de DNA debido a la enorme cantidad de material que debe ser analizado. Por eso, el desarrollo de arrays y biosensores es de un gran interés, ya que el diámetro de los spots es micro-nano y permite incrementar dramáticamente el número de spots que hay en un chip. Entre los métodos de la nanofabricación, el DPN resulta particularmente interesante porque permite posicionar las moléculas sobre un sustrato con 10 nm de resolución en un array prediseñado con un control completo sobre la densidad y el espaciado del punto.

La inmovilización directa de oligonucleótidos a escala micro y nanométrica se ha conseguido usando Dip-pen. Por ejemplo, Demers et al. fueron los primeros que escribieron directamente oligonucleiótidos en oro, en substratos de silica modificados.[39] Además se ha publicado la escritura de oligonucleótidos con modificaciones tiol,[40] amino[41] o silano[42] en diferentes substratos. Aunque ninguno de los trabajos mencionados describe un biosensor, son válidos para la inmovilización de oligonucleótidos a escala nanométrica.

Como se ha mencionado anteriormente, la **química click** puede ser una buena opción para inmovilizar moléculas en una superficie. Desde hace poco, se usa una cicloadicción 1,3-dipolar entre azidas y alquinos que da triazoles. Originalmente esta reacción fue descubierta por Huisgen[43] y mejorada por Meldal[44] y Sharpless[45], que introdujeron el uso de un catalizador para mejorar la regioselectividad y la eficiencia. Las aplicaciones incluyen la modificación de polímeros,[46,47] hidrogeles[48] y superficies bioactivas[49]. Además se ha utilizado con técnicas como la fabricación de microarrays,[50] microcontact printing,[51,52] y nanolitografía Dip-pen.[53,54,55,56]

2.2. RESULTADOS Y DISCUSIÓN

2.2.1. Oligo-tiol en vidrio modificado y tinta de tampón fosfato salino/gliceról

Para anclar una cadena de oligonucleótido con tiol en una superficie de vidrio, es imprescindible de modificar el vidrio (en este caso con un linker llamado SMPB). El oligo fluorescente y con grupo tiol se depositó usando una tinta líquida que consiste de un tampón fosfato salino y glicerol para minimizar la evaporación del líquido. La Figura 4 demuestra que la litografía tuvo éxito y se pudo depositar la tinta en la superficie. Sin embargo, después de lavar el substrato, la señal de fluorescencia disminuyó bastante. Como además hubo problemas con la homogenidad del patrón, este método se desechó.

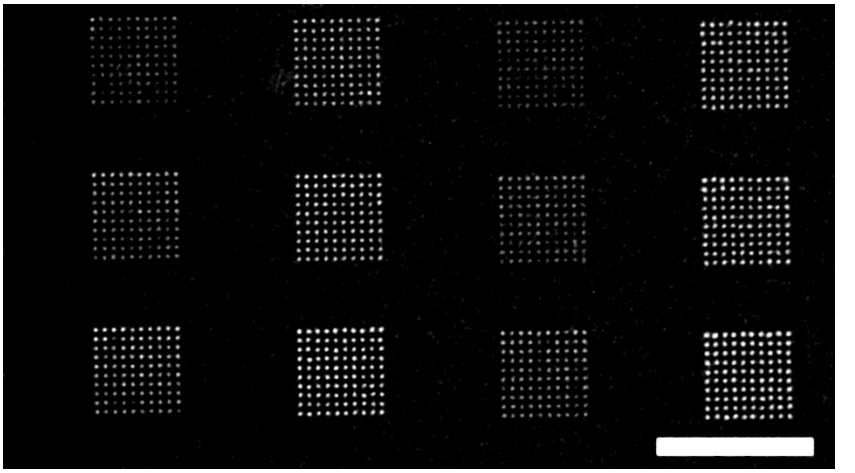

Figura 4: Imagen de fluorescencia de unos sets de arrays del oligo RRSoja escritos en vidrio modificado, después de la litografía. Cada columna corresponde a una punta diferente (se usaron multi puntas). La escala corresponde a 50 μm.

2.2.2. Oligo-tiol en oro y tinta de tampón fosfato salino/gliceról

Después de ajustar la concentración del oligo en la tinta, se consiguió depositar el oligo con suficiente concentración en la superficie y pudo ser hibridado con una cadena complementaria, como se puede ver en la Figura 5.

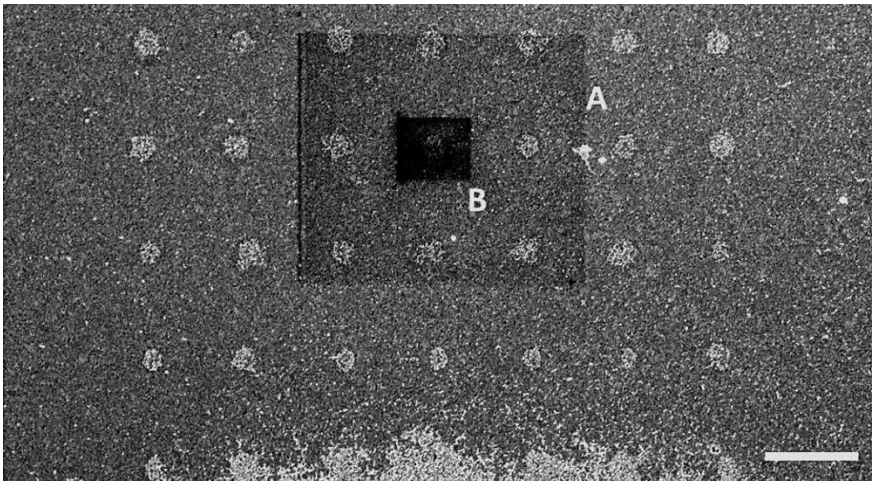

Figura 5: Imagen de microscopia electronica de barrido de un array del oligo "N3down" en oro con siguiente passivación e hibridación con el oligo complementario "N3up". El área del patrón se puede diferenciar bien contra el fondo. El color blanco de los spots es por las nanoparticulas de oro que lleva la cadena complementaria. La escala corresponde a 5 μm.

Aunque la litografía es exitosa, se producen agujeros debido al contacto entre la punta y la superficie (Figura 8). Como se puede ver también, hay pocas nanopartículas de oro (color blanco). Este hecho puede causar problemas a la hora de medir con un biosensor construido de esta manera ya que la señal que se obtiene puede ser errónea. Por eso se descartó esta vía de fabricación.

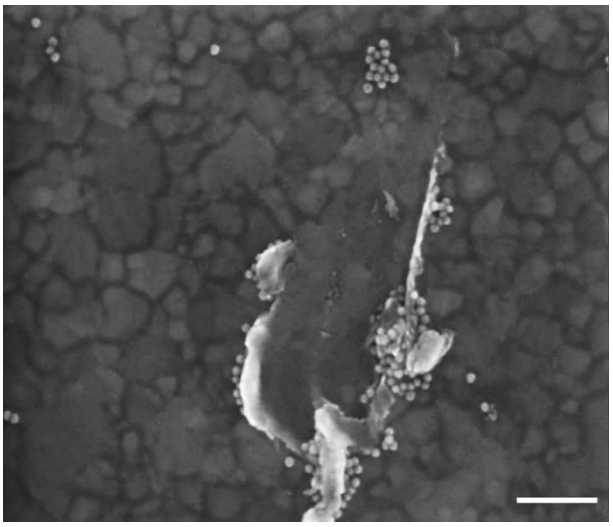

Figura 6: Imagen de microscopia electronica de barrido de un spot de un array del oligo "N3down", parecido a la Figura 5. Aquí, la pressión de la punta al hacer contacto con el oro ha sido demasiado y se produjo un agujero. La escala corresponde a 200 nm.

2.2.3. Oligo-azida en vidrio modificado usando química click

La Figura 7 muestra los pasos de funcionalización del vidrio (a y b) y una reacción click en superficie. Al acabar el paso b), se ha conseguido una plataforma estable para hacer química click en superficie.

Tanto los pasos de la funcionalización como el éxito de la reacción click en superficie, se examinaron con Espectroscopia de fotoelectrones emitidos por rayos X (XPS) y Espectroscopía de masas de iones secundarios mediante analizador por tiempo de vuelo (ToF-SIMS).

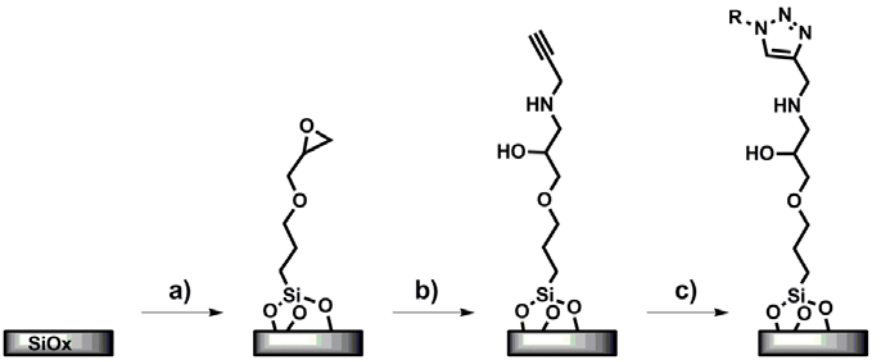

Figura 7: Estrategia de funcionalización de vidrio para facilitar una reacción click. A) Paso de silanización de la superficie con GPMTS. B) Apertura del grupo epoxy con la propargilamina. C) Reacción click en superficie con una azida. Se produce un anillo 1,2,3-triazol.

Se consiguió con éxito depositar una tinta para la química click en superficie con dos métodos de fabricación: Con el Nanoplotter se obtuvieron dots de un diámetro de ~250 µm y con la nanolitografía Dip-pen un diametro de 5.49 µm ± 0.39 µm (véase Figura 8). La imagen se tomó después de la litrografía y el proceso de lavar, passivar e incubar el substrato con la cadena complementaria. Aunque eso involucró varios pasos de lavado, se puede ver claramente el patrón.

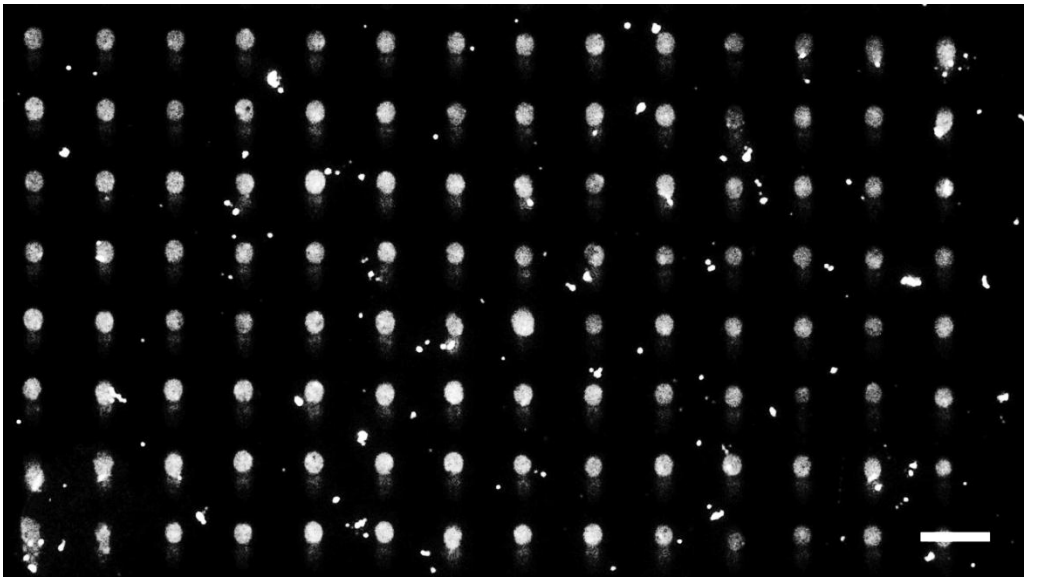

Figura 8: Imagen de fluorescencia de un array homogéneo de un oligo-azida depositado en vidrio modificado para la química click. La fluorescencia se obtuvo mediante hibridación con una cadena complementaria con fluorofor. La escala corresponde a 15 µm.

Para determinar la utilidad como biosensor, se hizo un ensayo con diferentes concentraciones de oligo complementario (de 100 pM a 10 µM). Tanto las fotos como la curva obtenida después de evaluar para cada concentración los 25 spots, se puede ver en Figura 9.

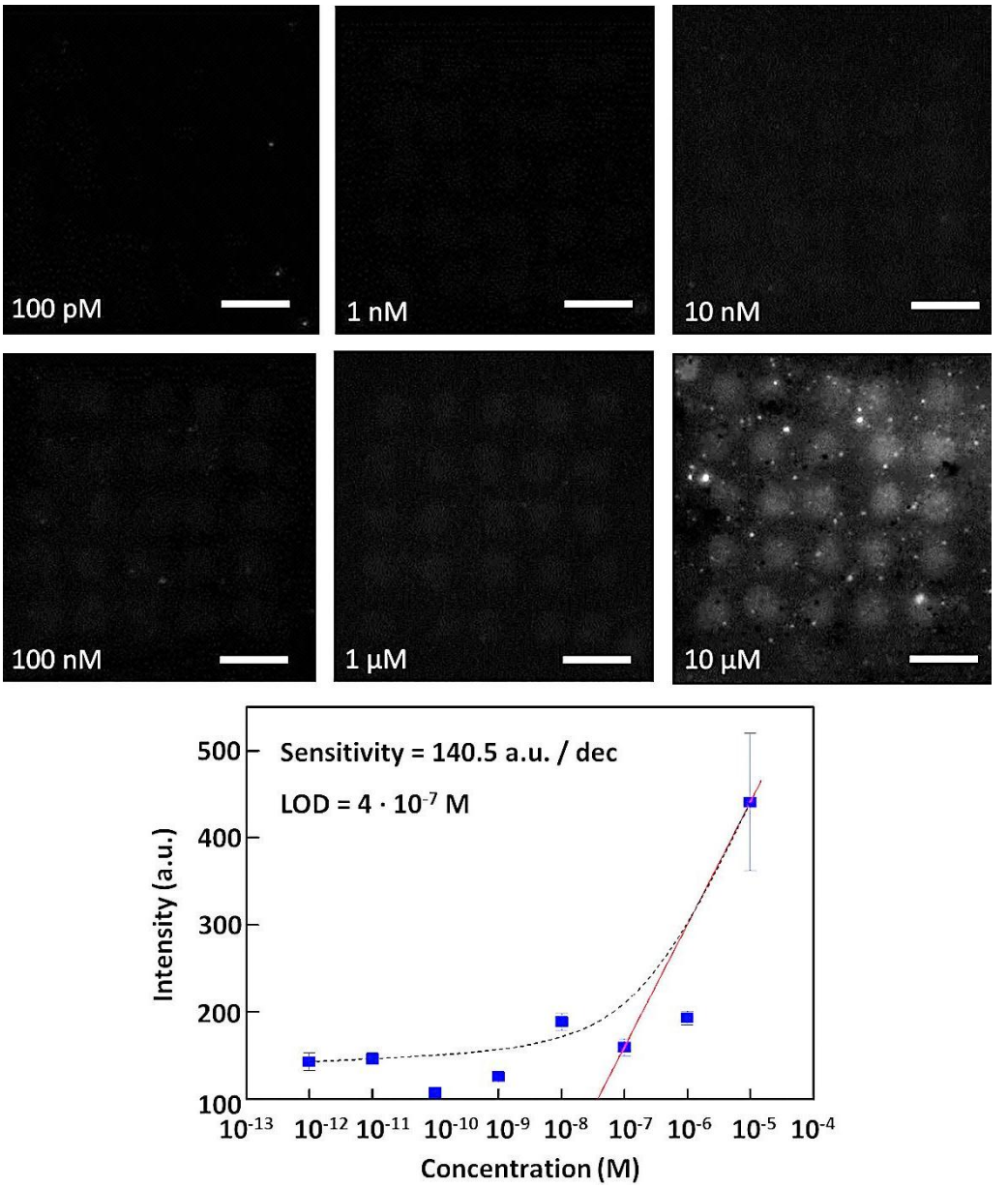

Figura 9: Imágenes de fluorescencia y plot de la intensidad normalizada de los spots (oligo complementario que lleva fluorofor). El plot representa la media normalizada de 25 spots del array de 5 x 5 spots. Las barras de error corresponden a la deviación estándar. La línea azul representa un fitting polinomico de segundo orden. Las escalas corresponden a 20 µm.

El limite de detección se determinó a LOD = 4 x 10^{-7} M de cadena complementaria.

2.3. CONCLUSIONES

El presente trabajo describe el desarrollo de la miniaturización de un biosensor basado en oligonucleótidos y fabricado via Nanolitografía Dip-pen.

Para eso se usaron dos substratos: oro y vidrio, y se probaron diferentes rutas de inmovilización covalente. Aunque se pudo conseguir con éxito el depósito de oligonucleótidos en oro, esta ruta no se continuó debido a la baja reproducibilidad del patterning y el problema casi inevitable de dañar el substrato.

Lo substratos de vidrio, en principio, son resistentes contra estos daños pero, al otro lado, requieren una previa funcionalización química para permitir una inmovilización covalente de las moléculas. Se probaron dos modificaciones diferentes de las cuales la química click resultó exitosa en cuanto a reproducibilidad y estabilidad.

La versatilidad de este enfoque de patterning directo usando química click se demostró usando dos técnicas de patterning directo a escala micro y "meso". Después de fabricar un array de dots de oligonucléicos, la capacidad biosensora se evaluó midiendo diferentes concentraciones de oligo complementario a la hora de la hibridación: de 100 pM a 10 μM. El límite de detección (LOD) se determinó a 4 x 10^{-7} M y aunque este limite parece alto, esta estrategia es prometedora ya que se consiguió una plataforma universal para un biosensor.

Futuro trabajo incluyera el depósito de 3 secuencias distintas de oligo (multiplexing) y posterior hibridación con una mezcla de cadenas complementarias para verificar el potencial de esta plataforma biosensora.

Capítulo 3. Patterning de grandes áreas de sustratos de oro y vidrio con nanolitografía Dip-pen y sus aplicaciones en los experimentos de diferenciación celular

3.1. INTRODUCCIÓN

Durante las dos últimas décadas, las nanotecnologías han dado paso a un nuevo campo de aplicación: la nanomedicina. El papel de la micro- y nanotecnología en este área es evidente ya que las tecnologías de fabricación actuales no pueden proveer acceso a estructuras a nanoescala. La razón de la importancia de la nanoescala se encuentra en las células: la adhesión celular es un proceso de anclaje crucial para las células que no pueden sobrevivir en suspensión.[57] Los receptores celulares que juegan un rol en el anclaje y la transducción de señales son micro- y nanométricos en sí mismos,[58] así como las proteínas intracelulares que activan las células para ejercer fuerzas sobre el sustrato.[59] Recientes estudios han demostrado que el orden geométrico del micro- y nano- patrón es importante y controla la proliferación e incluso la diferenciación celular.[60]

El cuerpo humano tiene muchos tipos de células diferentes que provienen todos de un único tipo que se crea durante de la fertilización. Las principales protagonistas del proceso de embriogénesis son las llamadas células madre, células que poseen la habilidad de regenerarse a si mismas, diferenciarse y regenerar tejidos. Estas células, también se encuentran en los individuos adultos, en tejidos como la médula ósea, sangre del cordón umbilical y tejido adiposo o neuronal. Éstas son las llamadas células multipotentes, que no son capaces de diferenciarse en cualquier tipo celular, pero sí en varios fenotipos distintos. Las células madre mesenquimales son células multipotentes que se puede diferenciar en osteoblastos, mioblastos y neuronas.[61]

Un cultivo de células madre necesita de una gran cantidad de control para alcanzar poblaciones homogéneas de células diferenciadas. Dicha homogeneidad

puede ser promovida administrando estímulos solubles exógenos o controlando el entorno celular, que consiste en proteínas de matriz extracelular (ECM) (Figura 10).

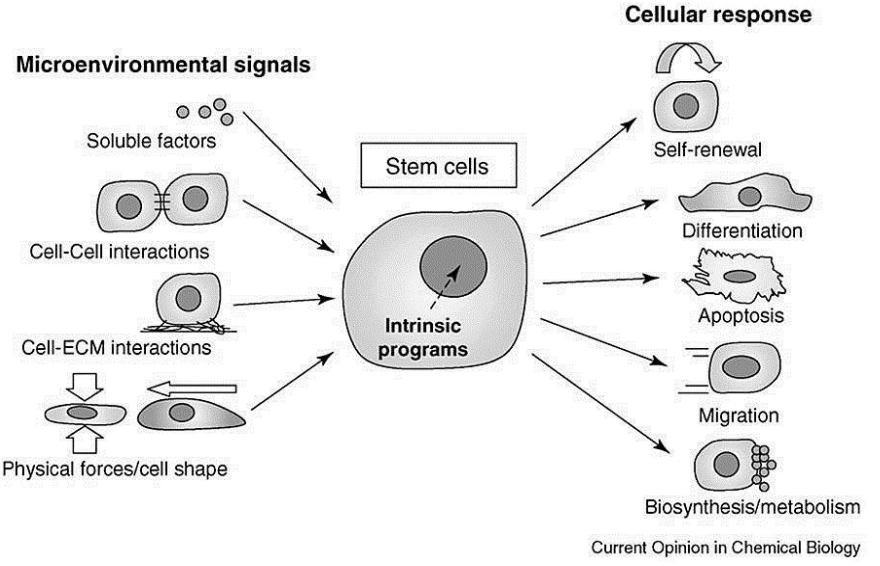

Figura 10: Señales de la matriz extracellular que influencian el destino de las células madre. ECM = matriz extracelular. Imagen tomado de la referencia 62.

Las proteínas de la ECM que normalmente se aplican en experimentos de células madre son la fibronectina, la laminina y el colágeno.[63,64] En vez de usar la proteína entera, también se inmovilizan pequeños motivos que son conocidos por tener influencia en la adhesión celular interactuando con proteínas de membrana llamadas integrinas, como la RGD.[65] Las moléculas usadas como factores solubles son los llamados factores de crecimiento. Hay varias familias de factores de crecimiento tales como el factor de crecimiento del fibroblasto (FGF), el factor de crecimiento transformante (TGF), la ruta de señalización Hedgehog y la ruta de señalización Wnt. De gran interés son las proteínas de la sub-familia de factores TGF β, las proteínas morfogénicas óseas, y en especial la proteína morfogénica ósea 2 (BMP-2), que se utiliza como terapia.[66,67] Con respecto a la diferenciación celular, la BMP-2 se ha utilizado para inducir efectivamente la formación y regeneración ósea.[68,69,70]

Una línea celular para estudiar los efectos de la BMP-2 en la diferenciación son las células C2C12, una línea mioblástica, que tiene sólo dos posibilidades al

diferenciarse (Figura 11). Según su presencia o no las células C2C12 se diferenciaran hacia osteoblastos o mioblastos, respectivamente.

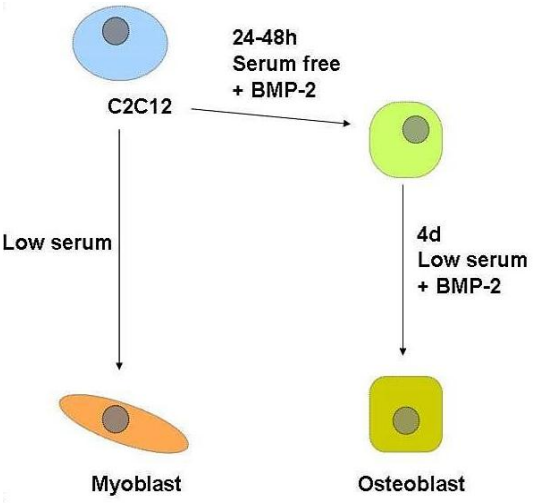

Figura 11: Camino de diferenciación de las células C2C12 con y sin la proteína BMP-2. Imagen adaptada de la referencia 71.

Inmovilizando la proteína BMP-2 en la superficie, se intenta minimizar los estímulos celulares no controlables. Una pre-condición importante para la inmovilización exitosa del factor es el completo control sobre su orientación y densidad en la superficie.[72] Hay varias posibilidades para inmovilizar una proteína sobre un sustrato, pero no todas ellas dejan la proteína activa para el reconocimiento celular. En vez de adsorción física o anclaje químico, nuestro grupo usa la estrategia del mecanismo de reconocimiento biotina-streptavidina. La biotina esta se ancla en la superficie y gracias a la fuerte unión entre biotina y streptavidina, una proteína biotinilada se quedará inmovilizada en la superficie de manera selectiva y estable.[73] El único paso crítico antes de unir la proteína al sustrato es el de biotinilización, que tiene que asegurar que la proteína permanece biológicamente activa.

3.2. RESULTADOS Y DISCUSIÓN

3.2.1. Inmovilización de 16-mercaptohexadecanoic acid en oro

Para realizar experimentos de cultivo celular en un substrato, el área total del patrón tiene que ser suficientemente grande (mínimo 500x500 μm²).[74] Hasta ahora, la fabricación de patrones homogéneos de áreas grandes ha sido un reto, especialmente si no se puede usar un array 2D (la molécula se tiene que evaporar para funcionalizar las puntas). Para validar la hipótesis de que se pueden fabricar áreas suficientemente grandes con un patrón homogéneo, se usaron multi puntas para depositar 16-mercaptohexadecanoic acid (MHA) en oro. Primero se probaron diferentes tiempo de permanencia (dwell time; dt) de la punta en la superficie y se determinaron los diámetros de los patrones creados: 312 ± 10 nm para 8 s; 250 ± 6 nm para 6 s; 215 ± 6 nm para 4 s; 206 ± 5 nm para 2 s (resultados no mostrados aquí). En otro experimento se determinó el diámetro para dts de 0.2 s y 0.1 s y se consiguieron los siguientes valores: diámetro de patrón entre 64 nm y 71 nm para 0.2 s y entre 35 nm y 45 nm para 0.1 s. Para fabricar un patrón de aproximadamente 1 mm² en un tiempo razonable, el dt tiene que ser suficientemente largo para no comprometer la calidad del patrón y suficientemente corto para no superar las 4 h. Por eso, se usó un dt de 0.2 s y se creó un patrón de 34 dots por 200 dots (cada punta) que ocupa un area total de 0.167 mm² (Figura 12).

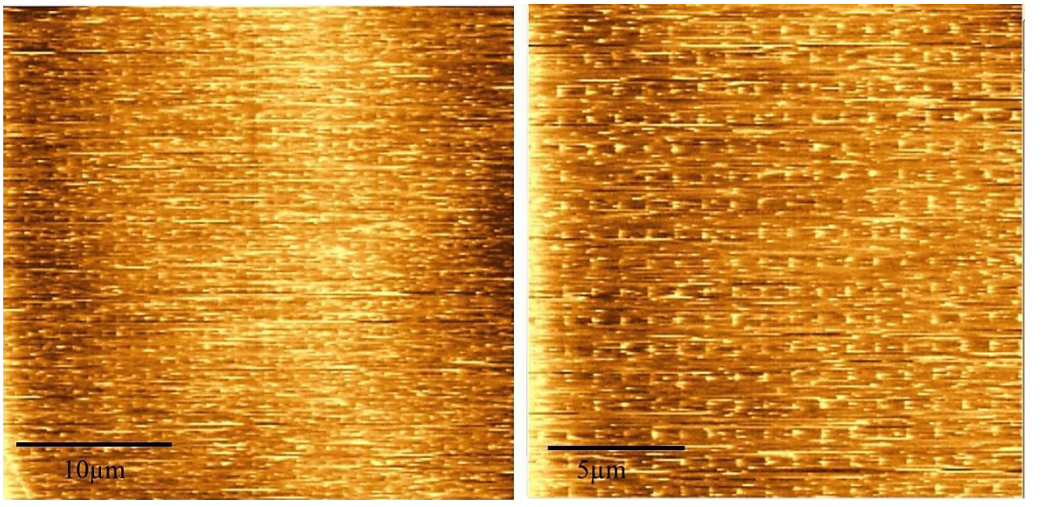

Figura 12: Imagen de topografía de microscopio de fuerzas atómicas (AFM) de dos zonas del área grande con patrón homogéneo.

Se consiguió la fabricación de patrones homogéneos suficientemente grandes para experimentos con células. El siguiente paso fue cambiar la molécula MHA por otra que facilite el anclaje fácil de biomolecular. Por eso se eligió la molécula biotina-PEG-tiol.

3.2.2. Biotina-PEG-tiol y "microcontact printing"

El set-up experimental se puede ver en Figura 13: la Biotina-PEG-tiol (en rojo) se inmoviliza en substratos de oro para crear una plataforma, junto con la streptavidina (en azul), en la cual se puede inmovilizar la BMP-2 biotinilada (en verde).

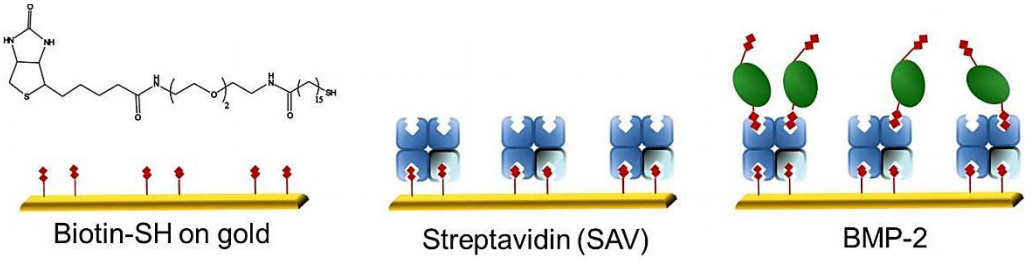

Figura 13: Set-up experimental para los experimentos de microcontact printing aplicados a cultivo celular.

Los substratos fabricados en este apartado comprenden: substratos con una capa homogénea de biotina (y también streptavidina); substratos con patrón circular de diámetro 5 µm (Figura 14) y substratos con patrón de líneas de anchura 5 µm (Figura 15). Las figuras mencionadas son imágenes de fluorescencia que muestran la co-localización de los patrones de streptavidina y BMP-2 biotinilada. Estos substratos se utilizaron para hacer experimentos de diferenciación celular.

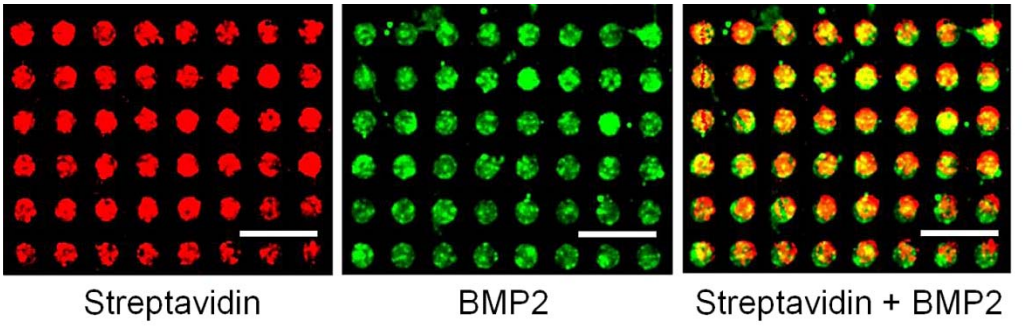

Figura 14: Imágenes de fluorescencia del patrón redondo de 5 µm: (lado izquierdo) streptavidina Texas-Red inmovilizada en biotina-PEG-thiol; (medio) BMP-2 biotinilada encima de streptavidina, detectada por imunofluorescencia; (lado derecha) co-localización de ambos imágenes de fluorescencia. La escala corresponde a 20 µm.

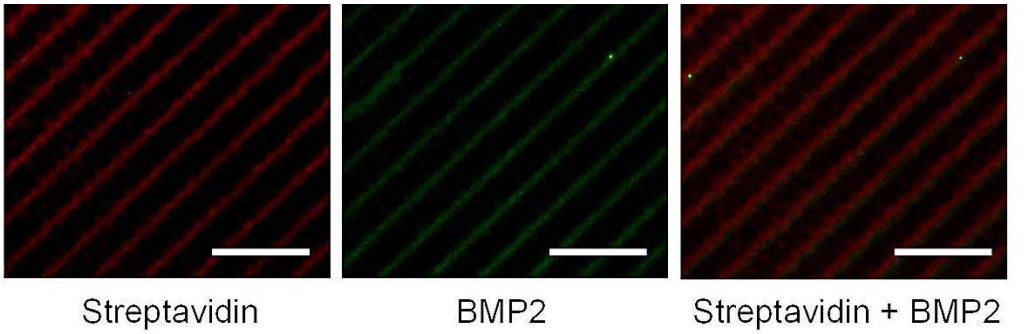

Figura 15: Imágenes de fluorescencia del patrón de líneas de 5 µm: (lado izquierdo) streptavidina Texas-Red inmovilizada en biotina-PEG-thiol; (medio) BMP-2 biotinilada encima de streptavidina, detectada por imunofluorescencia; (lado derecha) co-localización de ambos imágenes de fluorescencia. La escala corresponde a 50 µm.

3.2.3. Biotina-PEG-thiol y nanolitografía Dip-pen

También se intentó el depósito de la biotina-PEG-thiol usando un lípido, el DOPC, para facilitar el flujo de la tinta de la punta a la superficie. Para crear un área suficientemente grande, en vez de hacer la litografía sólo en la dirección y también se amplió en dirección x. Así se pudo conseguir una longitud en x de 1551 µm en vez de sólo 759 µm y patrones con un área mayor de 1 mm². Ajustando la densidad de los dots del patrón, se consiguió fabricar varios substratos con patrones homogéneos. La Figura 16 muestra las diferentes densidades que se probaron. Examinando todos los

substratos por microscopía de campo oscuro, se pudo determinar la homogeneidad del patrón en cuanto al tamaño de spot.

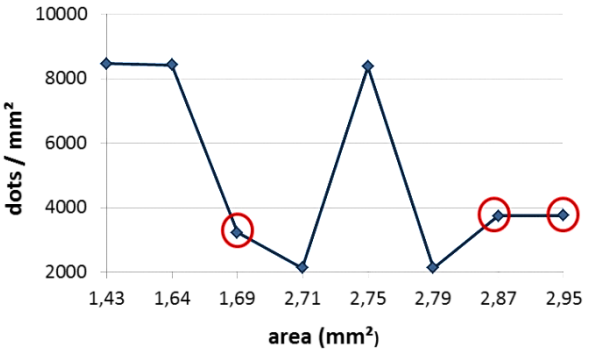

area (mm²)	dots	dots/mm²
1,43	12096	8459
1,64	13824	8429
1,69	5445	3222
2,71	5760	2125
2,75	23040	8378
2,79	5940	2129
2,87	10752	3746
2,95	11088	3759

Figura 16: Grafico y tabla para diferentes densidades de dots. La densidad se calculó a base del área total del patrón y el número total de dots depositados. Los círculos rojos indican las densidades óptimas para el resto de los experimentos.

En Figura 17 se puede ver un patrón de área grande y homogéneo. El diámetro promedio de de los dots es de 4.01 ± 0.90 µm (que corresponde a un área de 53.20 ± 23.89 µm²). En base a lo trabajos publicados,[75] se estimó la masa transferida mediante nanolitografía Dip-pen, depositando el lípido DOPC con biotina-PEG-tiol. Según la literatura áreas > 65 µm² corresponden a una masa de 1.59 ± 0.10 pg tinta/dot y áreas < 65 µm² a una masa de 0.08 ± 0.02 pg tinta/dot. El numero estimado de moléculas por dot varía entre 2.48 x 10^8 y 1.25 x 10^7. De esto puede deducirse que la cantidad de biotina-PEG-thiol depositada varía entre 411.82 amol y 20.72 amol. La densidad de biotina-PEG-tiol promedio es de 4.1 amol/µm², correspondiendo a 2.5 x 10^6 moléculas/µm². Una monocapa se puede estimar a 4.76 x 10^6 moléculas/µm².

Después de fabricar varios sustratos con idénticas características, éstos se han utilizado en cultivo celular. Para ello, se pasivaron con PEG-tiol y se incubaron con streptavidina y BMP-2 biotinilada.

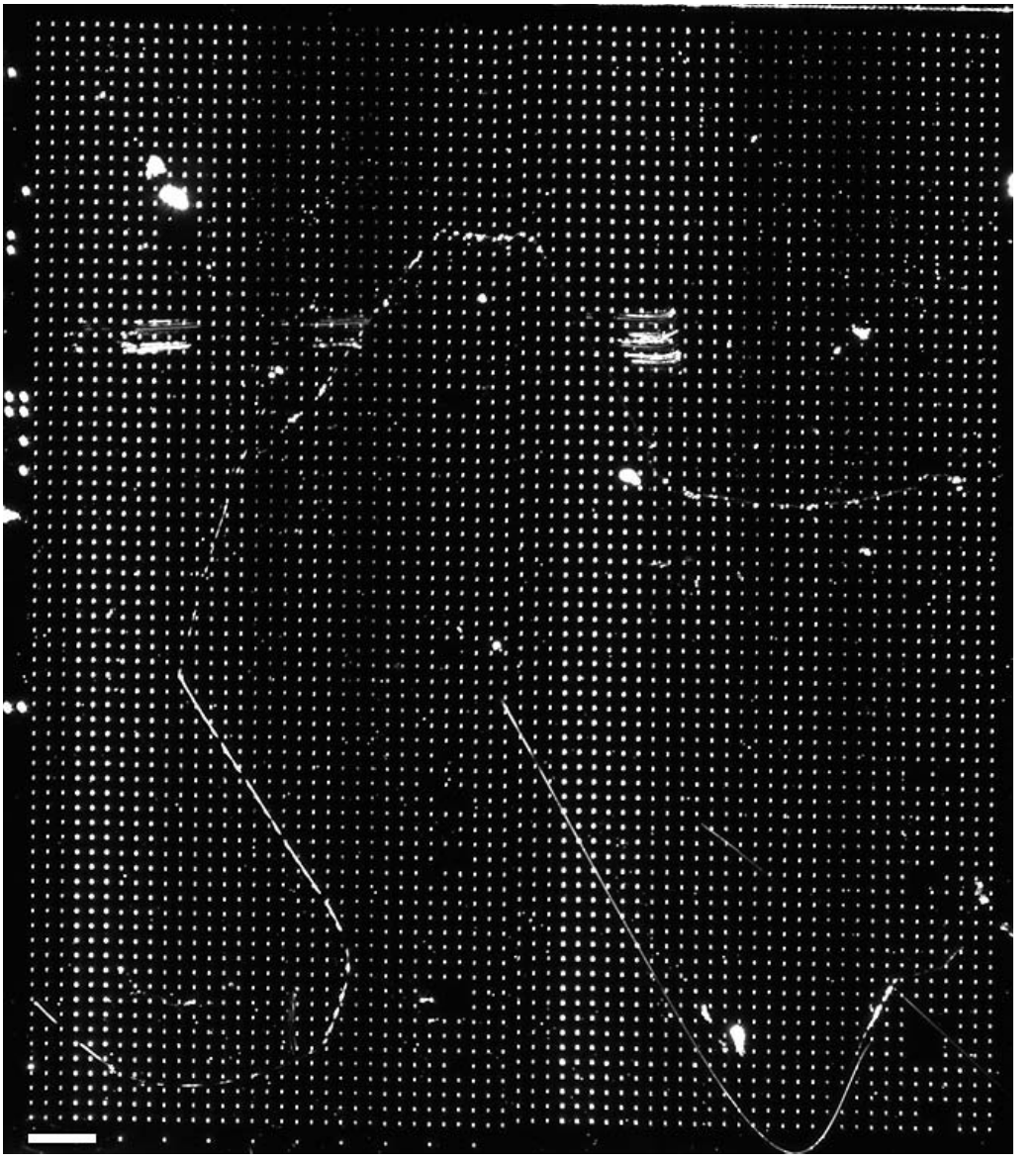

Figura 17: Imagen de microscopia de campo oscuro de un patrón de DOPC con biotina-PEG-tiol en oro. La homogeneidad del patrón se mejoró optimizando el proceso de litografía. La escala equivale a 100 μm.

3.2.4. Experimentos de diferenciación celular

Para medir el grado de diferenciación celular, las células se cultivaron durante de 24 h y después se fijaron en los substratos. A continuación se tiñeron con anticuerpos fluorescentes para detectar la proteína osterix (OSX) que es característica para células que se están empezando a diferenciar hacia osteoblastos. Entonces, esta

proteína se traslada del citosol hacia el núcleo. Por eso, las células con un núcleo vacío se contaron como negativas, respectivo a la diferenciación, y las células con color homogéneo verde o con un núcleo más brillante se contaron como positivas (Figura 18). Los substratos usados se presentan en la Tabla 1.

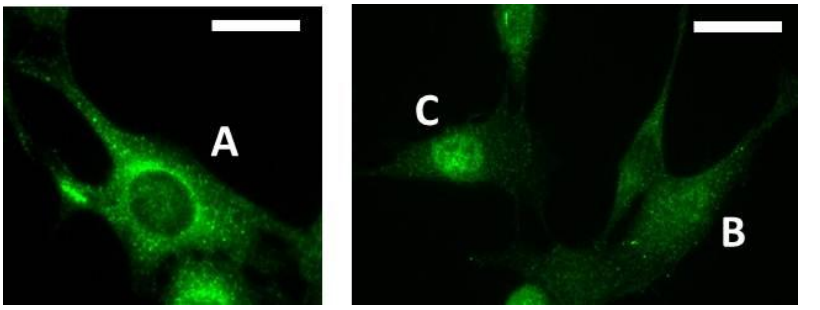

Figura 18: Tinción de la proteína Osterix (OSX) de las células C2C12. La célula de la izquierda (A) tiene el núcleo vacío y se considera negativa en cuanto a la diferenciación hacia osteoblastos. Las células al lado derecha tienen un color homogéneo (B) o incluso el núcleo más brillante (C) y se consideran positivas en cuanto a la diferenciación. La escala mide 25 µm.

Tabla 1: Resumen de los substratos usados para los experimentos de diferenciación celular y sus características.

Nombre	**homo**	**5-R**	**5-L**	**dots**
Método	Inmersión	µ-CP	µ-CP	Dip-pen
Tamaño	Monolayer	5 µm round	5 µm lines	4 µm dots
Espaciado	-	5 µm	5 µm	22 µm

La proteína BMP-2 inmovilizada en los substratos mantuvo su actividad biológica, como se puede ver en la Figura 19. Los substratos con BMP-2 tienen el porcentaje de células diferenciadas más alto que los substratos sin BMP-2 (las diferencias son significativas, como indican los asteriscos).

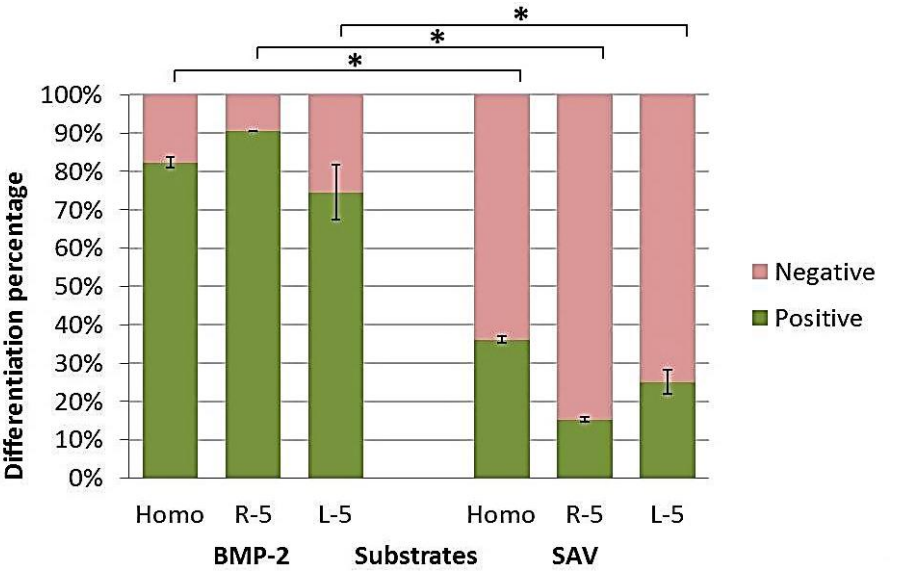

Figura 19: Grafica representando el porcentaje de diferenciación celular de las células C2C12 que han sido teñidos por la proteína osterix. Las células que han sido identificadas como positivas en cuanto a la diferenciación (hacía osteoblastos) se muestran en verde. Las células negativas en rojo. Los asteriscos indican diferencias significativas entre resultados.

Evaluando todos los substratos usados, se consigue la siguiente estadística de diferenciación celular, que se muestra en la Figura 20 y la Tabla 2.

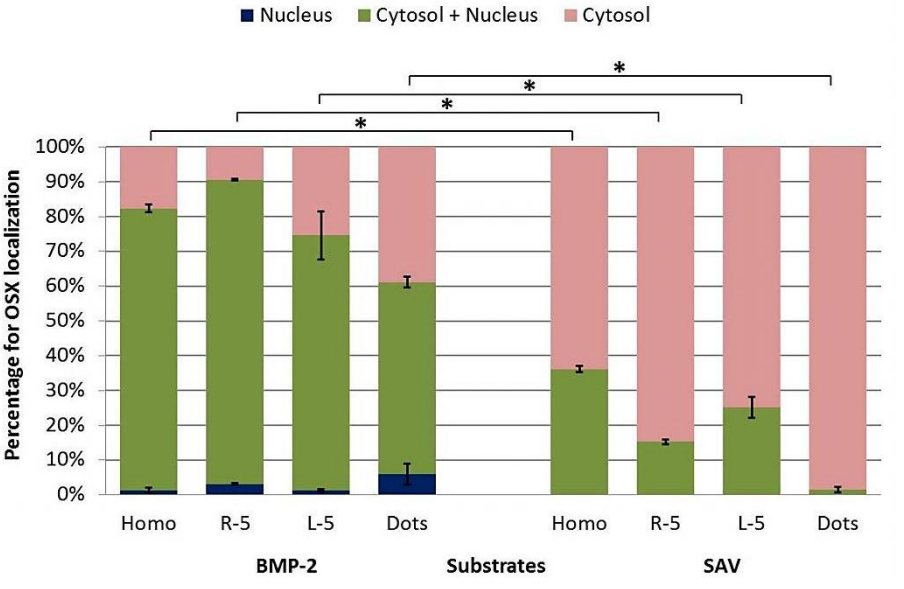

Figura 20: Grafica que representa el porcentaje de OSX en el citosol (rojo), en núcleo y citosol (verde) y en el núcleo (azul). El lado izquierdo representa los substratos con BMP-2, el lado derecha los substratos sin BMP-2 (correspondiendo a streptavidina). Los asteriscos indican diferencias significativas.

Tabla 2: Valores concretos para el porcentaje de diferenciación de células C2C12 hacia osteoblastos.

Substrato (+ BMP-2)	**5-L**	**Homo**	**5-R**	**dots**
Diferenciación %	74.59 ±14.35	82.32 ± 2.68	90.61 ± 0.02	61.31 ± 2.91

Las diferencias en respecto a los porcentajes de diferenciación en substratos con BMP-2 se pueden explicar de la siguiente manera: los substratos con patrón de líneas no favorecen la diferenciación hacia osteoblastos porque el patrón corresponde más al entorno natural de mioblastos.[76] Para los substratos homo, 5-R y dots, las diferencias en el porcentaje de diferenciación celular se pueden atribuir a la diferente densidad de BMP-2 en superficie. La Tabla 3 muestra las diferencias en la densidad de BMP-2. Muy importante, hay que diferenciar entre densidad local (en respecto a un área pequeño del substrato) y densidad total (en respecto a todo el substrato), véase Figura 21. Como se puede ver, la densidad total de los substratos 5-R y dots es mas pequeña que en los substratos homo. Sin embargo, la densidad local es más alta. Eso tiene un efecto importante en la diferenciación celular, como demuestran los substratos homo y 5-R.

Tabla 3: Diferencias en la densidad local y total de la BMP-2 en los diferentes substratos homo, 5-R y dots. La densidad local y total está indicada en Figura 21.

Substrato	**Homo**	**5-R**	**Dots**
Cubrimiento **local** de BMP-2	35.52%	100%	100%
Densidad **local** de BMP-2 (pmol/cm²)	**4.44**	**12.5**	**12.5**
Cubrimiento **total** de BMP-2	35.52%	28.27%	2.63%
Densidad **total** de BMP-2 (pmol/cm²)	**4.44**	**3.53**	**0.33**

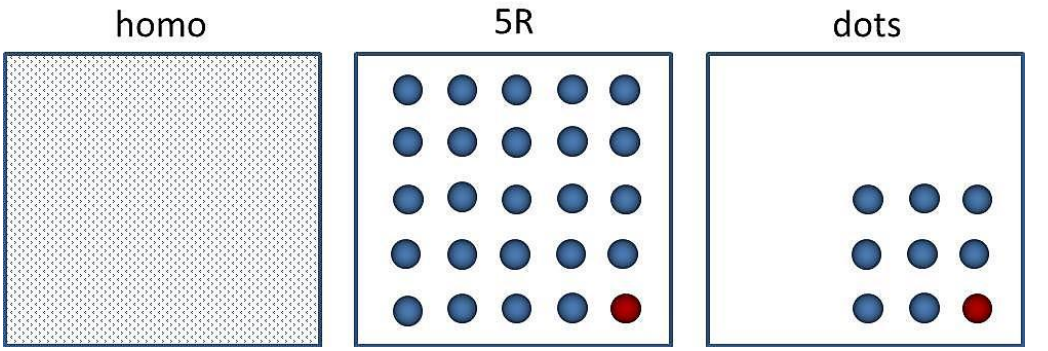

Figura 21: Figura esquemática que representa la densidad local y densidad total de BMP-2. La densidad local se refiere a un punto del patrón (en rojo), mientras la densidad total se refiere a la densidad de BMP-2 respectiva a toda la superficie.

3.3. CONCLUSIONES

En este capítulo, se ha demostrado que la nanolitografía Dip-pen puede ser aplicada de forma exitosa para el "patterning" de superficies de vidrio y oro y su consecuente aplicación para determinados estudios de diferenciación celular. A ese fin, se han evaluado varias formas de deposición de tinta para sustratos de vidrio y oro, con el objetivo de conseguir de manera reproducible, estable y localmente confinado un grupo biotina sobre la superficie. Para los sustratos de oro, esto se consiguió depositando una tinta que contenía un lípido como carrier para la actual molécula de interés (biotina-PEG-tiol). Para los sustratos de vidrio, una nueva estrategia de funcionalización fue desarrollada para facilitar la reacción click en la superficie con una biotina-azida. Ambos sustratos destacan debido a su sencillo "patterning" y al carácter robusto de la biotina covalentemente inmovilizada, que fue crucial en los siguientes pasos de derivación, y que deja como molécula final pendiente de la superficie a BMP-2. BMP-2 es conocida por inducir la diferenciación celular en la línea celular C2C12.

Solo los sustratos de oro pudieron ser evaluados después de los experimentos de diferenciación celular. Los resultados para la diferenciación celular sobre los sustratos de oro fueron evaluados con análisis estadísticos y mostraron que, incluso aunque el

porcentaje total de células diferenciadas sobre los sustratos era menor comparado con sustratos de referencia, las células diferenciadas lo hicieron en un 100%, lo cual es un resultado muy prometedor que anima a continuar estudios sobre este tipo de superficies, más aún debido a las pocas publicaciones que existen sobre estudios de diferenciación celular usando DPN.

3.4. REFERENCIAS

[1] Obtenido de http://www.nobelprize.org/educational/physics/microscopes/discoveries/index.html; en Junio 2012.

[2] R.P. Feynman. *There's plenty of room at the bottom*. Engineering and Science (California Institute of Technology) 1960. **23 (5)**: p.22-36.

[3] G.E. Moore. *Cramming more components onto integrated circuits*. Electronics 1965. **38 (8)**. Taken from the website "http://download.intel.com/museum/Moores_Law/Articles-Press_Releases/Gordon_Moore_1965_Article.pdf"; accessed in June 2012.

[4] B.D. Gates, Q. Xu, M. Stewart, D. Tyan, C.G. Willson and G.M. Whitesides. *New Approaches to Nanofabrication: Molding, Printing, and Other Techniques*. Chemical Reviews 2005. **105 (4)**: p. 1171-1196.

[5] E. A. Bayer, M. Wilchek and E. Skutelsky. *Affinity cytochemistry: The localization of lectin and antibody receptors on erythocytes via the avidin-biotin complex.* FEBS Letters 1976. **68**: p. 240-244.

[6] B.L. Weeks, M.W. Vaughn and J.J. DeYoreo. *Direct Imaging of Meniscus Formation in Atomic Force Microscopy Using Environmental Scanning Electron Microscopy*. Langmuir 2005. **21 (18)**: p. 8096-8098.

[7] R.D. Piner, J. Zhu, F. Xu, S. Hong and C.A. Mirkin. *"Dip-pen" Nanolithography.* Science 1999. **283 (5402)**: p. 661-663.

[8] Taken from the datasheet "2D nano PrintArray™", available at http://www.NanoInk.net; accessed June 2012.

[9] M. Su, M. Aslam, L. Fu, N. Wu and V.P. Dravid. *Dip-pen nanopatterning of photosensitive conducting polymer using a monomer ink.* Applied Physics Letters 2004. **84 (21)**: p. 4200-4202.

[10] F.S. Teixeira, R.D. Mansano, M.C. Salvadori, M. Cattani and I.G. Brown. *Atomic force microscope nanolithography of polymethylmethacrylate polymer.* Review of Scientific Instruments 2007. **78**: p. 0537021-0537023.

[11] H. Nakashima, M.J. Higgins, C. O´Connell, K. Torimitsu and GG. Wallace. *Liquid Deposition Patterning of Conducting Polymer Ink onto Hard and Soft Flexible Substrates via Dip-pen Nanolithography.* Langmuir 2011. **28 (1)**: p. 804-811.

[12] J.-W. Jang, A. Smetana and P. Stiles. *Multi-Ink Pattern Generation by Dip-pen Nanolithograph*y. Scanning 2010. **32**: p. 24-29.

[13] K. Salaita, Y. Wang and C.A. Mirkin. *Applications of Dip-pen nanolithography.* Nature Nanotechnology 2007. **2**: p. 145-155.

[14] K. Salaita, Y. Wang, J. Fragala, R.A. Vega, C. Liu and C.A. Mirkin. *Massively Parallel Dip-pen Nanolithography with 55000-Pen Two-Dimensional Arrays.* Angewandte Chemie, International Edition 2006. **45**: p. 7220-7223.

[15] A.J. Senesi, D.I. Roykiewicz, D.N. Reinhoudt and C.A. Mirkin. *Agarose-Assisted Dip-pen Nanolithography of Oligonucleotides and Proteins.* ACS Nano 2009. **3 (8)**: p. 2394-2402.

[16] E. Bellido, R. de Miguel, D. Ruiz-Molina, A. Lostao and D. Maspoch. *Controlling the Number of Proteins with Dip-pen Nanolithography.* Advanced Materials 2010. **22**: p. 352-355.

[17] E.J. Irvine, A. Hernandez-Santana, K. Faulds and D. Graham. *Fabricating protein immunoassay arrays on nitrocellulose using Dip-pen lithography techniques.* Analyst 2011. **136**: p. 2925-2930.

[18] H. Jiang and S.I. Stupp. *Dip-pen Patterning and Surface Assembly of Peptide Amphiphiles.* Langmuir 2005. **21 (12)**: p. 5242-5246.

[19] Y.-H. Shin, S.-H. Yun, S.-H. Pyo, Y.-S. Lim, H.-J. Yoon, K.-H. Kim, S.-K. Moon, S.W. Lee, Y.G. Park, S.-I. Chang, K.-M. Kim and J.-H. Lim. *Polymer-Coated Tips for Patterning of Viruses by Dip-pen Nanolithography.* Angewandte Chemie, International Edition 2010. **49**: p. 9689-9692.

[20] D. Grieshaber, R. MacKenzie, J. Vörös and E. Reimhult. *Electrochemical Biosensors – Sensor Principles and Architectures*. Sensors 2008. **8 (3)**: p. 1400-1458.

[21] A. Hulanicki, S. Glag and F. Ingman. *Chemical sensors definitions and classification*. Pure and Applied Chemistry 1991. **63 (9)**: p. 1247-1250.

[22] H. Harms, M.C. Wells and J. Roelof van der Meer. *Whole-cell living biosensors – are they ready for environmental application?* Applied Microbiology and Biotechnology 2006. **70 (3)**: p. 273-280.

[23] X. Zeng, Z. Shen and R. Mernaugh. *Recombinant antibodies and their use in biosensors.* Analytical and Bioanalytical Chemistry 2012. **402 (10)**: p. 3027-3038.

[24] P. Hollingen and P.J. Hudson. *Engineered antibody fragments and the rise of single domains.* Nature Biotechnology 2005. **23 (9)**: p- 1126-1136.

[25] J. Galbán, I. Sanz-Vicente, E. Ortega, M. del Barrio and S. de Marcos. *Reagentless fluorescent biosensors based on proteins for continuous monitoring systems.* Analytical and Bioanalytical Chemistry 2012. **402 (10)**: p. 3039-3054.

[26] T.A. Martin, C.T. Herman, F.T. Limpoco, M.C. Michael, G.K. Potts and R.C. Bailey. *Quantitative Photochemical Immobilization of Biomolecules on Planar and Corrugated Substrates: A Versatile Strategy for Creating Functional Biointerfaces*. ACS Applied Materials and Interfaces 2011. **3 (9)**: p. 3762-3771.

[27] R. Glatz and K. Bailey-Hill. *Mimicking nature's noses: From receptor deorphaning to olfactory biosensing.* Progress in Neurobiology 2011. **93 (2)**: p. 270-296.

[28] Y. Lei, W. Chen and A. Mulchandani. *Microbial biosensors*. Analytica Chimica Acta 2006. **568**: p. 200-210.

[29] F.R.R. Teles and L.P. Fonsecs. *Trends in DNA biosensors*. Talanta 2008. **77 (2)**: p. 606-623.

[30] B. Strehlitz, C. Reinemann, S. Linkorn and R. Stoltenburg. *Aptamers for pharmaceuticals and their application in environmental analytics.* Bioanalytical Reviews 2012. **4 (1)**: p. 1-30.

[31] C. Brioni and M. Moreno. *Applications of peptide nucleic acids (PNAs) and locked nucleic acids (LNAs) in biosensor development.* Analytical and Bioanalytical Chemistry 2012. **402 (10)**: p. 3071-3089.

[32] F. Mao, N. Mano and A. *Heller. Long tethers binding redox centers to polymer backbones enhance electron transport in enzyme "wiring" hydrogels*. Journal of the American Chemical Society 2003. **125 (16)**: p. 4951-4957.

[33] D. Avnir, T. Coradin, O. Lev and J. Livage. *Recent bio-applications of sol-gel materials.* Journal of Materials Chemistry 2006. **16 (11)**: p. 1013-1030.

[34] J.R. LaGraff and Q. Chu-LaGraff. *Scanning force microscopy and fluorescence microscopy of microcontact printed antibodies and antibody fragments.* Langmuir 2006. **22 (10)**: p. 4685-4693.

[35] R. Wacker, H. Schroder and C.M Niemeyer. *Performance of antibody microarrays fabricated by either dna-directed immobilization, direct spotting or streptavidin-biotin attachment: a comparative study*. Analytical Biochemistry 2004. **330 (2)**: p. 281-287.

[36] J. Labuda, A.M. Oliveira Brett, G. Evtugyn, M. Fojta, M. Mascini, M.Ozsoz, I. Plachetti, E. Palečec and J. Wang. *Electrochemical nucleic acid-based biosensors: Concepts, terms, and methodology (IUPAC Technical Report)*. Pure Applied Chemistry 2010. **82 (5)**: p. 1161-1187.

[37] M.J. Heller. *DNA MICROARRAY TECHNOLOGY: Devices, Systems and Applications.* Annual Revies of Biomedical Engineering 2002. **4**: p. 129-153.

[38] E. Engvall and P. Perlmann. *Enzyme-linked immunosorbent assay (ELISA). Quantitative assay of immunoglobulin G.* Immunochemistry 1971. **8 (9)**: p. 871-874.

[39] L.M. Demers, D.S. Ginger, S.-J. Park, Z. Li, S.-W. Chung and C.A. Mirkin. *Direct Patterning of Modified Oligonucleotides on Metals and Insulators by Dip-pen Nanolithography*. Science 2002. **296 (5574)**: p. 1836-1838.

[40] R.J. Stokes, J.A. Dougan and D. Graham. *Dip-pen nanolithography and SERRS as synergic techniques.* Chemical communications 2008. **44**: p. 5734-5736.

[41] A.J. Senesi, D.I. Rozkiewicz, D.N. Reinhoudt, and C.A. Mirkin. *Agarose-Assisted Dip-pen Nanolithography of Oligonucleotides and Proteins.* ACS Nano 2009. **3 (8)**: p. 2394-2402.

[42] D. Nyamjav and R.C. Holz. *Direct patterning of silanized-biomolecules on semiconductor surfaces*. Langmuir 2010. **26 (23)**: p. 18300-18302.

[43] R. Huisgen. *Centenary Lecture: 1,3-Dipolar Cycloadditions*. Proceedings of the Chemical Society 1961. p. 357-369.

[44] C.W. Tornoe, C. Christensen and M. Meldal. *Peptidotriazoles on Solid Phase: [1,2,3]-Triazoles by Regiospecific Copper(I)-Catalyzed 1,3-Dipolar Cycloadditions of Terminal Alkynes to Azides*. The Journal of Organic Chemistry 2002. **67 (9)**: p. 3057-3064.

[45] V.V. Rostovtsev, L.G. Green, V.V. Fokin and K.B. Sharpless. *A Stepwise Huisgen Cycloaddition Process: Copper(I)-Catalyzed Regioselective "Ligation" of Azides and Terminal Alkynes*. Angewandte Chemie, International Edition 2002. **41 (14)**: p. 2596-2599.

[46] R. A. Evans. *The Rise of Azide—Alkyne 1,3-Dipolar 'Click' Cycloaddition and Its Application to Polymer Science and Surface Modification.* Australian Journal of Chemistry 2007. **60 (6)**: p. 384-395.

[47] M. Bertoldo, G. Zampano, F. La Terra, V. Villari and V. Castelvetro. *Amphiphilic Amylose-g-poly(meth)acrylate Copolymers through "Click" onto Grafting Method.* Biomacromolecules 2011. **12 (2)**: p. 388-398.

[48] A. Koschella, M. Hartlieb and T. Heinze. *A 'click-chemistry' approach to cellulose-based hydrogels*. Carbohydrate Polymers 2011. **86 (1)**: p. 154-161.

[49] P. Dutta, S. Sawoo, N. Ray, O. Bouloussa and A. Sarkar. *Engineering Bioactive Surfaces with Fischer Carbene Complex: Protein A on Self-Assembled Monolayer for Antibody Sensing*. Bioconjugate Chemistry 2011. **22 (6)**: p. 1202-1209.

[50] P-C. Lin, S-H. Ueng, M-C. Tseng, J-L. Ko, K-T. Huang, S-C. Yu, A.K. Adak, Y-J. Chen and C-C. Lin. *Site-Specific Protein Modification through CuI-Catalyzed 1,2,3-Triazole Formation*

and Its Implementation in Protein Microarray Fabrication. Angewandte Chemie, International Edition 2006. **45 (26)**: p. 4286-4290.

[51] H. Nandivada, H-Y. Chen, L. Bondarenko and J. Lahann. *Reactive Polymer Coatings that „Click"*. Angewandte Chemie, International Edition 2006. **45 (20)**: p. 3360-3363.

[52] D.I. Rozkiewicz, D. Janczewski, W. Verboom, B.J. Ravoo and D.N. Reinhoudt. *„Click" Chemistry by Microcontact Printing.* Angewandte Chemie, International Edition 2006. **45 (32)**: p. 5292-5296.

[53] D.A. Long, K. Unal, R.C. Pratt, M. Malkoch and J. Frommer. *Localized "Click" Chemistry Through Dip-pen Nanolithography.* Advanced Materials 2007. **19 (24)**: p. 4471-4473.

[54] W.F. Paxton, J.M. Spruell and J.F. Stoddart. *Heterogeneous Catalysis of a Copper-Coated Atomic Force Microscopy Tip for Direct-Write Click Chemistry.* Journal of the American Chemical Society 2009. **131 (19)**: p. 6692-6694.

[55] H.Y. Chen, M. Hirtz, X. Deng, T. Laue, H. Fuchs and J. Lahann. *Substrate-Independent Dip-pen Nanolithography Based on Reactive Coatings.* Journal of the American Chemical Society 2010. **132 (51)**: p. 18023-18025.

[56] S.Oberhansl, M. Hirtz, A. Lagunas, R, Eritja, E. Martinez, H. Fuchs and J. Samitier. *Facile Modification of Silica Substrates Provides a Platform for Direct-Writing Surface Click Chemistry.* Small 2012. **8 (4)**: p. 541-545.

[57] R.G. Flemming, C.J. Murphy, G.A. Abrams, S.L. Goodman and P.F. Nealey. *Effects of synthetic micro- and nano-structured surfaces on cell behavior.* Biomaterials 1999. **20 (6)**: p. 573-588.

[58] J. Tagaki, B.M. Petre, T. Walz and T.A. Springer. *Global Conformational Rearrangements in Integrin Extracellular Domains in Outside-In and Inside-Out Signaling.* Cell 2002. **110 (5)**: p. 599-611.

[59] S.K. Mitra, D.A. Hanson and D.D. Schlaepfer. *Focal adhesion kinase: in command and control of cell motility.* Nature Review Molecular Cell Biology 2005. **6 (1)**: p. 56-68.

[60] E.A. Cavalcanti, P. Tomakidi, M. Bezler and J.P. Spatz. *Geometric organization of the extracellular matrix in the control of integrin-mediated adhesion and cell function in osteoblasts.* Progress in Orthodontics 2005. **6 (2)**: p. 232-237.

[61] M.F. Pittenger, A.M. Mackay, S.C. Beck, R.K. Jaiswal, R. Douglas, J.D. Mosca, M.A. Moorman, D.W. Simonetti, S. Craig and D.R. Marshak. *Multilineage potential of adult human mesenchymal stem cells.* Science 1999. **584 (5411)**: p. 143-147.

[62] G.H. Underhill and S.N. Bhatia. *High-throughput analysis of signals regulating stem cell fate and function.* Current Opinion in Chemical Biology 2007. **11 (4)**: p. 357-366.

[63] C.J. Flaim, S. Chien and S.N. Bhatia. *An extracellular matrix microarray for probing cellular differentiation.* Nature Methods 2005. **2 (2)**:119–125.

[64] C. Kuschel, H. Steuer, A.N. Maurer, B. Kanzok, R. Stoop and B. Angres. *Cell adhesion profiling using extracellular matrix protein microarrays.* Biotechniques 2006. **40 (4)**: p. 523–531.

[65] M. Kantlehner, P. Schaffner, D. Finsinger, J. Meyer, A. Jonczyk, B. Diefenbach, B. Nies, G. Hölzemann, S.L. Goodman and H. Kessler. *Surface Coating with Cyclic RGD Peptides Stimulates Osteoblast Adhesion and Proliferation as well as Bone Formation.* Chembiochem 2000. **1 (2)**: p. 107-114.

[66] H.G. Moghadam, M.R. Urist, G.K. Sandor and C.M. Clokie. *Successful mandibular reconstruction using a BMP bioimplant*. Journal of Craniofacial Surgery 2001. **12 (2)**: p. 119–127.

[67] U.M.E. Wikesjö, M. Qahash, Y-H. Huang, A. Xiropaidis, G. Polimeni and C. Susin. *Bone morphogenetic proteins for periodontal and alveolar indications; biological observations – clinical implications*. Orthodontics & Craniofacial Research 2009. **12 (3)**: p. 263–270.

[68] D. Chen, M. Zhao and G.R. Mundy. *Bone morphogenetic proteins.* Growth Factors 2004. **22 (4)**: p.233-241.

[69] V.Rosen. *BMP-2 signaling in bone development and repair.* Cytokine & Growth Factor Reviews 2009. **20 (5-6)**: p. 475-480.

[70] Y.Y. Yu, S. Lieu, C. Lu and C. Colnot. *Bone morphogenetic protein 2 stimulates endochondral ossification by regulating periosteal cell fate during bone repair.* Bone 2010. **47 (1)**: p. 65-73.

[71] S.A. Rodriguez Segui, University of Barcelona, PhD thesis 2009. *Development of cellular microarrays for stem cell culture and early stage differentiation evaluation.*

[72] K. Kashiwagi, T. Tsuji and K. Shiba. *Directional BMP-2 for functionalization of titanium surfaces.* Biomaterials 2009. **30 (6)**: p. 1166-1175.

[73] S.M. Kang, B. Kong, E. Oh, J.S. Choi and I.S. Choi. *Osteoinductive conjugation of bone morphogenetic protein-2 onto titanium/titanium oxide surfaces coated with non-biofouling poly(poly(ethylene glycol)methacrylate).* Colloids and Surfaces B: Biointerfaces 2010. **75 (1)**: p. 385-389.

[74] R. Derda, L. Li, B.P. Orner, R.L. Lewis, J.A. Thomson and L.L. Kiessling. *Defined substrates for human embryonic stem cell growth identified from surface arrays.* ACS Chemical Biology 2007. **2 (5)**: p. 347-355.

[75] S. Biswas, M. Hirtz and H. Fuchs. *Measurement of Mass Transfer during Dip-pen Nanolithography with Phospholipids.* Small 2011. **7 (14)**: p. 2081-2086.

[76] C.Y. Tay, M. Pal, H. Yu, W.S. Leong, N.S. Tan, K.W. Ng, S. Venkatraman, F. Boey, D.T. Leong and L.P. Tan. *Bio-inspired Micropatterned Platform to Steer Stem Cell Differentiation*. Small 2011. **7 (10)**: p. 1416-1421.

Barcelona - Such a beautiful horizon
Barcelona - Like a jewel in the sun
Por ti seré gaviota de tu bella mar
Barcelona - Suenan las campanas
Barcelona - Abre tus puertas al mundo
If God is willing
Friends until the end
Viva - Barcelona

Barcelona – Freddy Mercury and Montserrat Caballé